GLOBAL NEUROPROTECTION OF HUNTINGTIN IN CULTURE AND ALTERATIONS OF CORTICO-STRIATAL CONNECTIONS IN HUNTINGTON'S DISEASE CULTURE AND MOUSE MODELS

by

Caodu Buren

B.Sc., Jilin University, 2011

A THESIS SUBMITTED IN PARTIAL FULFILLMENT OF

THE REQUIREMENTS FOR THE DEGREE OF

DOCTOR OF PHILOSOPHY

in

The Faculty of Graduate and Postdoctoral Studies

(Neuroscience)

THE UNIVERSITY OF BRITISH COLUMBIA

(Vancouver)

April 2017

Abstract

Huntington's disease (HD) is a genetic neurodegenerative disorder caused by expansion of a CAG repeat in exon 1 of the *HTT* gene, encoding an elongated poly-glutamine repeat in the N-terminal region of the protein huntingtin (mutant huntingtin; mHtt). The average age of onset is 38, and the disease is characterized by psychiatric disorders and cognitive deficits that, in general, gradually develop over 10 years before the overt onset of the disease phenotype – difficulties in movement control. In the past two decades, many studies have focused on cell death that is obvious in mid to late stage of the disease when the overt disease symptoms become irreversible, despite the fact that altered neuronal/synaptic functions may underlie the mood/cognitive disorders that precede a motor diagnosis.

In order to uncover the potentially preventable and/or reversible changes in cortico-striatal (C-S) connections in pre- and early stages of HD, we first studied the C-S coculture platform that represents its *in vivo* counterparts in order to investigate the role of wild-type huntingtin (wtHtt) protein in cell-death and C-S synaptic malfunctions in HD. I found that coculture with low cortical-to-striatal neuronal plating ratio (1:3 plating ratio) is a closer replica of its *in vivo* origin with slight differences in membrane properties, but with a significant increase in extrasynaptic NMDA receptor portion and a decrease in cell-survival signaling compared with the control (1:1). On the other hand, we found that wtHtt provides neuroprotective effects to striatal, cortical and hippocampal neurons, in a phospho-CREB-independent way in the case of the latter two neuronal types. Finally, using the C-S coculture and acute brain slice to study C-S synapse development and functions, I found that mHtt impairs the connection not only via suppressing striatal dendritic tree

development but also by altering excitatory presynaptic vesicle release and recovery of the glutamate pool.

In summary, this work is a further proof of HD as synaptopathy, and is a foundation for future research of drug discovery for HD targeting synaptic malfunctions at the pre-symptomatic stage.

Preface

A version of chapter 2 (section 2.1, section 2.2, section 2.3 and section 2.4) has been published in: C. Buren, G. Tu, M. P. Parsons, M. D. Sepers, L. A. Raymond. Influence of cortical synaptic input on striatal neuronal dendritic arborization and sensitivity to excitotoxicity in corticostriatal coculture. J Neurophysiol.2016 Apr 27: jn.00933.2015. I designed the experiments with help from Dr. Matthew P. Parsons and Dr. Lynn Raymond. I conducted all of experiments and analysis except those shown in Table 2-1 and Figure 2-2 which were performed by Gaqi Tu. I drafted the manuscript except parts of the discussion and manuscript revisions contributed by Dr. Lynn Raymond.

A version of chapter 3 (section 3.1, section 3.2, section 3.3 and section 3.4) has been published in: C. Buren, L. Wang, A. Smith-Dijak, L. A. Raymond, Region-specific pro-survival signaling and global neuronal protection by wild-type Huntingtin. J Huntington's Dis. 2014;3(4):365-76. I conceived the experiments with help from Dr. Lynn Raymond. I performed all the experiments and analyzed all the data except that shown in Figure 3-1 Bi which was conducted by Liang Wang. I wrote the manuscript and Dr. Lynn Raymond revised the draft.

Part of chapter 4 (section 4.1, section 4.2.1, part of section 4.2.2, part of section 4.2.4, section 4.2.5, section 4.2.6, part of section 4.3.1, part of section 4.3.2, part of section 4.3.3, part of section 4.4.1 and part of section 4.4.2) has already been published in: C. Buren, M. P. Parsons, A. Smith-Dijak, L. A. Raymond. Impaired development of C-S synaptic connectivity in a cell culture model of Huntington's disease. Neurobiol Dis. 2016 Mar; 87:80-90. Dr. Matthew P. Parsons and I designed the experiments with help from Dr. Lynn Raymond. I conducted the experiments and analyses shown in following figures: Figure 4-2, part of Figure 4-3 C, D and E, part of Figure 4-4

A, B, C, D and E, Figure 4-5, Figure 4-6, Figure 4-7 A and B. Dr. Matthew P. Parsons conducted and analyzed work shown in following figures: Figure 4-3 Ai, Aii and B, part of Figure 4-3 C, D and E, part of Figure 4-4 A, B, C, D and E, Figure 4-4 F and G. Amy Smith-Dijak conducted the experiments shown in Figure 4-7 C, D, E and F. Dr. Matthew P. Parsons wrote the manuscript, Dr. Lynn Raymond and I revised it.

Other parts of chapter 4 are based mostly on Caodu Buren's work conducted in Dr. L. A. Raymond's laboratory at UBC, except for the imaging of synaptotagmin 1 uptake assay which was performed in Dr. Ann Marie Craig's laboratory at UBC and experiments of Figure 4-8 C and Figure 4-10 C which were conducted in Dr. Michael R. Hayden's laboratory at UBC. These results are the major part of an in-preparation manuscript titled "impaired presynaptic glutamate supply in corticostriatal connections of Huntington's disease model", C. Buren, M. Schmidt, G. Tu, M. R. Hayden, L. A. Raymond. I designed the experiments with help from Dr. Lynn Raymond, Dr. Peng Zhang, Dr. Anne Marie Craig and Dr. Matthew P. Parsons, except for experiments of Figure 4-8 C and Figure 4-10 C. I conducted the experiments and analyses shown in following figures: Figure 4-8 A and B, Figure 4-9, Figure 4-10 Ai, Aii, Bi and Bii, Figure 4-11, Figure 4-12, Figure 4-13 and Figure 4-14. Mandi Schmidt designed, performed experiments and analyses shown in Figure 4-8 C and Figure 4-10 C. Gaqi Tu conducted the experiments and analysis shown in Figure 4-1. AAV virus injection was performed by Pumin Wang in Dr. Timothy H. Murphy's lab at UBC.

All mice were bred, cared and sacrificed according to the requirements of the University of British Columbia and the Canadian Council for Animal Care. The University of British Columbia Animal Care Committee approved the animal research conducted in this dissertation (certificate numbers: RBH-1-15, 5549-12, LB-2012-125496 and CS-2012-125496).

Table of Contents

List of Tables

List of Figures

List of Symbols

%: percent sign

+: addition of

#: the number of

&: and

~: approximately

% ΔF/F: percent change in fluorescent intensity

List of Abbreviations

3-NP: 3-nitropropionic acid

4-AP: 4-aminopyridine

AAV: Adeno-associated virus

ACSF: artificial cerebrospinal fluid

Akt: protein kinase B

AMCA: aminimethylcoumrin

AMPA: α-amino-3-hydroxy-5-methyl-4-isoxazolepropionic acid

ANOVA: analysis of variation

ATP: adenosine triphosphate

AUC: area under curve

BAC: bacteria artificial chromosome

BACHD mouse: an HD mouse model which expresses full-length human mutant huntingtin with a 97 poly-glutamine tract in bacterial artificial chromosome

BDNF: brain-derived neurotrophic factor

BDNF-AS: brain-derived neurotrophic factor antisense

C-S: cortico-striatal

CA: cornus ammonis

CA1: region 1 of hippocampus proper

Ca^{2+}: calcium ion

$CaCl_2$: calcium chloride

CACNA1A: calcium voltage-gated channel subunit alpha1 A

CAG: cytosine-adenine-guanine

CaMKIV: calcium/calmodulin-dependent protein kinase type IV

Cas9: clustered regularly interspaced short palindromic repeats-associated protein 9

CB1: cannabinoid receptor type 1

CBP: CREB-binding protein

Cm: membrane capacitance

CNS: central nervous system

CO_2: carbon dioxide

Cop: Caspase recruitment domain only protein

CRE: cAMP response element

CREB: cAMP response-binding protein

CRISPR: clustered regularly interspaced short palindromic repeats

CsCl: caesium chloride

CSF: cerebrospinal fluid

CsOH: caesium hydroxide

CSP: cysteine string protein

CTX: cortical

D1: dopamine receptor subtype 1

D2: dopamine receptor subtype 2DARPP32: dopamine- and cAMP-regulated neuronal phosphoprotein

DARPP32+: dopamine- and cAMP-regulated neuronal phosphoprotein expressing

DMEM: Dulbecco's modified Eagle's medium

DIV: day *in vitro*

DNA: deoxyribonucleic acid

DNQX: 6,7-dinitroquinoxaline-2,3-dione

E18: embryonic day 18

EAAT: excitatory amino acid transporter

EGTA: ethylene glycol-bis(ß-aminoethyl ether)-N,N,N',N'-tetraacetic acid

EPSC: excitatory postsynaptic current

ERK: extracellular signaling-regulated kinases

F: fluorescence

FM1-43: *N*-(3-triethylammoniumpropyl)-4-(4-(dibutylamino) styryl) pyridinium dibromide

FVB/N mouse: an inbred mouse strain preferable for transgenic analyses

GDP: guanosine diphosphate

GFP: green fluorescent protein

GLAST: glutamate aspartate transporter

GLT1: glutamate transporter 1

GluA2: glutamate ionotropic receptor AMPA type subunit 2

GluN2B: glutamate ionotropic receptor NMDA type subunit 2B

GluN3A: glutamate ionotropic receptor NMDA type subunit 3A

GPe: external segment of globus pallidus

GPi: internal segment of globus pallidus

GRIN2A: glutamate ionotropic receptor NMDA type subunit 2A

GRIN2B: glutamate ionotropic receptor NMDA type subunit 2B

GTP: guanosine triphosphate

HAP1: huntingtin-associated protein 1HD: Huntington's disease

Hdh: the murine homologue gene of human *HTT*

HEPES: 4-(2-hydroxyethyl)-1-piperazineethanesulfonic acid

HIP14: huntingtin interacting protein 14

HPA: hypothalamic pituitary-adrenal

HTT gene: gene encoding huntingtin, and it is mutated in Huntington's disease

Htt: huntingtin protein

HTT-AS: huntingtin antisense

iGluSnFr: intensity-based Glutamate-sensing fluorescent reporter

$I_{injected}$: current injected

IPSC: inhibitory postsynaptic current

Iss: steady-state current

I-V: current-voltageJNK: c-Jun N-terminal kinase

KCl: potassium chloride

KOH: potassium hydroxideMAP2: microtubule-associated protein 2

MAP2+: microtubule-associated protein 2 expressing

MAPK: mitogen-activated protein kinases

mEPSC: miniature excitatory postsynaptic current

mHtt: mutant huntingtin

MgATP: adenosine 5'-triphosphosphate magnesium salt

$MgCl_2$: magnesium chloride

mIPSC: miniature inhibitory postsynaptic current

MK801: dizocilpine

mPTP: mitochondrial permeability transition pore

MRI: magnetic resonance imaging

MSN: medium-sized spiny neurons

N17: first 17 amino acids in animo terminal

Na_2GTP: guanosine 5'-triphosphate sodium salt

NaCl: sodium chloride

NaOH: sodium hydroxide NeuN: Hexaribonucleotide Binding Protein-3

NGS: normal goat serum

NMDA: *N*-Methyl-D-aspartate

NMDAR: NMDA receptor

n.s.: no significance

N terminal: amino terminal

p38 MAPK: p38 mitogen-activated protein kinases

p53: tumor protein p53

p75NTR: p75 neurotrophin receptor

PBS: phosphate-buffered saline

PBST: PBS with 0.03% Triton X-100

pCREB: phosphorylated cAMP response element binding protein

PET: positron emission tomography

PFA: paraformaldehyde

PGC-1α: peroxisome proliferator—activated receptor gamma coactivator 1-alpha

PI3K: phosphoatidylinositol 3 kinase

PPARγ: peroxisome proliferator-activated receptor gamma

PSP: paired-sucrose pulse

PSD-95: postsynaptic density protein 95

PTEN: phosphatase and tensin homolog

PTX: picrotoxin

R6/1 mice: a truncated transgenic HD mouse model expressing around 115 CAG repeats

Rab3a: Ras-related protein Rab-3A

Rab11: Ras-related protein Rab-11A

REST/NRSF: RE1-silencing transcription factor/neuron-restrictive silencer factor

Rip2: Receptor interacting protein-2

RNA: ribonucleic acid

ROI: region of interest

RRP: readily releasable pool

RT: room temperature

SNAP: synaptosomal-associated protein

SNAP-25: synaptosomal-associated protein 25

SNPs: single nucleotide polymorphisms

SNc: substantia nigra pars compacta

SNr: substantia nigra pars reticularis

SPN: spiny projection neuron

STEP: Striatal-Enriched protein tyrosine phosphatase

STN: subthalamic nucleus

Syt1: synaptotagmin 1

TIFF: tag image file format

TrkB: tropomyosin receptor kinase B

TrkB-Fc: TrkB receptor fused with fragment crystallizable region of antibody

TTX: tetrodotoxinVAMP1: vesicle-associated membrane protein 1vGlut1: vesicular glutamate transporter 1

vGlut1+: vesicular glutamate transporter 1 expressing

vGlut2: vesicular glutamate transporter 2

vGlut2+: vesicular glutamate transporter 2 expressingvs.: versus

WT: wild-type

wtHtt: wild-type huntingtin

YAC: yeast artificial chromosome

YAC128: an HD mouse model that expresses human *HTT* with 128 CAG repeats on yeast artificial chromosome.

YAC18: an HD mouse model that expresses human *HTT* with 18 CAG repeats on yeast artificial chromosome.

YFP: yellow fluorescent protein

Acknowledgements

This dissertation was fulfilled with the support and cooperation from many people.

At first, I offer my enduring gratitude to my dear supervisor Dr. Lynn A. Raymond for cultivating me as a scientist for the past several years. Working with her I learned far more than science. I appreciate her kindness, considerateness and her careful supervision.

I thank all my committee members: Dr. Timothy O'Connor, Dr. Timothy H. Murphy, Dr. Kurt Haas and Dr. Lynn A. Raymond, for their guidance and support during my PhD. I owe Dr. Matthew P. Parsons a debt of gratitude for his mentorship as a postdoc, I learned more than electrophysiology and scientific writing that he taught me working with him side-by-side.

I thank Dr. Anne Marie Craig and Dr. Peng Zhang at the University of British Columbia for giving their intellectual help and for providing technical support.

The work performed in this dissertation was supported by Canadian Institutes of Health Research, CHDI foundation and Michael Smith Foundation for Health Research.

Special thanks are owed to my dear parents and to my sister, who have supported me emotionally and financially throughout the years of education.

To my dear parents

For their unspoken love

Chapter 1: Introduction

HD, as a progressive neurodegenerative and motor disorder, is manifested by difficulties in movement control and coordination, along with neuronal death in striatum and other neighboring brain regions (1). The movement dysfunction starts at mid-to-late adulthood, and gradually worsens over 15-30 years, making it difficult for the patients to take care of themselves (2) and eventually disabling the patient's speech and mental abilities (3), to death (4). It affects 10 to 13 in 100,000 people of European descents [an estimated close to 50,000 people in United States and Canada (5); prevalence in British Columbia, Canada is 13.7 per 100,000 in the general population, and 17.2 per 100,000 in the Caucasian people (5)], whereas the occurrence is relatively low in Asian populations (5–9).

Current treatments of HD are capable to ameliorate symptoms like hyperkinetic movement, but unable to cure the neurodegeneration (2,10–14). Anti-psychotic and anti-depressant drugs are often prescribed along to treat the accompanying mood and cognitive disorders of HD (15). The social cost of caring for HD patients is staggering, especially in developed countries (an estimated annual cost per HD patient is £21,605 in UK) (16).

Much of the previous research about HD was focused on the mechanisms of the striatal neuronal death which occurs at mid-to-late stage of the disease. But the mechanism underlying striatal-selective neurodegeneration is still elusive.

Notably, more than a decade prior to clinical diagnosis HD mutation carriers begin to exhibit personality change (17), cognitive decline (18,19), memory (20) and motor deficits (21), along striatal atrophy and white matter loss (22,23), which suggest deficits in cortico-striatal (C-S) connections (24,25) before the unstoppable neuronal death in the striatum and neighboring

regions. Indeed, recent investigation of has been shifted more to study synaptopathy of HD (26–28).

1.1 Huntington's Disease

1.1.1 Genetics of Huntington's Disease

The age of HD onset is inversely correlated with the CAG repeat length, which encodes the poly-glutamine tract in N-terminal region of Huntingtin (Htt) (3,29–32). The CAG repeat of *HTT* is unstable and may expand from generation to generation, so that unaffected persons carrying an intermediate number of repeats (from 28 to 35) may be followed by full-penetrant offspring (3).

Ninety percent of all the HD cases originate from a parent affected by HD, while the rest is caused by new mutations (9). In juvenile cases of HD (1-15% of all HD cases (33)), which manifests in childhood or adolescence (34), patients express one mutant allele with fairly long CAG trinucleotide repeat (over 60) (33,34). In comparison, adult HD is much more common with a trinucleotide repeat of 40-66 and with onset at an average age of 35-44 (3), whereas HD carriers with 36-39 CAG repeats often have much later starts, or may not even manifest disease symptoms within their normal lifetimes (3).

Besides, genetic background (i.e. presence and absence of background genes and single nucleotide polymorphisms (SNPs)) and environmental factors affect the disease penetrance, age of onset as well as progression (3,29,35–40). For instance, variations in kainate-specific glutamate receptor GluR6 genotype were shown to influence age of onset (41), as well as SNPs within GRIN2A and GRIN2B (35).

1.1.2 Clinical Symptoms

As the disease symptoms progress gradually, most of the tasks that require muscle control are affected (3) and it disables patients' self-care (42), accompanied with cognitive deficits (43), age-dependent sleep disorder and circadian abnormalities (44), even seizures in case of juvenile HD (45).

Many years before the disease onset, cognitive abilities start to decline and become progressively impaired (19); largely affected are executive functions, including problem solving (46), cognitive flexibility, abstract thinking, rule acquisition, initiation of appropriate actions, and inhibition of inappropriate actions, and ultimately these lead to subcortical dementia (47–49). Some studies found that HD has different impacts on sub-domains of executive functions, for example, accuracy in problem solving is reduced over the disease progression while planning time remains the same between early and late stage HD patients (46). Memory impairments appear as the disease progresses (both short-term and long-term memories), including episodic, procedural and working memories (47).

Emotion (mood) is another aspect compromised in HD patients. Patients often experience depression (50) and anxiety (51), and have difficulties in understanding negative/positive emotion (52). For instance, HD patients cannot well evaluate sincere, sarcastic vs. 'paradoxical sarcastic' statements (52). Suicide thoughts and attempts are more frequent than in the general populations (3,53). Even at the prodromal stage, neuropsychiatric symptoms are apparent, such as apathy, in the mutant gene carriers (54). In HD, depression, anxiety, irritability, obsessive-compulsive disorder and, less frequently, psychosis are treated with the same range of medications used for patients who do not have HD.

HD patients have increased weight loss compared with age-matched controls over the course of the disease (55), mainly due to muscle wasting that accounts for about 40% of body weight in normal person (56). The exact mechanism of muscle atrophy in HD is not well understood, but researchers proposed a hypothesis that imbalance of hypertrophic and atrophic signals from central nervous system (CNS) contributes to the muscle atrophy in HD (56). In an HD mouse model, skeletal muscle loss was also reproduced (57), and there is increased neurotransmitter release at the neuromuscular junctions at early stages (58). Inflammation is another feature of HD, both in the nervous system and in peripheral systems (59). Postmortem studies found significant microglial activations in striatum, globus pallidus and cortex of HD patients (60,61). A recent review has nicely covered inflammation of HD in both CNS and peripheral systems (59).

Furthermore, in peripheral tissues, HD patients often exhibit cardiac failure, impaired glucose tolerance, osteoporosis, testicular atrophy (62), stress susceptibility (63), and alterations in lipid transport (64). HD mouse models possess more brown-like adipocytes than control mice and increased thermogenic release of stored energy (65).

1.1.3 Clinical Treatments

The major treatments for HD are medications prescribed to suppress hyperkinetic symptoms, along with anti-psychotic drugs that ameliorates the accompanying psychosis. The most commonly used is tetrabenazine, which depletes dopamine stores via reversible inhibition of the vesicular monoamine transporter (14). Because the tonic level of dopamine in HD condition is higher (66), this activates the high-affinity D2 type of dopamine receptors, suppresses D2 receptor-expressing SPNs and further represses indirect pathway, and finally increases the motor outcome-

hyperactivity. Whereas tetrabenazine reduces extracellular dopamine level and removes the suppression on indirect pathway.

Additionally, special diet and increased involvement in activity may slow down disease progression (14,67–70). Anthocyanins, water-soluble vacuolar pigments in plants such as blueberry, have been shown to improve brain functions in aging and to suppress irritability in R6/1 mice (68), an HD mouse model that expresses truncated exon 1 of *HTT*, likely through functioning as anti-oxidants (71) but with no improvement in behavioral performances in rotarod test (72). Evidence suggesting that physical therapy is beneficial in HD is that stationary cycling helped HD patients have better fitness, but with reduced body weight by week 13 (67), possibly by elevating brain-derived neurotrophic factor (BDNF) generation in the brain (73). A larger scale study with longer track time for the disease progression is necessary to elucidate whether and how exercise can slow down the developments of disease phenotypes.

Deep brain stimulation, a widely used therapy for neurological diseases such as Parkinson's disease and depression, is also applied as an additive to HD on top of the main symptomatic treatments described above (74). This therapy is performed as chronic electrical stimulation of deep brain structures, such as basal ganglia, by pinpointing to target regions of interest (75). A double-blinded, pallidal deep brain stimulation study showed significant reduction of HD chorea and improvements in mood and in cognition after a 6-month treatment in HD patients (76).

Another study demonstrated that varenicline, a nicotinic agonist used as a smoking cessation aid, is able to improve executive functions and emotional recognition in a touch screen computer-based neurocognitive test battery in patients with early HD with poorly known mechanism (77).

1.1.4 Therapeutic Research

To rescue patients in mid-to-late HD, cell/tissue transplantation is under heavy investigation (78). In a recent study, injection of microencapsulated sertoli cells, a type of nursing cells of testicles, improved motor performance and extended life expectancy of a HD mouse model by modulating immune responses (79). However, other scientific and clinical questions remain unaddressed, such as immunological reactions between host and graft in CNS(80).

Other emerging HD therapeutics target the mutant gene at either DNA (81,82) or transcription level (83) to either correct the mutation or silence its expression. Selective silencing of mHtt with CRISPR/Cas9 (81,82), antisense oligonucleotide (83) or microRNA therapies (84) based on allele-specificity, are all under study as potential disease-modifying therapies.

1.2 Huntington's Disease Models

1.2.1 Neurotoxin Animal Models

Before the discovery of the gene *HTT* in 1993 (4), quinolinic acid and kainic acid were used to create HD models based upon an assumption that both acids spare the specific population of striatal neurons that are also resistant to neurodegeneration in HD (85). Unarguably, the largest disadvantage of these neurotoxin-induced animal models is that they genetically and molecularly do not reproduce many key disease features of HD.

1.2.2 Genetically Modified Rodent Models

Numerous genetically modified HD models have been created to reproduce not only neurodegeneration in striatum and related chorea, but also cognitive declines and increased emotional instabilities, including aggression, anger, anxiety and irritability, as well as immune

reactions (86,87). Those models were covered nicely in a few recent HD murine model reviews (88,89). Table 1-1 shows the most common genetically modified HD mouse models.

Transgenic Models

Transgenic HD mouse models generally were created by utilizing yeast artificial chromosome (YAC) or bacteria artificial chromosome (BAC) as a vector for expressing human *HTT*, where related promotors and enhancers have or have not be inserted. In YAC HD models that express full-length human *HTT* in the FVB/N background, its copy number and CAG trinucleotide repeat length vary from line to line, so do disease onset and progression (90,91). The YAC128 mouse model that expresses *HTT* with 128 CAG repeats (the expression of mHtt is 75% of endogenous protein level (90)) reproduces the key pathology of HD, such as hyperactivity at early and hypoactivity at late stage (90) as well as gradual and specific loss of striatal neuronal loss (90,92). This mouse model starts to display motor learning deficits from 2 months (93), decreased performance in the rotarod test from 6 months (90,93), striatal atrophy from 9 months (90) and neuronal loss from 12 months (90). Most importantly, it is an adult-onset HD model that shows slow disease progression, which allows us to study the gradual development of HD synaptopathy with long time window. As a control line, the Hayden lab also created YAC mice that express *HTT* with 18 CAG repeats (94). This mouse line could also be used as a wild-type Htt (wtHtt)-overexpressing model (the human wtHtt expression is about one half of the endogenous Htt expression) (94).

Truncated Models

The earliest developed and the most widely used transgenic mouse model is R6/2, an aggressive HD model which expresses human Htt N-terminal fragments with 141-157 poly-glutamine repeats under human *HTT* promotor (95). It is regarded as a model for the juvenile form of HD (95). These mice develop the HD motor phenotype from 5-7 weeks of age and it rapidly worsens to death at 12-15 weeks (96). Therefore, this HD mouse model is not suitable for our current study. Another truncated HD mouse model is R6/1 which expresses exon 1 of *HTT* (with 111-119 CAG repeat length) with low mRNA level (96) and develops the disease phenotypes more slowly compared with R6/2 (97). However, R6/1 mice hardly show neuronal death – one of the key phenotypes of HD (97).

Knock-in Models

Recently, knock-in models of HD are widely accepted because they are genetically closer to HD compared to the transgenic models. One of them is the CAG140 model that expresses chimeric human/mouse Htt with 140 poly-glutamine repeats (98). However, CAG140 mice show greater age-dependent resistance to excitotoxicity than YAC128 (99). The Q175 model is another popular knock-in mouse model on the C57B/16J background (100). This HD model reproduces multiple HD phenotypes, including disrupted circadian rhythms (101), altered excitatory and inhibitory inputs to striatal neurons (102) as well as behavioral and neuropathological abnormalities (103). However, Q175 mice show the motor phenotype of HD later than YAC128 mice (104).

A genetically modified rat model is also used in HD research, but with shorter CAG repeats (105). The cost of maintaining the rat model is higher than that of mice. Furthermore, transgenic non-human primate models of HD are also used in research (106). But research on them is

restricted to unique aspects of HD that those models reproduce better than rodent models, such as mood (87). One reason is because the expense is higher than that of mouse models.

Htt as an evolutionarily conserved protein that has its homolog in Drosophila (107). Researchers created the Drosophila HD model and have investigated synaptic functions largely on the neuro-muscular junction (108). But its brain structure is not appropriate to study synaptopathy basis of the central nervous system, especially the cortical-striatal (C-S) connections of HD.

	Genetic background	CAG repeat length	Reduced performance on Rotarod at	Impaired motor learning on Rotarod at	Hyperactive at	Hypoactive at
YAC128 - line55, transgenic	FVB/N (90)	Full-length human Htt with 128 CAG repeats on YAC (90)				
YAC128 - line53, transgenic	FVB/N (90)	Full-length human Htt with 128 CAG repeats on YAC (90)	6 months (90,93)	2 months (93)	3 months (90)	12 months (90)
R6/2, transgenic	CBA x C57BL/6 (96)	141-157 CAG repeats (96)	5-6 weeks (109)			5-7 weeks (110)
R6/1, transgenic	CBA x C57BL/6 (96)	111-119 CAG repeats (96)	5 months (111)		4 weeks (112)	6 weeks (112)
BACHD, transgenic	FVB/NJ (113)	Full-length human Htt with 97 a mix of CAA-CAG repeats on BAC (113)	2 months (113)			
Q175, knock-in	129Sv x C57BL/6J (114)	A chimeric human/mouse exon 1 carrying the region of expanded 188 CAG repeats and the human proline region (104)	30 weeks in both homozygous and heterozygous (104)			8 weeks in the homozygous; 20 weeks in heterozygous (104)
CAG140, knock-in	129Sv x C57BL/6J (114)	Chimeric *HTT/Hdh* exon 1 with 140 CAGs (114,115)	4 months (98)		1 month (115)	4 months (115)

	Age of onset	DARPP32 reduction	Striatal volume reduction at	Striatal neuronal loss at	Inclusions present in striatum at	Death at	Note
YAC128 - line55, transgenic							
YAC128 - line53, transgenic	6 months (90)		15% reduction at 9 months (90)	15-18% decrease at 12 months (90)	18 months (90)	Normal (90)	Twice more copies human Htt RNA than line 55 (90)
R6/2, transgenic	8-11 weeks (96,109,116)				3.5 weeks (117)	12-15 weeks (96)	
R6/1, transgenic	15-21 weeks (96)	5 months (111)				32-40 weeks (96)	
BACHD, transgenic			28% reduction at 12 months (113)	14% of striatal neurons starts to degenerate but not disappear at 12 months (113)	12 months, but largely in cortex and less in striatum (113)		
Q175, knock-in		12-18 weeks (118)				76-104 week in the homozygous; 25% of the heterozygous die at 104 weeks (104)	Also named as zQ175 (104)
CAG140, knock-in	20 months (98)		20-26 months (98)	20-26 months (98)	6 months (115)		Also named as Hdh140 (114) and Q140 (119)

Table 1-1 Most widely used genetically-modified mouse models of HD

1.2.3 Culture Models

Mono-culture

To study the neurodegeneration of HD, which initiates from striatal SPNs selectively and spreads out to the neighboring brain regions, with precise control over the extracellular environment, researchers have developed striatal neuronal culture HD models (120) from either primary neurons of HD mouse models (121) or induced-pluripotent stem cells originated from human HD patient somatic cells via induced differentiation (122). These culture models of HD lack modulatory dopaminergic or excitatory glutamatergic inputs of neurons originated from other brain regions, which exist *in vivo*. Therefore, these culture models are very useful to study cell-autonomous features of striatal SPNs, but not suitable to investigate C-S connections that undergo malfunctions prior to striatal SPNs death in HD.

Cortical-striatal Coculture

Invention of coculture prepared with primary neurons from different brain regions (123) (133) made it possible to study striatal neurons in a closer *in vitro* condition by co-plating striatal neurons with cortical neurons (124). Importantly, C-S coculture develops abundant C-S synapses, thus, we can investigate the C-S connections in various conditions with cell culture-unique methods (124). For example, by co-plating striatal or cortical neurons from FVB/N wild-type mice together with cortical or striatal neurons from transgenic mice, either YAC18 or YAC128, we are able to study how expression of wtHtt (over-expression) or mHtt in either side of C-S synapses contributes to changes in C-S connections (125).

1.3 Huntingtin

1.3.1 Huntingtin

The gene *HTT* is located in chromosome 4 short arm and encodes for the protein Htt (4). The poly-glutamine tract near the N-terminal of Htt is translated from the CAG triplet repeat in exon 1 of *HTT* (4). The molecular mass of the protein is estimated to be around 350kD with about 3144 amino acids depending on the poly-glutamine tract length. Both wtHtt and mHtt are expressed ubiquitously in the body (4).

The protein is evolutionarily conserved (126). However, the exact functions of the protein are poorly understood with limited knowledge of its spatial structure. It is known that severe reduction in wtHtt level leads to impaired development of nervous system (127) and its deletion is even lethal at embryonic stage (128–130). Interestingly, solo expression of mHtt can rescue Htt knockout embryos (131,132). These data suggest that HD mutation in *HTT* has little influence on embryonic development and it functions at least at embryonic stage likely through its non-poly-glutamine domains to promote nervous system development.

On the other hand, protein interaction studies suggested several hundreds of potential interactors of Htt (wild-type and/or mutant) distributed throughout cytosol and cell nucleus (133,134). Htt appears as an interaction hub that modulates numerous aspects of a cell, from gene transcription, post-translational modification, cell metabolism to intracellular cargo transportation (133,134). But the roles of Htt in cell signaling and synaptic transmission are still largely elusive (134,135). After translation, the expanded poly-glutamine tract of mHtt forms hydrogen bonds with one another due to the polarized nature of glutamine amino acid (136), thereby producing misfolded protein that aggregates (136) instead of interacts properly with its partner proteins (8).

Htt (wild-type and/or mutant) can be phosphorylated (137), acetylated (138–140), palmitoylated (141,142) and SUMOylated (143). Post-translational modification of the mutant form is an essential factor that mediates both neurodegeneration and behavioral abnormalities. For instance, elevated phosphorylation of serine 421 facilitates clearance of mHtt from the cell via protein degradation and mitigates cell-death and even improves behavioral outcomes in HD murine models (144). Lysine 48 ubiquitination partially determines proteasome-mediated clearance of mHtt (145). Thus, accelerated phosphorylation-dependent or ubiquitin-dependent degradation of mHtt potentially postpones accumulation of mis-folded Htt and suppresses aggregate formation, although Htt aggregates may not be detrimental to the cell (146). Furthermore, phosphorylation of serine residues within the first 17 amino acids in the N terminal (N17) region of Htt enhances dissociation of Htt from endoplasmic reticulum membrane and facilitates subsequent nuclear retention (147). In contrast, acetylation in N17 accelerates the formation of poly-glutamine aggregates, and disrupts lipid bilayer morphology by binding to the lipid membrane (148). Thus, N17 is under heavy investigation. In addition, SUMOylation of the pathogenic fragment of mHtt reduces aggregate formation, but enhances its ability to suppress transcription in cultured cells (143) and worsens neurodegeneration in a Drosophila model of HD (143). Htt was also found to interact well with and be palmitoylated by Htt-interacting protein 14 (HIP14) (141,142). Notably, the palmitoylation of Htt was shown to be required for its correct subcellular distribution and functions (142). In HD, mHtt does not properly interact with and is insufficiently palmitoylated by HIP14 (142), thus forming inclusion and inducing neuronal toxicity (142).

mHtt undergoes proteolysis and produces a toxic form of N-terminal Htt fragment (149), which forms insoluble aggregates that accumulate in both nuclei and cytoplasm of the affected

neurons (150). The cleavage sites encoded by *HTT* exon 12 (151) (Figure 1-1: amino acid 552 is a cleavage site for caspase-2 and caspase 3 (152), amino acid 586 is for caspase-6 (153)) are under investigation in order to prevent generation of insoluble fragments (151). Furthermore, calpain cleaves Htt at 469 and 536 and produces fragments that accumulate in the nucleus (154). Calpain-resistant mHtt undergoes less proteolysis, forms less aggregation and is less toxic to cultured cells (154). Moreover, calpain expression and activation were found elevated in striatum and cortex of HD Htt150 knock-in mouse model (154). Pharmacological suppression of calpain activation in the BACHD rat model resulted in improved cognitive and psychiatric phenotypes, reduced Htt fragmentation and decreased nuclear accumulation of mHtt (155).

The transcriptional process of mHtt may also be dysregulated in HD (156). In HD postmortem brains, researchers found a highly toxic, small N-terminal fragment from exon 1 of *HTT* generated from mis-splicing of transcripts instead of proteolysis (157). Consistently, expression of *HTT* exon 1 alone leads to an early onset of HD symptoms in mouse (96).

Nevertheless, the roles of these aggregates in HD are still under debate, because the presence of visible aggregates does not correlate well with striatal neurodegeneration (115) and careful studies observed little overlap between apoptotic neurons and aggregate-containing cells (158,159), suggesting that the formation of the aggregates might be neuroprotective instead of deleterious.

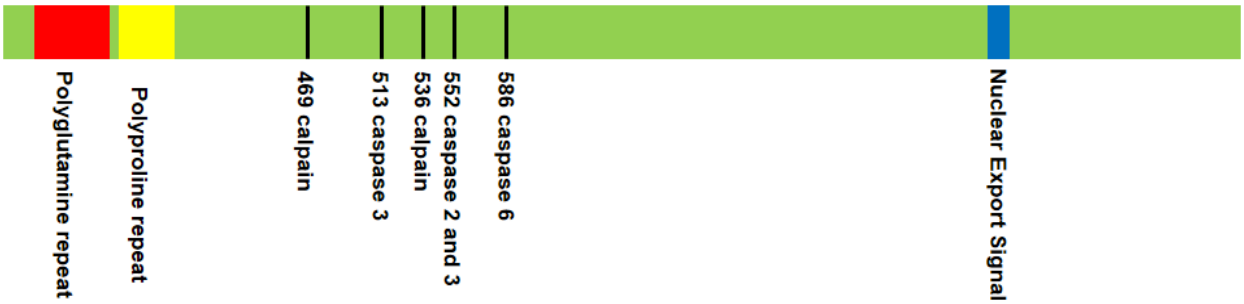

Figure 1-1 Calpain and caspase cleavage sites on Htt

1.3.2 Huntingtin Functions and its Protein Interactions

Although the full, domain-based understanding of functionalities of Htt has not yet been achieved, wtHtt importance in embryonic development and its neuroprotective role in striatum are well-known (160,161).

A study found that genetically modified HD mice models that express reduced levels of homozygous mutant *Hdh*, the murine homologue gene of human *HTT*, displayed abnormal brain development and perinatal death, while those expressing normal level of mHtt appeared healthy during the development (127). This suggests that the Htt domain(s) required for neurodevelopment is(are) likely located outside the poly-glutamine repeat region. Consistently, deletion of the CAG triplet from *Hdh* in mouse gene does not affect embryonic development, only slightly impairs performance in the Barnes circular maze learning and memory test without compromising motor coordination (162). In addition, homozygous deletion of the proline-rich region of Htt, a flanking region of the poly-glutamine tract, that modulates the protein structure and is a binding site of several interacting proteins has little influence on the embryonic development, general motor functions or motor learning in adult (163), except that 18 month-old male mice displayed reduced performance in the Morris water maze task (163).

Htt protects neurons from cell death in various ways. *In vitro* study showed that Htt puts a brake on apoptotic enzyme caspase 9 activation by suppressing its cleavage induced by excitotoxic stimuli, such as toxic levels of glutamate (164). Suggestion of another way comes from an investigation where mHtt was shown to affect membrane trafficking and distribution of NMDA-type glutamate receptors (165–167), because synaptic and extrasynaptic NMDA receptors signal to pro-survival and pro-death signaling, respectively (although debated) (168,169). Therefore,

change in the membrane distribution of NMDA receptors by Htt is possible and would likely impact the pro-survival and pro-death balance of the cell.

Moreover, in a protein interaction study, using mass spectrometry, high-throughput yeast two-hybrid screening and affinity pull-down assay Kaltenbach et al. identified 234 high-confidence wtHtt and/or mHtt fragments-associated proteins (39). In another study, Shirasaki et al. revealed a total of 747 candidate proteins that form complexes with full-length human/murine wtHtt and/or mHtt in cortex, striatum and cerebellum from 2- and 12-month old control mice and BACHD mice (134). Based on this protein interactome, Shirasaki et al. grouped the candidate proteins into several modules, which span from intracellular transport, synaptic transmission, protein folding, generation of precursor metabolites and energy to cytoplasmic membrane-bound organelles and nucleotide binding (134). Recently, the same group also identified 790 genes in 5 striatal modules which interact with Htt in a CAG length-dependent manner and confirmed 22 striatal genes as mHtt toxicity modifiers at the protein level from brain samples of HD knock-in mouse models with a range of CAG repeat lengths (170). Among these proteins, we are interested in the synaptic proteins that directly or indirectly interact with wtHtt and/or mHtt.

A number of presynaptic proteins are common Htt (wtHtt vs. mHtt) interactors (171), and have been reported to undergo altered expressions, abnormal post-translational modifications or changed functions in the presence of mHtt (172,173). On the presynaptic side, Htt interacts with clathrin-coated vesicles, endosomal compartments, and microtubules that traffic vesicles (174–176), whereas mHtt is more strongly associated with presynaptic vesicles and its related proteins [such as Htt associated protein 1 (HAP1)], and inhibits glutamate release (177). On the postsynaptic side, wtHtt and/or mHtt interact with scaffolding proteins and receptors (133,171). For example, postsynaptic density protein 95 (PSD-95), the major postsynaptic scaffolding protein

of excitatory synapses such as C-S glutamatergic synapses, binds to Htt but less to mHtt (178), and was found reduced in R6/2 (179), R6/1 (180,181) and knock-in models (103,182).

In addition, in HD a number of synaptic proteins that are not known to interact directly with mHtt or wtHtt display altered expression and/or changed synaptic localization. For instance, expression of complexin II, a small SNARE complex-associated protein that positively regulates the size of the readily releasable pool (RRP) (183), is progressively reduced throughout the brain (including striatum, hippocampus, neocortex and cerebellum) of 10 to 18-week old R6/2 HD mice (184) as well as in grade 0-III HD postmortem striatal tissue, but elevated in hippocampus as western blotting showed (185). Consistently, the behavioral phenotype of complexin II knockout mice resembles that of the R6/2 (186) and deletion of complexin II in 9 to 12-week old R6/2 mice does not worsen the HD phenotypes, suggesting a possible occlusion effect of complexin II loss of function in HD (187). Similarly, expression level of the SNARE protein SNAP-25 is reduced in motor cortex of grade I-IV HD patients (188) and in R6/2 mouse brain at 6, 12 and 15 weeks (189). Rabphilin 3a, a protein critically involved in exocytotic transmitter release, is specifically decreased in postmortem human HD brain tissue (grade III-IV) (188) as well as in HD animal models (in R6/1 at 4-10 months) (190). Interestingly, treatment with BDNF rescued synaptic functions in Hdh(Q92) and Hdh(Q111) HD knock-in mouse models (191). Apart from these, numerous other synaptic protein expressions are altered in HD, including synaptobrevin 2, Ras-related protein Rab-3A (rab3A), vGlut1, vGlut2, vesicle-associated membrane protein 1 (VAMP1) and synaptosomal-associated protein- α (SNAP-α) (185,188,192) [There is a recent review on the progress of understanding alteration of presynaptic terminals in HD (172)]. Thus, the precise mechanisms underlying HD-associated synaptopathy are likely to be complex, highlighting a need for a rapid and accessible screening platform to thoroughly study synaptic functions in HD . Using

the C-S coculture system to understand the roles of these proteins in presynaptic dysfunctions of HD is of great interest for future studies.

Htt was also found to not only interact with HIP14 (141,142), but also modulate HIP14 enzymatic activity (193). In HD, mHtt does not properly interact with HIP14 (142), this causes improper palmitoylation of other substrates of HIP14 (194,195), many of which are synaptic proteins (141). For example, HIP14 was found to palmitoylate synaptotagmin 1 and SNAP-25 (141), but how presence of mHtt would affect palmitoylations and functions of these synaptic proteins is still unclear. Furthermore, deletion of HIP14 resulted in behavioral, biochemical and neurological abnormalities similar to those of HD mice (189).

At transcriptional level, expression of mHtt distorts the brain transcriptome from early development by disturbing functions of transcription factors, chromatin-modeling proteins and noncoding RNAs, and eventually upregulates or downregulates expressions of neuronal survival and death genes (196). For instance, studies suggested that transcription factor cAMP-response element binding protein (CREB) binding protein (CBP) interacts with mHtt (197) and causes suppression of downstream CREB-dependent pro-survival genes (197,198), such as BDNF (135). Another example is that in prefrontal cortex of HD patients RNA sequencing revealed increased inflammatory and developmental gene expressions, suggesting altered gene transcription (199). Thus, altered gene transcription and disrupted splicing may largely contribute to neurodegeneration of striatal SPNs as well as to the preceding synaptopathy (200). One of the novel therapies being tested in the laboratory is a treatment that potentially could recover epigenetic dysregulations (196) and thereby rescue the altered gene expression, cell signaling and the imbalance of cell survival and death signaling in HD.

Additionally, interactions of other transcriptional factors and proteins with *HTT* vs. expanded *HTT* and their transcripts may differ significantly. For instance, wig1, a downstream target of p53, preferentially upregulates the level of mHtt over wtHtt via enhanced binding with mHtt transcripts (201); cysteine string protein (CSP), a synaptic vesicle release modifier, interacts with mHtt but not wtHtt (202).

1.4 Neurodegeneration of Huntington's Disease

1.4.1 Neurodegeneration Anatomy

Basal ganglia

Basal ganglia, the major region of degeneration in HD, are composed of interconnected nuclei that play important roles in mood and movement (203). Basal ganglia include structures of the caudate and putamen (dorsal striatum), nucleus accumbens (ventral striatum), subthalamic nucleus (STN), globus pallidus segments and substantia nigra (204,205).

Striatum

Striatum, which is a collection of nuclei inside the basal ganglia, receives glutamatergic inputs from the cerebral cortex (Figure 1-2), hippocampus, amygdala and thalamus (206,207), and dopaminergic projections from the ventral tegmental area and substantia nigra pars compacta (SNc) (208,209), and projects to the rest of the basal ganglia nuclei. It has been well-recognized for its involvements in motor control and refinement (210,211), as well as for its contributions to reward (212,213), decision-making (213) and social behaviors (214–216) by integrating of sensory, motor, cognitive and motivational information (213,214).

Anatomically and functionally, striatum can be divided roughly into two sub-regions – dorsal striatum and ventral striatum (217). Dorsal and ventral striata play different roles in instrumental learning (218), drug addiction (219) and cognition (220). In primates, dorsal striatum is further subdivided into caudate nucleus and putamen by a white matter tract called the internal capsule, whereas the ventral striatum is made up of the nucleus accumbens and olfactory tubercle (221). In HD, neuronal loss starts from the tail of the caudate nucleus and progresses from dorsal to ventral, from rostral to caudal (222,223).

At the cellular level, spiny projection neurons (SPNs), which are also commonly referred as medium spiny neurons (MSNs), constitute 90-95% of the total neuronal population in the striatum (224). The other major class of striatal neurons is aspiny interneurons, which are relatively spared in HD (223) and can be divided into four different types based on peptide and enzyme expressions (224). The striatal SPN spine heads receive glutamatergic inputs while spine necks are innervated by dopaminergic afferents from outside the striatum (225,226). These fine localizations of distinct synapses form a complex mechanism for modulating of SPN activity.

Based on receptor expression and output projections, the striatal SPNs can be divided into two main groups(227,228): those that express D1-type dopamine receptors (D1 SPNs) project to internal segment of globus pallidus (GPi) and substantia nigra pars reticularis (SNr) and form part of the direct pathway of motor control; the others express D2-type dopamine receptors (D2 SPNs), project to external segment of globus pallidus (GPe), and form part of the indirect pathway of the motor control circuit (229) (shown in Figure 1-2). It is widely accepted that activation of the direct pathway processes movement initiation commands (230,231), while activation of the indirect pathway executes movement inhibition (230,231); thus, they play opposite roles in motor control (230,231). These two classes of SPNs are homogenously distributed throughout the striatum (221).

It is confirmed that striatal SPNs receive inputs from cortical pyramidal neurons located in layer II-VI, with the most dense projections from layer V (232). However, the cortical projections form stronger connections with D2 SPNs than with D1 SPNs (233–235).

One prevailing hypothesis states that at the early stage of the disease D2 SPNs show dysfunction and are first to undergo neuronal death leading to disinhibition of movement control and hyperkinesia (236–239), while at the intermediate and late stages D1 SPNs are conspicuously affected eventually resulting in hypokinesia (236,237,240). However, the pre-manifest and early stage symptoms are mainly attributed to dysfunctions of C-S connections instead of cell death (3).

Although SPNs are affected by neurodegeneration most, the striatal interneurons also undergo pathological changes. For instance, at pre-manifest and early stages HD mice have smaller cholinergic interneurons with a significantly reduced dendritic tree, although the density of vGlut2-expressing synapses along dendrites remains the same (241). These alterations may contribute differently to striatal direct vs. indirect pathways.

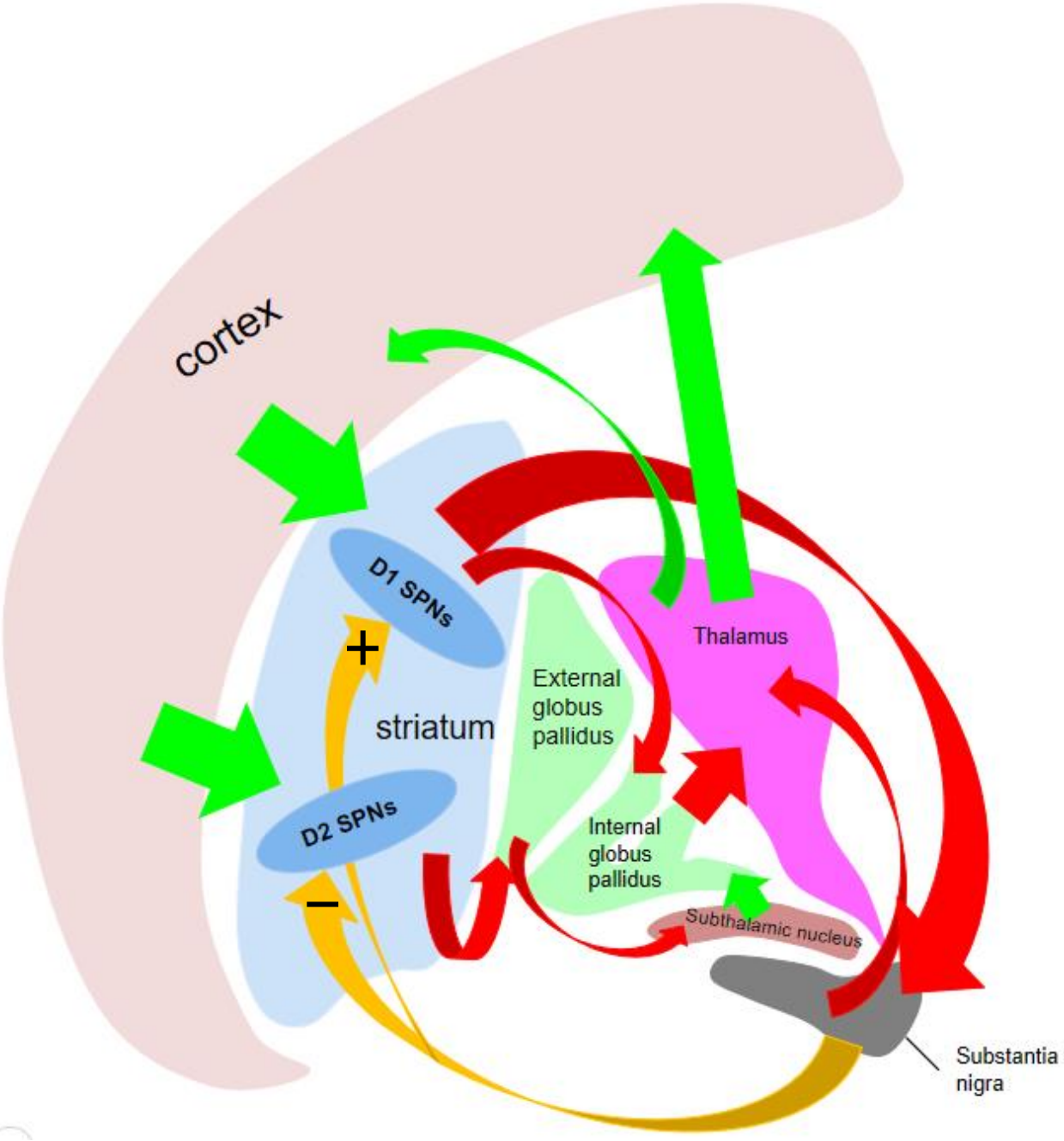
cortex
D1 SPNs
+
striatum
D2 SPNs
−
External
globus
pallidus
Internal
globus
pallidus
Thalamus
Subthalamic nucleus
Substantia
nigra

Figure 1-2 Projections of direct and indirect pathways of basal ganglia

Excitatory projections are shown in green, inhibitory in red and modulatory in yellow. Striatal D1 SPNs and D2 SPNs distribute homogenously throughout the striatum and receive excitatory cortical (and thalamic, not shown) projections. D1 SPNs project (inhibitory) to GPi and SNr, while D2 SPNs give inhibitory projections to GPe. GPe projects (inhibitory) to STN, which in turn provides glutamatergic excitatory inputs to GPi. The GPi then inhibits thalamus that projects excitatory inputs back to the cerebral cortex. Dopaminergic neurons of SNc project onto both D1 and D2 SPNs in the striatum and modulate their activity, but oppositely.

Substantia nigra

Substantia nigra is one of the numerous nuclei in the brain affected by neurodegeneration in HD (242). In clinic, substantia nigra hyper-echogenicity detected by transcranial sonography is well described in hypokinetic HD (243), likely indicating fatty deposits. The role of dopamine released from SNc has been a focus of HD study for a long time as it modulates C-S synaptic transmission (244–246). A theory proposed is that at the early stage of the disease increased tonic level of dopamine leads to hyperkinetic movements, while at the later stage reduced extracellular dopamine level results in hypokinesia (247).

Globus pallidus and subthalamic nucleus

The GPe is the major target of D2 SPNs, whereas GPi is that of D1 SPNs. Neurons in globus pallidus display reduced soma volume and increased death in HD (248). There is decreased GABAergic transmission in GPe starting from the asymptomatic stage in R6/1 mice (249). In these mice, both structural and functional inhibitory synapses onto GPe neurons gradually become rare along with development of locomotor deficits (249).

STN structure (250) and activity (251) were also found altered in HD mouse models.

Cerebral cortex

In HD, neurodegeneration occurs widely in cerebral cortex (3) where pyramidal neurons in layer III, V, and VI show most severe death (252,253). Even in prodromal stage HD patients researchers detected atrophy in cortical gray matter with magnetic resonance imaging (MRI) (254). Certainly, the HD symptoms are correlated with the affected cortical regions. For instance, in an autopsy study of brain tissue, those HD patients with predominantly motor symptoms showed

marked neurodegeneration in the motor cortex, while mood changes in HD were attributed to atrophy in the anterior cingulate gyrus of cerebral cortex (255).

Other regions of central nervous system

Although thalamus innervates striatum with considerable amount of glutamatergic inputs, evidence of neurodegeneration in thalamus of human HD is rare (3).

However, hippocampus was reported repeatedly (254,256–258) as one of the major brain regions of atrophy in HD patients (254,256–258), who also experience difficulties in memory formation. Interestingly, neurodegeneration preferentially occurs in the CA1 region of hippocampus (256).

Cerebellum, which expresses a comparable amount of Htt to striatum, also degenerates in HD, but with much later occurrence in the disease (259,260), affecting cognitive processing (260). In cerebellum of HD patients, researchers discovered loss of Purkinje cells and nerve cells of the fastigial, globose emboliform and dentate nuclei (259).

Circadian rhythm, sleep (261,262) and hypothalamic pituitary-adrenal (HPA) (263) axis disturbances were also reported, suggesting that a wide variety of brain regions are affected in HD (264).

1.4.2 Mechanisms of Neuronal Death in Huntington's Disease

When it comes to neurodegeneration of striatal SPNs as well as cortical (252) and hippocampal neurons in HD, there are many hypotheses that have been put forward with supportive evidences.

Reduced BDNF in HD

The BNDF deficit in HD is the outcome of multiple abnormalities (Figure 1-3). In one theory, PGC-1α is involved in HD pathology, a transcriptional coactivator of metabolic genes (265) and of BDNF (135) - mHtt suppresses expressions of PGC-1α (267) and BDNF (135) by abnormally interacting with transcription factors required for CREB-dependent transcriptions (266), such as CBP (267), and thereby represses cell survival signaling pathways (268). Consistently, deletion of PGC-1α in mice showed a hyperkinetic movement phenotype and neurodegeneration in striatum similar to those of HD (269), likely by reducing BDNF expression in the brain. Another theory states that mHtt's inability to sequester RE1-silencing transcription factor/neuron-restrictive silencer factor (REST/NRSF), which represses BDNF transcription, in the cytoplasm contributes to the BDNF deficit (135,270). However, such a suppression of BDNF is most effective in cortical neurons which provide the neurotrophic support for the striatal SPNs that do not express BDNF (271,272).

In addition to the changes in BDNF transcription, the presence of mHtt or loss of wtHtt interferes with anterograde transport of BDNF in cortical axons (158) through insufficient or abnormal interactions with modulator proteins of cargo transport. A well-known modulator is (HAP1, which interacts with dynactin as well as Htt in a poly-glutamine length-dependent way (273,274). wtHtt facilitates vesicular transport of BDNF along microtubules by interacting with HAP1 and p150(Glued) subunit of dynactin (158).

The BDNF hypothesis of HD was also supported by evidences that conditional knockout of BDNF in the cortex caused gradual degeneration of striatal neurons (275) and that reducing BDNF expression in an HD mouse model led to an earlier disease onset and exacerbated motor phenotypes (276,277).

Furthermore, signaling through BDNF receptors and their expressions are likely impaired in HD (278–280). Evidence suggests that BDNF activation of TrkB receptors is intact in HD condition (281), but activations of Ras/MAPK/ERK1/2 by TrkB receptors (279,281), as well as TrkB receptor expression (278), is disrupted. Moreover, mHtt increases protein phosphatase 1 level and disrupts the p75NTR receptor/TrkB receptor balance, and thereby reduces activation of Akt and increases c-Jun N-terminal kinase (JNK) phosphorylation, phosphatase and tensin homolog (PTEN) signaling (282) and activation of apoptotic cascades (280). Thus, imbalance of pro-survival vs. pro-death signaling of BDNF in striatal neurons is likely a factor contributing to the neurodegeneration in HD.

Treatment that increases BDNF level in the brain is expected to ameliorate disease phenotypes (283). Indeed, rescue of BDNF and other striatal-specific gene expressions by epigenetic methods successfully ameliorated mHtt-induced neuronal toxicity in primary cortical and striatal neurons (284). Another example is that pridopidine, a drug originally described as a dopamine stabilizer, showed promising results in clinical trials most likely by upregulating the BDNF pathway in a sigma 1 receptor-dependent manner (285). However, attempts to transplant BDNF over-expressing cells failed to give a significant rescue in mouse models of HD (286). Along with the unbalanced signaling of BDNF, the low affinity BDNF receptor p75NTR has been under heavy investigation because it was found to modulates both cell-death and survival pathways, as well as synapse degeneration (287).

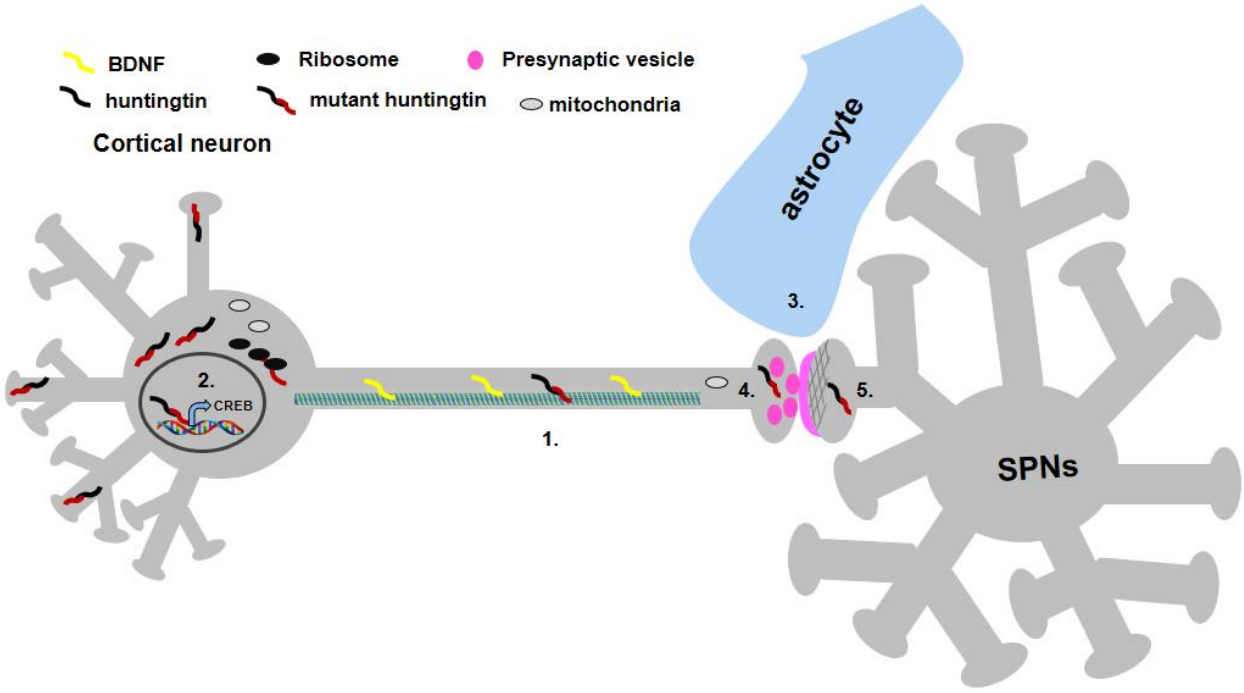

Figure 1-3 mHtt expression impacts cortical and striatal neurons in various ways.

mHtt:

1. abnormally interacts with microtubules, thereby interfering with cargo transportation in axon, including transport of BDNF.

2. impedes gene transcription such as via CREB, and reduces BDNF transcription.

3. role in astrocytes is under debate.

4. in presynaptic cortical terminal interacts with multiple vesicular proteins and disrupts neurotransmitter release.

5. in postsynaptic striatal neuron interrupts protein sub-localizations, such as NMDA receptors.

Altered glutamate receptors of striatal SPNs in HD

A functional NMDA receptor, a type of ionotropic glutamate receptors, is a heterotetramer composed of two obligatory GluN1 subunits and two subunits of GluN2 (i.e., one or more of four distinct subunits: GluN2A, GluN2B, GluN2C and GluN2D) and/or GluN3 (with two distinct subunits: GluN3A and GluN2B) (288). Although it is controversial and still under debate, there is strong evidence suggesting that NMDA receptors play a critical role in cell survival and death (289); namely, NMDA receptors at synapses where the GluN2A subunit dominates (290) promote cell-survival when activated, whereas those at extrasynaptic sites which mainly contain GluN2B subunit (291,292) signal cell-death in hippocampal (293,294), cortical (295,296,124) and striatal neurons (124,168,297) (Figure 1-4), through their differential intracellular domains, to which downstream proteins bind.

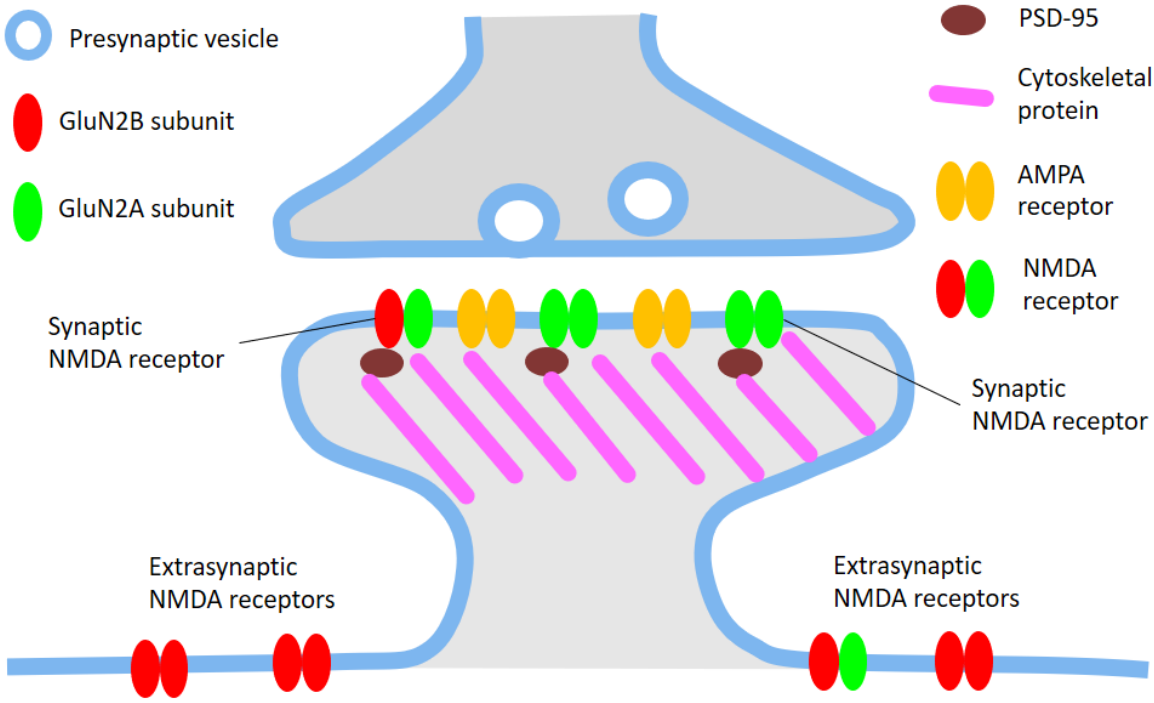

Figure 1-4 Synaptic and extrasynaptic NMDA receptors

Previously, we found that in YAC128 HD mouse model the GluN2B subunit-containing NMDA receptor expression on the SPN surface is elevated at the pre-symptomatic stage (166,298,299); this enhances cell-death signaling over cell-survival signaling through extrasynaptic NMDA receptors from an early age (299). Tonic activation of the extrasynaptic NMDA receptors results in increased Ca^{2+} influx that in turn activates calpain, Striatal-Enriched protein tyrosine phosphatase (STEP) 61 and STEP33 and causes failure to dephosphorylate p38 MAPK, which enhances downstream apoptotic signaling in the YAC128 model at the pre- and early stages of the disease (300–302). It was found that altered STEP expression, activation, and downstream signaling at early and late stages of the YAC128 HD model (302), as well as increased interaction of GluN2B-containing NMDA receptors with PSD-95, contribute to elevated vulnerability of SPNs to excitotoxic stimuli (303), signaling through p38 MAPK when NMDA receptors are activated (300). Furthermore, memantine blockade of extrasynaptic NMDA receptors can rescue synaptic dysfunction (304) and suppress pro-death signaling in YAC128 HD mice (304). Interestingly, the STEP level was found to be also regulated by BDNF in primary cortical culture (305,306).

In another study, GluN3A expression was found elevated in the same HD mouse model and suppression of GluN3A expression rescued reduced spine density, elevated NMDA and AMPA current ratio, increased falling in the rotarod test, decreased strategy shifting in T-maze swimming test, striatal volume reduction and neuronal loss, but not hypoactivity in the symptomatic YAC128 HD model (307). These results suggest that these two subunits of NMDA receptor may form a single receptor complex in the HD striatum. Interestingly, protein kinase C and casein kinase substrate in neurons protein 1 (PACSIN1), an endocytic adaptor specific for GluN3A, is sequestered by mHtt (307,308) allowing the NMDA receptor containing GluN3A subunits to stay

on the SPN surface at the pre-symptomatic stage (307). The interaction of PACSIN1 with mHtt becomes stronger proportionately to the mHtt poly-glutamine length (308). Together, these suggest that the lack of PACSIN1 at synapse caused by mHtt contributes to the elevated surface level of extrasynaptic NMDA receptor, increased caspase activation and cell death signaling.

In the HD mouse model, mHtt promotes the interaction between PSD-95 and GluN2B subunit (266,275). One factor that may contribute to elevated interaction of PSD-95 with NMDA receptors is potentially reduced palmitoylation of PSD-95 by HIP14 in HD (141), resulting from the altered modulation of HIP14 by mHtt (173). Both palmitoylation and nitrosylation of PSD-95 determine the synaptic localization of PSD-95 (310).

Another type of ionotropic glutamate receptor is the AMPA receptor, which is less permeable to Ca^{2+} than the NMDA receptor when activated. By conducting electrophysiological recording from acutely dissociated SPNs of striatal tissue, Joshi et al. found elevated AMPA receptor surface expression in pre-symptomatic 2-month old YAC128 mice compared with control mice (311), but the expression was gradually reduced back to the normal level when the HD mice aged up to 12 months (symptomatic). Thus, it is possible that the elevated expression of AMPA receptors at the pre- and early stages of the disease promotes neighboring NMDA receptor activation by inducing more local depolarization, thereby enhancing cell survival or death signaling depending on the NMDA receptor distribution and/or composition. However, an increase in AMPA receptor current was not found in recordings from striatal neurons in acute brain slice of HD mice (91), so it is possible that the elevation of AMPA receptor-mediated current found in acutely dissociated striatal neurons (312) was restricted to the cell soma rather than at dendritic synapses.

Increased tonic level of extracellular glutamate of HD

One hypothesis about HD pathology is that an elevated level of tonic glutamate in the striatal extracellular environment, as a result of increased release of glutamate from cortical terminals in response to action potential (312) and/or impaired re-uptake of the extracellular glutamate by neurons/astrocytes (313–321), contributes to excitotoxicity of striatal SPNs in HD.

Evidence from the YAC128 HD mouse model suggested increased release of glutamate from cortical neurons onto striatal SPNs in response to action potential (312) at the pre-phenotype stage; over the course of disease development, it gradually diminishes to become glutamate release deficits in the late stage of the disease (312). A similar type of biphasic change was observed at C-S synapses of R6/2 (322). HD patients at prodromal stage may also have enhanced release of glutamate from cortex.

On the other hand, a number of *ex vivo* experiments suggested impaired glutamate re-uptake by neighboring astrocytes via glutamate transporters (323,317). For example, in postmortem studies low level of the major glutamate transporter of astrocyte - glutamate transporter 1 (GLT1) mRNA in HD striatum was correlated well with the disease severity (313) and glutamate uptake ability was impaired by 43% in prefrontal cortex of HD patients compared with controls (318), although there was increase in the number of GLT1-expressing astrocytes (313,318). In HD animal models, researchers also found impaired glutamate uptake. R6 lines of HD models exhibited decreased GLT1 mRNA level in striatum as well as cortex, and reduced uptake of glutamate prior to neurodegeneration, as shown by Lievens et al. (314). Indeed, mHtt accumulates in the glia nuclei and suppresses the expressions of glutamate transporters in HD brains (316). Selective expression of mHtt in striatal astrocytes repressed expressions of both GLT1 and glutamate aspartate transporter (GLAST), as well as DARPP-32 in SPNs (319). Consistently, increasing GLT1

expression in R6/2 with ceftriaxone (324,325) elevates glutamate uptake as shown by Miller et al. (325), as well as improves neurological signs of the mice including clasping, performance in plus maze and climbing behavior in the open field (325). However, another study on R6/2 mice detected similar level of extracellular glutamate compared with control mice (315) with microdialysis from freely moving animals, but partial inhibition of glutamate transport showed age-dependent increase in the extracellular glutamate level in R6/2 compared with controls (315). Moreover, decreased expression of GLT1 did not affect weight loss, performance in rotarod test, climbing and paw-clasping in R6/2 HD mice (326). Besides, a study of HD knock-in mice showed lower surface expression of excitatory amino acid transporter (EAAT3, also named EAAC1), the neuronal glutamate transporter, and it was attributed to aberrant Rab11-dependent trafficking of EAAT3 to the cell membrane (320), but a cell line model of HD detected increased expression of EAAT3 on the cell surface and elevated Na^+-dependent glutamate uptake (321). In contrast to the above studies, a recent work in acute brain slice prepared from early age (pre-manifest) and late HD YAC128 and R6/2 mice did not detect a significant difference in clearance of extracellular glutamate or in astrocyte transporter current between the HD mice and controls by imaging extracellular glutamate level with glutamate sensor and conducting electrophysiological recording from astrocytes (327), and it disagreed with the hypothesis. The common side of these two hypotheses is the assumption that enhanced level of extracellular glutamate is upstream of the HD neuropathology, for example such a long-term elevated level of extracellular glutamate (either tonic or action potential release-based) may lead to increased activation of NMDA receptor-dependent cell death signaling at the pre-symptomatic stage of the disease and underlie the later neuronal death in the striatum of HD (168,169).

Caspase activation

Another aspect of HD regarding striatal neurodegeneration is unbalanced cell survival and death signaling due to increased activation of pro-death caspases (328). In cell culture studies, wtHtt was shown to suppress caspase 9 activation by inhibiting its cleavage induced by increased release of cytochrome c from mitochondria in response to excitotoxic stimuli (164,329,330). In HD animal, study on R6/2 mice showed elevated activation of caspase 1 at 7 weeks following the phenotype onset, that of caspase 3 and caspase 8 at 9 weeks and caspase 9 at 12 weeks (331). The early activation of caspase 1 is likely induced by elevated level of caspase 1 activator Receptor interacting protein-2 (Rip2) and reduction of caspase 1 inhibitor Caspase recruitment domain only protein (Cop) in HD (332). In HD postmortem study, caspase 9 activation, as well as cytochrome c release from mitochondria, was detected along with striatal neuronal degeneration (328).

In contrast, in HD caspase 6 is activated by reduced palmitoylation by HIP14 (333) whose enzymatic activity is mediated by the level of wtHtt (193). The activated caspase 6 in turn cleaves mHtt at amino acid 586 (153) and generates toxic forms of Htt fragments that translocate into the nucleus (334) and suppress transcription of pro-survival genes, preceding neurodegeneration (335) in pre-symptomatic HD mutation carriers and pre-phenotypic murine HD models (153). Consistently, expression of caspase 6 cleavage-derived N-terminal fragments of mHtt alone can result in neurologic abnormalities with inclusion pathology (336). Moreover, expression of caspase 6 cleavage-resistant mHtt in mice did not show increased striatal neuronal death (337,338) or depressive behavior (339), but reduced aggregate formation (337), while caspases 3-resistant did (338). Loss of caspase 6 in YAC128 mice rescued body weight gain, normalized depression-like phenotype and reduced, not eliminated, mHtt-586 cleaved fragment (340), and caspase 8 was attributed to the generation of the rest of mHtt-586 cleaved fragment (341).

Caspase 2 activation and its cleavage of mHtt may contribute to striatal neuronal pathology because it was shown to be required for death of primary striatal neurons induced by mHtt in YAC72 HD mice (152) and caspase 2 interacts with mHtt in a poly-glutamine length-dependent manner (152). The latter recruits caspase 2 into an apoptosome-like complex (152). Caspase 2 activation was also found elevated in pre-symptomatic YAC72 HD mice (152).

Mitochondria dysfunction and biogenesis

The elevated release of cytochrome c from mitochondria in HD results from mitochondria dysfunction (342–344). mHtt causes mitochondria fragmentation, interferes mitochondria biogenesis (266) and trafficking (345), and lowers its membrane potential through abnormal handling of Ca^{2+} (342–344). The disrupted biogenesis of mitochondria is a result of suppressed expression of PGC1-α by mHtt as Cui et al. showed(266). Furthermore, in the presence of mHtt, mitochondria production of ATP is reduced due to repressed expression of oxidative phosphorylation enzymes that regulate ATP generation (346,347). Also, the mitochondrial permeability transition pore (mPTP) was found malfunctional when mHtt is present (348). As expected from results of these mechanistic studies, numerous mitochondria-based drugs have been suggested by pre-clinical studies (349,350).

Cannabinoid receptors

Cannabinoid receptor type 1 (CB1) expression and transmission are attenuated in basal ganglia in HD rodent models (351–354) as well as in HD patients (355). CB1 is neuroprotective when activated (356–358) and its activation was also shown to alleviate hyperkinetic motor phenotypes in 3-nitropropionic acid (3-NP)-induced rat model of HD (359) but not in R6/1 mouse (360).

Evidence in N171-82Q transgenic HD model suggested that CB1 receptor deletion worsens its motor performances (361).

1.5 Glia Cells in Huntington's Disease

Not only just neurons, but also glia cells influence HD pathology (362). Expression of mHtt specifically in striatal glia cells is enough to impact neuronal properties, such as resulting in hyperexcitability of striatal neurons (363), and to impair motor coordination in rotarod test compared with control mice transplanted with wtHtt-expressing glia progenitor cells as shown by Benraiss et al. (363). Conversely, engrafting wtHtt-expressing glia progenitors cells to HD mice rescued electrophysiological deficits and behavioural phenotypes, slowed down the disease progression and extended the life expectancy (363). Surprisingly, in contrast to neuronal loss in the striatum the number of glia cells increases significantly in HD during the disease development (364,365).

Astrocytes

Astrocytes were proven as an important source of BDNF for neuroprotection in human neuroblastoma cells (348) and cortical neurons (367,368). It was demonstrated that mHtt or its truncated N-terminal fragment (369) impairs BDNF transcription (369) and secretion (370) from astrocytes by disrupting conversion of Rab3a-GTP to Rab3a-GDP (371), a protein that regulates exocytosis. Moreover, elevating the BDNF expression in astrocytes of HD mouse models (R6/2 and YAC128) by glatiramer acetate improved motor performance, reduced body weight loss and increased their life expectancy, suggesting that astrocytes do shape the disease phenotypes (283).

Microglia

One of the early changes observed in HD mice is accumulation of intracellular ferritin in microglia in striatum of 2 to 4-week old R6/2, a blood cell protein that carries iron (372). Those microglia are dystrophic and appear with thick, twisted processes (372). Similar pathology was observed in grade 0-IV HD patient brains (372), suggesting impaired iron metabolism. This change is followed by further morphological alterations of microglia, including bulbous swellings and long stringy processes, (373) preceding an accelerated reduction in microglial density in the same HD model compared with age-matchedcontrol mice (373). However, a study of HD postmortem brain observed a gradual accumulation of microglia in both cortex and striatum over the course of the disease (61,374–376), an opposite observation to that from the animal studies (373). Interestingly, the quinolinic acid and 3-NP-induced models of HD showed increased microglia in the striatum (377,378). Moreover, Chakraborty et al. found that quercetin, a dietary flavonoid with free radical-scavenging property and ability to attenuate microglia activation, improved motor coordination but increased astrocyte number and failed to protect SPN death in the 3-NP HD model (378). Finally, whether and how microglia would change SPN vulnerability and C-S connections are still poorly understood.

Other glia cells

Oligodendrocytes are another widely recognized neuroglia cells whose membrane forms myelin sheath wrapping around neuronal axons in such a way that allows electrical signals to propagate more efficiently. In HD, early research suggested mHtt causes degeneration of myelin sheaths (379) by suppressing of expression of myelin-related transcripts (380), and thereby impairs the microstructure of white matter between cortex and striatum long before the actual onset of

phenotypes and neuronal loss in HD mouse models (380). However, little work was done to uncover to what extent and how myelination degeneration contributes to the disease progression.

1.6 Changes in Huntington's Disease Preceding Neuronal Death

Numerous lines of studies uncovered that HD mutation carriers and early HD patients exhibit cognitive (381,382) and psychiatric impairments (383) along with striatal atrophy (22) and brain white matter loss (22,23) many years before the neuronal death.

In an age and IQ-matched study of 54 subjects, HD carriers showed reduced cognitive flexibility in a test of attentional set shifting (381), which suggests circuitry dysfunction within the prefrontal cortex (384,385), and decreased performance in a test of semantic verbal fluency (381), which indicates impairment in frontal lobe (386,387). Consequently, the study attributed these changes to deficits in inhibitory control mechanisms involving frontal-striatal circuits (381). Earlier, the same study group revealed impaired executive functions of early HD in another cognitive assessment test (388), named Cambridge Neuropsychological Test Automated Battery. Interestingly, a later work of the group uncovered correlation of cognitive impairments with reduced striatal dopamine receptor levels with positron emission tomography (PET) scan in asymptomatic HD mutation carriers (389), and based on previous research Lawrence et al. concluded that dysfunction of C-S circuits is the major cause of impaired cognitive functions in HD (390). Other groups also observed similar cognitive declines in various tasks in HD carriers (391–393).

Indeed, using 3 Tesla MRI Crawford et al. detected reduced volume of corpus callosum, the largest white matter structure in the brain through which cortical neurons massively project to striatum and other subcortical nuclei, in premanifest and early HD groups (23). In the early HD

group, the researchers also observed a significant association of reduced volume of corpus callosum with poor performance in the Circle Tracing Indirect (23) task that measures cognitive abilities, suggesting early disconnection of C-S projections and its contribution to cognitive impairments in prodromal HD. With MRI imaging, other studies detected striatal atrophy as well as reduction of cortical white matter in premanifest HD (22). It is noteworthy that at pre-symaptomatic stage and early stage of HD, there is no detectable neuronal loss in either striatum or cerebral cortex.

On the other hand, presympatomatic HD gene carriers also display detectable motor changes, such as alterations in movement time and in movement time with decision, correlated with CAG repeat length of their *HTT* genes (21). Numerous more studies detected similar motor dysfunctions. In one study, researchers revealed more rapid longitudinal decline of psychomotor speed in pre-symptomatic HD carriers compared with controls (394), which indicates impairments in cognitive abilities and/or motor functions. Another study observed slower movement responses of pre-symptomatic HD group for auditory and visual reactions clues than controls (395), as well as chorea and dystonia of their extremities (395). These pre-symptomatic motor dysfunctionalities suggest significant pathology in the C-S circuits of HD before neuronal death.

Consistently, in HD mouse at the pre-phenotype stage studies many lines of evidence suggest the same underlying pathological changes observed in prodromal HD in various tests. For example, YAC128 HD mice showed poor motor performance in rotarod test starting from 6 months (90,93), hyperactivity at 3 months (90) and slow motor learning beginning from 2 months (93) compared with controls, long before striatal and cortical volume reductions at 9 months measured with stereological software by immunostaining (90) and striatal neuronal loss at 12 months examined with immunostaining for neuronal nuclei with Hexaribonucleotide Binding Protein-3 (NeuN)

antibody (93). In the same study, Van Raamsdonk et al. also detected significant deficit in YAC128 mice in choosing the correct direction in a simple swimming test at 8 months (93) and difficulty in shifting strategy in the T maze swimming test even at 2 months (93) when motor factors were eliminated. These indicate cognitive impairments at pre- and early symptomatic stages of the HD mice. Using MRI on the same HD mice, Carroll et al. detected white matter loss (corpus callosum) and reduced striatal volume starting from 3 months (92), and increased ventricular volume beginning from 8 months (92). Similar pathologies were observed in R6/2 mice (396) that develop HD phenotype as early as 5 weeks (109). Zhang et al. found reduced brain volume and neocortex volume as early as 4 weeks (396), and reduced striatal volume and increased lateral ventricle volume beginning from 5 weeks (396). Other HD model showed comparable brain volume reductions at pre-symptomatic and early symptomatic stage as well (397).

At the synaptic level, in Joshi et al.'s study presymptomatic 1-month old YAC128 mice displayed elevated release of presynaptic glutamate-containing vesicles from cortical terminals onto striatal SPNs in response to electrical stimulation in cortical layer V-VI (312), whereas in Cepeda et al.'s investigation early symptomatic 5 to 7-week old R6/2 mice exhibited reductioned spontaneous EPSC frequency as well as decreased miniature EPSC frequency (322). In HD mouse models, researchers observed altered SPN input resistance, abnormal rheobase and changed excitatory paired-pulse facilitation from pre-symptomatic-to-early symptomatic animals (40-day old R6/2 mice, 1 to 6-month old YAC128, and 3 to 4-month Q175) (91,398–400).

Together, evidence of HD patients and HD animal models suggests severe synaptopathy of C-S connections during pre- and early stages. Thus, early treatments of synaptopathy are much more valuable than attempts to prevent cell-death after neuronal circuits become severely dysfunctional (401).

1.7 Rationale, Hypotheses and Objectives

The creation of C-S coculture is a step forward to investigate C-S connections and both types of neurons in a system closer to its *in vivo* environment in *in vitro* ways (124). However, the coculture preparation method and C-S neuronal plating ratio vary from study to study (123,124). **In Chapter 2, we hypothesized that cortical-to-striatal neuronal plating ratio affects striatal neuronal properties as well as formation of C-S connections**.

The neuroprotective effect of wtHtt is well known in striatal neurons (164,329,402). However, questions remain regarding how wtHtt protects striatal SPNs and whether cortical and hippocampal neurons, which are also subjects to neurodegeneration in HD, can also be protected by wtHtt in the same way. **In Chapter 3, we test a hypothesis that wtHtt provides a neuroprotective effect for all striatal, cortical and hippocampal neurons in a nuclear phospho-CREB-dependent way**.

HD has been regarded as a synaptopathy, as increasing number of evidences suggest that synaptic changes occur well before the HD neurodegeneration. However, much remains to be addressed regarding how neuronal connections are affected by mHtt at the pre-symptomatic stage and the early stage of HD. **In Chapter 4, we test our hypothesis that mHtt damages C-S connections in various ways, including synapse formation and functions**.

Objectives:

Aim 1. To uncover a closer plating ratio of cortical and striatal neurons in C-S coculture to more closely reproduce *in vivo* C-S connections in cell culture.

Aim 2. To examine how wtHtt protects striatal neurons in C-S coculture and whether it also protects neuronsfrom cortex and hippocampus by promoting pro-survival signaling through phospho-CREB.

Aim 3. Test how mHtt impacts C-S connections in C-S coculture and in a HD mouse model at the early phenotypic stage.

Chapter 2: Investigation on Optimizing of Cortico-striatal Coculture System

2.1 Introduction

Since the groundbreaking finding that immature neurons can develop and be maintained *in vitro* (403,404), cultured neuronal systems as models of their *in vivo* counterparts have played an essential role in neuroscience investigation for over a century (405). Generally, neuronal cultures are generated from primary neurons dissociated from a single brain region such as cortex, hippocampus or striatum; however, a culture from one type of tissue cannot reproduce any inter-regional connections that exist in the brain. This shortcoming was addressed when coculture of neurons from different brain tissues was developed, providing a valuable tool for studying the interactions of neurons from distinct brain regions (124,406,407). The coculture system is also used to study neuron/non-neuron cell interactions, such as neuron-muscle (404) or neuron-glia (408,409), or to distinguish contribution of pre- vs. postsynaptic neuronal expression of a disease-causing gene to malicious phenotype (125,299). Despite these achievements, a few questions remain, including that of how to optimize the ratio of different neurons in culture to more closely represent the physiological condition in the brain.

Studies of neurodegenerative diseases suggest that synaptic alterations precede overt clinical manifestations and neuronal loss (28,297,410). In Huntington's disease (HD), an inherited disorder in which the striatum shows the most severe degeneration, one of the earliest pathogenic changes is impairment of glutamatergic cortical connections to GABAergic striatal medium-sized spiny projection neurons (SPNs) (91,298,322). Consequently, cortico-striatal (C-S) coculture is superior to striatal-only culture as an *in vitro* model for investigating pathogenic mechanisms in such a neurodegenerative disorder. Moreover, SPNs in coculture are morphologically and synaptically

more developed and similar to striatal neurons in the brain (124,406,411,412). However, coculture preparation methods vary between studies, and the influence of cortical-to-striatal neuron plating ratio in coculture on striatal SPN physiology, including dendritic arborization, NMDA-type glutamate receptor subcellular distribution and survival-death signaling — an important focus of HD research — has not been explored. In this chapter, we address this question by varying the coculture ratio of cortical to striatal neurons and comparing striatal SPN physiology and morphology, receptor distribution, pro-survival signaling and sensitivity to cell death.

2.2 Methods

2.2.1 Cell Culture

All procedures and animal care were approved by the University of British Columbia, according to the guidelines of the Canadian Council for Animal Care. All cultures were prepared from wild-type (WT) FVB/N embryonic day 18 (E18) mouse cortical and striatal tissue, as previously described (125); each E18 brain yielded ~1.5 million striatal and 3 million cortical neurons. Briefly, after the mother was anesthetized, the embryos were extracted, and their brains were quickly removed and dissected in ice-cold Hank's balanced salt solution (Invitrogen). Tissues were chopped, followed by digestion in trypsin (Invitrogen) and dissociation in trypsin inhibitor solution (Invitrogen). Striatal neurons were labeled by transfection with yellow fluorescent protein (YFP) construct on a β-actin promoter (a gift from A.M. Craig, the University of British Columbia) to be identified from cortical neurons as follows: 1.5 million striatal cells were suspended in 100 µl of electroporation buffer (Mirus Bio. LLC, Madison, WI) mixed with 2 µg of DNA, and then electroporated (program 05, AMAXA nucleofector, Amaxa, Lonza bio. Inc., Walkersville, MD, USA) in a cuvette, according to the manufacturer's instructions. Transfected striatal neurons then were blended with 1.5 or 0.5 million cortical neurons, and the mixture was diluted in DMEM (Invitrogen) with 10% fetal bovine serum (Sigma) to give the same final concentration of cells for the two different mixtures. Five hundred microliters of the mix were plated in each well with an approximate cell density of 650 cells/mm^2 in a 24-well plate. Each well had a 12-mm coverslip (Marienfeld, Lauda-Konigshofen, Germany) precoated with poly-D-lysine hydrobromide (P6407, Sigma) in borate buffer (12.5 mM Borax, 50 mM boric acid; Sigma). Two to four hours after the cells were plated, the medium was switched to 500 µl of plating medium (Neurobasal medium, B27, glutamine, and penicillin/streptomycin; Gibco). At 3 to 4 days *in vitro* (DIV), an extra 500

µl of plating medium was added to each well, and subsequent half-medium changes occurred every 3-7 days thereafter. All experiments were conducted at DIV17-19. YFP-positive cells with SPN morphological characteristics (medium-sized soma with less polarized dendritic tree) were chosen for assessment in both immunocytochemical and electrophysiological experiments, as previously described (413).

2.2.2 Electrophysiology

Whole cell patch-clamp recordings were carried out under voltage clamp condition. The Axopatch 200B amplifier (Axon Instruments) and pClamp 10.2 software (Molecular Devices, Palo Alto, CA) were used to acquire the data. Coverslips were transferred to the recording chamber and perfused with external bath solution prepared with (in mM): 167 NaCl, 2.4 KCl, 10 Glucose, 10 HEPES, 2 $CaCl_2$, 1 $MgCl_2$, 0.05 picrotoxin (PTX), 0.0003 tetrodotoxin (TTX), pH 7.3 with NaOH, 310-320 mOsm (125). The miniature excitatory postsynaptic currents (mEPSC), recorded at a holding potential of -70 mV, were digitized at 10 kHz and filtered at 1 kHz. Recording electrodes (3-6 MΩ) were filled with an internal solution consisting of (in mM): 145 K-Gluconate, 1 $MgCl_2$, 10 HEPES, 1 EGTA, 2 adenosine 5'-triphosphate magnesium salt, and 0.5 guanosine 5'-triphosphate sodium salt; 280 mOsm. The access resistance was typically between 10-20 MΩ but not higher than 25 MΩ. To assess SPN excitability, TTX and PTX were omitted from the recording solution, and membrane potential was measured in response to a series of 400-ms current pulses of amplitudes ranging from -250 to 300 pA, incremented by 50 pA. For the input-output curve, the same protocol was applied except that the bath solution contained TTX (0.3µM) and PTX (50µM). The curve was plotted based on the mean values of stable membrane potentials recorded during the final 100ms of each current pulse.

To record whole cell and extrasynaptic NMDA currents, coverslips were placed in bath solution consisting of (in mM unless stated otherwise): 167 NaCl, 2.4 KCl, 10 glucose, 10 HEPES, 2 $CaCl_2$, 10 μM $MgCl_2$, 100 μM PTX, 0.3 μM TTX, and 10 μM glycine; pH 7.3 with NaOH, 310-320 mOsm. Internal recording solution consisted of (in mM): 130 Caesium methanesulfonate, 5 CsCl, 4 NaCl, 1 $MgCl_2$, 10 HEPES, 5 EGTA, 5 lidocaine, 0.5 GTP, 10 sodium phosphocreatine, and 5 adenosine 5'-triphosphate magnesium salt; pH 7.2, 290 mOsm. Rapid application of drugs or wash solution was achieved by using a perfusion system with a theta tube (Harvard Apparatus, Saint-Laurent, Quebec). *N*-Methyl-D-aspartate (NMDA; 1 mM; M3262; Sigma-Aldrich) was applied for 3 s every 30 s at a holding potential of -70 mV while the initial whole cell NMDA current was recorded and to measure extrasynaptic NMDA current after synaptic NMDA receptors were blocked with MK801 (10 μM, Sigma). Blockade of synaptic NMDA receptors was achieved by holding cells at -80 mV, superfusing for 2 min with 4-aminopyridine (4-AP; 10μM; Tocris) to maximize synaptic activity, and superfusion with 4-AP together with MK801 for 3 min, followed by washout for 30 s. Cells in which the access resistance changed by >25% were discarded. The peak current was normalized to cell capacitance (Cm), and charge transfer density was calculated as total area of evoked NMDA current (pA × ms) normalized to cell capacitance.

2.2.3 Apoptotic Assay

SPN sensitivity to excitotoxicity was assessed as previously described (414). Briefly, in a 37^{o}C, 5% CO_2 humidified incubator, cultures were treated with NMDA at concentrations of 30 and 50 μM in conditioned medium for 15 min, washed twice with new plating medium, switched back to the conditioned medium, and incubated for 1 h. Cultures were then fixed with 4% paraformaldehyde (PFA) (30 min), permeabilized with 1% Triton X-100 (Sigma) in PBS (5 min),

and incubated with 10% normal goat serum (NGS, Vector Laboratories) at room temperature (RT; 40min) in 0.03% Triton X-100 in PBS (PBST). To detect YFP, the neurons were incubated with a chicken polyclonal anti-green fluorescent protein (GFP) antibody (1:1,000; ab13970; Abcam) in 2% NGS PBST at RT for 3 h. Neurons were then washed 3 times with PBST, incubated with a goat anti-chicken Alexa Fluor 488 antibody (1:1,000; A-11039; Invitrogen) in 2% NGS PBST at RT for 1.5 h, washed again 3 times with PBST, stained with 5 µM Hoechst 33342 (Invitrogen) at RT for 10 min in PBST, and washed again 3 times with PBST, and the coverslips were mounted on slides with Fluoromount-G (0100-01; SouthernBiotech). Cells with round, small, densely compacted nuclei and few neuritic processes were counted as apoptotic neurons, whereas cells with loosely compacted, large nuclei and extensive dendritic projections were regarded as healthy cells (414). At least 200 YFP-positive cells were counted in each condition of each culture batch under a 63x oil-immersion lens (1.4 numerical aperture) with a Zeiss Axiophot epifluorescence microscope.

2.2.4 Immunostaining

Basic characterization of cell populations was carried out using Hoechst 33342 to assess nuclear morphology, an antibody against microtubule-associated protein 2 [MAP2; 1:200; MA5-12823; Thermo Scientific; Alexa Fluor 568 (1:1,000; A-11031; Invitrogen) was used as secondary antibody] to label all neurons, and an antibody against dopamine and cAMP regulated phosphoprotein 32 [DARPP-32; 1:500; 2306S; Cell Signaling Technologies; Alexa 488 (1:1,000; A-11008; Invitrogen) was used as secondary antibody] to identify striatal SPNs. At DIV17-19, cells were fixed, permeabilized, blocked, and immunostained with primary antibodies in 2% NGS PBST at RT for 3 h. Neurons were then washed, incubated with secondary antibodies in 2% NGS

PBST at RT for 1.5 h, washed, stained with Hoechst 33342, washed, and mounted. Basic characterization images were acquired in 20x fields using a Zeiss Axiophot epifluorescence microscope. Live cells were differentiated from dead cells on the base of their nuclear morphology (as described above) (414), and counted with the Cell Counter plugin in ImageJ software (1.47v; NIH, Bethesda, MD) with or without merging channels for overlapping signals. Results are displayed in Table 1 as average numbers $\pm$ standard error in a single 20x field. A total of 77-78 20x fields from 5 batches of cocultures were used for live cell and DARPP-32 staining analysis, whereas 15-18 20x fields from 2 culture batches were assessed for MAP2 staining statistics.

Sholl analysis was conducted in ImageJ using the Sholl analysis plugin (http://fiji.sc/Sholl_Analysis). The dendritic tree of striatal SPNs was visualized by immunostaining against DARPP-32 and was traced with the segmented line tool in ImageJ. Concentric circles with radii from 10 to 200 μm, stepped by 5 μm, were centered on the soma, and the number of intersections with the traced lines was measured. The total dendritic length is a summation of lengths of all traced lines.

Analysis of excitatory synapses was conducted with the same immunostaining protocol, with the following exceptions: PBS was used for wash instead of PBST; methanol (-20^{o}C, 5 min) and PBST (RT, 5 min) were applied for permeabilization; primary antibodies were the chicken polyclonal anti-GFP antibody (to label striatal SPNs, as above), a mouse anti-postsynaptic density protein 95 (PSD-95) antibody (1 h at RT, 1:1,000; MA 1-045; Thermo Scientific) and a guinea pig anti-vesicular glutamate transporter 1 (vGlut1) antibody (at 4^{o}C overnight, 1:4,000; AB 5905; Chemicon) in 2% NGS PBST; and secondary antibodies were Alexa Fluor 488 goat anti-chicken, Alexa Fluor 568 goat anti-mouse, and aminimethylcoumrin (AMCA)-conjugated goat anti-guinea pig (1:1,00; 706-155-148; Jackson ImmunoResearch) at RT for 1.5 h. Coverslips were washed

with PBS for three to four times before being mounted. Images were acquired with a Zeiss Axiophot epifluorescence microscope under a 63X oil-immersion lens (1.4 numerical aperture) by taking 10-15 sections with 0.23-μm steps in the *z*-plane with the same exposure time for each channel on each sample. The three best-focused sections were extracted to average, using the extended depth of focus function, and were exported as gray-value TIFF files for individual channels. Blinded to conditions and using the green channel, the experimenter chose three 15- to 30-μm segments of primary and/or secondary dendrite at a distance of 40 to 100 μm from the soma with polygon selection tool in ImageJ. The PSD-95 and vGlut1 images were thresholded manually within the chosen dendritic segments to remove background staining and to isolate puncta. Binary images of puncta were generated and analyzed for puncta density and colocalization using the Analyze Particles tool and the colocalization plugin of ImageJ (125). Average values of the three chosen areas of interest from individual cells were used in the final analyses.

For measuring phosphorylated cAMP response element binding protein (pCREB), a reflection of pro-survival signaling, we used the chicken polyclonal anti-GFP antibody (to identify striatal SPNs, as above) and a mouse monoclonal anti-pCREB antibody [1:500; 05-667; Millipore; Alexa Fluor 568 (A-11031, Invitrogen) was used as secondary antibody]. Cells were stained as described above. Images for pCREB signal analysis were acquired with a Zeiss Axiophot epifluorescence microscope under a 63× oil-immersion lens. Nuclear-to-cytoplasmic pCREB ratios were obtained by comparing the average pCREB signal intensity in the nucleus to that of three randomly chosen areas covering most of the cytoplasmic region (as illustrated in Figure 2-6 Ai) using ImageJ.

2.2.5 Data Analysis

Pooled data are presented as mean ± s.e.m. Figures were prepared with Prism 5 (GraphPad Software), and graphs were created with Adobe Illustrator CS5 (Adobe Systems). In all figures, n values represent the numbers of cells analyzed in given measurements, followed by the culture batch numbers in parentheses.

2.3 Results

2.3.1 Influence of Cortical-striatal Plating Ratio on Survival and Basic Membrane Properties of Striatal SPNs after 18 Days in Culture

To determine the effect of cortical neuron abundance on the properties of striatal SPNs, we cocultured cortical and striatal neurons at a cortical-striatal plating ratio of 1:1 vs. 1:3 and then compared these two conditions at DIV18 for all experiments. Cell population density at DIV18 was characterized using Hoechst-stained nuclear morphology to determine density of live cells, MAP2 staining to identify all neurons, and an antibody against DARPP-32 as a marker of striatal SPNs (413,415). Results are shown in Table 2-1. We found that the average number of live cells per 20x field (441x330 μm), including both cortical and striatal neurons as well as MAP2-negative cells, was significantly lower in cocultures plated at the 1:3 vs. 1:1 ratio, as was the density of MAP2-positive cells (~23%). Moreover, despite a 50% higher plating density of striatal neurons in the 1:3 coculture condition, the density of DARPP32-positive cells was similar at DIV18 for 1:3 and 1:1 cocultures. Taken together, our results suggest that cocultures plated at the lower cortical ratio (1:3) undergo greater loss of striatal SPNs. As well, the relatively low ratio of DARPP-32-positive neurons compared to MAP2-positive cells (all neurons) in both coculture conditions suggests that striatal SPNs are generally more fragile in these cocultures and/or slow to fully mature (i.e., some may not express detectable levels of DARPP-32 by DIV18). Although we cannot make definite conclusions from these results about the ratio of cortical glutamatergic pyramidal neurons to striatal SPNs at DIV18, our data indicate that the density of live MAP2-positive/DARPP-32-negative (mainly cortical) neurons at DIV18 is only ~25% lower in the cocultures plated at a 1:3 vs. 1:1 ratio, whereas there is no significant difference in striatal SPN density.

To determine how a change in cortical input affects basic membrane properties of SPNs, we measured the resting membrane potential, action potential firing rates, current-voltage (I-V) response, membrane capacitance, and input resistance of SPNs in C-S cocultures plated at the 1:1 and 1:3 ratios. SPNs in the cocultures plated at the lower cortical ratio showed significantly reduced membrane capacitance (Figure 2-1 A), suggesting that a reduction in cortical-striatal ratio decreases the soma size and/or dendritic growth of striatal SPNs. However, the input resistance (Figure 2-1 B) and resting membrane potential (Figure 2-1 C) were similar for SPNs in the two cocultures, indicating that the reduction of cortical neurons does not significantly alter these basic striatal neuronal membrane properties. In addition, SPN excitability curves (Figure 2-1 Di and Dii) were similar, and the I-V response curve (Figure 2-1 Ei and Eii) only trended toward depressed in the cocultures plated at the lower cortical ratio. Together, these results show that the C-S ratio has only a modest impact on the SPN basic membrane properties.

	1:1	1:3	P value (paired t-test)
Live cells	30.0 ± 2.3	22.9 ± 1.5	0.0011**
MAP2+	21.3 ± 2.2	16.4 ± 1.2	0.0216*
DARPP32+	3.4 ± 0.2	3.3 ± 0.3	0.5761
MAP2+ & DARPP32-	17.2 ± 1.7	12.7 ± 1.0	0.0172*

Table 2-1 Characterization of cell density in C-S cocultures plated at 1:1 and 1:3 ratios

Values are average (±SE) numbers of cells in a single 20x microscope field. The *n* values in legend indicate the numbers of 20x microscope fields (a 20x field is 441x330 µm)counted, with the numbers of culture batches shown in parenthesis. Despite the same plating density, both the number of live cells and the number of MAP2-positive cells per 20x field are significantly lower in 1:3 compared with 1:1 cocultures [live cell density: n=77(5) for 1:1 and n=78(5) for 1:3 plating ratio; by paired t-test, **p=0.0011; MAP2+ cell density: n=15(2) for 1:1 and n=18(2) for 1:3 plating ratio; by paired t-test, *p=0.0216]. Surprisingly, the density of DARPP-32+ cells is similar between conditions even though the MAP2+ but DARPP32- cell density is low in 1:3 cocultures (DARPP-32+ cell density: n=77(5) for 1:1 and n=78(5) for 1:3 plating ratio; paired t-test p=0.5761; MAP2+ and DARPP32- cell density: n=15(2) for 1:1 and n=18(2) for 1:3 plating ratio; paired t-test, *p=0.0172).

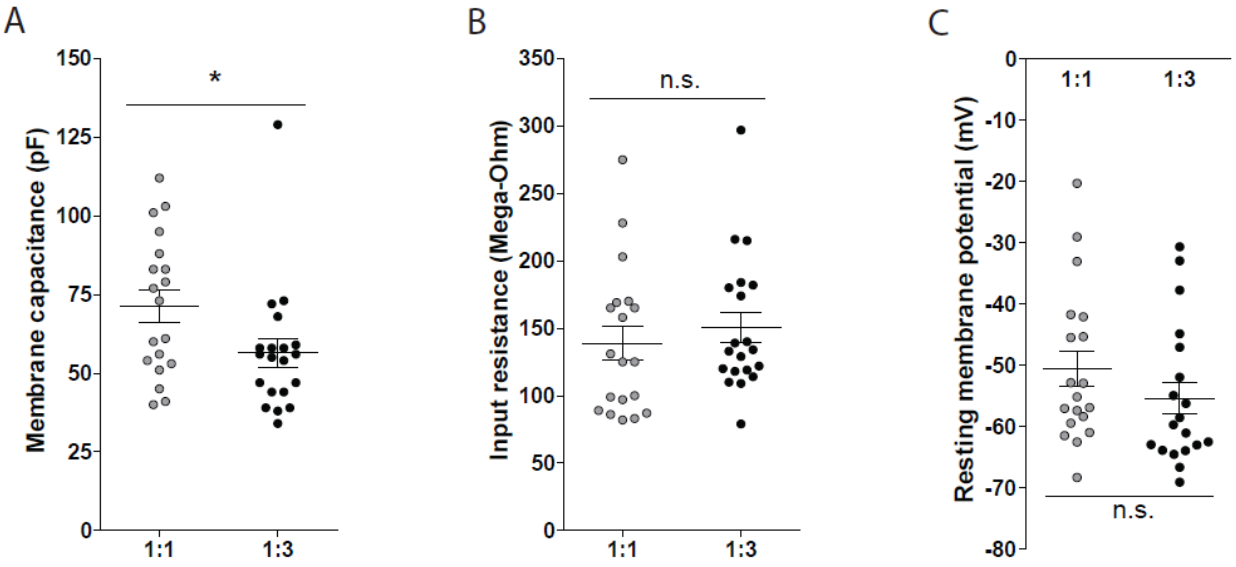
A
Membrane capacitance (pF)
150
125
100
75
50
25
0
*
1:1
1:3
B
Input resistance (Mega-Ohm)
350
300
250
200
150
100
50
0
n.s.
1:1
1:3
C
Resting membrane potential (mV)
0
-10
-20
-30
-40
-50
-60
-70
-80
1:1
1:3
n.s.

Di

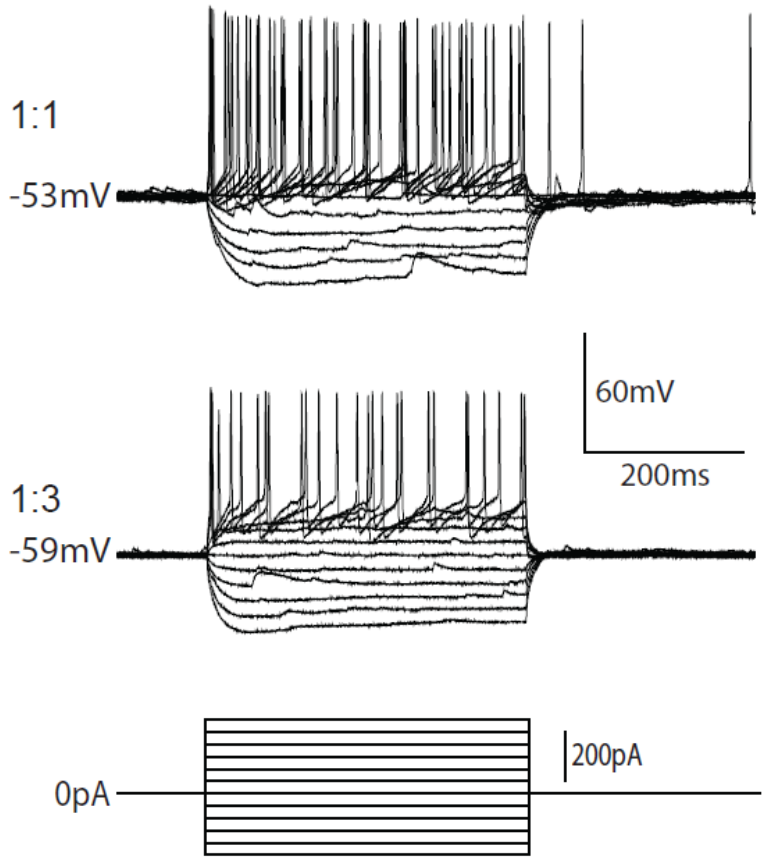
1:1
-53mV
60mV
200ms
1:3
-59mV
200pA
0pA

Dii

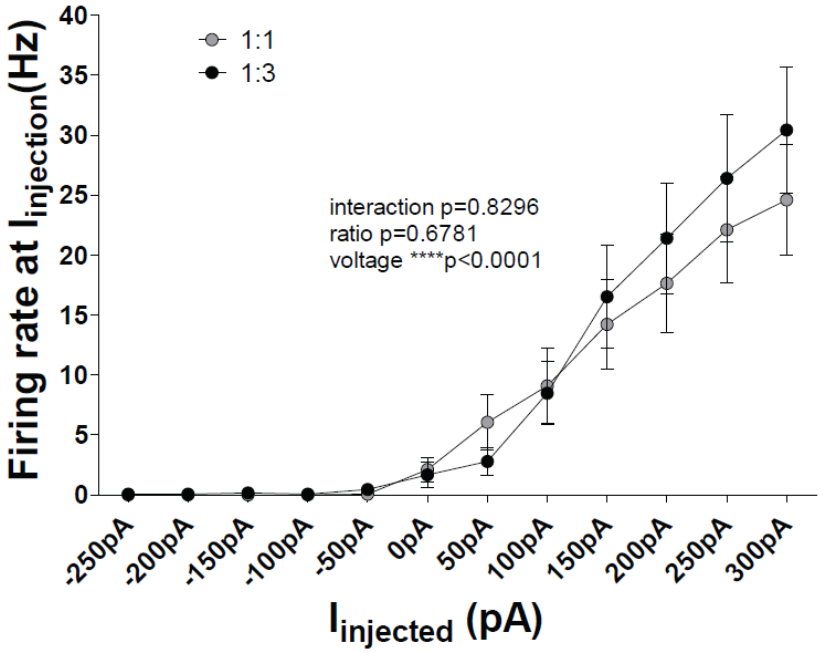
1:1
1:3
interaction p=0.8296
ratio p=0.6781
voltage ****p<0.0001
Firing rate at I injection (Hz)
I injected (pA)
-250pA
-200pA
-150pA
-100pA
-50pA
0pA
50pA
100pA
150pA
200pA
250pA
300pA

Ei

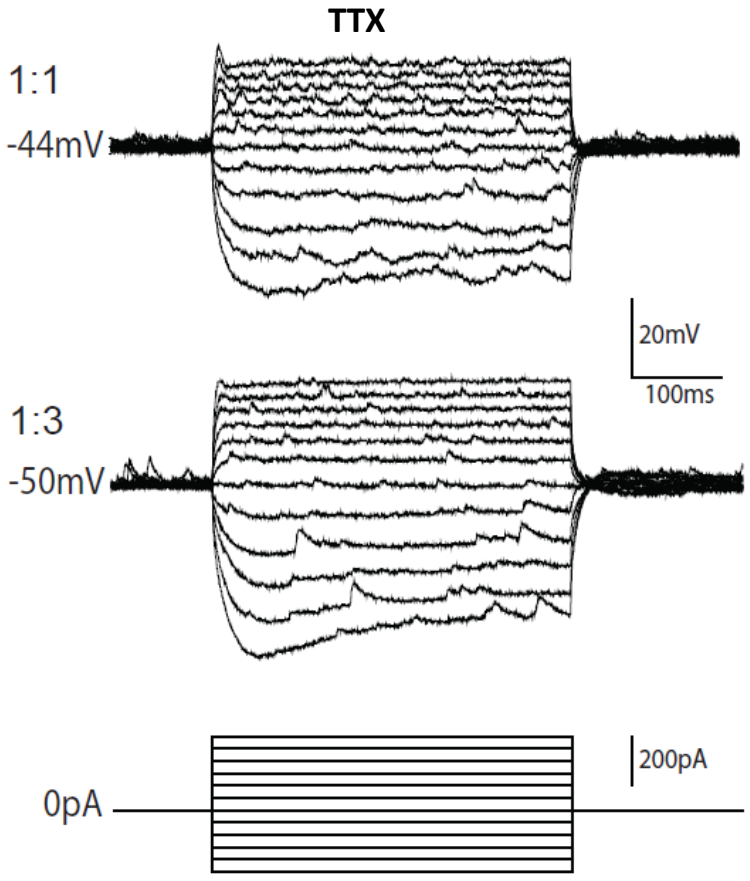
TTX
1:1
-44mV
20mV
100ms
1:3
-50mV
200pA
0pA

Eii

TTX

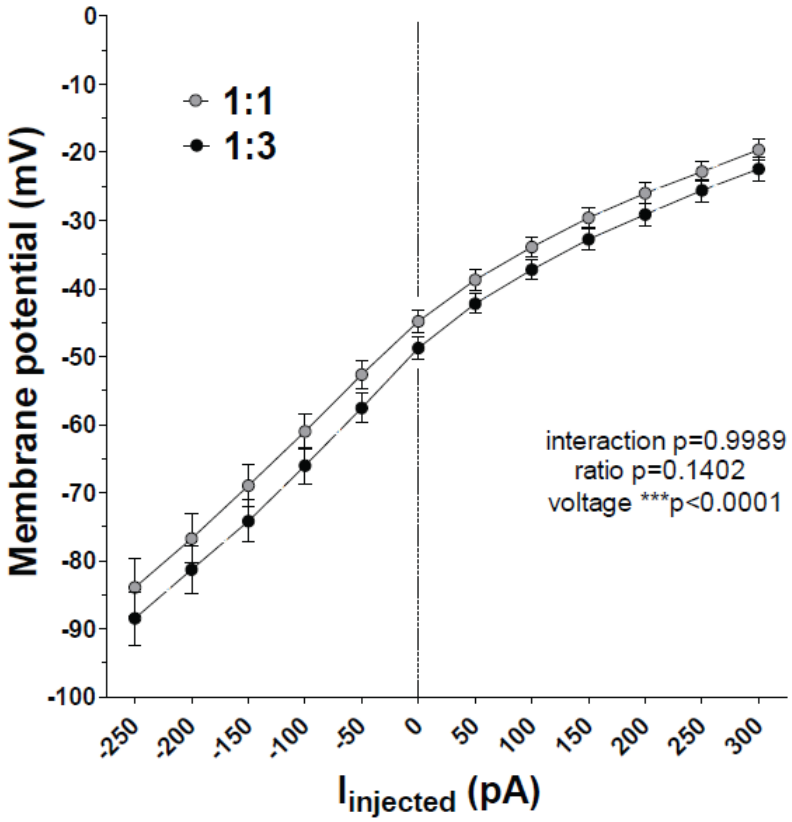
1:1
1:3
Membrane potential (mV)
0
-10
-20
-30
-40
-50
-60
-70
-80
-90
-100
-250
-200
-150
-100
-50
0
50
100
150
200
250
300
I injected (pA)
interaction p=0.9989
ratio p=0.1402
voltage ***p<0.0001

Figure 2-1 Cortical-to-striatal neuron ratio affects some SPN membrane properties in coculture.

The numbers of cells analyzed are presented as *n* values with the culture batch numbers in parentheses. ***A.*** SPN membrane capacitance is significantly smaller in C-S cocultures plated at 1:3 than at 1:1 ratio [n=19(3) in 1:1 and n=20(4) in 1:3 ratio; *p<0.05 by unpaired t-test]. ***B.*** and ***C.*** Membrane input resistance [***B.*** n=19(3) in 1:1 and n=20(4) in 1:3 ratio; unpaired t-test, p>0.05] and resting membrane potential [***C.*** n=19(3) for both ratios; unpaired t-test, p>0.05] are similar for the 2 coculture conditions. ***D.*** Current-induced firing rate is not significantly different. ***Di.*** Representative traces of membrane potential change under current injections; ***Dii.*** Pooled data for current injection-induced firing rates [n=19(3) for 1:1 and n=18(3) for 1:3; repeated-measures 2-way ANOVA, interaction p=0.8296, cortical-striatal ratio p=0.6781, and current ****p<0.0001]. ***E.*** I-V curve is not significantly different between the 2 coculture conditions in the presence of TTX and PTX. ***Ei.*** Representative traces for membrane potential change in response to a range of current injections; ***Eii.*** Pooled data for I-V curve [n=24(4) for 1:1 and n=22(4) for 1:3 ratio; repeated-measures 2-way ANOVA, interaction p=0.9989, cortical-striatal ratio p=0.1402, and current ***p<0.0001].

2.3.2 Impaired SPN Dendritic Arborization in Cocultures Plated at the Lower Cortical-to-Striatal Ratio

The reduction in SPN membrane capacitance in the cocultures plated at the lower cortical ratio suggests that cortical neuronal abundance influences striatal SPN dendritic length, soma size and/or spine density. To test this, we assessed dendritic arborization by visualizing striatal SPNs with antibody staining against DARPP-32. Our results showed a significant reduction in the total dendritic length of SPNs in cocultures plated at the lower cortical ratio (Figure 2-2 A and B), suggesting underdevelopment of the dendritic arbor. Consistent with that result, Sholl analysis indicated a reduced complexity of dendritic arborization in cocultures plated at the 1:3 (Figure 2-2 C). Altogether, these data suggest that a relative change in cortical neuron abundance affects SPN neurite growth and/or maintenance.

A

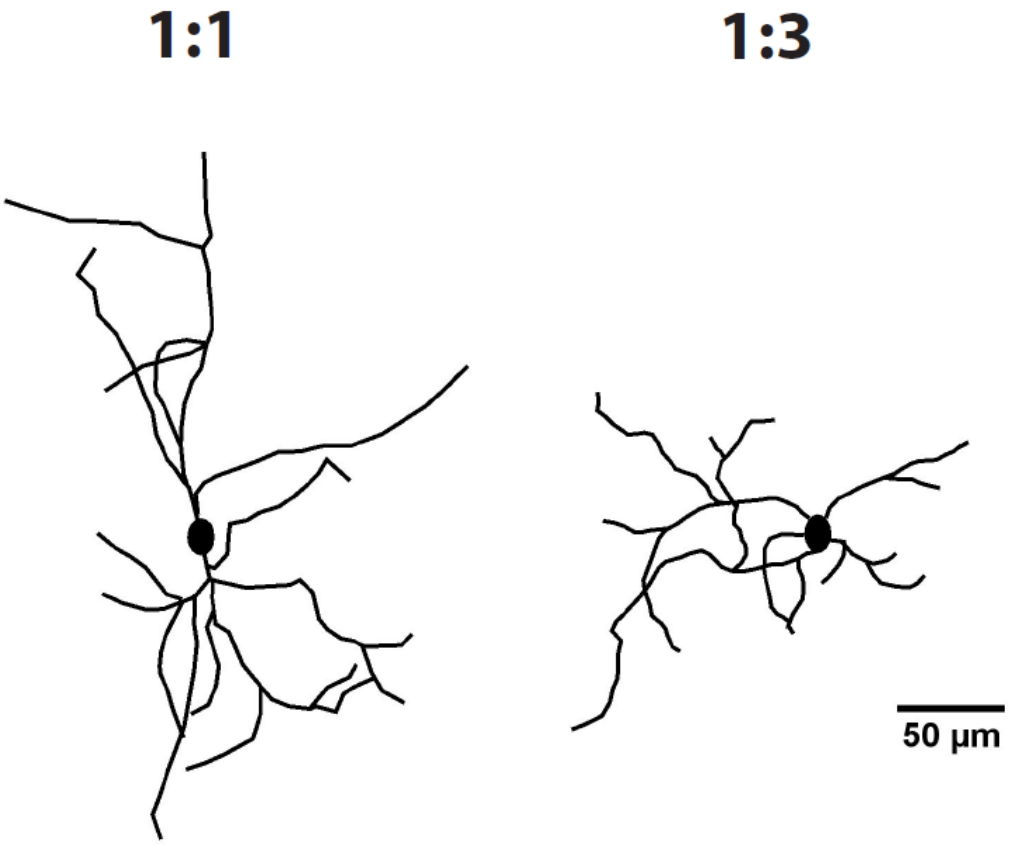
1:1
1:3
50 µm

B

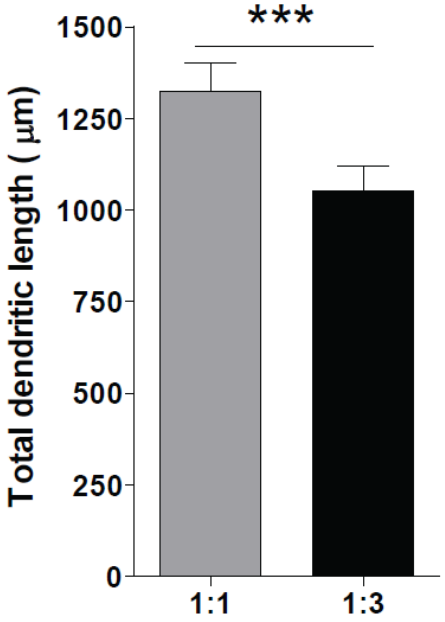
***
1500
1250
1000
750
500
250
0
Total dendritic length (µm)
1:1
1:3

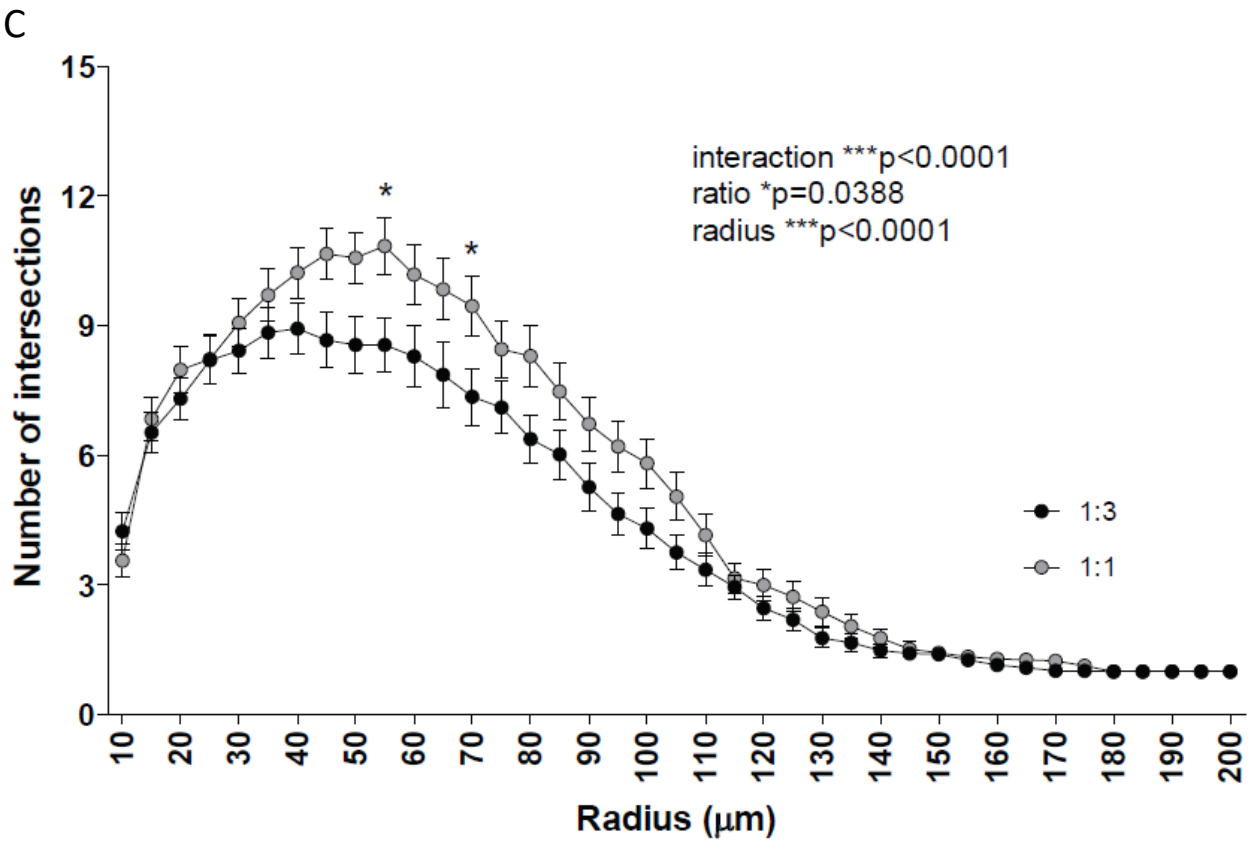

Figure 2-2 Change in cortical relative to striatal cells regulates SPN dendritic arborization.

A. Representative tracings of SPN dendritic arbor from both conditions. ***B.*** SPNs grown with lower cortical cell ratio (1:3) have shorter total dendritic length compared to the other condition [n=44(4) and 45(4) for 1:1 and 1:3 conditions, respectively; paired t-test, ***p<0.0001]. Moreover, dendritic complexity indicated by Sholl analysis is reduced significantly in coculture plated at lower cortical ratio [***C.*** n=44(4) and 45(4) for 1:1 and 1:3 conditions, respectively; interaction ***p<0.0001, ratio *p=0.0388 and radius ***p<0.0001 by repeated measures two-way ANOVA; by Bonferroni's post-tests, *p<0.05 at 55 and 70 μm].

2.3.3 Cortical-striatal Ratio Affects the Density of Excitatory Synapses onto SPNs

To determine if the cortical-striatal ratio in cocultures influences excitatory cortical synapses onto SPNs, we measured spine density and excitatory synapse density along dendritic segments >40 μm away from the soma with immunocytochemistry, staining the pre- and postsynaptic markers vGlut1 and PSD-95, respectively. Our results showed a trend towards reduction in spine density per unit length (~15%; Figure 2-3 A and Bi) and a significant decrease in the density of colocalized puncta of PSD-95 and vGlut1 along the dendrites (~24%; Figure 2-3 A and Bii) in cocultures plated at the 1:3 compared with 1:1 ratio. Interestingly, the density along dendrites of both individual PSD-95 and vGlut1 puncta only showed a trend toward reduction in the cocultures plated at the lower cortical ratio (Figure 2-3 Ci and Cii), suggesting that cortical-striatal ratio does not significantly affect development of major pre- and postsynaptic elements of striatal excitatory synapses, but only synapse formation in culture.

Miniature EPSC frequency recorded from SPNs in cocultures plated at the lower cortical ratio showed a strong trend toward a lower mean (~26% decreased; p=0.1389 by Mann Whitney test) in comparison with cocultures plated at the higher cortical ratio (Figure 2-4 A and Bi). The cumulative probability analysis of the event frequency showed a shift toward lower frequency distribution in cocultures plated at the lower cortical ratio (Figure 2-4 Bii; significant interaction effect by repeated-measures 2-way ANOVA). Although the mean mEPSC amplitude was almost identical (Figure 2-4 Ci), a cumulative probability plot suggested a difference in distribution of amplitudes with slightly smaller amplitude events for the 1:3 cocultures (Figure 2-4 Cii; significant interaction effect by repeated-measures 2-way ANOVA). Together, these data suggest that a change in the cortical-striatal ratio has little effect on SPN synaptic AMPA receptor current but does impact excitatory synapse number in cocultures.

A **WT**

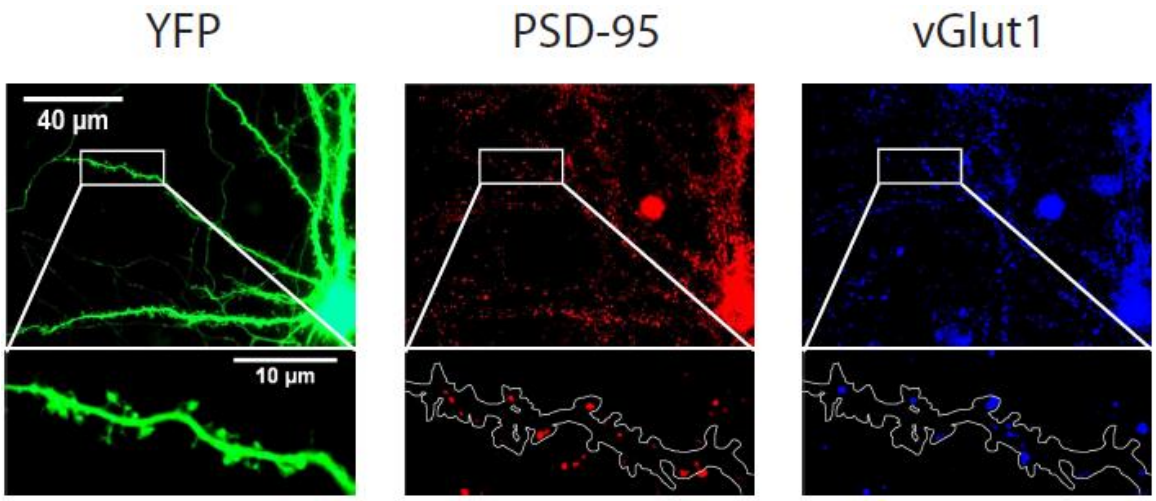

PSD-95 + vGlut1

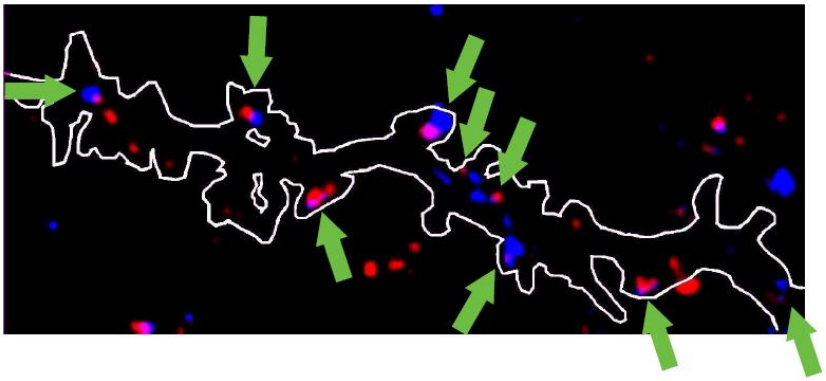

YAC128

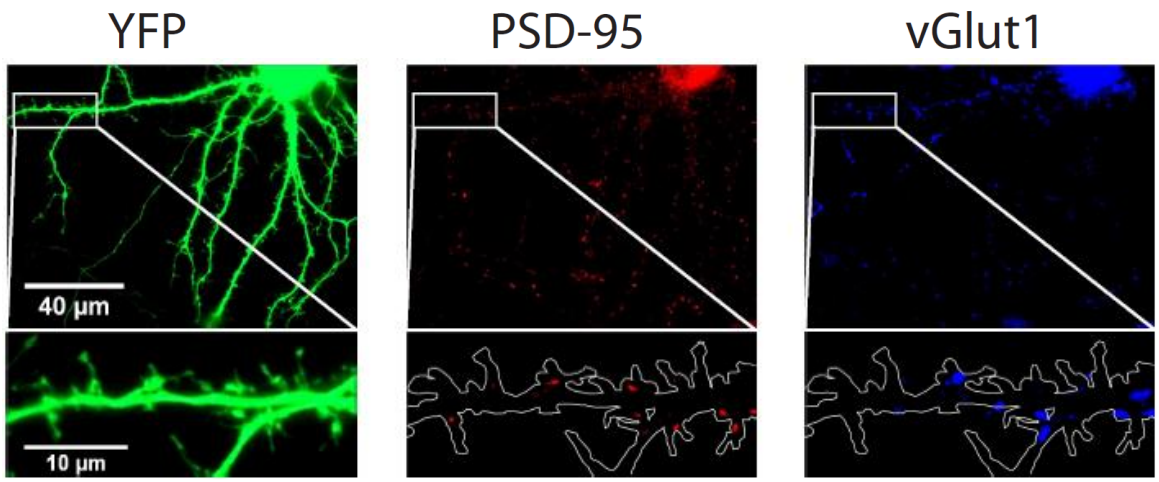

PSD-95 + vGlut1

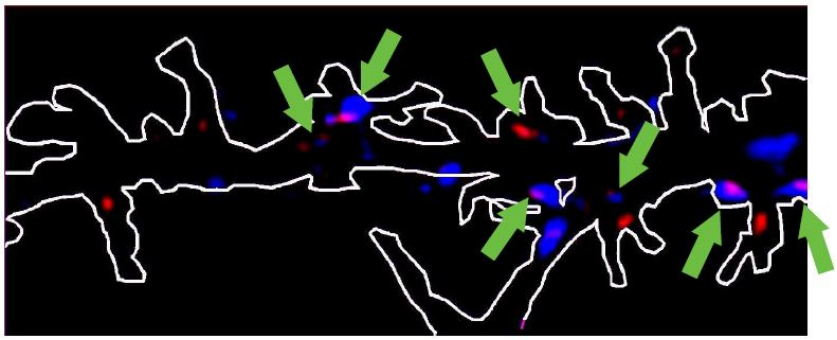

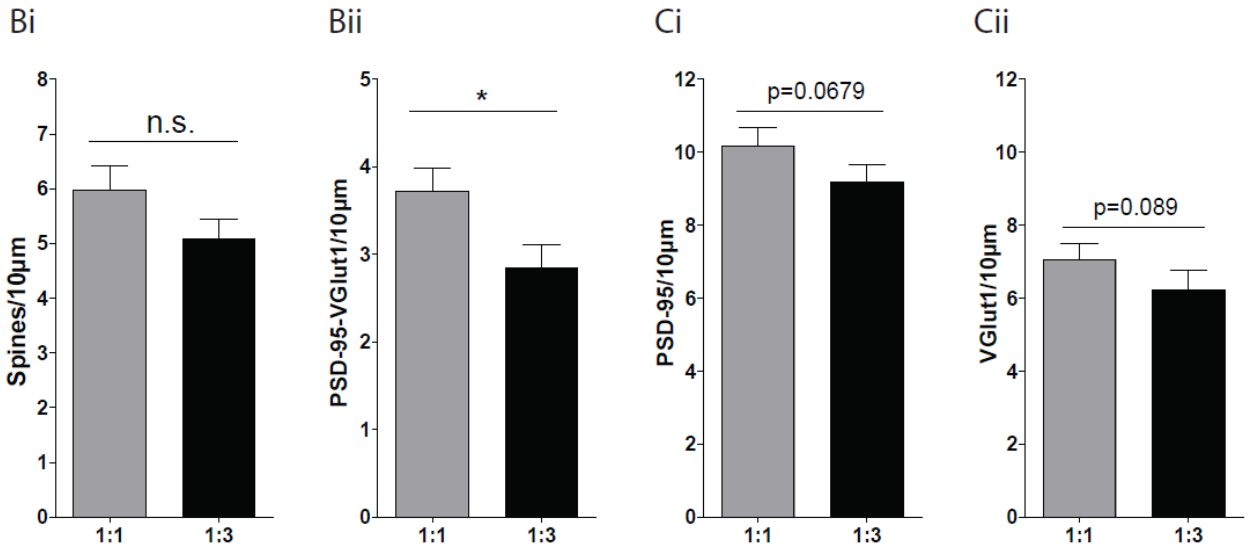

Figure 2-3 Cortical-to-striatal neuron ratio in coculture impacts dendritic excitatory synapse density.

A. Representative photomicrographs of immunostaining for YFP, PSD-95 and vGlut1. White lines, generated in ImageJ, outline the shapes of spines and dendrites in higher magnification graphs. Green arrows indicate colocalized PSD-95 and vGlut1 puncta (far right). ***Bi.*** Spine density along the SPN dendrites >40 μm away from soma shows a nonsignificant (n.s.) decrease in 1:3 compared to 1:1 ratio coculture [n=45(3) for both 1:1 and 1:3 plating-ratio; paired t-test, p=0.1127]. ***Bii.*** Density of colocalized PSD-95 and vGlut1 puncta along dendrites is lower in 1:3 than in 1:1 plating-ratio [n=45(3) for both 1:1 and 1:3 conditions, paired t-test, *p=0.0213]. ***C.*** Individual PSD-95 (***Ci.***) and vGlut1 (***Cii.***) puncta densities along dendrites trend lower for 1:3 condition compared with SPNs from 1:1 C-S cocultures, but neither is statistically significant. [***Ci.*** PSD-95 puncta density: n=45(3) for both 1:1 and 1:3 conditions; paired t-test, p=0.0679; ***Cii.*** vGlut1 puncta density: n=45(3) for both conditions; paired t-test, p=0.089].

A

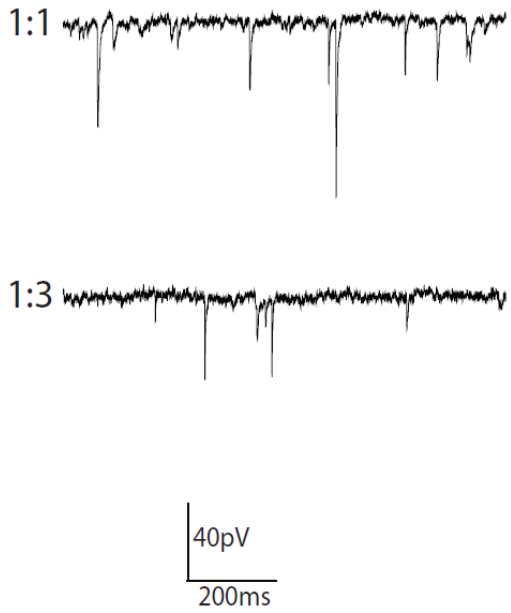
1:1
1:3
40pV
200ms

Bi

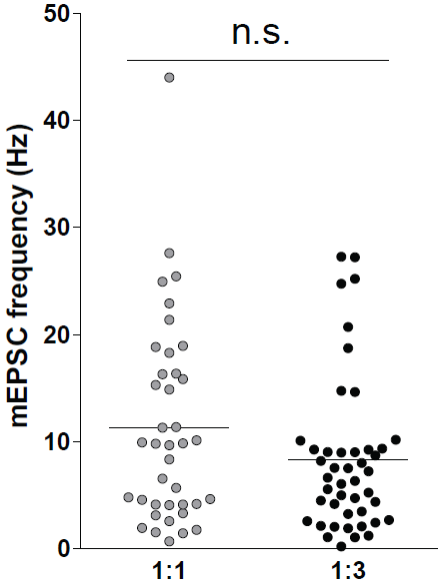
n.s.
mEPSC frequency (Hz)
50
40
30
20
10
0
1:1
1:3

Bii

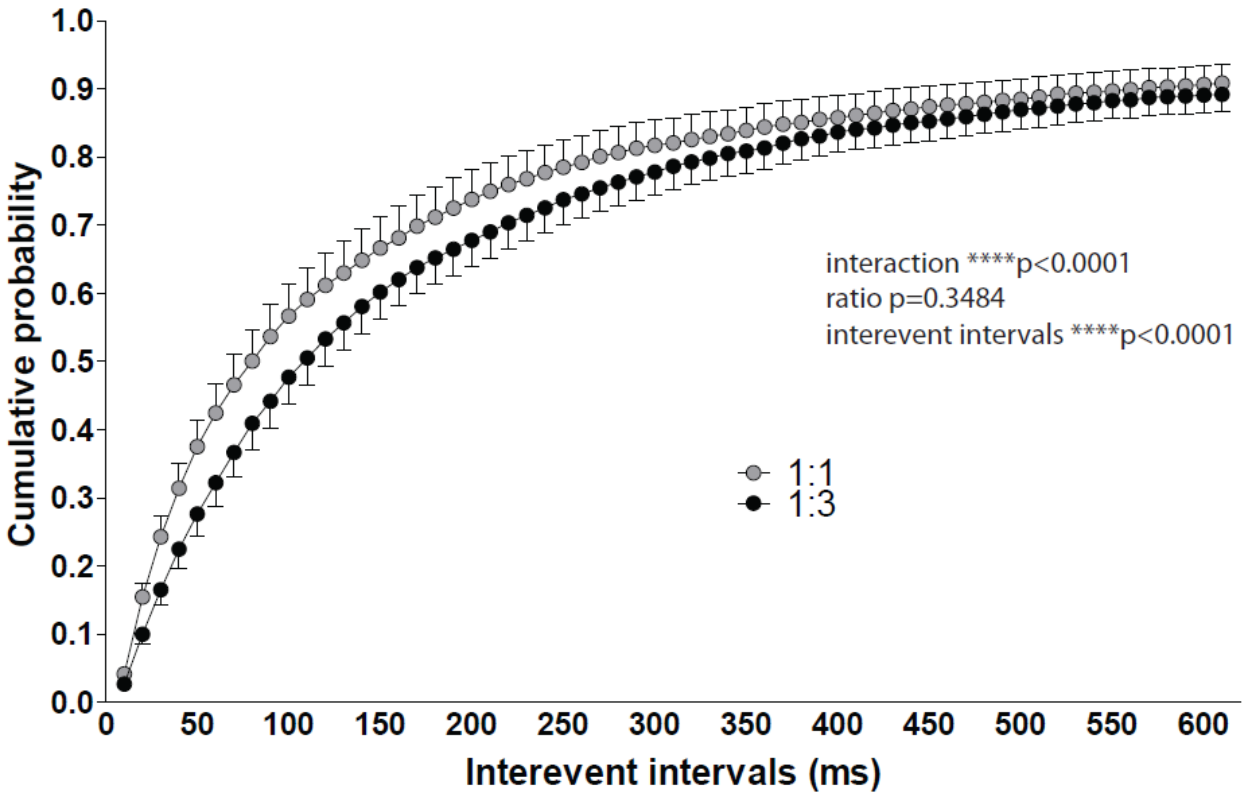
Cumulative probability
1.0
0.9
0.8
0.7
0.6
0.5
0.4
0.3
0.2
0.1
0.0
0
50
100
150
200
250
300
350
400
450
500
550
600
Interevent intervals (ms)
interaction ****p<0.0001
ratio p=0.3484
interevent intervals ****p<0.0001
1:1
1:3

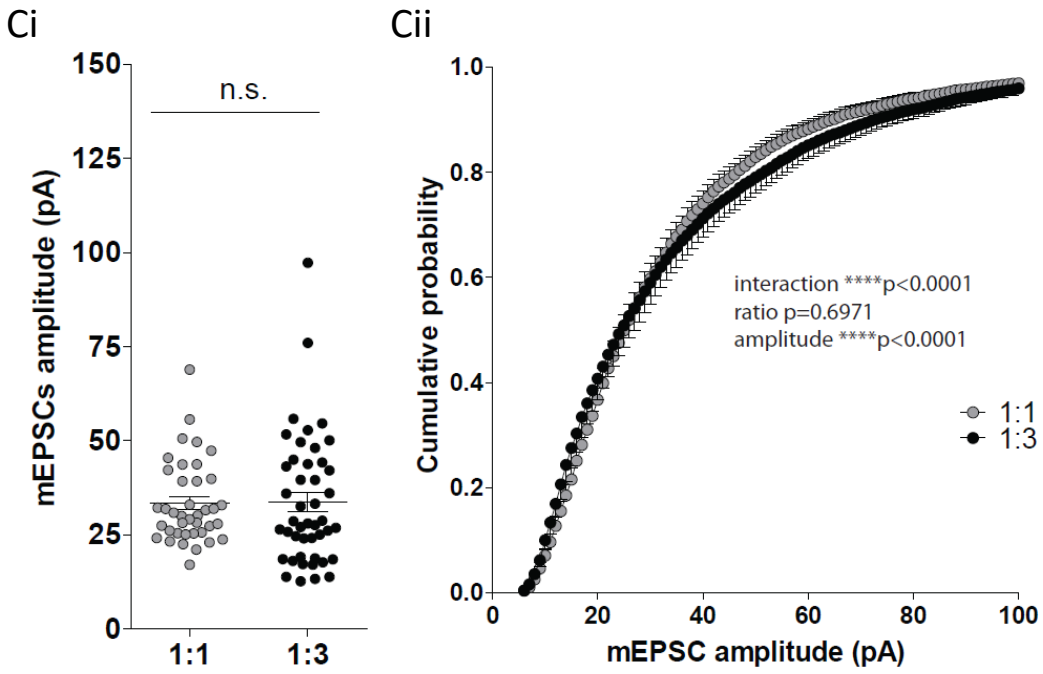

Figure 2-4 The proportion of cortical neurons to striatal SPNs in coculture affects SPN miniature excitatory postsynaptic current (mEPSC) frequency.

A. Typical current traces of mEPSCs at DIV18 show a decreased number of events in SPNs from coculture plated at a 1:3 ratio. ***Bi.*** Mean mEPSC frequency trends lower in SPNs in 1:3 than in 1:1 coculture [n=39(6) for 1:1 and n=45(7) for 1:3 ratio; Mann Whitney test, p=0.1389]. ***Bii.*** Cumulative probability of interevent intervals shows a rightward shift, toward longer interevent intervals for SPNs in 1:3 coculture [n=39(6) for 1:1 and n=45(7) for 1:3 ratio; by repeated-measures 2-way ANOVA, interaction ****p<0.0001, and cortical-striatal ratio p>0.05]. ***Ci.*** Mean amplitude of striatal mEPSCs is similar in the 2 different cocultures [n=39(6) for 1:1 and n=45(7) for 1:3 ratio; unpaired t-test, ratio p=0.9347], but its cumulative probability plot (***Cii.***) shows a small difference at higher mEPSC amplitudes between the 2 coculture conditions [***Cii.*** n=39(6) for 1:1 and n=45(7) for 1:3 ratio; repeated-measures 2-way ANOVA, interaction ****p<0.0001, and ratio p>0.05].

2.3.4 Level of Cortical Abundance Influences the NMDA Receptor Distribution on SPN Cell Membrane

NMDA receptor distribution and activity at synaptic and extrasynaptic sites have been shown to determine neuronal survival vs. cell death signaling (169). Since, in our study, the decrease of cortical neuronal abundance relative to striatal neurons in cocultures downregulated the density of glutamatergic synapses on striatal SPNs (Figure 2-3 Bii), we were interested to know whether this reduction would shift the balance of synaptic and extrasynaptic NMDA receptors in striatal neurons. To address this question, we measured the total whole cell NMDA receptor current and compared this to the extrasynaptic NMDA receptor current isolated by specifically blocking synaptic receptors with MK801 within each cell (Figure 2-5 Ai). Our results showed that the charge transfer density (Figure 2-5 Aii and Bi) and peak current density (Figure 2-5 Ci) of striatal SPNs were similar for total whole cell NMDA receptor current in both 1:1 and 1:3 conditions; however, the proportion of current carried by extrasynaptic NMDARs was significantly larger in the 1:3 cocultures (Figure 2-5 Bii and Cii), suggesting that increased cortical input upregulates synaptic and downregulates extrasynaptic NMDA receptors. Altogether, these data demonstrate that a change in the amount of cortical neurons relative to SPNs does not impact the overall density of NMDA receptors on the cell membrane, but it does influence their surface membrane distribution.

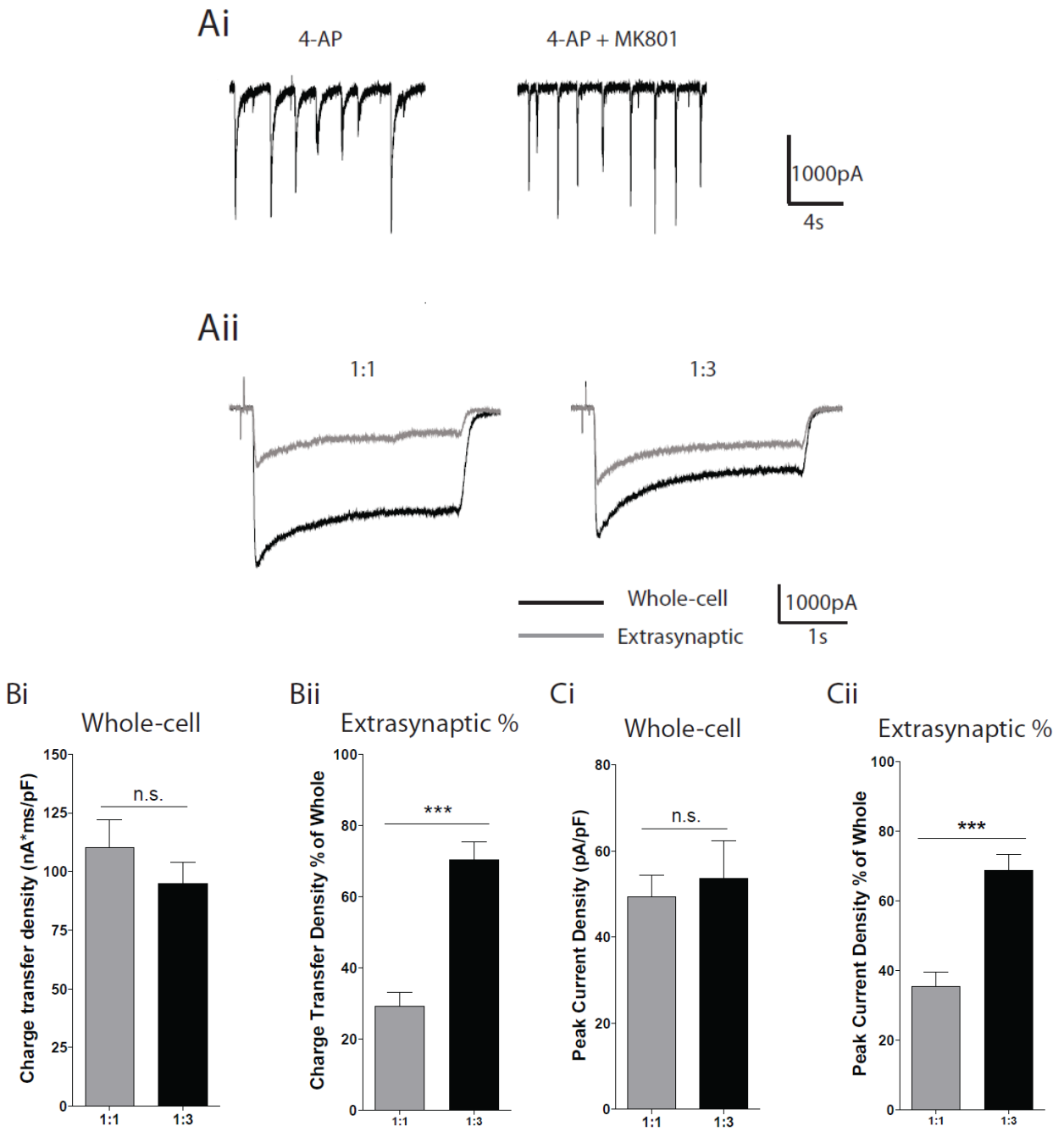
Ai
4-AP
4-AP + MK801
1000pA
4s
Aii
1:1
1:3
Whole-cell
Extrasynaptic
1000pA
1s
Bi
Whole-cell
Charge transfer density (nA*ms/pF)
n.s.
1:1
1:3
Bii
Extrasynaptic %
Charge Transfer Density % of Whole
***
Ci
Whole-cell
Peak Current Density (pA/pF)
n.s.
Cii
Extrasynaptic %
Peak Current Density % of Whole
***

Figure 2-5 Reduced abundance of cortical neurons enhances proportion of extrasynaptic NMDA receptors in cocultured SPNs.

Ai-ii. Representative current traces before and after MK801 application to block synaptic NMDA receptors (NMDARs), and in response to NMDA application. Black traces represent total (synaptic and extrasynaptic) currents, whereas light grey traces represent currents through extrasynaptic NMDARs (***Aii***). The charge transfer density of the total NMDAR current (***Bi.***) is similar [n=10(4) for 1:1 and n=9(3) for 1:3 ratio; p=0.3206], but the proportion of current carried by extrasynaptic NMDARs (***Bii.***) is significantly higher in cocultures with a 1:3 ratio [n=10(4) for 1:1 and n=9(3) for 1:3 ratio; ***p<0.0001]. Moreover, the whole cell NMDAR peak current density (***Ci.***) is similar [n=10(4) for 1:1 and n=9(3) for 1:3 ratio; p=0.1221], whereas the proportion of peak current mediated by extrasynaptic NMDARs (***Cii.***) is higher in 1:3 than in 1:1 cocultures [n=10(4) for 1:1 and n=9(3) for 1:3 ratio; ***p<0.0001]. Unpaired t-tests were conducted in all statistical analyses.

2.3.5 Increased Cortical-striatal Ratio Upregulates SPN Basal Level Pro-survival Signaling and Resistance to Apoptosis

Because our study suggested that cortical neuronal abundance impacts NMDA receptor membrane distribution on SPNs, a factor that determines the neuronal survival-death signaling balance, we wondered whether altering the proportion of cortical to striatal neurons would change SPN vulnerability to a harmful stimulus. We measured the basal level of pro-survival signaling as reflected by activation of the master pro-survival transcriptional regulator, nuclear pCREB, by assessing the ratio of nuclear to cytoplasmic pCREB (pCREB ratio) (124,414) (Figure 2-6 Ai) in order to eliminate inter-culture difference. The pCREB ratio measured in SPNs was significantly lower in cocultures plated at the lower cortical ratio (Figure 2-6 Aii), suggesting that the reduction in cortical-striatal neuronal ratio decreases the basal level of pro-survival signaling through pCREB. We also exposed 1:1 and 1:3 ratios to different concentrations of NMDA in conditioned medium at DIV17-19 for 15 min and waited for 1 h to let the cells respond (Figure 2-6 Bi). Our result showed that the apoptotic cell percentage was significantly higher in cocultures plated at the lower cortical ratio (Figure 2-6 Bii), indicating that the reduction of cortical neurons renders striatal SPNs more vulnerable to an apoptotic stimulus. Together, these data support our conclusion that the proportion of cortical neurons determines the cell survival capacity of striatal SPNs *in vitro*.

Ai

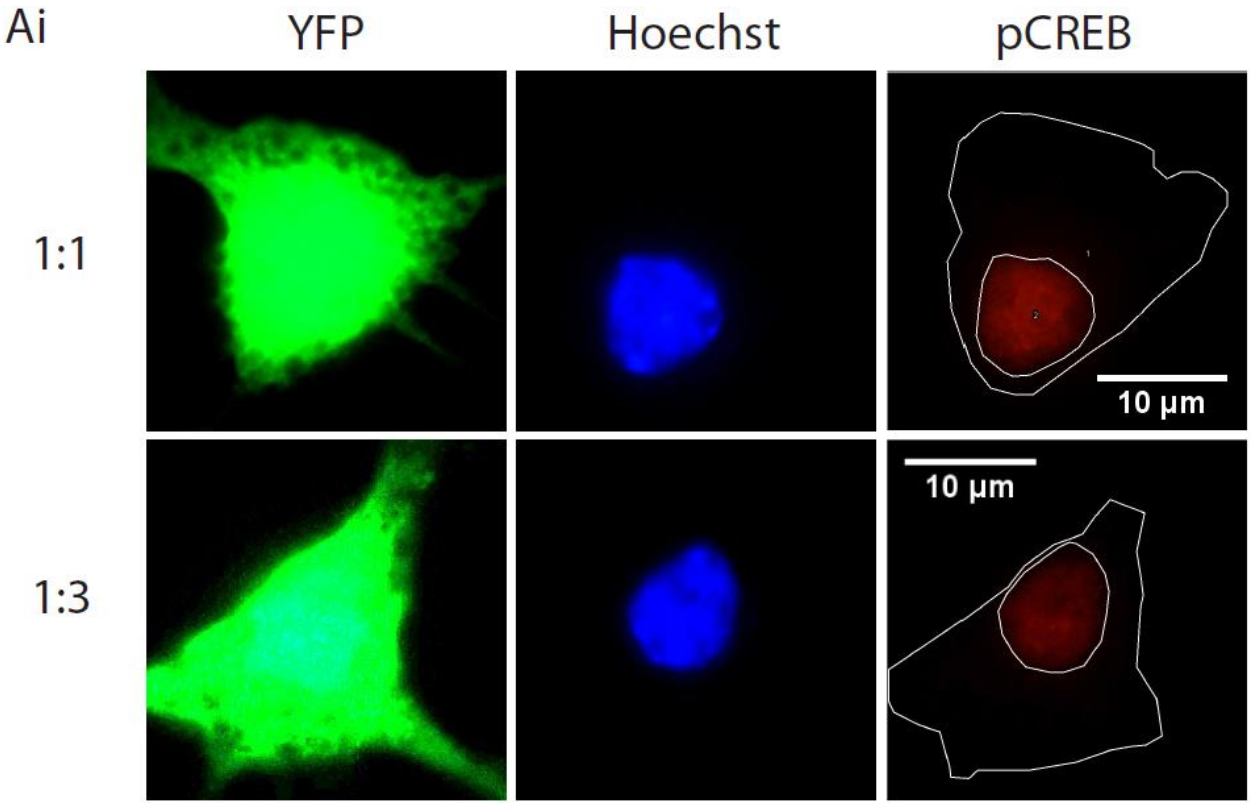
YFP
Hoechst
pCREB
1:1
1:3
10 µm
10 µm

Aii

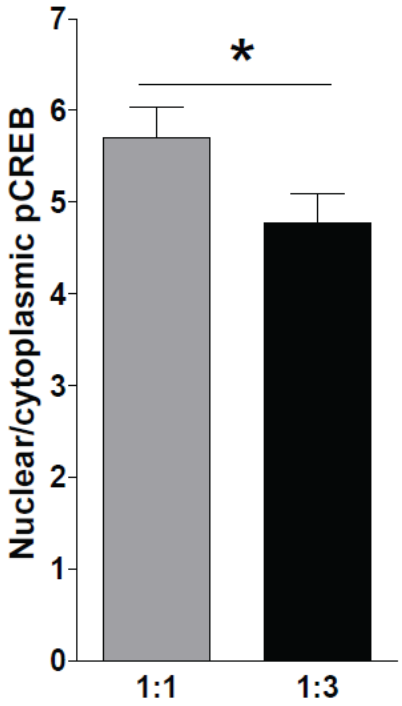
Nuclear/cytoplasmic pCREB
0
1
2
3
4
5
6
7
*
1:1
1:3

Bi

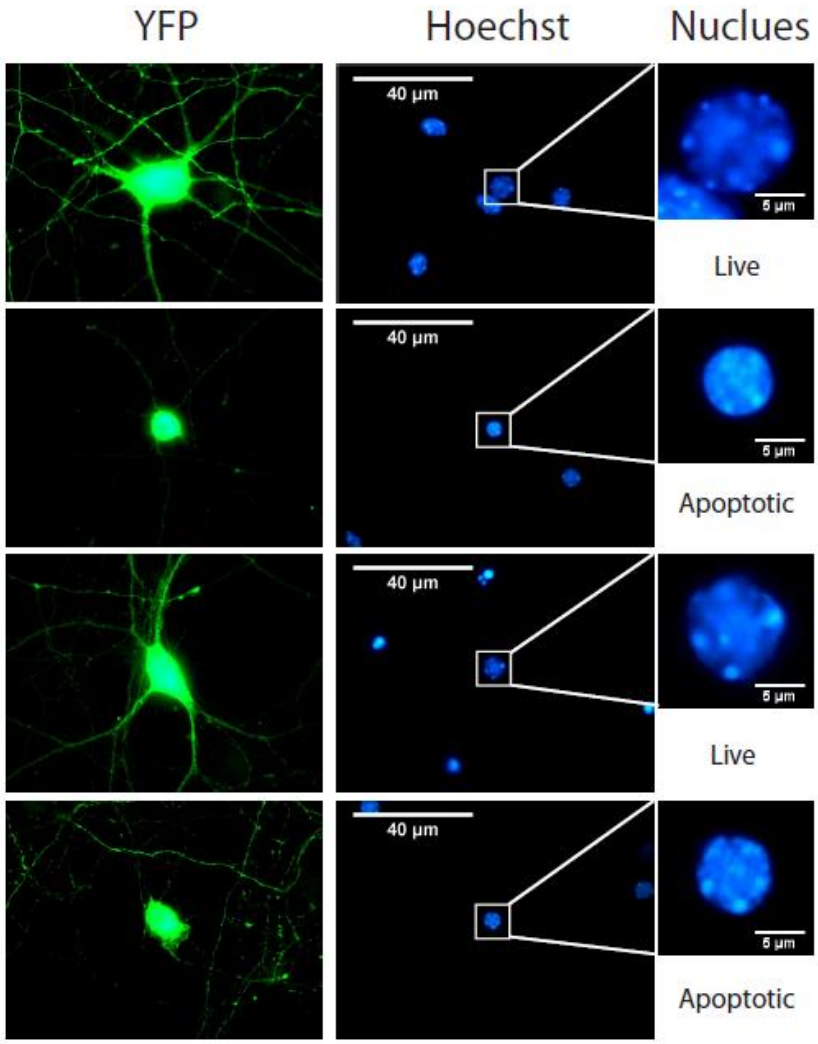
YFP
Hoechst
Nuclues
1:1
1:3
40 µm
5 µm
Live
Apoptotic
Live
Apoptotic

Bii

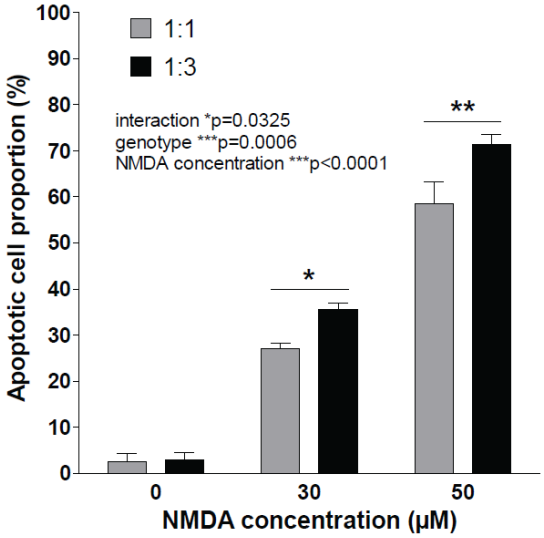
1:1
1:3
interaction *p=0.0325
genotype ***p=0.0006
NMDA concentration ***p<0.0001
Apoptotic cell proportion (%)
NMDA concentration (µM)
0
30
50
*
**

Figure 2-6 Reduction in cortical neuron proportion reduces pro-survival signaling of striatal SPNs and enhances their vulnerability to excitotoxic injury.

Ai. Typical photomicrographs of striatal SPNs (soma) labeled with YFP, whose signal is enhanced with green secondary antibody; cell nuclei are visualized with Hoechst (blue), and pCREB staining is shown in red. ***Aii.*** The nuclear-to-cytoplasmic pCREB ratio is significantly lower in SPNs in coculutres plated at 1:3 vs. 1:1 ratio [n=67(4) for both conditions; paired t-test, *p<0.05]. ***Bi.*** Representative photomicrographs of live and apoptotic striatal SPNs in C-S cocultures plated at 1:1 and 1:3 ratios. Live neurons have a large, loosely compacted nucleus and show abundant dendritic processes, whereas a small, round, compacted nucleus associated with few if any dendritic processes is a signature of an apoptotic cell. ***Bii.*** 1:3 C-S coculture exhibits a higher proportion of apoptotic cells after NMDA challenge (culture batch n=5, 5, and 4 for both 1:1 and 1:3 plating ratios at 0, 30, and 50 μM NMDA; by 2-way ANOVA, interaction *p=0.0325, ratio ***p=0.0006 and NMDA concentration ***p<0.0001; by Bonferroni's post-tests *p<0.05 at 30 μM, and **p<0.01 at 50 μM NMDA).

2.4 Discussion

Cocultures composed of neurons that originate from distinct brain regions that are synaptically connected *in vivo* have become a popular platform to study these connections in a well-controlled *in vitro* system. Although most previous work has combined cortical and striatal neurons in equal numbers to generate C-S connections in culture, we hypothesized that a lower proportion of cortical neurons could more closely recapitulate conditions in the striatum *in vivo*, which receives robust glutamatergic cortical (and thalamic) afferents but is composed of >90% GABAergic medium-sized spiny projection neurons (SPNs). In this chapter, we compared C-S cocultures with two different concentrations of cortical neurons to understand how the ratio of cortical to striatal neurons impacts striatal SPN physiology, dendritic morphology, membrane receptor distribution and vulnerability to excitotoxic stress. Our results indicate that manipulation of cortical-striatal neuronal ratio does not substantially alter many of the striatal neuronal basic membrane properties. However, striatal SPNs in coculture with a lower cortical neuron proportion (plating ratio of 1:3) showed reduced membrane capacitance and dendritic arborization, decreased numbers of excitatory synapses, and enhanced vulnerability to an excitotoxic challenge associated with reduced basal pCREB and an increased proportion of extrasynaptic NMDA receptors.

It is interesting that despite the reduction in cortical neurons and excitatory synapses on striatal SPNs in cocultures plated at the 1:3 ratio, the SPN input resistance, resting membrane potential, and excitability were not substantially changed. On the other hand, SPN resting potential showed a strong trend towards being more hyperpolarized in the 1:3 cocultures. One possible reason for this difference may be in the contribution of leak and/or inwardly rectifying potassium channels. Moreover, in our coculture system, the resting membrane potential was considerably depolarized (~ -51 to -55 mV) compared with the dominant “downstate” resting membrane potential *in vivo* (~

-86mV) (416), and striatal SPNs showed an apparent lack of inwardly rectifying potassium current (Figure 2-1 Di), which would be consistent with the absence of dopaminergic input in our cocultures, as suggested by a previous study (417). Further experiments would help clarify these potential differences. Still, the resting potential of SPNs in coculture with the lower ratio of cortical neurons was relatively closer to that of the *in vivo* condition, as previously reported (418).

We found that the reduction in the density of excitatory synapses along striatal SPN dendrites, as reflected by the colocalization of PSD-95 and vGlut1, was only ~24% for the cocultures plated at the lower cortical ratio, whereas the number of cortical neurons per striatal neuron plated was decreased by ~67%. However, as shown in Table 2-1, further examination revealed that the density of MAP2-positive cells that were DARPP32-negative (putative cortical neurons) in our cocultures was only ~25% lower in the 1:3 vs. 1:1 plating ratio, while the density of DARPP32-positive cells (striatal SPNs) was nearly identical. These results suggest that over the course of development *in vitro*, cortical and striatal cells in our coculture experience a compensatory alteration in rate of differentiation and/or apoptosis, which acts to normalize the relative abundance of cells with different origins. Thus, the modest reduction in functional (~26% for mean mEPSC frequency; not significant) and morphological measures of excitatory synapses of striatal SPNs in the cocultures plated at the lower cortical ratio is roughly commensurate with the modest difference in cortical-striatal SPN cell density. That said, we still cannot exclude the possibility of alteration in cortical glutamatergic presynaptic terminals, such as a compensatory enhancement in synaptic vesicle release probability in 1:3 cocultures, since the combination of reduced SPN dendritic length and synaptic density by immunostaining would predict a more robust, and significant, reduction in mEPSC frequency than we observed.

Some features of striatal SPNs in our cocultures differ from those found in *ex vivo* brain slices or other coculture conditions. Recordings made from SPNs in acute striatal slice from 2-month old mice show mEPSC frequency of ~2.5-3 Hz (102,419), which includes excitatory projections from thalamus as well, whereas SPNs in our cocultures show mean mEPSC frequencies of ~8.3 and ~11.3 Hz for 1:3 and 1:1 plating ratios, respectively. Still, the lower cortical ratio coculture once again more closely matches the *ex vivo* condition than the 1:1 ratio coculture.

Moreover, the density of spines on striatal SPNs that we observed in both sets of cocultures is ~50% that reported in a previous study (411). However, Tian and colleagues (411) started with postnatal day 1 and 2 (P1-2) striatal tissue, which was then cocultured with E17-18 cortical neurons; in this study, we started with E18 cortical and striatal tissue. After 18 days *in vitro*, the striatal SPNs in our cocultures may not have achieved the same level of maturity, which could contribute to the reduced spine density. The reduced absolute cell density at the time of plating in our study compared with that of the previous study could also be a factor.

In this study, we also found that although the overall density of surface NMDA receptors, reflected by the whole cell NMDA-evoked current normalized to cell capacitance, was similar for SPNs from the two coculture conditions, the proportion of extrasynaptic NMDA receptors was increased, suggesting a corresponding reduction in synaptic NMDA receptors, in the 1:3 cocultures. According to a variety of studies (169), such a change in NMDA receptor distribution would be expected to alter cell survival/death signaling and shift SPNs toward enhanced susceptibility to harmful stimuli. Consistent with this idea, we found that basal pro-survival signaling through pCREB was reduced by ~16%, whereas sensitivity to NMDA-induced apoptotic cell death was increased by ~22 – 32% in SPNs from 1:3 cocultures. Thus, as predicted by the

prevailing model (169), in our coculture system the change in NMDA receptor distribution is closely correlated with dephosphorylation of nuclear CREB, and weakening of neuronal health.

Together, our results demonstrate that culture conditions, in this case the plating ratio of two different neuronal types, influence key characteristics of mature cultured neurons. In our studies, cortical neuronal abundance influenced striatal SPN membrane area, dendritic arborization, excitatory synapse numbers, NMDA receptor distribution, pro-survival signaling and susceptibility to stressful stimuli. As well, the lower cortical ratio resulted in striatal SPN resting membrane potential and mEPSC frequency that more closely matched recordings from striatal SPNs in acute brain slice or *in vivo*. Moreover, our data highlight the fact that changes in neuronal type proportion can affect experimental outcome measures, especially NMDA receptor distribution and vulnerability to excitotoxicity.

Chapter 3: Neuroprotective Role of Wild-type Huntingtin in Neurons Originated from Distinct Brain Regions in Cortico-striatal Coculture versus Hippocampal Monoculture

3.1 Introduction

Huntington's disease (HD) is a dominantly inherited neurodegenerative disorder, caused by expansion in the poly-glutamine-encoding CAG repeat of the huntingtin gene, *HTT*; HD occurs when the CAG repeat expands beyond 35 (4). The disease develops progressively and manifests with a movement disorder, along with psychological disturbances and cognitive deficits, over a period of 15 to 30 years until death. HD causes atrophy and neuronal loss in a variety of brain regions (420–422), of which the striatum is most severely affected.

Although HD is thought to result primarily from a gain-of-function mutation in huntingtin (Htt), a variety of studies indicate that loss of wild-type huntingtin (wtHtt) function contributes to pathophysiology (423). Evidence suggests that striatal neurodegeneration in HD is caused, in part, by over-activation of NMDA-type glutamate receptors (NMDAR), especially extrasynaptic NMDAR (297,298,424,425). Interestingly, previous work has shown that wtHtt protects cells from apoptotic death, including NMDAR-mediated excitotoxicity in striatal medium-sized spiny neurons [MSN, i.e. spiny projection neurons (SPN)] in primary culture and *in vivo* (402) as well as 3-nitropropionic acid-induced oxidative stress in an immortalized striatal cell line (329). Although atrophy and neuronal loss occur first in the striatum, cortical (254,422) and hippocampal (3,256) neurons also degenerate in later stages of the disease. Thus, it is of interest to investigate whether Htt can provide neuroprotection for cortical and hippocampal neurons.

cAMP response element-binding protein (CREB) is a cellular transcription factor that binds to cAMP response element (CRE) DNA sequences and thereby modifies downstream gene transcription. Not only does CREB have a well-documented role in neuronal plasticity (426), it also links to cell survival signaling in neurons (427) by increasing the transcription of pro-survival genes. CREB is activated by phosphorylation to form pCREB (phosphorylated CREB), and it has been reported that higher pCREB to CREB ratios correlate with greater transcription of cell survival genes in an undifferentiated cell line (428,429). In the YAC128 mouse model of HD, which expresses human Htt with an ~128 glutamine repeat on FVB/N genetic background, the nuclear pCREB level is reduced in striatum (298) but can be restored by treatment with the extrasynaptic NMDAR-selective inhibitor memantine (304), which also rescues neuropathology and motor function (424). These data suggest that pro-survival signaling, as reflected by nuclear pCREB levels, is correlated with neuronal resistance to cell death, but this relationship has not been tested throughout the brain yet.

Cortical afferent projections are the primary input for the striatum. They are glutamatergic, synapsing mainly on spine heads of medium-sized spiny projection neurons in striatum, and the main source of brain-derived neurotrophic factor (BDNF) that is required for striatal neuronal survival. Many lines of research suggest that cortical BDNF transcription, trafficking and release, which is regulated by wtHtt (135,158), are reduced in cortex of HD (Figure 1-3), both in human patients and animal models (135). BDNF transcription was shown to be regulated by CREB in cortical neurons (430). However, it remains to be determined to what extent striatal neuronal properties are modulated by the cortical projections relative to striatal-itself, such as pro-survival signaling and neuronal resistance to apoptosis via the BDNF signaling pathway.

Here, we used primary hippocampal and cortical-striatal neuronal cocultures to determine whether pro-survival signaling, as reflected in nuclear pCREB levels, and sensitivity to NMDA-induced apoptosis were altered by overexpression of wtHtt. Further, mixed-genotype cocultures, selectively overexpressing wtHtt in cortical vs. striatal neurons, were used to distinguish cell-autonomous from cell-cell interaction effects of wtHtt. Together, our results extend understanding of wtHtt's role in neurons from different brain regions, which may help guide treatment in HD.

3.2 Methods

3.2.1 Transgenic Mice

All data were acquired from neurons of FVB/N wild-type (WT, control) and YAC18 (line 212) mice; the latter express full-length human wtHtt with an 18 poly-glutamine repeat on an FVB/N background (94).

3.2.2 Primary Neuronal Culture Preparation

Animal care and all procedures were approved by the University of British Columbia, according to guidelines of the Canadian Council for Animal Care. All primary neuronal cultures were prepared from embryonic day 18 (E18) WT mice and YAC18 transgenic mice as previously described (125,300). Briefly, the density of cells was approximately 650 cells/mm^2 except for experiments testing excitotoxicity in coculture, in which a density of 436 cells/mm^2 cells was used. Brains were removed rapidly and placed on ice. Striatal, cortical and hippocampal neurons were dissociated from the tissues and counted. On the day of plating (day in vitro – DIV – 0), one cell population (either striatal, cortical or hippocampal) was labeled with yellow fluorescent protein (YFP) plasmid on a β-actin promoter (gift from Ann Marie Craig, the University of British Columbia) (124) for identification from the other by transfecting in electroporation buffer (Mirus Bio. LLC; Madison, WI) with nucleofection (Amaxa; Lonza bio.; Walkersville, MD) according to manufacturer's guidelines. YFP-transfected striatal cells were co-plated with untransfected cortical cells or YFP-transfected cortical neurons were cocultured with untransfected striatal neurons, at a 1:3 ratio (cortical:striatal) for excitotoxicity and 1:1 ratio for all the other coculture experiments, on 12-mm poly-D-lysine pre-coated coverslips in a 24-well plate. YFP-transfected hippocampal neurons were supplemented with the same amount of untransfected hippocampal

neurons and plated. Since >90% of neurons from rodent striatal tissue are medium-sized spiny projection neurons, we refer to striatal neurons as "MSN" throughout.

All cultures were maintained in DMEM (Invitrogen) with 10% fetal bovine serum (DMEM+) for 3 h, then switched to serum-free NeuroBasal plating medium (Gibco), supplemented with B27, penicillin/streptomycin, glutamine (Gibco) in a humidified 37^0C, 5% CO_2 incubator, and refreshed every 5-7 days by a half-medium change.

3.2.3 Excitotoxicity Assay and Immunostaining

The excitotoxicity assay was conducted at DIV14 or 18. *N*-Methyl-D-aspartic acid (NMDA; M3262; Sigma-Aldrich) of different micromolar concentrations was applied to the cultured neurons for 15 min, followed by twice washes with plating medium, and cultures were then switched to conditioned medium for 1 h in a humidified 37^0C, 5% CO_2 incubator to allow apoptosis to develop. Then cells were fixed with 4% paraformaldehyde (PFA) for 30 min, permeabilized with 1% Triton X-100 in PBS for 5min, and incubated with 0.03% Triton X-100 in (PBST) with 10% normal goat serum [NGS; 40 min, at room temperature (RT)]. The neurons were immunostained with chicken polyclonal anti-green fluorescent protein (GFP) antibody (binds to YFP as well; 1,000; ab13970; Abcam) with or without mouse monoclonal anti-phosphorylated CREB antibody (1:500; 05-667; Millipore) in PBST with 2% NGS for 3 h at RT. Neurons were then washed (PBST, ×3), incubated with goat anti-chicken Alexa Fluor 488 (1:1,000; A-11039; Invitrogen) with or without goat anti-mouse Alexa Fluor 568 (1:1,000; A-11031; Invitrogen) in PBST with 2% NGS for 1.5 h at RT, washed again (PBST, ×3), incubated with 5μM Hoechst 33342 (10 min at RT) in PBST, washed again (PBST, ×3), and mounted on slides with Fluoromount-G (0100-01; SouthernBiotech). Cells with round, small, densely compacted nuclei

were counted as apoptotic, whereas those with loosely compacted, large nuclei were regarded as healthy cells (Figure 3-3 A and B); apoptotic neurons were assessed as a proportion of at least 200 total GFP-positive cells in each condition of hippocampal culture, and 50 total GFP-positive cells for corticostriatal (C-S) cocultures. Images for representative photomicrographs and pCREB signal analysis were acquired under a 63× oil lens with Zeiss Axiophot microscope. Nuclear-to-cytoplasmic pCREB ratios were acquired by comparing the average pCREB signal intensity over the entire area of the nucleus to an average of three randomly chosen regions in the cytoplasm (Figure 3-1 A), using ImageJ software (1.47v; NIH, USA).

3.2.4 Drug Treatment

Brain-derived neurotrophic factor (BDNF; 2837-human; Tocris) was applied to the neuronal cultures at DIV10, 14, 17, or 21 at a concentration of 5 nM for 1 or 2 h in 500 μl conditioned medium in a 37^0C, 5% CO_2 incubator. Alternatively, the neuronal cultures were treated with TrkB-Fc (recombinant human TrkB-Fc chimera; 688-TK-100; R & D) of different concentrations (0.7, 1.5, 3, 6 μg/ml) in conditioned medium for 1 or 4 h at 37^0C, 5% CO_2. All treatments were followed by fixation with 4% PFA, permeabilization, blocking, and immunostaining with primary antibodies (chicken polyclonal anti-GFP antibody and mouse monoclonal anti-pCREB^{ser133}) and secondary antibodies (goat anti-chicken Alexa Fluor 488 and goat anti-mouse Alexa Fluor 568) as described above (Excitotoxicity and Immunostaining sections); nuclei were labeled with Hoechst 33342, and slides were mounted as for the excitotoxicity assay. Out of a total of 50 batches of cultures in which pCREB levels were compared with/without BDNF treatment, one (WT hippocampal) showed a >20% decrease in average

nuclear pCREB intensity and nuclear to cytoplasmic pCREB ratio for BDNF-treated compared to untreated neurons within the same culture, these results were excluded from further analysis.

3.2.5 Data Analysis

All data were analyzed, presented as means ± S.E., and figures were created with Prism (4.00, 2003; GraphPad Software). Graphs were built with Adobe Illustrator CC (2014.0.0; Adobe Systems).

3.3 Results

3.3.1 Region-specific Pro-survival Signaling Alteration by wtHtt Overexpression

Scaffolding proteins in the postsynaptic density protein 95 (PSD-95) family facilitate assembly and stabilization of postsynaptic receptors in excitatory synapses (431). Indeed, enhanced levels of PSD-95 in synapses are linked to increased numbers of synaptic AMPA receptors in hippocampal and cortical neurons (432–434). Interestingly, overexpression of wtHtt, in a comparison of primary neuronal cultures from WT vs. YAC18 mice, increased synaptic levels of PSD-95 but failed to alter levels of synaptic AMPA receptors in striatal neurons cocultured with cortical neurons (125), suggesting brain region-specificity. To test if this specificity is a general rule and if it applies to pro-survival signaling, we cultured YFP-labeled striatal neurons with cortical neurons, YFP-labeled cortical neurons with striatal neurons, or YFP-labeled hippocampal neurons with unlabeled hippocampal neurons, and immunostained against pCREB at DIV14, comparing WT and YAC128 cultures (Figure 3-1 A). As our work in the previous chapter (Chapter 2) on C-S coculture suggested that the abundance of cortical neurons has a minor influence on SPN membrane properties, I chose to use a plating ratio of 1:1 cortical-to-striatal neurons (unless otherwise indicated) because of its wide application in previous studies. Because many of these experiments comparing the two genotypes were done in an unpaired manner, using cultures prepared on different days and immunocytochemical staining with different batches of antibodies, the absolute levels of nuclear pCREB fluorescence intensity varied widely between experiments; therefore, the ratio of nuclear to cytoplasmic pCREB levels was assessed within each cell to reduce inter-batch variability. We have utilized this method in previous studies of striatal neurons in this cortical-striatal coculture system (124) and observed a tight correlation between an increase in the

nuclear-to-cytoplasmic pCREB ratio by immunocytochemistry and increased fluorescence from the CRE-luciferase reporter, in response to stimuli known to enhance survival signaling (124).

As shown in Figure 3-1 A and B the nuclear-to-cytoplasmic pCREB ratio to eliminate staining difference from batch to batch (herein referred to as "pCREB ratio") of YAC18 striatal MSN was significantly higher than that of WT (Figure 3-1 Bi). By contrast, this ratio was similar between genotypes in cortical and hippocampal neurons (Figure 3-1 Bii and Biii), suggesting brain region-specific elevation of pro-survival signaling in striatal neurons by wtHtt overexpression. To test whether any genotype differences in the pCREB ratio could be due to a shift from cytoplasm to nucleus, we compared pCREB levels in the cytoplasm of WT and YAC18 striatal neurons in paired experiments. The cytoplasmic pCREB level was similar between the two genotypes (the mean cytoplasmic pCREB for YAC18 normalized to WT is 0.930 in 8 paired coculture experimtents). This result gave us confidence that a change in nuclear-to-cytoplasmic pCREB ratio largely reflected modulation of nuclear pCREB levels.

Previously, we found that presynaptic wtHtt overexpression in cortical neurons (from YAC18 mice) enlarges PSD-95 cluster size in non-transgenic postsynaptic striatal neurons in coculture, likely through enhanced BDNF release from cortical terminals (125). Since BDNF can also induce nuclear CREB phosphorylation via TrkB receptors and activation of mitogen-activated protein kinases (MAPK)/extracellular signaling-regulated kinases (ERK) and phosphoatidylinositol 3 kinase (PI3K)/Akt pathways (435), we tested regional specificity in all three neuronal types by treating with BDNF to upregulate the pro-survival signaling via pCREB. We treated cultured neurons with 5 nM BDNF and measured the pCREB immunostaining two hours later. Since these were paired experiments (comparisons of pCREB levels within the same culture, immunostained at the same time, in wells treated or not with BDNF), we assessed both

absolute nuclear pCREB intensities and the nuclear-to-cytoplasmic pCREB ratio (Figure 3-1 Ci and Cii). In all three neuronal types, the pattern of response to BDNF treatment was identical whether assessed by absolute or relative (nuclear-to-cytoplasmic ratio) pCREB levels. The BDNF-induced elevation in nuclear pCREB was significantly greater in WT than in YAC18 striatal MSN (Figure 3-1 Ci), suggesting that BDNF-induced downstream signaling is relatively occluded in YAC18 striatal neurons. In contrast, the increase in nuclear pCREB was significantly greater in YAC18 than WT cultures for both cortical and hippocampal neurons (Figure 3-1 Ci). The nuclear-to-cytoplasmic pCREB ratio showed the same pattern as nuclear pCREB did (Figure 3-1 Cii). Together, these results indicate that wtHtt regulates pro-survival signaling in a neuronal type- and/or region-specific manner.

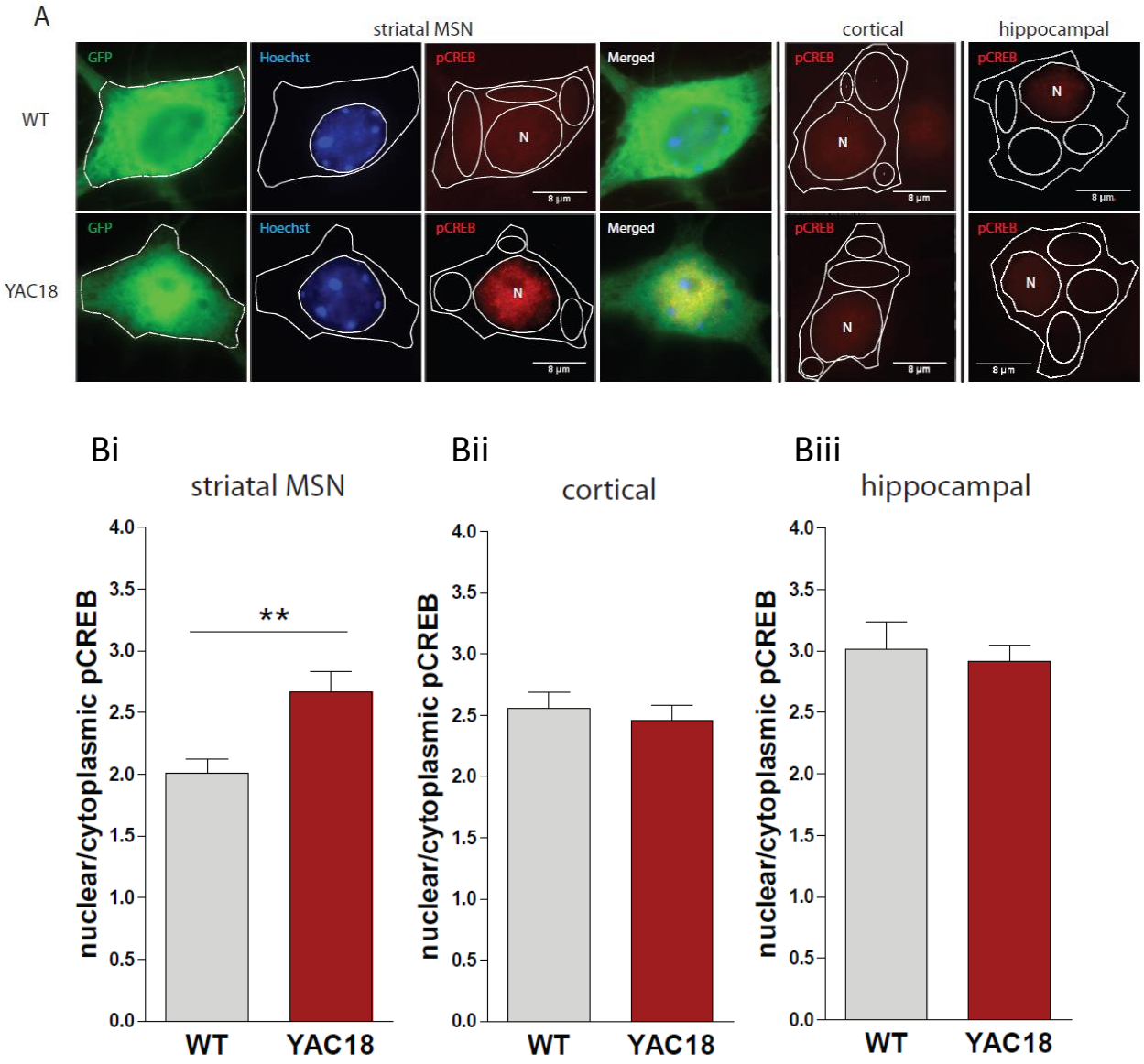
A
striatal MSN
cortical
hippocampal
WT
YAC18
GFP
Hoechst
pCREB
Merged
N
8 µm
Bi
striatal MSN
Bii
cortical
Biii
hippocampal
nuclear/cytoplasmic pCREB
4.0
3.5
3.0
2.5
2.0
1.5
1.0
0.5
0.0
**
WT
YAC18

Ci

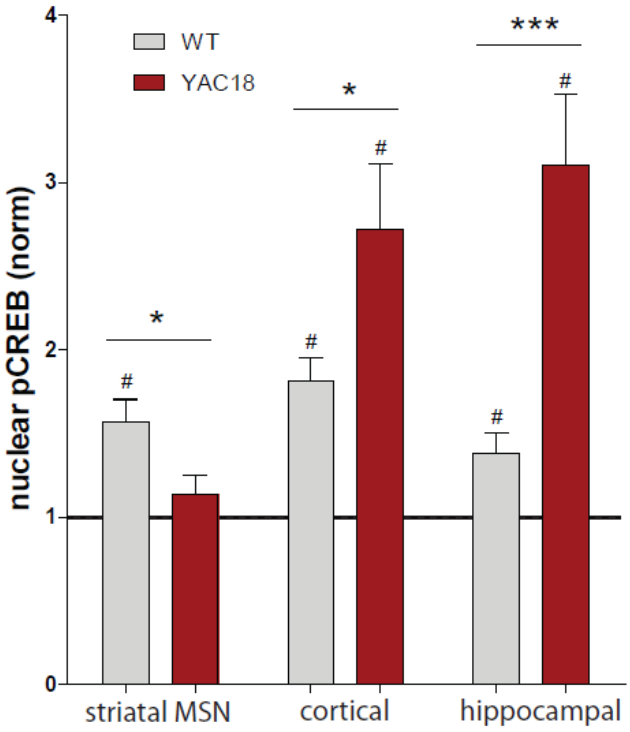
WT
YAC18
nuclear pCREB (norm)
0
1
2
3
4
*
*
***
#
striatal MSN
cortical
hippocampal

Cii

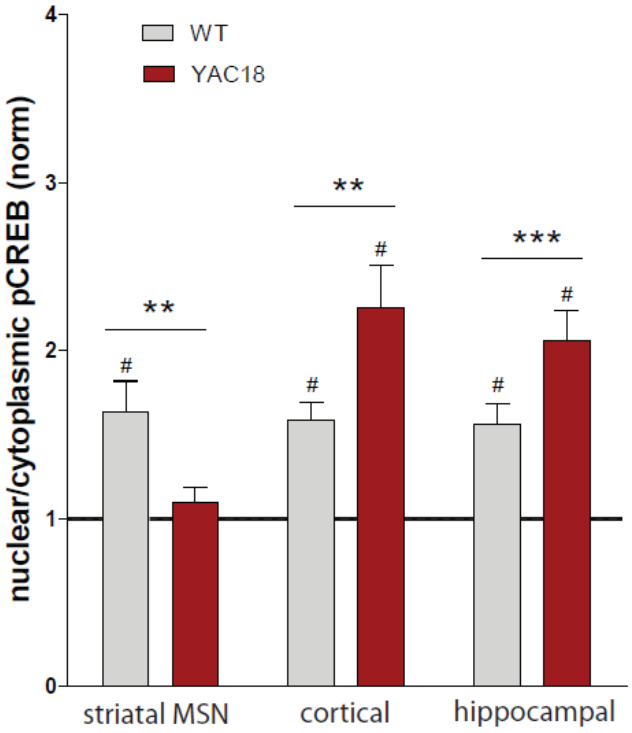
WT
YAC18
nuclear/cytoplasmic pCREB (norm)
0
1
2
3
4
**
**
***
#
striatal MSN
cortical
hippocampal

Figure 3-1 wtHtt overexpression has region-specific impact on phosphorylated CREB levels in YAC18.

A. Representative photomicrographs showing nuclear-to-cytoplasmic pCREB ratio measurement in representative neurons from the striatum, hippocampus and cortex in culture. N indicates the nucleus. ***B.***, ***C.*** Comparison of basal and BDNF-induced pCREB ratio between genotypes in different neuronal types. In all experiments, the number of different neurons measured is indicated as *n*, and the number of independent culture batches is shown in parentheses. wtHtt overexpression enhances the basal pCREB ratio in striatal MSN [***Bi.***: WT n=66(5) and YAC18 n=67(5); by unpaired t-test $**p<0.01$; DIV14], but not cortical [***Bii.***: WT n=60(6) and YAC18 n=62(6); by unpaired t-test $p>0.05$; DIV14] or hippocampal neurons [***Biii.***: WT n=82(8) and YAC18 n=70(7); by unpaired t-test $p>0.05$; DIV14]. Treatment with BDNF (5 nM for 2 h) increases the nuclear pCREB more in WT than YAC18 striatal MSN [***Ci.*** striatal MSN: WT n=40(4) and YAC18 n=40(4); by unpaired t-test $*p<0.05$; DIV17]; in contrast, BDNF enhances the nuclear pCREB more in cortical and hippocampal neurons from YAC18 than from WT mice [***Ci.*** cortical: WT n=50(4) and YAC18 n=35(3); by unpaired t-test $*p<0.05$; DIV17; ***Ci.*** hippocampal: WT n=40(3) and YAC18 n=35(3); by unpaired t-test $***p<0.001$; DIV17]. The nuclear-to-cytoplasmic pCREB ratio showed the same pattern [***Cii.*** striatal MSN: WT n=40(4) and YAC18 n=40(4); by unpaired t-test $**p<0.01$; DIV17; ***Cii.*** cortical: WT n=50(4) and YAC18 n=35(3); by unpaired t-test $**p<0.05$; DIV17; ***Cii.*** hippocampal: WT n=40(3) and YAC18 n=35(3); by unpaired t-test $***p<0.001$; DIV17). # indicates significant increase of nuclear pCREB intensity and the pCREB ratio for BDNF-treated compared with control of same genotype.

3.3.2 Nuclear pCREB Augmentation in Striatal Neurons Requires wtHtt Overexpression in both Cortical and Striatal Neurons

Since the striatum is most susceptible to neurodegeneration in HD, and wtHtt overexpression increased basal pro-survival signaling selectively in striatal MSNs, we next examined the contribution of cortical (presynaptic) and striatal (cell-autonomous) wtHtt overexpression in elevating basal striatal nuclear pCREB levels. We prepared chimeric cocultures of cortical (CTX) and striatal (MSN) neurons from WT and YAC18 mice and measured the pCREB ratio in the striatal neurons. The pCREB ratio was highest in YAC18/YAC18 cocultures, although the difference was only significant when compared with MSN in the WT/WT and WT MSN/YAC18 CTX (by 1-way ANOVA and Bonferroni's posttests; Figure 3-2 A). Moreover, although there was a trend toward increasing pCREB in YAC18 MSN/WT CTX > WT MSN/YAC18 CTX > WT/WT (Figure 3-2 A), there were no significant differences among these groups. These results indicate that overexpression of wtHtt is required in both cortical and striatal neurons to significantly elevate the pCREB ratio in striatal neurons.

Because wtHtt overexpression upregulates transcription of BDNF in cortex (135), we postulated that BDNF conducts signals from cortical to striatal neurons that contribute to the increase in YAC18 striatal nuclear pCREB, as suggested in Figure 3-1 Ci. To further test our hypothesis that an increased BDNF level in wtHtt-overexpressing (YAC18) cortical neurons enhances pro-survival signaling in striatal MSN, we investigated the effect of modulating extracellular BDNF levels on the pCREB ratio over the course of development in WT and YAC18 cocultured striatal MSN. BDNF (5 nM for 1h) brought the pCREB ratio to a similar level in WT and YAC18 at all time-points (not shown), and the fold-increase in pCREB ratio induced by BDNF was greater in WT than YAC18 MSN at DIV14 and 21 (Figure 3-2 B), suggesting saturation of

the pro-survival signaling pathway in YAC18 MSN by BDNF. However, at DIV10 there was no difference in basal (not shown) or BDNF-induced increases in pCREB ratio between WT and YAC18 MSN (Figure 3-2 B), indicating that striatal neurons show a genotype difference only at more mature culture stages. Moreover, we reduced endogenous, extracellular BDNF levels with TrkB-Fc, a soluble scavenger, and found that a 4-fold higher concentration of TrkB-Fc was required to reduce the pCREB ratio by ~40% in YAC18 compared to WT MSNs (Figure 3-2 C). These results are consistent with the idea that overexpression of wtHtt upregulates nuclear pCREB in striatal MSN in part via BDNF signaling – likely as a result of cortical release; however, we cannot rule out a strong striatal cell-autonomous effect on pCREB (see Figure 3-2 A), independent of BDNF, that occludes the effect of modulating extracellular BDNF levels.

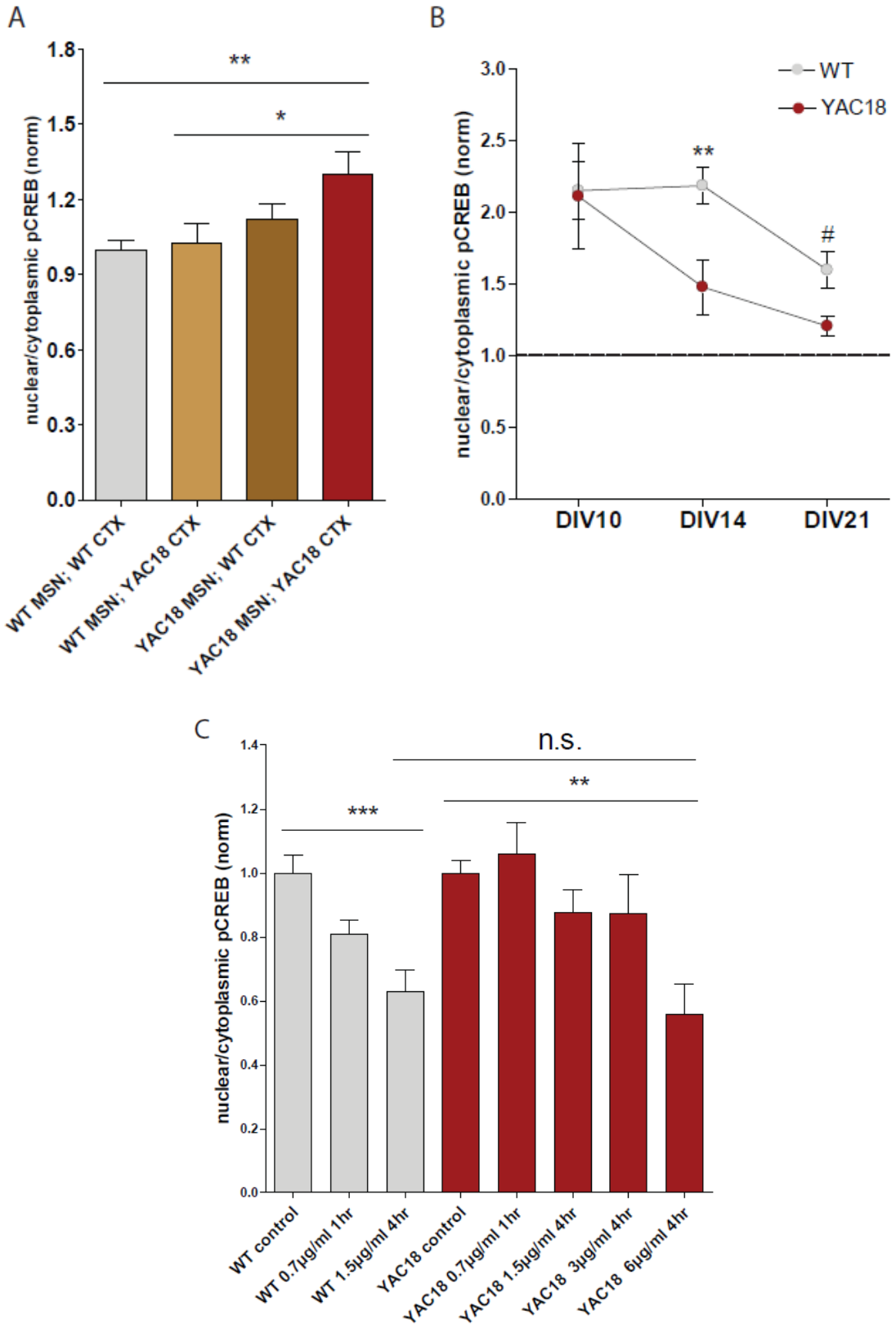
A
nuclear/cytoplasmic pCREB (norm)
1.8
1.5
1.2
0.9
0.6
0.3
0.0
**
*
WT MSN; WT CTX
WT MSN; YAC18 CTX
YAC18 MSN; WT CTX
YAC18 MSN; YAC18 CTX
B
nuclear/cytoplasmic pCREB (norm)
3.0
2.5
2.0
1.5
1.0
0.5
0.0
WT
YAC18
**
#
DIV10
DIV14
DIV21
C
nuclear/cytoplasmic pCREB (norm)
1.4
1.2
1.0
0.8
0.6
0.4
0.2
0.0
n.s.
**
***
WT control
WT 0.7µg/ml 1hr
WT 1.5µg/ml 4hr
YAC18 control
YAC18 0.7µg/ml 1hr
YAC18 1.5µg/ml 4hr
YAC18 3µg/ml 4hr
YAC18 6µg/ml 4hr

Figure 3-2 The basal elevation in pCREB ratio in YAC18 striatal MSN depends on both cortical projections as well as striatal cell-autonomous effects.

A. Nuclear-to-cytoplasmic pCREB ratios measured in striatal MSN in chimeric DIV14 cocultures of cortical and striatal neurons from WT and YAC18 mice. In all experiments, the number of different neurons measured is indicated as *n*, and the number of independent culture batches is shown in parentheses. The basal pCREB ratio is significantly higher in striatal MSN from YAC18/YAC18 compared with WT/WT striatal MSN/cortical cocultures [n=92(8) and n=86(8), respectively; by 1-way ANOVA and Bonferroni's post-test, $**p<0.01$]. wtHtt overexpression in both MSN and CTX significantly increases the pCREB ratio compared with wtHtt overexpression in CTX only (YAC18/YAC18 vs. WT MSN/YAC18 CTX) [n=92(8) and 87(8) in each; by 1-way ANOVA and Bonferroni's post-test, $*p<0.05$]. Also, the basal pCREB ratio for MSN in purely YAC18 cocultures shows a strong trend towards being higher than MSN in cocultures overexpressing wtHtt in MSN only (YAC18 MSN/WT CTX) [n=92(8) and 89(8) in each; by one-way ANOVA and Bonferroni's post-test, t=2.301]. Moreover, there is no significant difference in WT/WT, YAC18 MSN/WT CTX, and WT MSN/YAC18 CTX pCREB ratios. ***B.*** Genotype difference in response to BDNF treatment (5 nM, 1 h) is significant for DIV14 and DIV21 [DIV10, 14, 21: WT n=17(3), 45(4), 32(4) and YAC18 n=19(3), 23(3), 26(5); 2-way ANOVA and Bonferroni's post-test showed DIV10 $p>0.05$, DIV14 $**p<0.01$, DIV21 $p>0.05$, genotype $*p<0.05$, DIV $***p<0.001$, and interaction $p>0.05$; by unpaired t-test, at DIV10 $p>0.05$, at DIV14 $**p<0.01$, and at DIV21 $\#p<0.05$]. ***C.*** A 4-fold higher concentration of TrkB-Fc is required in YAC18 than in WT cocultures to significantly reduce the basal MSN pCREB ratio by 40% (from left to right: WT n=68(8), 38(4), 30(3) and YAC18 n=63(9), 28(3), 18(2), 18(2), 18(3); by 1-way ANOVA and Bonferroni's post-test, 1.5μg/ml for 4hr treatment in WT is significantly

different from control, ∗∗∗p<0.001, whereas in YAC18, only the 6μg/ml for 4hr treatment is significantly different from control, ∗∗p<0.01).

3.3.3 Increased Expression of wtHtt Protects Hippocampal, Striatal, and Cortical Neurons against NMDA-induced Excitotoxicity in Culture

Numerous lines of evidence suggest that early-stage NMDAR-mediated upregulation of cell death pathways contributes to neurodegeneration in later stages of HD (425,436–438). Furthermore, in HD mouse models expression of mutant Htt renders striatal neurons more vulnerable to excitotoxic insults (121,439) via elevating extrasynaptic NMDAR expression (298). In contrast, wtHtt overexpression enhances striatal neuronal survival both *in vitro* and *in vivo* (402). However, the relationship between susceptibility to NMDA-induced apoptosis and basal levels of cell survival signaling as reflected in nuclear pCREB levels has not been fully explored, nor has the functional role of wtHtt in cortical or hippocampal neurons, which also undergo degeneration during the disease progression.

To determine whether wtHtt has a neuroprotective role in neurons from other brain regions, monocultured hippocampal neurons and cocultured cortical-striatal neurons were labeled with YFP at the time of plating for later identification, and challenged with NMDA at a time not earlier than DIV14. Cortical and striatal neurons were plated at a 1 : 3 ratio, as described in a previous study (412) to better represent the physiological condition (Chapter 2). Assessment of apoptosis was based on the nuclear morphology, as described in Methods. Figure 3-3 A and B are excitotoxicity examples from cultured hippocampal neurons. Healthy neurons showed relatively large, polygon-shaped nuclei, whereas apoptotic neurons had small, round nuclei with fewer dendrites, and shrunken soma (Figure 3-3 A). Nuclear size measurement indicated that treatment of hippocampal neurons with 50 μM NMDA for 15 min resulted in a shift to significantly smaller nuclei compared to a nontoxic 5 μM-NMDA treatment (Figure 3-3 B). The same pattern was observed for cortical and striatal neurons. Despite differences in relative pCREB ratios at baseline,

all three neuronal types -- hippocampal, striatal and cortical neurons -- showed significantly less NMDAR-mediated cell death in YAC18 compared with WT cultures (Figure 3-3 Ci, Cii and Ciii), suggesting that neuroprotection by overexpression of wtHtt is not region-specific and is also not well correlated with its effect on pCREB-dependent pro-survival signaling.

A

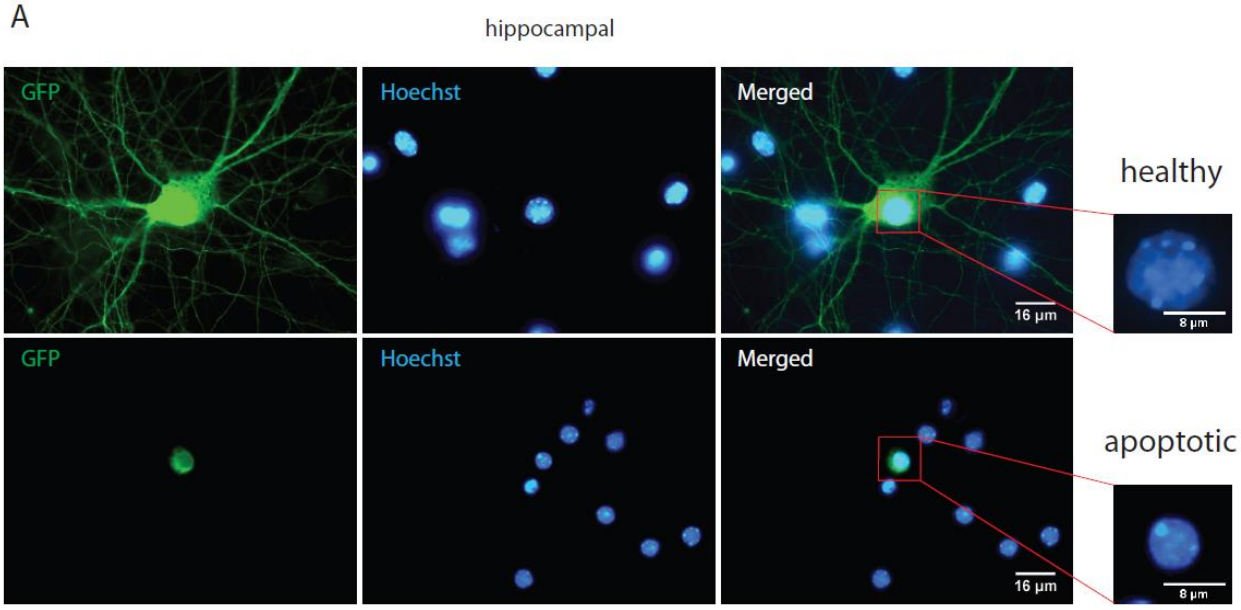
hippocampal
GFP
Hoechst
Merged
healthy
16 µm
8 µm
GFP
Hoechst
Merged
apoptotic
16 µm
8 µm

B

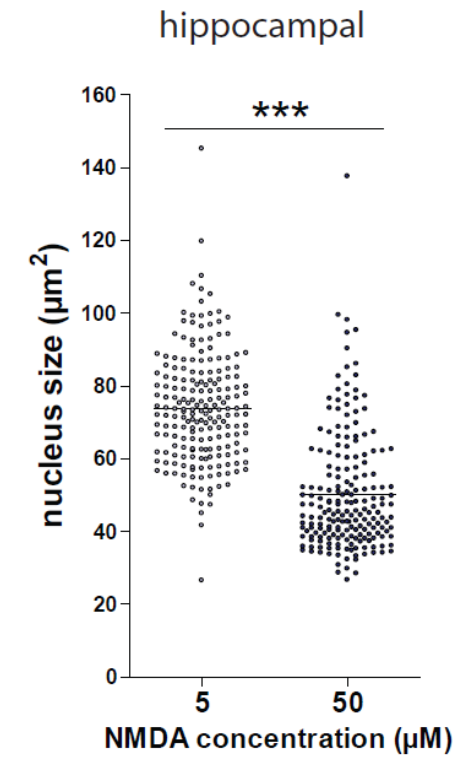
hippocampal
***
nucleus size (µm²)
160
140
120
100
80
60
40
20
0
5
50
NMDA concentration (µM)

Ci

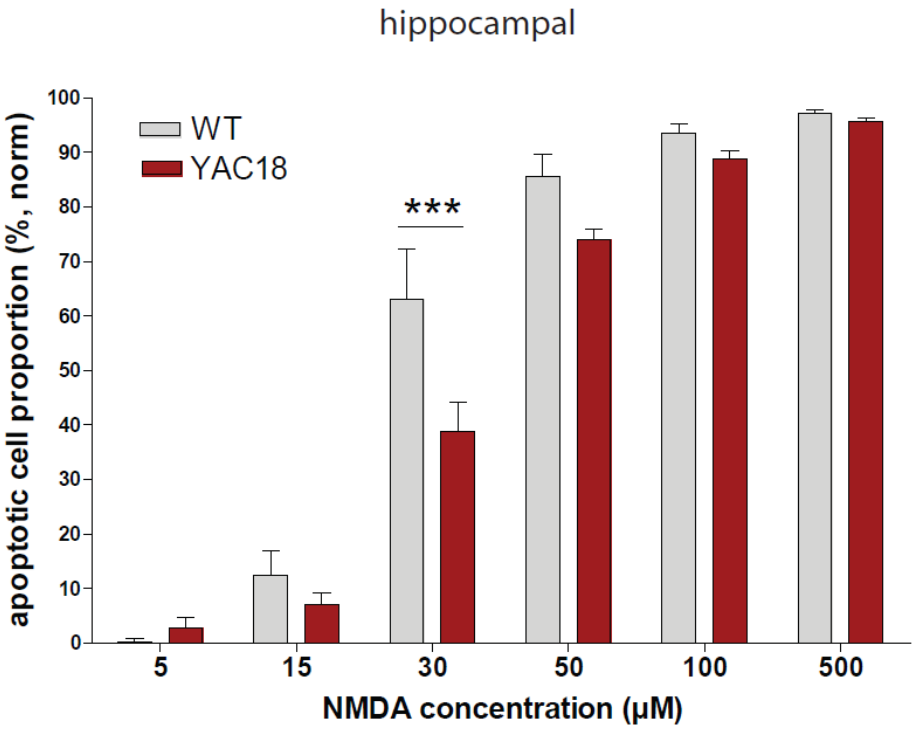
hippocampal
WT
YAC18
***
apoptotic cell proportion (%, norm)
NMDA concentration (μM)
5
15
30
50
100
500

Cii

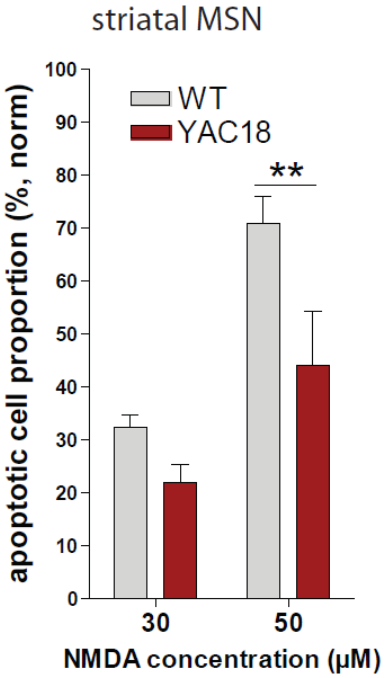
striatal MSN
WT
YAC18
**
apoptotic cell proportion (%, norm)
NMDA concentration (μM)
30
50

Ciii

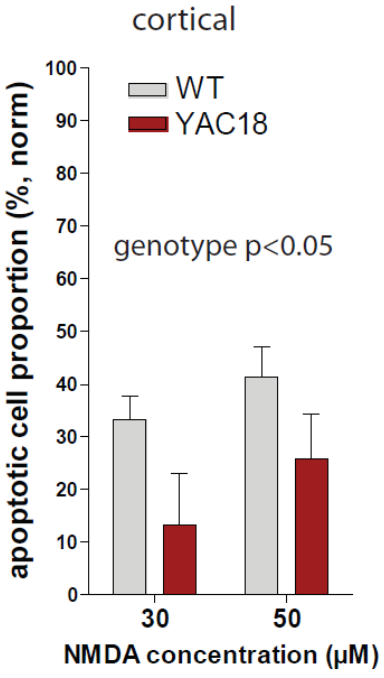
cortical
WT
YAC18
genotype p<0.05
apoptotic cell proportion (%, norm)
NMDA concentration (μM)
30
50

Figure 3-3 wtHtt overexpression protects hippocampal, cortical and striatal neurons, which is not predicted by basal pCREB ratios in those neuronal types.

A. Representative photomicrographs from excitotoxicity assay in hippocampal neurons in monoculture. Healthy neurons have larger, relatively oval, loosely compacted nuclei (upper), whereas apoptotic neurons have smaller, round and condensed nuclei and also lack or have fewer processes (lower). Cortical and striatal neurons also showed same pattern. ***B.*** Representative graph from one experiment in cultured hippocampal neurons shows that 50 µM NMDA dramatically decreases the nuclear size compared with the 5 µM NMDA condition (the number of nuclei assessed was 200 for 50 µM and 197 for 5 µM, respectively; by paired t-test, ∗∗∗p<0.0001). ***Ci.*** Hippocampal neurons are protected from NMDA-induced excitotoxicity in YAC18 compared with WT cultures (normalized to untreated controls; YAC18 n=6 and WT n=6 different batches of cultures; genotype ∗∗p<0.01 by 2-way ANOVA; by Bonferroni's post-tests, at 30µM ∗∗∗p<0.001). ***Cii.*** wtHtt overexpression also protects striatal neurons (normalized to untreated controls; DIV18; WT n=9 at 30 µM and 8 at 50 µM, and YAC18 n=7 at 30 µM and 6 at 50 µM different batches of cultures; genotype ∗∗p<0.01 by 2-way ANOVA; by Bonferroni's post-test, ∗∗p<0.01 at 50 µM) and cortical neurons (***Ciii.***: normalized to untreated controls, DIV18; WT n=8 and YAC18 n=9; Bonferroni's post-test does not show significant difference between individual doses, but by 2-way ANOVA, genotype ∗p<0.05).

3.4 Discussion

Expansion of the CAG repeat over 35 in the *HTT* gene leads to development of Huntington's disease (HD), and extensive study has contributed to understanding the role of mutant huntingtin (mHtt) in disease development, including the pathological alteration of synapses, degeneration of neurons, and regional brain atrophy (28,425,440). Despite discovery of a large number of Htt interaction partners (133,161,171,441) and general function of wtHtt in axonal trafficking, regulation of gene transcription – especially the striatal growth/survival factor BDNF, and neuroprotection in the striatum (161,402,423), little is known about the impact of wtHtt on cell survival signaling pathways. Moreover, because of the imminent implementation of pan-specific Htt knockdown strategies for treatment of HD, there is an increasing necessity for understanding wtHtt function on cell resistance to excitotoxic insults in brain regions affected in HD. Here, we reveal both a tissue-specific role in basal pro-survival signaling and more global impact on neuronal resistance to excitotoxic insult in striatal, cortical and hippocampal neuronal cultures from YAC18 mice, which overexpress wtHtt.

We find that the overexpression of wtHtt provided protection against NMDA-induced apoptotic death in primary cultures of cortical, striatal and hippocampal neurons. These results are consistent with previous reports in many different cell lines, implicating wtHtt in resistance to a variety of insults via interference with formation of the C3/C9 apoptosome and/or caspase 8 activation (164,329,330,442–444). Moreover, wtHtt protects against NMDA-mediated toxicity in primary neuronal cultures from striatum, lacking any cortical synaptic input or BDNF (402). Together with our data showing a universal neuroprotective effect of wtHtt in primary neuronal culture from different brain regions, these studies strongly suggest that modulation of BDNF levels and/or transport and release is not required for wtHtt-mediated neuroprotection.

The attenuated response of YAC18 MSN nuclear pCREB in cortical-striatal cocultures to treatment with exogenous BDNF (Figure 3-2 B) and TrkB-Fc (Figure 3-2 C) is consistent with enhanced BDNF release from YAC18 cortical neurons. Further, the elevated release of BDNF from cortical neurons can reduce the toxic extrasynaptic NMDA receptor signaling to cell-death by via synaptic NMDA receptors (445). However, we cannot exclude the possibility that wtHtt upregulates striatal TrkB receptor expression and/or signaling, especially since overexpression of wtHtt in CTX alone was insufficient to upregulate the pCREB ratio in WT MSN. Many studies indicate that mutant Htt interferes with TrkB receptor trafficking (446), expression (278), and its downstream signaling (279) in striatal neurons. Moreover, recent studies show that TrkB receptor agonists ameliorate neuropathology, motor function and extend survival in HD mouse models (447–449). Liot and colleagues also found that silencing wtHtt reduces vesicular transport of TrkB in striatal neurons (446). Further study is needed to determine whether increased levels of wtHtt can also upregulate the TrkB receptor expression level and/or increase its trafficking.

When activated by phosphorylation, nuclear CREB regulates transcription of hundreds of genes, many of which promote cell survival, such as BDNF (428,429). Notably, previous studies have linked synaptic/extrasynaptic NMDA receptor (NMDAR) activation to regulation of pCREB levels and demonstrated that upregulation of pCREB correlated with resistance to NMDA-induced neuronal apoptosis in hippocampal (168) and cortical cultures (450). Those experiments assessed pCREB response to acute NMDAR stimulation, and one study showed that activation of the calcium-dependent phosphatase calcineurin mediated CREB shut-off upon bath application of NMDA while enhanced synaptic NMDAR activity increased pCREB via CaMKIV and ERK activation (450). By extension, a variety of studies have assumed that basal pro-survival signaling, as reflected in nuclear pCREB, is predictive of resistance to neurodegeneration (168,304,450). Our

results challenge this idea, since the ratio of phosphorylated CREB in the nucleus, as normalized to cytoplasmic levels, prior to NMDA application, was not predictive of neuronal resistance to NMDA-induced apoptosis. This is particularly surprising given reports that CREB activation results in enhanced expression of PGC1-α (451,452), a transcriptional regulator of energy metabolism genes, whose expression shows an inverse correlation with levels of extrasynaptic NMDARs in cortical and striatal neurons (453) and that provides resistance against excitotoxicity (453–456). On the other hand, resistance to NMDAR-mediated apoptosis mediated by overexpression of wtHtt in YAC18 striatum is not likely to occur via down-regulation of extrasynaptic NMDAR levels, as these are similar for wild-type and YAC18 striatal tissue (298). Further studies are required to determine the precise mechanisms of wtHtt-mediated protection from NMDAR toxicity.

Together, our results suggest wtHtt confers region-specific basal pro-survival signaling, but a global neuroprotection for neurons with different tissue origins. This provides us with further understanding of wtHtt function, and may assist us in developing effective therapeutics against HD.

Chapter 4: Mutant Huntingtin Impairs Cortico-striatal Connections in both Cortico-striatal Coculture and Early-symptomatic Huntington's Disease Mouse Model

4.1 Introduction

Neurodegenerative disorders are characterized by progressive neuronal death; however, substantial variability exists in the rate, magnitude and neuronal selectivity of cell death. Despite this variability, a recent surge of evidences indicate that early synaptic dysfunction can be detected well in advance of cell death in neurodegenerative diseases (457–459). The emerging view that such diseases are initially disorders of the synapse, or "synaptopathies," is accompanied by the hypothesis that early interventions aimed to restore synaptic functions are likely to provide greater therapeutic value than belated attempts to prevent cell death when neurons have been severely compromised (26). This highlights the importance of understanding the specific mechanisms of early synaptic dysfunction associated with neurodegenerative disease.

Huntington's disease (HD) is a neurodegenerative disorder that has strong evidence for synaptic dysfunction preceding cell death (26,28). HD is caused by a mutation in gene *HTT*, which results in a toxic gain of function of protein huntingtin (Htt) and can also interfere with the normal physiological function of Htt (460). Htt is known to interact with a wide variety of intracellular proteins, many of which are responsible for synaptic neurotransmission (171), and the mutant Htt (mHtt) or altered expression of wild-type Htt (wtHtt) can influence its interaction with, and the localization of, synaptic proteins (125,298,303,461). The effects of mHtt are particularly striking

in the striatum, and therefore, most studies have focused on the synaptic dysfunction that occurs at a major excitatory projection to the striatum; the cortico-striatal (C-S) synapse.

Cortical projections to striatal spiny projection neurons (SPNs), the most vulnerable cell type in HD, represent the predominant excitatory input to this region, and the majority of excitatory synapses in the striatum are comprised of vesicular glutamate transporter 1 (vGlut1)-expressing cortical terminals that synapse onto SPN dendritic spines (119). Our lab and others have studied this synapse in relative isolation through the use of a cell coculture model in which embryonic or early postnatal cortical neurons are simultaneously grown on coverslips with striatal neurons. Under such conditions, robust excitatory connectivity develops between the cortical and striatal neurons (124,406). As cell cultures are highly amenable to genetic manipulation and therapeutic screening, the C-S coculture system may provide a useful platform for identifying both the mechanisms underlying HD-associated synaptic dysfunction as well as potential treatments that may prevent or restore these synaptic alterations. Indeed, in the YAC128 mouse model of HD, we have previously shown that the early increase in cell death-associated extrasynaptic NMDA receptors detected in brain slice is also recapitulated in this coculture model, suggesting that at least some of the synaptic phenotype observed in animal models can be modeled in this isolated system.

From animal models, it has been reported that the *HTT* mutation can also affect release probability at C-S synapses, promote the loss of C-S connectivity and SPN dendritic complexity, and reduce cell survival signaling, in a disease stage-dependent manner (197,312,398,462). Here, we used C-S cocultures from wild-type (WT; FVB/N) and YAC128 mice to study C-S synaptic connectivity, SPN morphology and intracellular signaling as the cocultures developed up to three weeks *in vitro*. Our results demonstrate that a number of HD-associated synaptopathic features are

recapitulated in cocultures within this three-week period. We discuss the potential value of this system to unlocking the mechanisms and treatment of synaptic dysfunction in HD.

4.2 Methods

4.2.1 Culture Preparation

All procedures were approved and guided by the University of British Columbia Committee on Animal Care and Canadian Council on Animal Care regulations. Cultures were prepared on embryonic day 17-18 (E17-18) from wild-type (WT) FVB/N mice and/or transgenic YAC128 (line 55; FVB/N background) mice expressing full-length human Htt with 128 CAG repeats (90). Cocultures were prepared and maintained as previously described (125,299).

4.2.2 Electrophysiology

Whole cell patch-clamp recordings were performed with an Axopatch 200B amplifier and pClamp 10.2 software (Molecular Devices; Palo Alto, CA). Yellow fluorescent protein (YFP)-expressing SPN were targeted for recording at various stages of coculture development, which are described in the text. Cells were clamped at -70 mV and intrinsic membrane properties were determined by the current response to a 10 mV hyperpolarizing step applied immediately after achieving whole cell access. For all experiments, a series resistance of up to 25 MΩ was tolerated, with the large majority of recordings under 20 MΩ. Striatal SPNs were identified for assessment based on intrinsic membrane properties (membrane resistance, Rm < 500 MΩ and membrane capacitance, Cm > 30 pF). mEPSCs were recorded in artificial cerebrospinal fluid (ACSF) containing (mM): 167 NaCl, 2.4 KCl, 10 Glucose, 10 HEPES, 2 $CaCl_2$, 1 $MgCl_2$, 0.05 picrotoxin (PTX; to block $GABA_A$ receptors), 0.0003 tetrodotoxin (TTX; to block action potentials), pH 7.3 with NaOH, 310-320 mOsm. The recording electrode (3-6MΩ) was filled with internal solution containing (mM): 145 K-Gluconate, 1 $MgCl_2$, 10 HEPES, 1 EGTA, 2 MgATP, 0.5 Na_2GTP, pH 7.3 with KOH, 280-290 mOsm. For miniature inhibitory postsynaptic currents (mIPSCs), cells

were also clamped at -70 mV, but with a high chloride internal solution containing (mM): 145 CsCl, 1 $MgCl_2$, 10 HEPES, 1 EGTA, 2 MgATP, 0.5 Na_2GTP, pH 7.3 with CsOH, 280-290 mOsm. The ACSF used for mIPSCs was as above, except with 10 µM DNQX (to block AMPA-type glutamate receptors) instead of PTX. Both mEPSCs and mIPSCs were recorded for approximately 2 min; typically, 100-1000 consecutive events were analyzed per cell.

To assess the size of the readily-releasable pool (RRP) of presynaptic vesicles (463), ACSF containing 500 mM sucrose was applied for 4 seconds through a theta tube placed in close proximity to the recorded cell, controlled by pressure system (MILJOCO) and six channel valve controller (Warner Instrument Corporation). Recording conditions were as above (in the first paragraph of section 4.2.2) for mEPSCs (for excitatory vesicles) or mIPSCs (for inhibitory vesicles). The rate of replenishment of the RRP was assessed by a second application of sucrose 3 seconds after the termination of the first application in initial experiments, and later with various inter-pulse intervals (1, 4, 7, 10, 13, 16 and 30 s) for both excitatory and inhibitory vesicle pools.

In experiments where cortical neuronal action potential firing rate was assessed, membrane potential was recorded in response to various current injections as previously described (Chapter 2, methods section).

Recovery of the excitatory RRP in acute brain tissue was examined on C-S slices prepared from 6-month old WT and YAC128 mice, as previously described (91). Briefly, 6-month mice were anaesthetized with isoflurane and sacrificed, their brains were rapidly collected and sliced (300 µm; sagittal plane) with a vibratome (VT 1200S; LEICA) in oxygenated (95% O_2 and 5% CO_2), ice-cold, low-Ca^{2+} ACSF [consisted of (mM): 125 NaCl, 2.5 KCl, 25 $NaHCO_3$, 1.25 NaH_2PO_4, 2.5 $MgCl_2$, 0.5 $CaCl_2$ and 25 glucose; pH 7.3-7.4; ~310 mOsm]. Whole cell patch-clamp was conducted in a recording chamber perfused with oxygenated ACSF (containing 1 mM

Mg^{2+}, 2 mM Ca^{2+} and 100µM PTX) on striatal SPNs identified by their characteristic membrane properties [typically Cm > 90 pF, 400> Rm >100 MΩ and membrane Tau >1 ms). Recording pipettes were filled with internal solution containing (mM): 130 caesium methanesulphonate, 5 CsCl, 4 NaCl, 1 $MgCl_2$, 5 EGTA, 10 HEPES, 5 QX-314, 0.5 GTP, 10 Na_2-phosphocreatine and 5 MgATP; pH 7.3; 280-290 mOsm]. Paired electrical train stimuli (300-500 µA; 20 Hz, 4 s) with changing inter-train intervals (1, 4 and 7 s) was generated within corpus callosum, 150-450 µm away from the recorded cell, with a glass pipette (0.5-1 MΩ) filled with recoding ACSF, allowing a 60 s full-recovery interval between pairs. Cells with shifted baseline, access resistance >25MΩ, an area-under-curve <20,000 pA x ms in response to the initial train stimuli, or with a decreasing recovery percentage against increasing inter-train intervals were removed from the final data.

All electrophysiological data were analyzed in Clampfit software (10.2; Molecular Devices).

4.2.3 Imaging with Intensity-based Glutamate-sensing Fluorescent Reporter

Expression of the intensity-based glutamate sensing fluorescent reporter (iGluSnFr) in 4- to 6-week old WT and YAC128 mice was achieved as previously reported (327) by *in vivo* injection of 1µl of AAV2/1.hSyn.iGluSnFr.WPRE.SV40 (327) into the striatum. The stereotaxic co-ordinates were (in mm): 0.75 anterior, 2.0 lateral, 2.5 ventral with respect to Bregma. At 6 months of age, mice were anaesthetized with isoflurane and sacrificed, the sagittal brain slices (300µm in thickness) of cortex and striatum were obtained using a vibratome in chilled, low-Ca^{2+} ACSF as described previously (327). After 30 to 40 min-recovery in 37^{o}C with constant oxygenation in recording ACSF, the slice was moved to a recording chamber perfused [2-3 ml/min at room temperature (RT)] with oxygenated ACSF containing PTX (100µM). A tungsten micro-

electrode (tip diameter 2-3 µm; E30030.1A5; MicroProbes) was placed in the corpus callosum next to the dorsal striatum where iGluSnFr was highly expressed. The fluorescent signal was produced by a 470-nm LED and recorded with a CCD camera (1M60; Pantera; Dalsa) installed with a pair of lenses (50 mm, 1.4f; 135 mm, 2.8f) and a 530-nm bandpass filter. The baseline fluorescence intensity was typically between 800 and 2,000 in a 12-bit scale after manual adjustment of the LED intensity. The electrical stimulation and light were controlled with Clampex software, A-M systems isolated pulse stimulator (Model 2100) and stimulus isolator (A385; World Precision Instruments). A series of images (128 x 128 pixels) were generated with XCAP software (EPIX; 150Hz; 8 x 8 pixel binning) (327).

To examine action potential (AP)-dependent vesicle release, the baseline response was established as the average response to six stimuli (in pairs, 10-ms apart, each with 300 µA intensity) applied at 30s intervals, followed by a train stimulation (100Hz for 500ms) with the same intensity stimulus. For assessing RRP recovery in acute slice with iGluSnFr, pairs of train stimulation (100Hz for 500ms) with 60-s full-recovery time between pairs, were used with incrementing inter-train intervals (4, 7 and 10 s). The images were processed as previously described (327) in ImageJ software (NIH) with the exception that a 6 x 6 pixel region of interest (ROI) was adopted throughout the analysis.

4.2.4 Cell Death Analysis, pCREB and Synaptic Protein Immunoflurescence

To quantify nuclear localization of phosphorylated cAMP response element-binding protein (pCREB), cells were fixed at DIV14 or DIV21, as indicated, in 4% paraformaldehyde (PFA) + 4% sucrose for 15-20 min, washed with phosphate-buffered saline (PBS), permeabilized with PBST (1% Triton-X in PBS) and blocked for 45 min with normal goat serum (NGS; 10% in

PBST). Cultures were then incubated with a mouse monoclonal anti-pCREB antibody (1:500; 05-667; Millipore) together with a chicken anti-GFP antibody (1:1,000-1:2,000; ab13970; AbCam) in 2% NGS-containing PBST at RT for 3 h under 40 rpm agitation. After thorough washing with PBST, cultures were incubated with goat anti-mouse Alexa 568 (1:1000; A-11031; Invitrogen) and goat anti-chicken Alexa 488 (1:1000; A-11039; Invitrogen) secondary antibodies in 2% NGS-containing PBST for 1.5 h at RT with 40 rpm agitation. Following another extensive wash with PBST, coverslips were subject to 10 min of Hoechst 33342 staining (5μM; Invitrogen), followed by a final wash prior to mounting on glass slides (2948-75×25; Corning) with Fluoromount-G (0100-01; SouthernBiotech). Images were acquired with a Zeiss Axiovert 200M epifluorescence microscope (63x magnification; 1.4 NA) running ZEN 2012 software (Zeiss). Using a z-step of 0.23 μm, 10-15 images were taken per cell and the best 3-5 sections, including the focal planes of the cell body, were flattened using the extended focus function within the ZEN 2012 program. Flattened images were saved as TIFF files and imported into ImageJ, where they were analyzed for pCREB fluorescence intensity in the nucleus (defined by Hoechst staining) and in the cytosol (defined by the average of three regions of interest drawn within the YFP-filled cell body but outside of the Hoechst-stained nucleus; these were drawn to optimize coverage of the maximum cytoplasmic area). The nuclear-to-cytoplasmic (n/c) ratio was calculated by dividing the nuclear pCREB staining intensity by the average of the 3 regions of cytoplasmic pCREB staining intensity.

To characterize cell survival, cocultures were immuno-stained to visualize neurons and striatal SPNs. After fixation, cells were permeabilized and blocked as above. Neurons were identified with an anti-microtubule-associated protein 2 antibody [MAP2; 1:200; MA5-12823; Thermo Scientific; Alexa Fluor 568 (1:1,000; A-11031; Invitrogen) was used as secondary antibody], whereas striatal SPNs were distinguished with an antibody against dopamine and cAMP

regulated phosphoprotein 32 [DARPP-32; 1:500; 2306S; Cell Signaling Technologies; Alexa 488 (1:1,000; A-11008; Invitrogen) was used as secondary antibody] by immunocytochemistry as described in a previous chapter (Chapter 2, Methods). Hoechst staining was used to visualize all cell nuclei and to discern live cells based on nuclear morphology (Chapter 2, Methods). Pictures were taken and data were processed as in Chapter 2.

For synaptic receptor protein staining, cells were live-stained for AMPA receptor subunit GluA2 using a previously published protocol (464). Live cells were incubated at 37˚C and 5% CO_2 with mouse anti-GluA2 antibodies (1:200; Millipore) diluted in plating medium for 1 h, followed by 1.8 mL of plating medium for another 1 h. Coverslips were then fixed with 4% PFA and 4% sucrose for 20 min and washed 3 times with PBS. Coverslips were blocked in PBS with 10% normal goat serum (NGS; 30 min at RT) and incubated with secondary antibodies for 1.5 h at RT. The secondary antibody mixture consisted of Alexa Fluor 568-conjugated goat anti-mouse (1:500; A11031; Invitrogen) diluted in PBS with 2% NGS. Cells were washed three times with PBS and then permeabilized with methanol (5 min at -20˚C), washed three more times with PBS, and incubated in PBS with 0.03% Triton X-100. Coverslips were blocked in PBS with 10% NGS (30 min at RT) and incubated with primary antibodies for 1 h at RT and then overnight at 4˚C. The primary antibody mixture consisted of guinea pig anti-vGlut1 (1:1000; AB5905; Millipore) and the chicken anti-GFP diluted in PBS with 2% NGS. Coverslips were washed three times with PBS and then incubated with secondary antibodies for 1.5 h at RT. The secondary antibody mixture consisted of AMCA-conjugated donkey anti-guinea pig (1:100; 706-155-148; Jackson ImmunoResearch Laboratories) and Alexa Fluor 488-conjugated goat anti-chicken (1:1000; A11039; Invitrogen). Coverslips were washed three times with PBS and then slide-mounted with Fluoromount-G. Images were acquired at 63x as above for the pCREB experiments. Exposure

times were kept constant throughout the experiment. The TIFF images were imported into ImageJ and a region of interest (ROI) was drawn around one dendrite in each image according to the YFP signal. This ROI was then superimposed onto the GluA2 and vGlut1 images, which were then manually thresholded within the ROI to eliminate background while preserving puncta staining. All thresholding was done with genotypes interleaved and experimenter blinded to genotype. The binary thresholded images were then analyzed for puncta size, density and co-localization using the Analyze Particles tool and the co-localization plug-in for ImageJ. Values for the ROI in the three images for each cell were averaged to generate a mean value for each cell.

The same protocol was applied for synaptotagmin1 (Syt1) and cysteine string protein (CSP). The antibodies used for staining: is mouse-anti-Syt1 (1:10,000; MAB4364; R&D) as primary and Alexa Fluor 568-conjugated goat anti-mouse (1:1,000; A11031; Invitrogen) as secondary antibody for Syt1; polyclonal rabbit-anti-CSP (1:3,000; ADI-VAP-SV003-E; Enzo) as primary and Alexa Fluor 488-conjugated goat anti-rabbit (1:1,000; A11008; Invitrogen) as secondary antibody for CSP. Images were taken under confocal microscope.

In order to evaluate vesicle release at C-S synapses, striatal SPNs were transfected with a PSD95-GFP construct when plated with cortical neurons. At DIV21, the Syt1 luminal domain was live-stained by incubating cocultures with a rabbit polyclonal anti-Syt1 antibody (1:200; 105 103C5; Synaptic Systems) tagged with Oyster®650 in plating medium (Neurobasal medium with B27, penicillin/streptomycin and glutamine; Gibco) for 5, 10 and 20 min when assessing AP-dependent, and for 30, 60 and 90 min with TTX (0.3µM) when measuring AP-independent vesicle release, in a 37^{o}C, 5% CO_2 humidified incubator. The vehicle-only condition was DMSO (1:200) in plating medium. Coverslips were fixed, permeabilized, blocked, and incubated in primary antibodies (the chicken anti-GFP antibody and the guinea pig anti-vGlut1 at 4 ^{o}C overnight as

previously described) and secondary antibodies (Alexa Fluor 488-conjugated goat anti-chicken antibody and the AMCA-conjugated donkey anti-guinea pig as above described) prior to being mounted onto slides with Fluoromount-G. Pictures were taken using an epifluorescence microscope under 63x objective (oil lens). Entire dendritic tree was selected with automated thresholding and opposed to vGlut1 channel which was thresholded manually in ImageJ software (NIH, USA) in order to remove background signals, while the experimenter was blinded to the conditions. vGlut1 puncta were further used to generate ROIs for these puncta with the analyze particle tool. Syt1 puncta intensity in raw picture was measured under vGlut1 puncta mask and used as final data.

4.2.5 SPN Morphology

The SPN morphology and protrusions were visualized by YFP staining. Images were acquired and flattened as above. The protrusion density was manually determined for each cell by counting the number of protrusions (0.3-3 μm in length) under 63x from three different dendritic branches (typically 40-120μm away from soma) that were at least 40 μm away from the soma. In order to examine the dendritic complexity, one image was acquired for each cell at 20x with the soma in the center and YFP-expressing neurons were traced manually in ImageJ. An ImageJ plugin (http://fiji.sc/Sholl_Analysis) was used for Sholl analysis to detect the number of dendritic crossings with concentric circles – ranging from 10 - 157.5 μm in radius – radiating out from the center of the soma. In all cases of counting and tracing, the experimenter was blinded to the condition.

4.2.6 Statistical Analysis

All statistics were performed in GraphPad Prism. Reported n-values refer to the total number of cells analyzed from a minimum of 3, and typically 4 or more, independent cocultures unless described elsewhere. For slice electrophysiological experiments, n-values indicates the number of acute brain slices for analysis, while the number of mice is shown in parenthesis. Two-way ANOVA and unpaired (2-tailed) t-tests were used throughout and is indicated in the text. Bonferroni's post-tests were used subsequent to overall ANOVA significance. All data are reported as mean ± s.e.m. and p-values less than 0.05 were considered significant.

4.3 Results

4.3.1 Cell Survival in Cortical-striatal Coculture by Three Weeks *in vitro*

Many lines of evidences suggest that Huntington's disease (HD), particularly in its early stages, can be classified as a synaptopathy, in which subtle alterations in synaptic function are detectable well in advance of cell death (28,298). Thus, we were interested in asking whether a distinct synaptopathic phenotype could be observed at C-S synapses in a coculture system obtained from YAC128 mice that express full-length human mutant *HTT*. To study C-S connections at a time point when synaptic malfunctions are present but cell survival is still comparable between the disease and wild-type conditions, we characterized the health status of C-S cocultures (cortical:striatal = 1:1) at day *in vitro* 21 (DIV21), prepared from WT (FVB/N) and YAC128 embryonic mice. The cells were stained/immuno-stained for nuclei (with Hoechst), microtubule-associated protein2 (MAP2, a neuron-specific protein) and dopamine- and cAMP-regulated neuronal phosphoprotein 32 [DARPP32, which is highly enriched in striatal spiny projection neurons (SPNs)]. We found that the densities of live cells, MAP2-positive cells and DARPP32-positive cells were comparable between WT and YAC128 in DIV21 C-S coculture (Figure 4-1 A, B, C and D). As expected, nearly all DARPP32-positive cells were MAP2-positive (Figure 4-1 E). These data indicate that there is neither a decrease in live neurons nor in SPNs for YAC128 vs. WT cocultures by three weeks *in vitro.*

A

WT

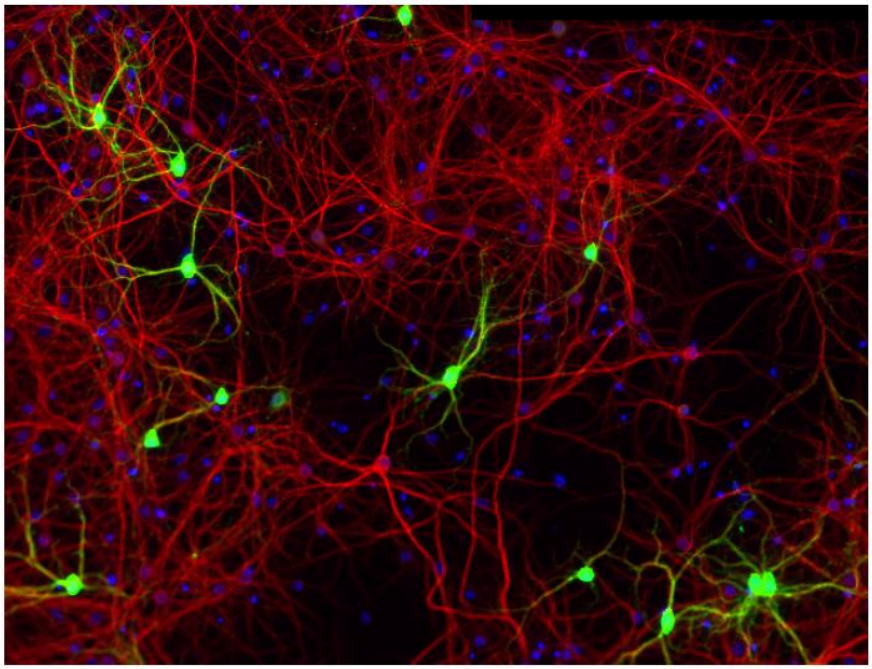

YAC128

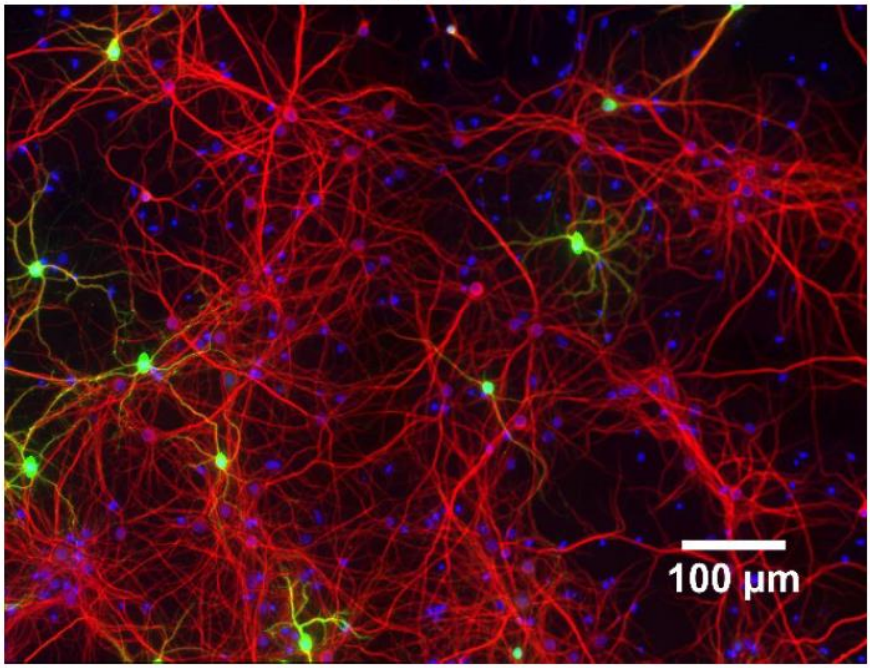

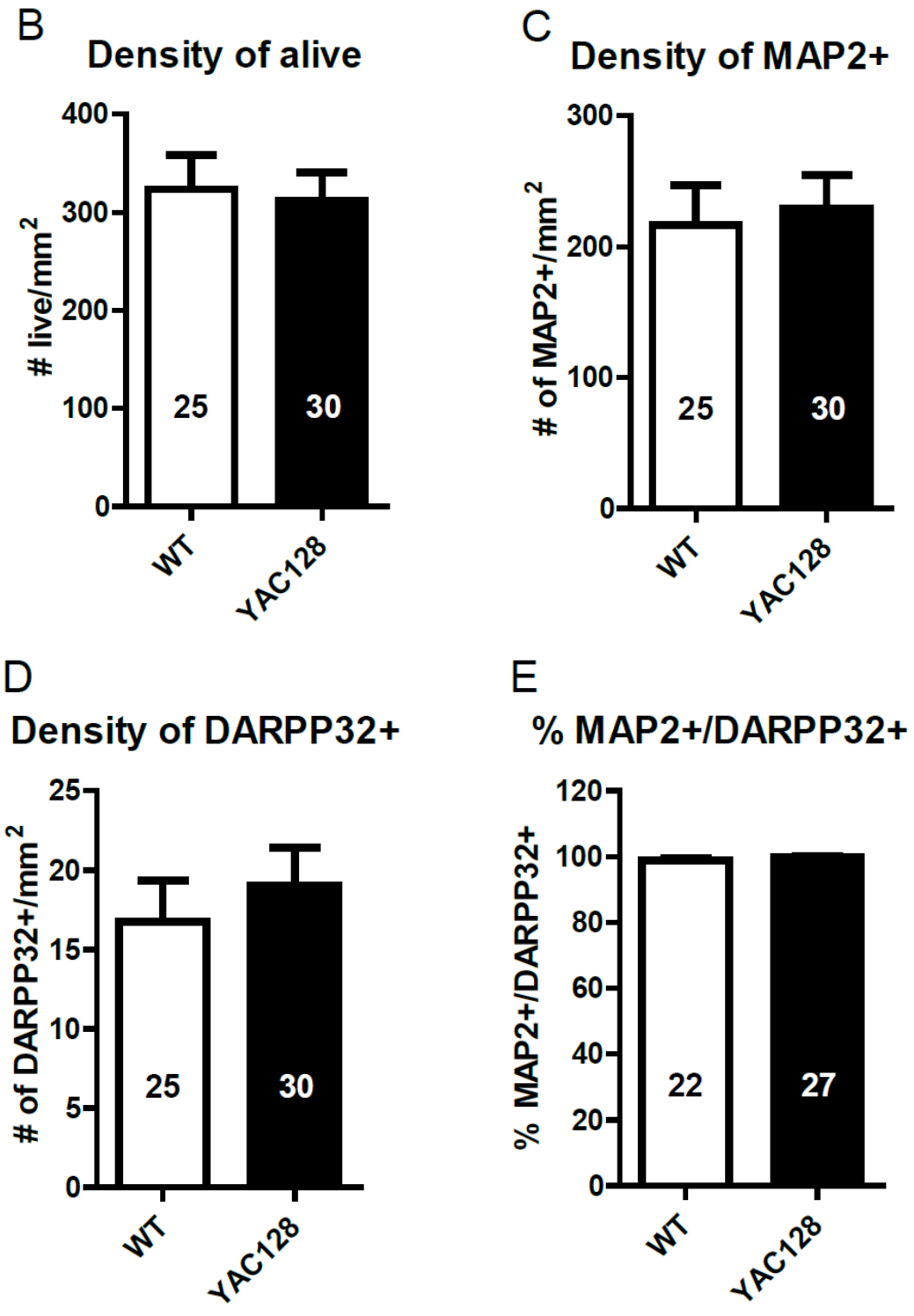
B
Density of alive
live/mm2
400
300
200
100
0
25
30
WT
YAC128
C
Density of MAP2+
# of MAP2+/mm2
300
200
100
0
25
30
WT
YAC128
D
Density of DARPP32+
# of DARPP32+/mm2
25
20
15
10
5
0
25
30
WT
YAC128
E
% MAP2+/DARPP32+
% MAP2+/DARPP32+
120
100
80
60
40
20
0
22
27
WT
YAC128

Figure 4-1 Cell survival in corticostriatal (C-S) coculture at DIV21.

The n's in the figure represent the number of 20x pictures (four pictures were tiled into one) used in analysis and the culture batch number is shown in parenthesis. ***A.*** Representative pictures of staining of Hoechst (stains cell nuclei; blue), microtubule-associated protein 2 (MAP2; red) and dopamine- and cAMP-regulated neuronal phosphoprotein 32 (DARPP32; green) for visualizing live cells (morphology-based identification), neurons and striatal spiny projection neurons (SPNs), respectively, in WT and YAC128 C-S cocultures at DIV21. The density of live cells [***B.***: WT n=25(3) and YA128 n=30(4); by unpaired t-test p=0.7943], that of MAP2-positive cells [***C.***: WT n=25(3) and YA128 n=30(4); by unpaired t-test p=0.7537] and that of DARPP32-positive cells [***D.***: WT n=25(3) and YA128 n=30(4); by unpaired t-test p=0.5186] are similar between WT and YAC128. ***E.*** Expectedly, the percentage of DARPP32-positive cells that are also MAP2-positive is close to 100% in both genotypes [WT n=22(3) and YA128 n=27(4); by unpaired t-test p=0.0997].

Previously, we detected a higher percentage of cell death in YAC128 than in WT SPNs after exposure to cell-toxic levels of NMDA (300). Thus, we asked whether there is intrinsically reduced basal cell-survival signaling in YAC128 SPNs. To test this, we quantified the basal nuclear-to-cytosolic ratio of phosphorylated cAMP response element binding protein (pCREB; thereafter referred as "pCREB ratio"), a well-established regulator of pro-survival gene transcription (Figure 4-2 A). As coculture developed from DIV14 to 21, the pCREB ratio significantly increased in WT SPN (Figure 4-2 B). There was also a significant increase in the mean pCREB ratio in YAC128 SPN from DIV 14 to 21, and no significant interaction effect was observed (interaction $p=0.459$; Figure 4-2 B). These data suggest that the expression of mutant huntingtin (mHtt) has no effect on basal pro-survival signaling in the current coculture conditions.

Together, our results demonstrate that at DIV21 there is no accelerated cell death or weak pro-survival signaling, at least through pCREB, in SPNs in YAC128 coculture, and therefore it is a valid time point to investigate synaptic functions.

A

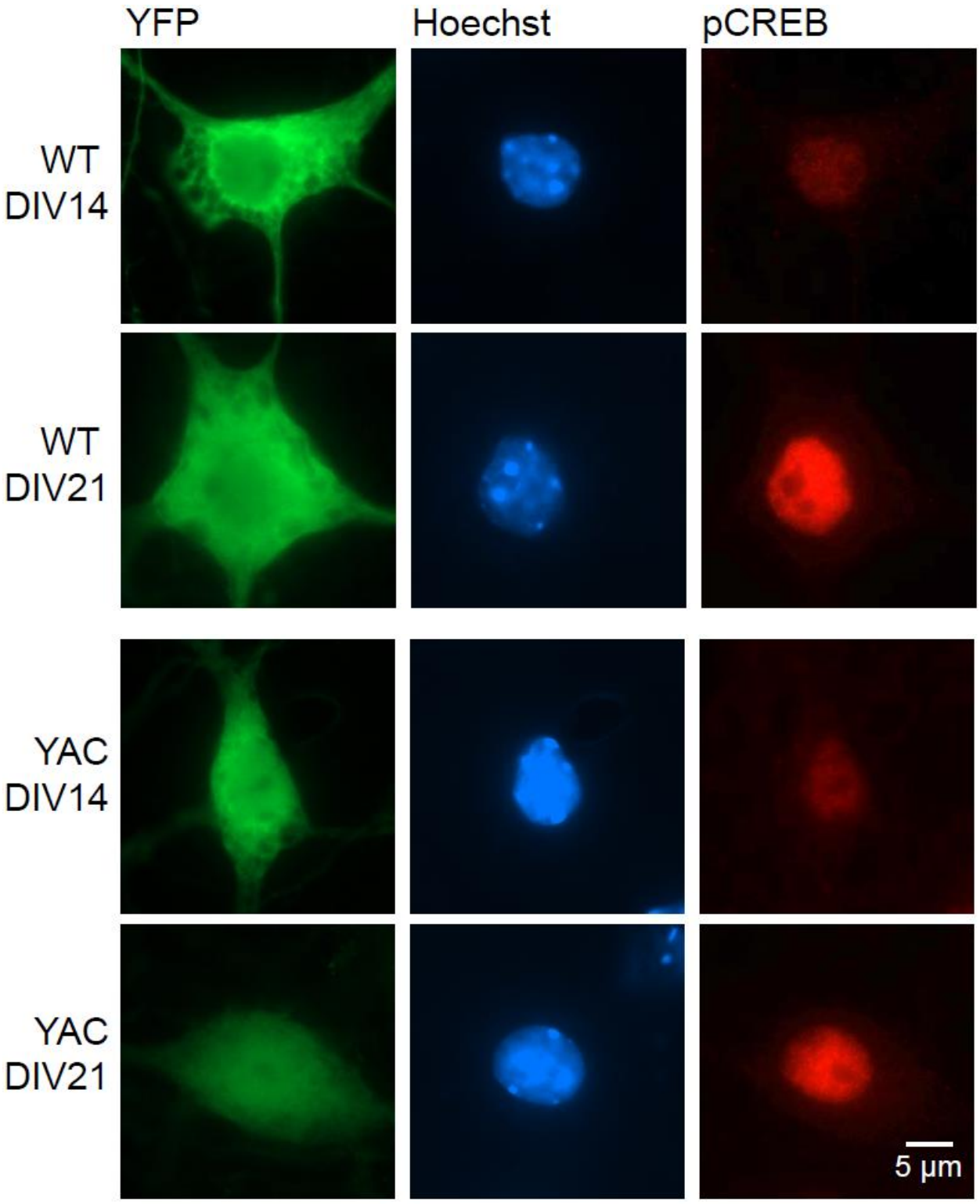

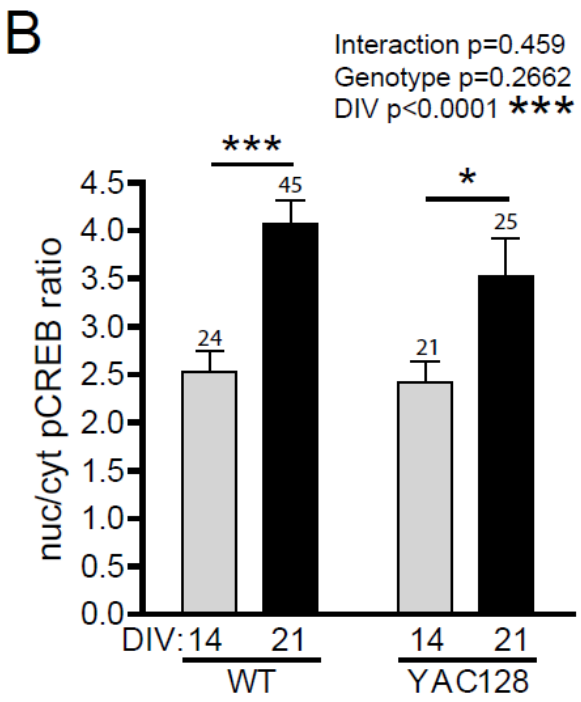

Figure 4-2 No effect of the Huntington's disease (HD) mutation on nuclear pCREB levels in cocultured SPNs.

A. Representative images showing yellow fluorescent protein (YFP; transfected to label striatal SPNs), pCREB and Hoechst staining in WT and YAC128 SPNs at DIV 14 and 21. ***B.*** Bar graph showing the nuclear-to-cytoplasmic ratio of pCREB (pCREB ratio) staining intensity. pCREB ratios increased from DIV 14 to 21 in both genotypes (by 2-way ANOVA DIV ***p<0.0001; ***p<0.001 for WT and *p<0.05 for YAC128 by posthoc tests). No genotype (p=0.2662) or interaction (p=0.459) effects were observed (n=21 to 45 cells per bar from 4-8 culture batches).

4.3.2 Altered Functions of Excitatory Synapses in Striatal SPNs from YAC128 Cortical-striatal Coculture

To thoroughly explore C-S synaptic functions in YAC128 throughout coculture development, we first assessed the time-course of functional C-S excitatory synapse formation by recording miniature excitatory postsynaptic currents (mEPSCs) from YFP-transfected striatal SPNs in coculture with non-transfected cortical neurons. Recordings were obtained at DIVs 7, 10, 14, 18 and 21 from both WT and YAC128 cocultures, as well as cocultures from YAC18 mice, which express a non-pathological version of full-length human *HTT*. WT SPNs exhibited a rapid and continuous growth in mEPSC frequency from DIV7 up to DIV21 (Figure 4-3 A and B), suggesting robust excitatory synaptogenesis during this period *in vitro*. The same results were obtained for mEPSCs recorded from YAC18 mice coculture (Figure 4-3 B), suggesting that the presence of wild-type human Htt does not significantly alter these measures of C-S synaptic connectivity. However, in YAC128 cocultures, SPN mEPSC frequency was found to increase from DIV7 up to DIV14, at which point no further growth was observed (Figure 4-3 B). From the results of this experiment, we designed subsequent experiments and analyses to focus on DIV14 and DIV21 in WT and YAC128 cocultures in order to facilitate the comparison of genotype differences between these two critical time points. With this approach, genotype differences in the development of a given parameter from DIV 14 to 21 were determined by a two-way ANOVA interaction effect, and Bonferroni's post-hoc tests were used to determine the strength of parameter development from DIV 14 to 21 within a given genotype. When mEPSC frequency is quantified in this manner from the cocultures shown in Figure 4-3 B combined with recordings from additional batches of WT and YAC128 cocultures (total of 7 and 9 independent coculture batches for WT and YAC128, respectively; cell number is shown above each bar), a significant interaction

effect is observed, as well as a significant post-hoc increase in mEPSC frequency for WT SPNs from DIV 14 to 21 that did not occur in YAC128 SPNs (Figure 4-3 C). When we compared mEPSC amplitude at these two time-points with the additional coculture batches, there was a significant interaction effect, reflected by the increase and decrease in the mean mEPSC amplitude in WT and YAC128 SPN, respectively, from DIV14 to DIV21 (Figure 4-3 D). Notably, YAC128 mEPSC amplitude was significantly smaller than that of WT in DIV21 cocultures [WT n=27(5) and YAC128 n=37(7); by unpaired t-test *p=0.0244]. We also observed a similar interaction effect and lack of growth in YAC128 SPNs in measurements of the membrane capacitance of the recorded neurons (Figure 4-3 E), which may reflect a mHtt-induced attenuation in the development of overall SPN cell size from two to three weeks *in vitro*.

A

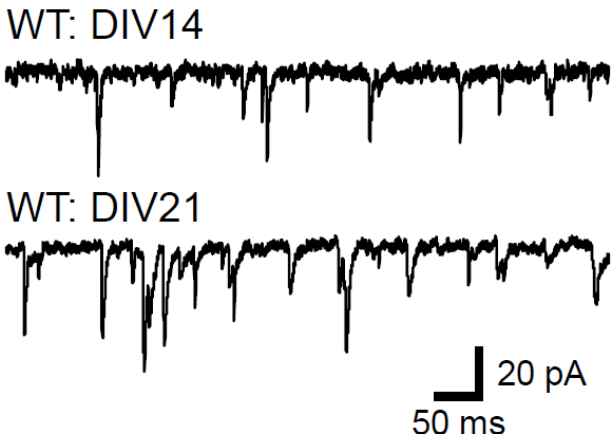
WT: DIV14
WT: DIV21
20 pA
50 ms

Aii

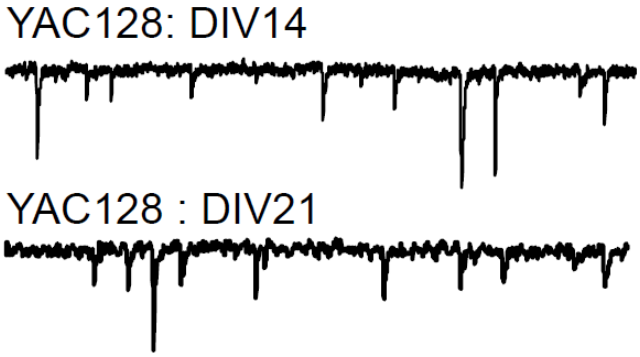
YAC128: DIV14
YAC128 : DIV21

B

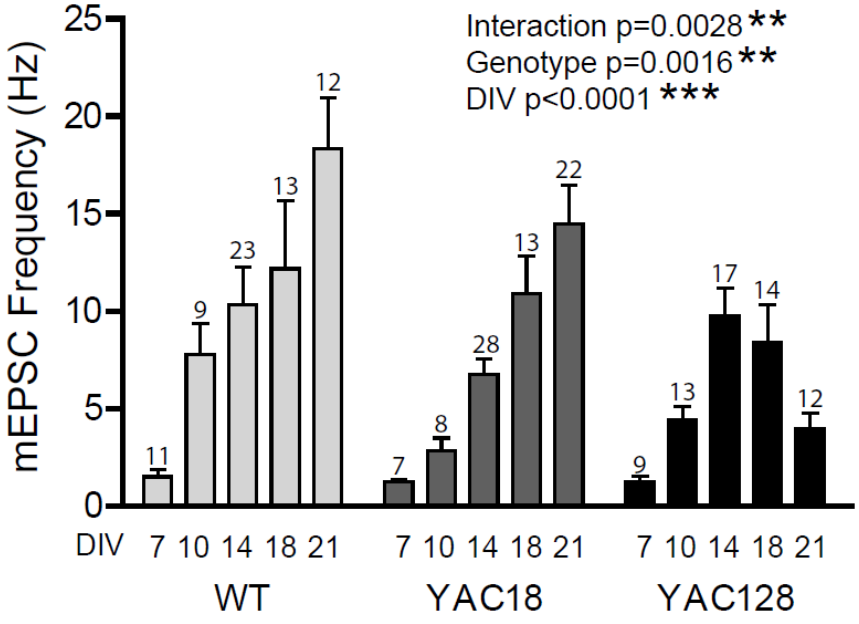
mEPSC Frequency (Hz)
25
20
15
10
5
0
Interaction p=0.0028 **
Genotype p=0.0016 **
DIV p<0.0001 ***
11
9
23
13
12
7
8
28
13
22
9
13
17
14
12
DIV 7 10 14 18 21
7 10 14 18 21
7 10 14 18 21
WT
YAC18
YAC128

C

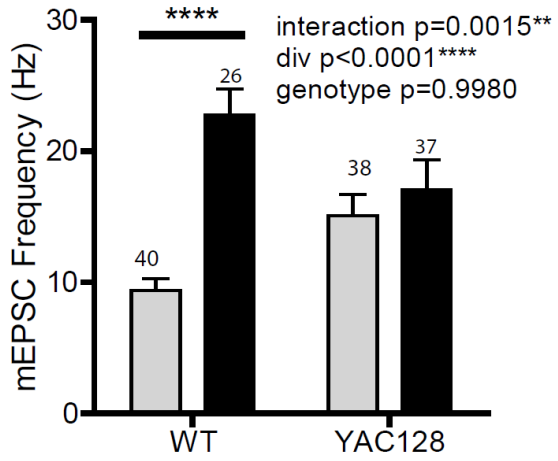
****
interaction p=0.0015**
div p<0.0001****
genotype p=0.9980
mEPSC Frequency (Hz)
30
20
10
0
26
40
38
37
WT
YAC128

D

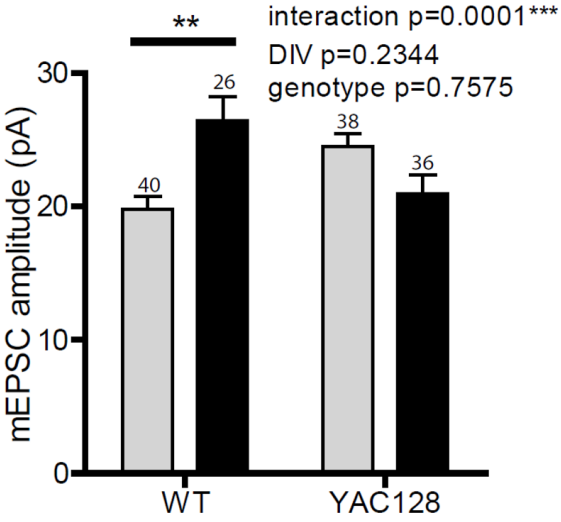
**
interaction p=0.0001***
DIV p=0.2344
genotype p=0.7575
mEPSC amplitude (pA)
30
20
10
0
26
40
38
36
WT
YAC128

E

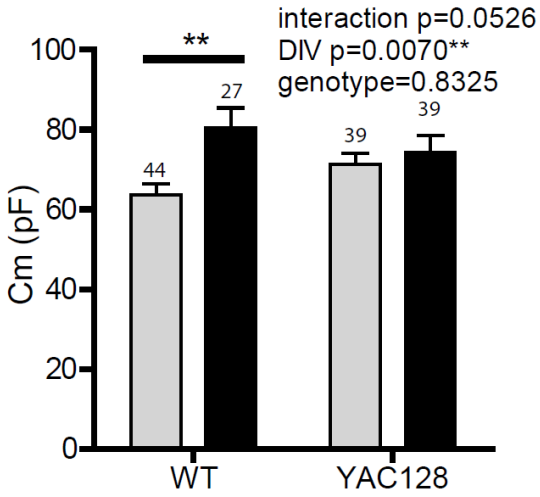
**
interaction p=0.0526
DIV p=0.0070**
genotype=0.8325
Cm (pF)
100
80
60
40
20
0
27
44
39
39
WT
YAC128

Figure 4-3 mEPSC frequency is reduced after DIV14 in YAC128 C-S cocultures.

Ai-Aii. Representative traces showing mEPSC events recorded from striatal SPNs in coculture with cortical neurons. Shown are traces from DIV 14 and 21 from WT (***Ai***) and YAC128 (***Aii***) cocultures. ***B.*** Bar graphs showing mean mEPSC frequency at DIVs 7, 10, 14, 18 and 21 from 3 independent batches each of WT, YAC18 and YAC128 cocultures. Two-way ANOVA revealed a significant genotype (**p=0.0016) and DIV (***p<0.0001) effect, as well as a significant interaction effect (**p=0.0028). n=7-28 cells per bar. ***C.*** Data from ***B*** together with a new set of data from additional coculture batches, analyzed as a 2-way ANOVA to focus solely on changes in WT and YAC128 cocultures between DIV 14 and 21. By this approach, a significant interaction effect (**p=0.0015; n=26-40 cells per bar) indicates a genotype difference in the change in mEPSC frequency from DIV 14 to 21. Post-hoc analysis revealed a significant increase in mean mEPSC frequency in WT SPNs from two to three weeks *in vitro* (****p<0.0001), but not in YAC128 SPNs (p>0.05). ***D.*** Bar graph showing mean mEPSC amplitude in WT and YAC128 cocultures at DIVs 14 and 21. A significant interaction effect was observed by 2-way ANOVA (***p=0.0001; n=26-40 cells per bar) and there was a significant increase in mean amplitude from DIV 14 to 21 for WT SPNs by post-hoc test (**p<0.01). ***E.*** Mean membrane capacitance did not demonstrate a significant interaction effect (p=0.0526; n=27-44 cells per bar), but only WT showed a significant increase from DIV 14 to 21 by post-hoc test (**p<0.01). Data in ***C – E*** were generated from 7 and 9 independent coculture batches for WT and YAC128, respectively.

Next, we used hypertonic sucrose-containing artificial cerebrospinal fluid (ACSF) to ask whether the reduced mEPSC frequency in DIV21 YAC128 cocultures is associated with a reduced size of the readily releasable pool (RRP) of excitatory vesicles. Sucrose experiments were restricted to DIV21, the time point at which a deficit in YAC128 mEPSC frequency, but no significant difference in cell-death (Figure 4-1), was observed. When sucrose (500 mM) was applied for 4 s to deplete the RRP, large inward currents that decayed to a steady-state were readily recorded from SPNs (Figure 4-4 A). There was a trend towards a smaller peak density recorded from YAC128 SPN, although this did not reach significance (Figure 4-4 B). This trend, combined with a significant reduction in the total charge carried by the sucrose-induced current (Figure 4-4 C), is suggestive of a reduction in the size of the RRP in YAC128 C-S synapses in cocultures; however, since the mEPSC frequency is lower for YAC128 vs. WT SPNs at DIV21, we cannot rule out a contribution of lower excitatory synapse density as a factor in reduced peak current and total charge evoked by a maximal sucrose challenge. As the steady-state current is thought to represent the rate of RRP replenishment (465), the strong trends toward smaller steady-state currents (Figure 4-4 D) and faster decay time course (Figure 4-4 E) in YAC128 SPN hinted that there may also be a deficit in the rate of RRP replenishment following its depletion. This possibility was explored further by quantifying the area under the curves (AUC) in response to paired sucrose pulses, with an inter-pulse interval of 3s. By dividing the AUC of the second response to that of the first, we revealed a significant reduction in the recovery of sucrose-induced responses in YAC128 SPNs (Figure 4-4 F and G). Genotype differences are unlikely to be accounted for by a difference in the degree of AMPA receptor desensitization or internalization, as normalization of the second pulse to the first within genotype eliminates any potential genotype differences in the function of individual AMPA receptors. Moreover, there was no differential genotype effect on

the amplitude of mEPSC events recorded immediately before and after sucrose application (2-way ANOVA interaction p=0.888, not shown). Together, these data indicate that mHtt may alter synaptic function by reducing the RRP size and replenishment rate at C-S synapses.

Additionally, we observed a significant genotype difference in the amplitude of mEPSC events recorded from striatal SPNs before and after the sucrose pulse between the two genotypes. WT mEPSC amplitude (in pA) was 34.59$\pm$2.001 before and 29.05$\pm$1.661 after sucrose, whereas YAC128 mEPSC amplitude (pA) = 30.51$\pm$2.091 before and 24.93$\pm$1.255 after sucrose [n = 16(4) for both WT and YAC128; by 2-way ANOVA genotype *p = 0.0249 and sucrose **p = 0.0028; by Bonferroni's post-test there was no significant reduction of mEPSC amplitude within both genotypes after sucrose; not shown]. These data are consistent with the reduced amplitude of YAC128 SPN basal mEPSC events (Figure 4-3 D), indicative of less glutamate content per presynaptic vesicle or decreased expression of AMPA glutamate receptors on the postsynaptic SPN cell membrane in YAC128 coculture at DIV21.

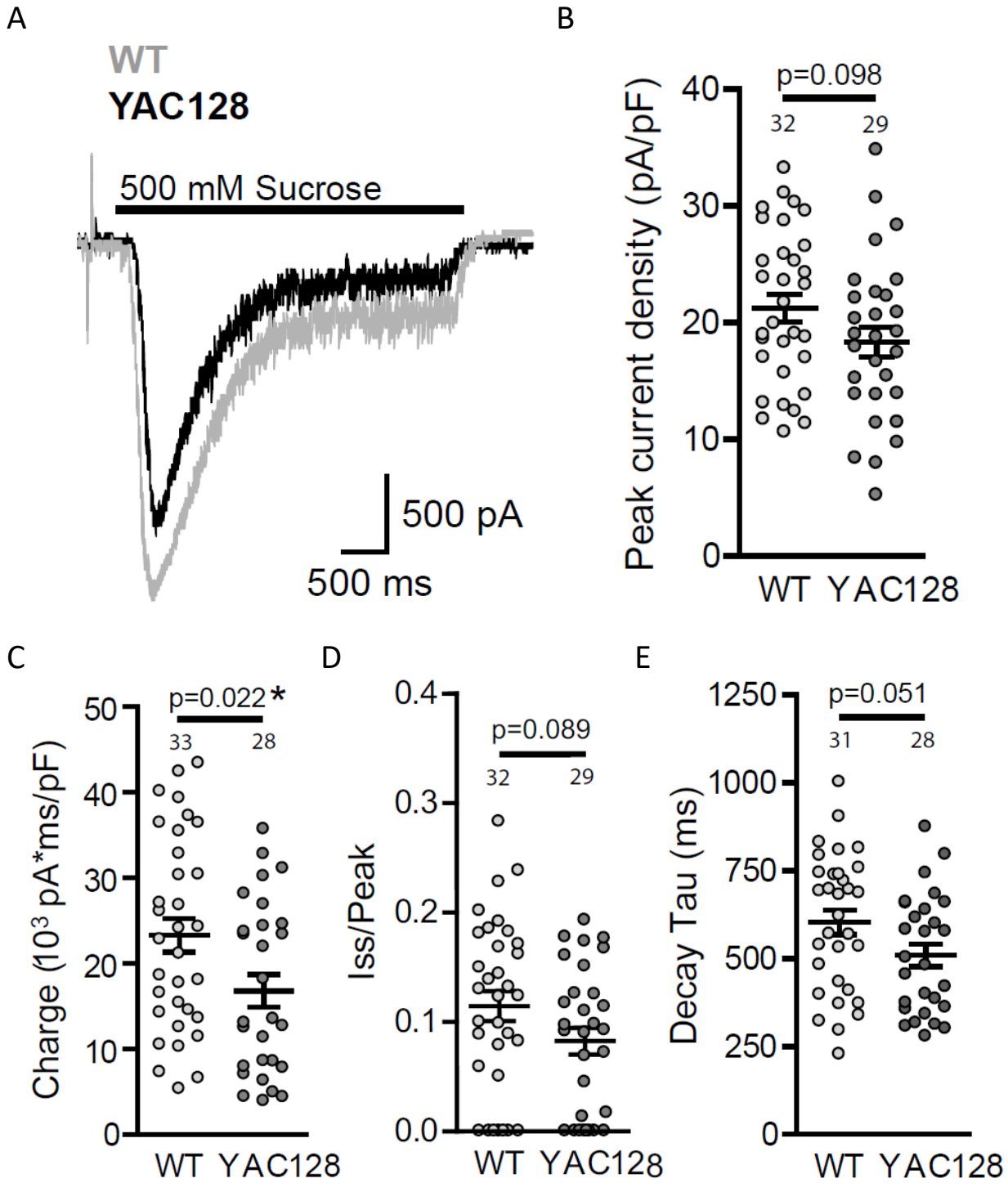
A
WT
YAC128
500 mM Sucrose
500 pA
500 ms
B
p=0.098
32
29
Peak current density (pA/pF)
40
30
20
10
0
WT YAC128
C
p=0.022*
33
28
Charge (10³ pA*ms/pF)
50
40
30
20
10
0
WT YAC128
D
p=0.089
32
29
Iss/Peak
0.4
0.3
0.2
0.1
0.0
WT YAC128
E
p=0.051
31
28
Decay Tau (ms)
1250
1000
750
500
250
0
WT YAC128

F

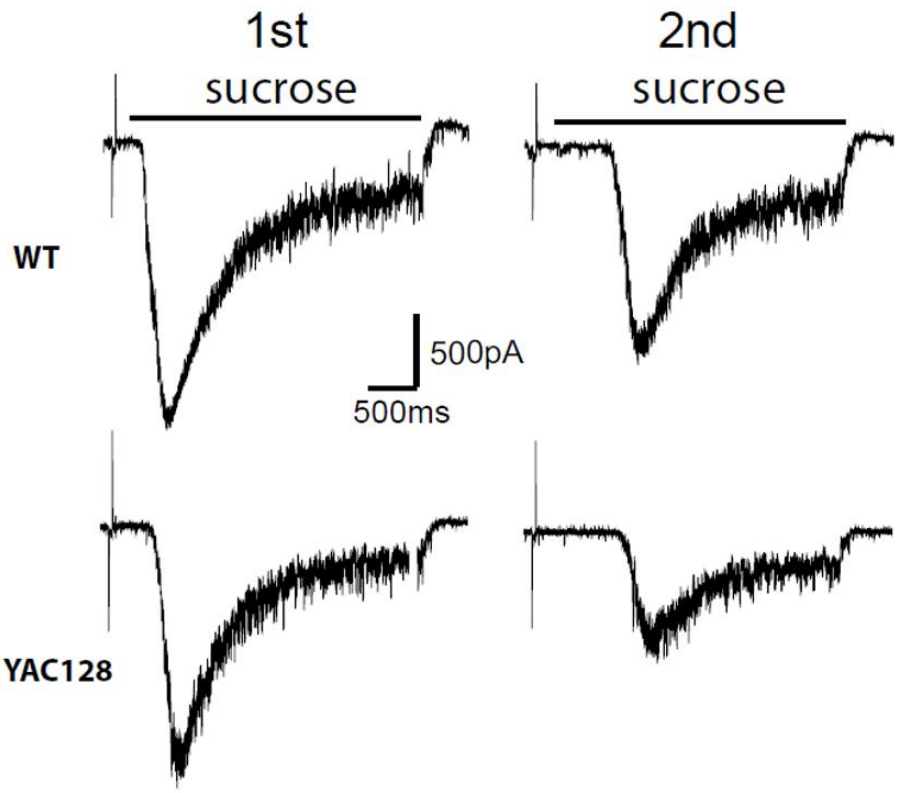
1st
sucrose
2nd
sucrose
WT
500pA
500ms
YAC128

G

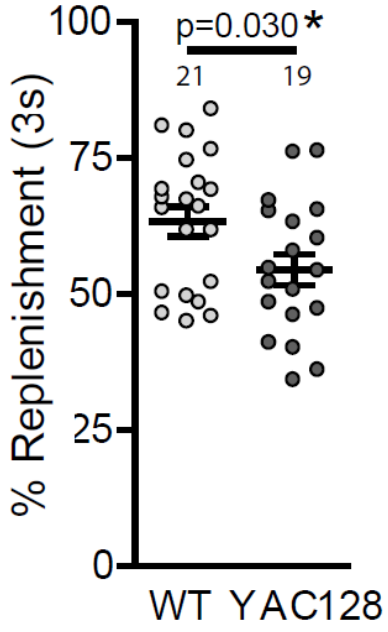
100
75
50
25
0
% Replenishment (3s)
p=0.030*
21
19
WT YAC128

Figure 4-4 Reduced size and rate of replenishment of the readily-releasable pool (RRP) of vesicles in DIV21 C-S cocultures from YAC128 mice.

A. Representative traces of sucrose-induced EPSCs recorded from WT (grey) and YAC128 (black) SPNs. ***B-E.*** Graphs show mean ± s.e.m. as well as individual data points for the peak (***B***), charge (***C***), steady-state (***D***) and decay tau (***E***) of sucrose-induced EPSCs recorded from WT and YAC128 SPNs. Measurements of peak and charge were normalized to cell capacitance and steady-state current (Iss) to the peak current. ***F.*** Representative traces for paired-pulse sucrose-induced EPSCs with a 3-second interval. ***G.*** Graph showing the rate of replenishment of sucrose-induced EPSCs as determined by calculating the area of a second sucrose EPSC divided by that of the first. p-values are shown in the graphs and cell numbers, displayed as individual data points within the graphs, are from at least 3 independent cocultures per genotype.

To determine whether the observed synaptic phenotype was specific to excitatory synapses, we recorded mIPSCs at DIV 14 and 21 from WT and YAC128 SPN in coculture with cortical neurons. In this culture, much of the inhibitory synaptic connectivity is likely to result from connections forming among the SPN themselves. Like mEPSCs, frequency of mIPSCs also significantly increased from DIV14 to DIV21 in WT cocultures (Figure 4-5 A and C), suggesting a rapid rate of functional inhibitory synapse formation during this period. However, unlike mEPSCs, this growth in mIPSCs also occurred to a similar degree in YAC128 cocultures, and there were no significant genotype or interaction differences for mIPSC frequency (Figure 4-5 B and C). There was also a lack of genotype or interaction effects on mIPSC amplitude, although post-hoc comparisons only revealed a significant increase in YAC128 mIPSC amplitude from DIV 14 to 21 (Figure 4-5 D). Thus, it appears that the presently reported synaptic phenotype in YAC128 C-S cocultures is restricted to excitatory synapses. These data also demonstrate that the excitatory synaptic phenotype is unlikely to be attributed to poor overall cell health in DIV21 YAC128 cocultures, as inhibitory connectivity is fully intact.

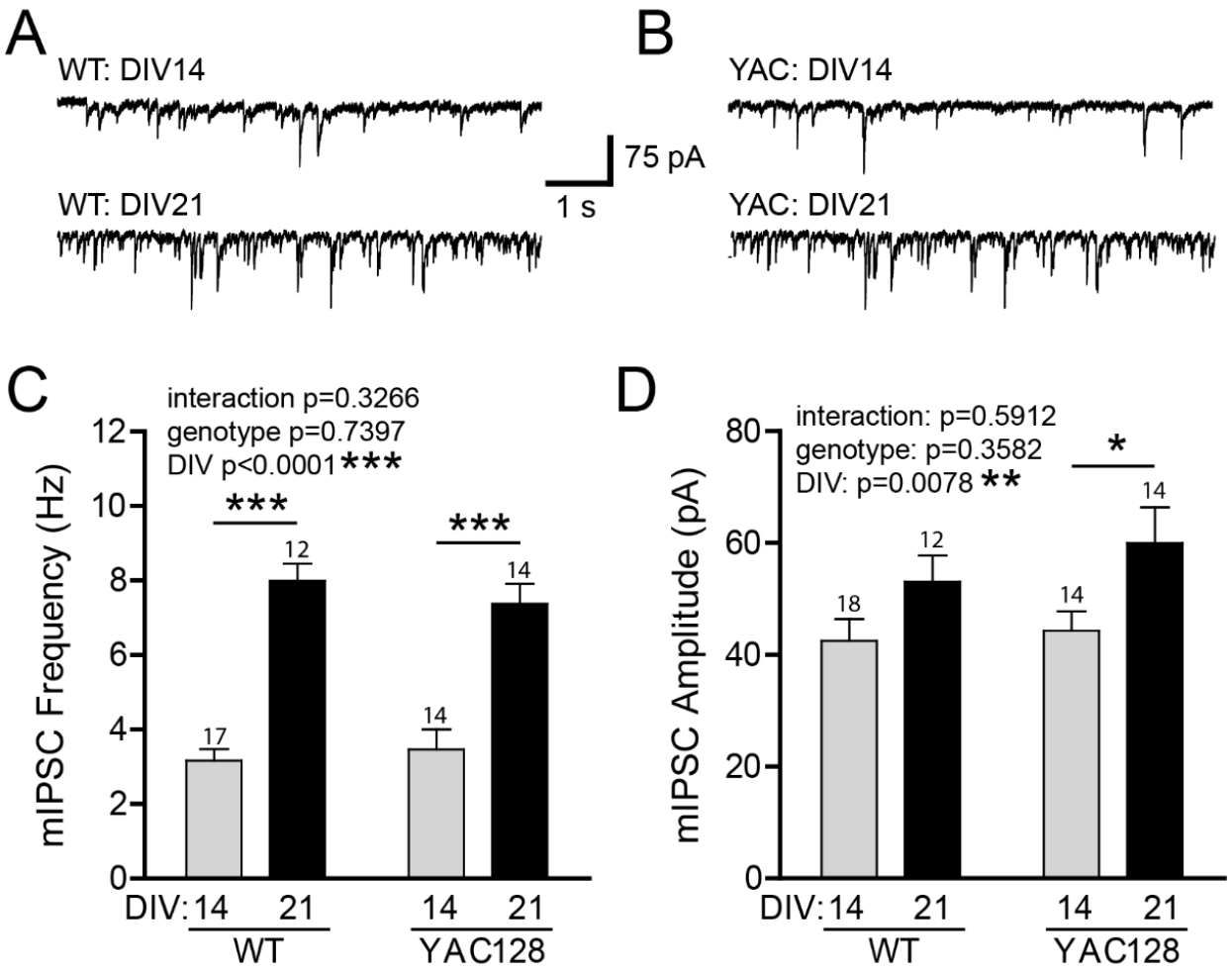
A
WT: DIV14
WT: DIV21
75 pA
1 s
B
YAC: DIV14
YAC: DIV21
C
interaction p=0.3266
genotype p=0.7397
DIV p<0.0001***
mIPSC Frequency (Hz)
DIV: 14 21 14 21
WT
YAC128
D
interaction: p=0.5912
genotype: p=0.3582
DIV: p=0.0078 **
mIPSC Amplitude (pA)
DIV: 14 21 14 21
WT
YAC128

Figure 4-5 mIPSCs are unaffected in YAC128 C-S cocultures.

A-B. Representative traces showing mIPSC events recorded from SPNs in coculture with cortical neurons. Shown are traces obtained at DIV 14 and 21 from WT (***A.***) and YAC128 (***B.***) cocultures. ***C.*** Mean mIPSC frequency at DIV 14 and 21 recorded from WT and YAC128 SPNs. mIPSC frequency increased significantly in both genotypes from DIV 14 to 21, as indicated by both a 2-way ANOVA effect of DIV (***$p<0.0001$) and post-hoc Bonferroni's tests (***$p<0.0001$ for both genotypes). There was no significant effect of genotype ($p=0.7397$; n=12-17 cells per bar). ***D.*** Mean mIPSC amplitude from DIV 14 and 21 recorded from WT and YAC128 SPNs. mIPSC amplitude increased significantly from DIV 14 to 21, as indicated by a 2-way ANOVA effect of DIV (**$p<0.0078$). Post-hoc analysis only revealed a significant increase in mIPSC amplitude from DIV 14 to 21 in YAC128 SPNs (*$p<0.05$), although no overall genotype ($p=0.3582$) or interaction ($p = 0.5912$; n = 12-18 cells per bar) effects were observed.

4.3.3 Attenuated Dendritic Arborization in YAC128 Striatal SPN

To determine whether morphological alterations accompany the functional excitatory synapse deficit that occurs between 2 to 3 weeks *in vitro* in YAC128 cocultures, coverslips were fixed at either DIV14 or DIV21, and YFP-transfected SPNs were imaged under 20x or 63x magnification. At 20x, the dendrites from randomly selected YFP-positive cells were manually traced (Figure 4-6 A), and a Sholl analysis was performed in ImageJ. At DIV14, there was no difference in WT and YAC128 SPN dendritic arborization as measured by Sholl analysis (Figure 4-6 A and B). However, at DIV21, dendritic complexity was found to be significantly reduced (Figure 4-6 A and C), and the number of crossings at the most distal circle – 157.5 μm radius from the soma – was significantly lower (Figure 4-6 D) in YAC128 SPN compared to WT. When we quantified the total dendritic length, there was a significant interaction effect, reflecting the increase and decrease of the mean dendritic length in WT and YAC128 SPN, respectively, from DIV 14 to 21 (Figure 4-6 E). Thus, a mHtt-induced reduction in SPN dendritic arborization is evident in cocultures by 3 weeks *in vitro*.

A

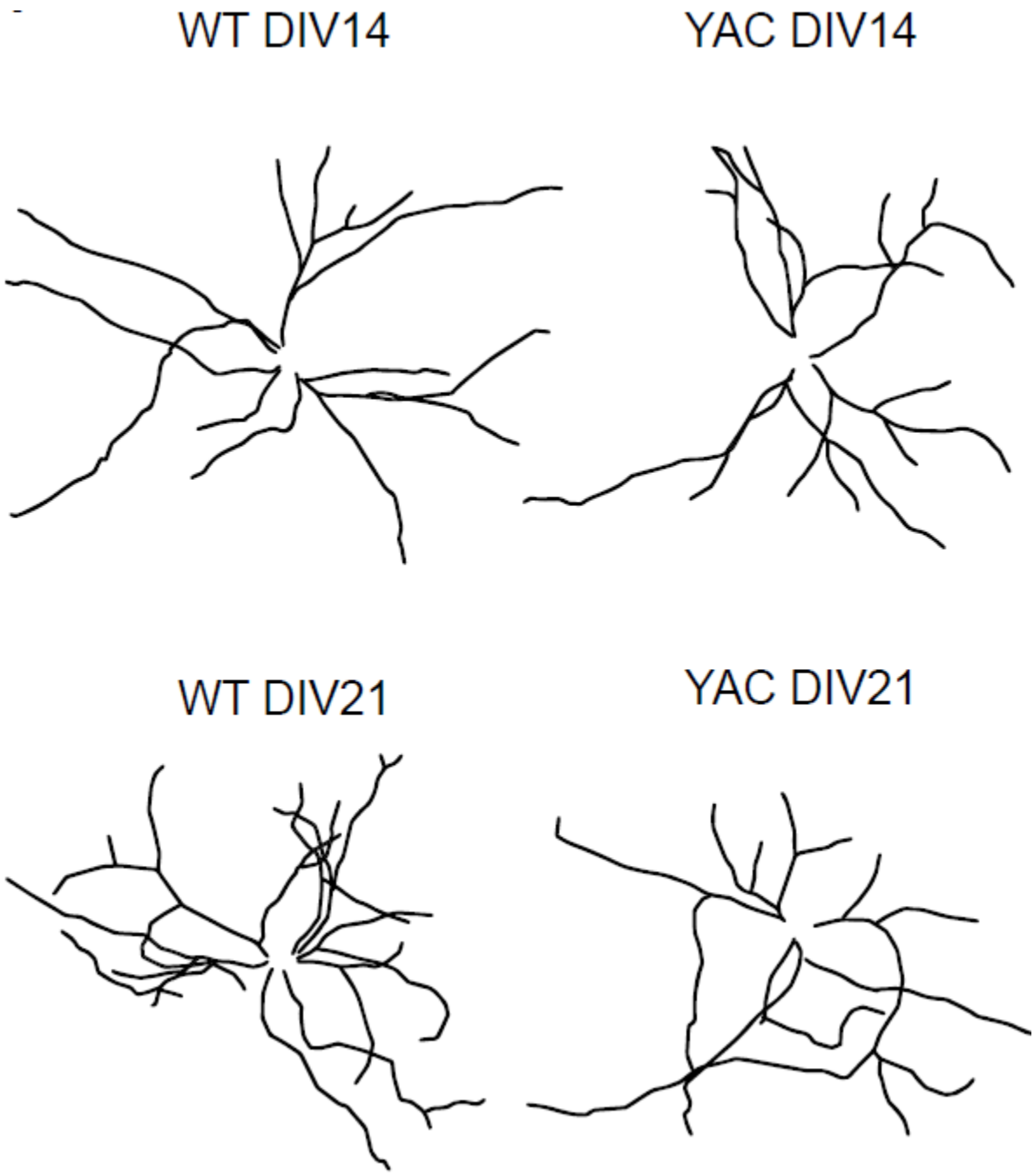

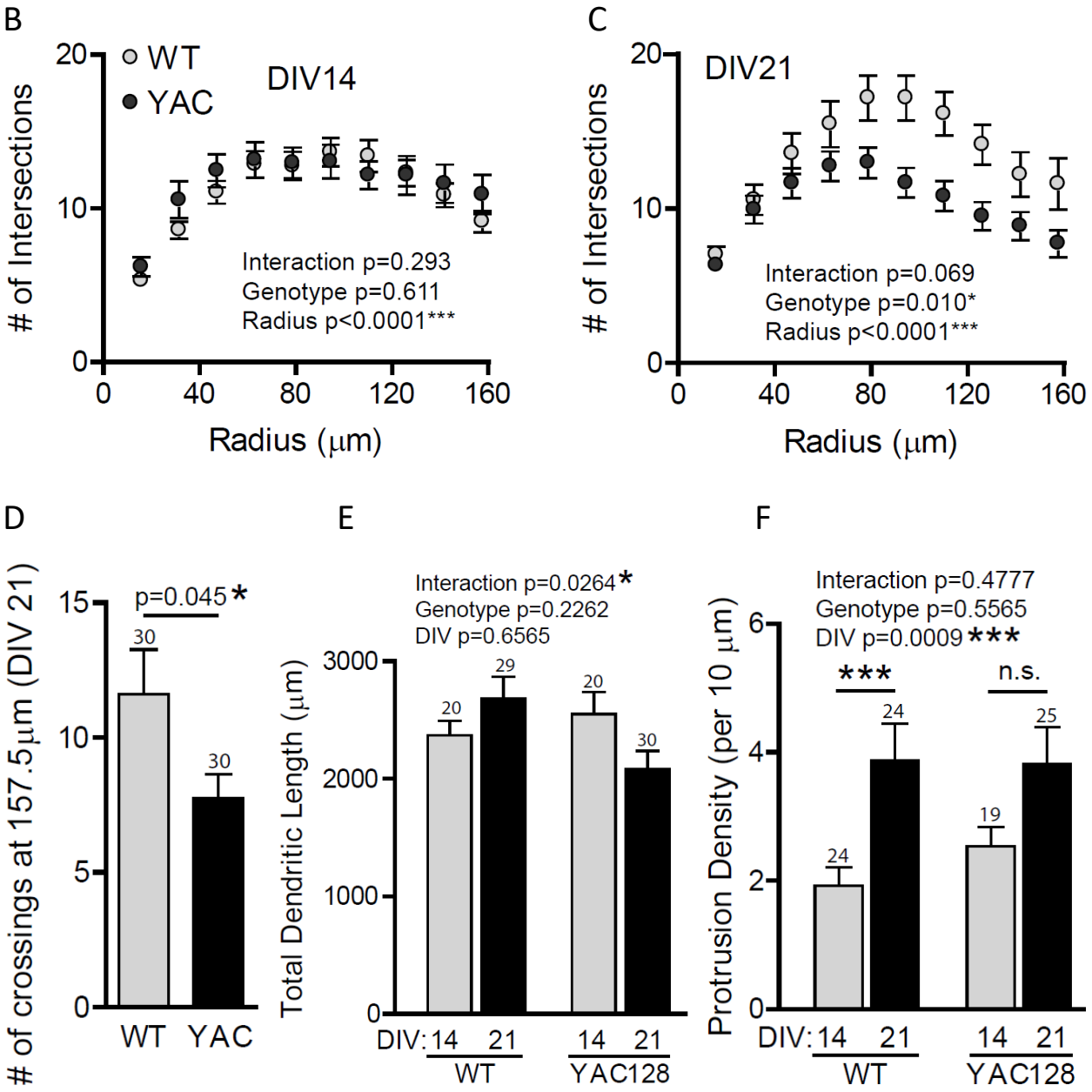
B
WT
YAC
DIV14
# of Intersections
Radius (μm)
Interaction p=0.293
Genotype p=0.611
Radius p<0.0001***
C
DIV21
# of Intersections
Radius (μm)
Interaction p=0.069
Genotype p=0.010*
Radius p<0.0001***
D
# of crossings at 157.5μm (DIV 21)
p=0.045*
WT
YAC
E
Total Dendritic Length (μm)
Interaction p=0.0264*
Genotype p=0.2262
DIV p=0.6565
DIV: 14 21 14 21
WT
YAC128
F
Protrusion Density (per 10 μm)
Interaction p=0.4777
Genotype p=0.5565
DIV p=0.0009***
***
n.s.
DIV: 14 21 14 21
WT
YAC128

Figure 4-6 Reduced dendritic arborization of YAC128 SPNs at DIV21 in C-S cocultures.

A. Representative traces of SPN dendritic trees from both WT and YAC128 SPNs at DIV 14 and 21. ***B.*** Sholl analysis showing no significant difference at DIV14 between genotypes for the number of dendritic intersections with concentric circles, centered at the soma and drawn with a radius of 10 to 157.5 μm in 16.4 μm increments (2-way ANOVA, genotype $p = 0.611$; $n = 20$ cells per genotype). ***C.*** Sholl analysis showing a significant reduction of dendritic complexity in YAC128 SPNs at DIV21 (2-way ANOVA, genotype **p=0.010; n=30 cells per genotype). ***D.*** Bar graph showing the total number of dendritic crossings of a circle drawn with a 157.5 μm radius from the center of the soma (*p=0.045, unpaired t-test). ***E.*** Bar graph showing the total dendritic length from WT and YAC128 SPNs at DIV 14 and 21. A significant interaction effect is observed (2-way ANOVA, interaction *p=0.0264, genotype p=0.2262). ***F.*** Bar graph showing the density of spine-like dendritic protrusions on WT and YAC128 SPNs dendrites at DIV 14 and 21. Protrusion density increased from DIV 14 to 21 (2-way ANOVA, DIV ***p=0.0009), but the increase was significant by post-hoc analysis for WT SPNs only (***p<0.001); no genotype (p=0.5565) or interaction (p=0.4777) effect was observed (n=19-25 cells per bar).

Co-culturing SPNs with cortical neurons promotes the growth of dendritic protrusions that are readily visible on the dendritic surface of YFP-transfected SPNs (124). Small, spine-like protrusions emerging from the dendritic shafts were manually counted in ImageJ. Not surprisingly, there was a robust increase in the number of dendritic protrusions from DIV 14 to 21 in WT SPN (Figure 4-6 F). While we also observed an increase in the mean of YAC128 SPN dendritic protrusions, post-hoc analysis only detected a significant increase from DIV14 to DIV21 in WT, and not YAC128 SPN, suggestive of a more robust effect in WT SPN (Figure 4-6 F). However, as there was no interaction effect ($p=0.478$), we conclude that any effects of the Htt mutation on the development of SPN protrusions during this time period is minimal. Similarly, when we assessed structural excitatory synapse density by quantifying colocalization of vGlut1 with the postsynaptic scaffolding protein, PSD-95 (Figure 4-7 A and B), we found no evidence for a reduction in YAC128. A similar result was seen when we analyzed functional synapses at DIV21 by immunofluorescence labeling of AMPA receptor GluA2 subunits and the presynaptic marker vGlut1 (Figure 4-7 C-F). The densities of GluA2 (Figure 4-7 D) and vGlut1 (Figure 4-7 E) puncta were similar between genotypes, as was the size of GluA2 (WT: 0.138 ± 0.013 μm^2, n=32, YAC: 0.138 ± 0.009 μm^2, n=32) and vGlut1 puncta (WT: 0.213 ± 0.019 μm^2, n=32; YAC: 0.176 ± 0.015 μm^2, n=32). Colocalization of the two markers was also not significantly affected by genotype (Figure 4-7 F). These data suggest that despite a reduction in overall dendritic arborization, the synapse density for a given area of dendrite is normal in YAC128 cocultures up to three weeks *in vitro.* Moreover, the similar density of vGlut1 puncta along dendrites of both WT and YAC128 SPNs at DIV21 is strong evidence to indicate similar survival of cortical neurons and their input to SPNs in cocultures from the two genotypes.

Given that we previously observed smaller mEPSC amplitude (Figure 4-3 D), the fact that we observed no change in GluA2 puncta size or density suggests reduced glutamate content in presynaptic vesicles in C-S synapses in YAC128 coculture at DIV21 compared with WT. Interestingly, using confocal microscopy, we found a small but significant reduction in vGlut1 puncta size [WT=0.341$\pm$0.006 μm^2 and YAC128=0.321$\pm$0.005 μm^2 ; n=117(12) for both WT and YAC128; by unpaired t-test **p=0.0024; not shown], and no change in its density, in YAC128 compared with WT SPNs. Together with the ~17% (non-significant) reduction of vGlut1 puncta size (above paragraph) observed with epifluorescence microscopy, we conclude that mHtt causes a modest decrease of vGlut1 expression in C-S synapses, which likely contributes to reduced glutamate loading into presynaptic vesicles.

A

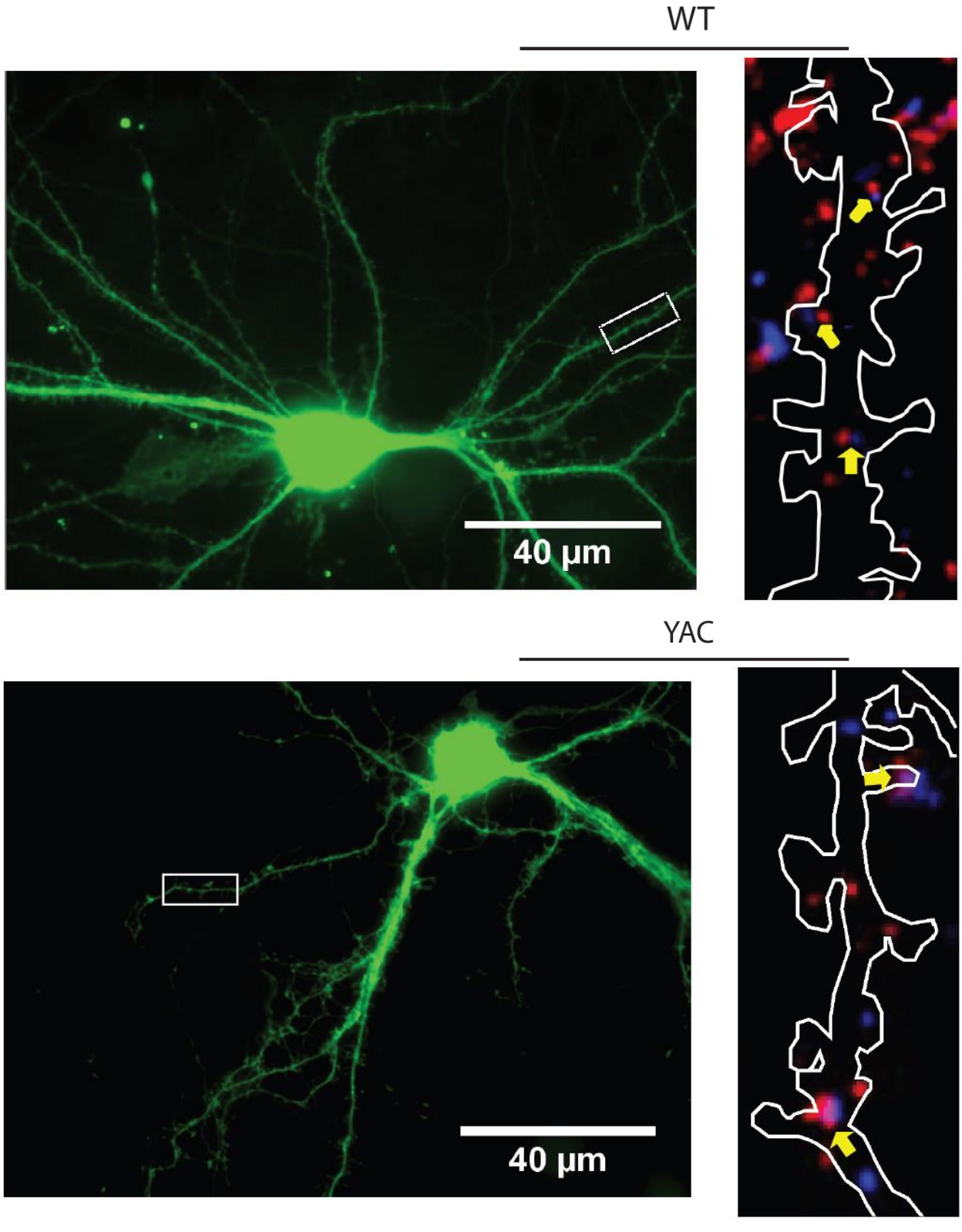

B

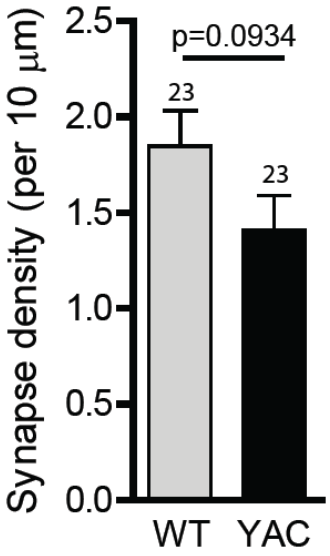
Synapse density (per 10 µm)
2.5
2.0
1.5
1.0
0.5
0.0
p=0.0934
23
23
WT
YAC

C

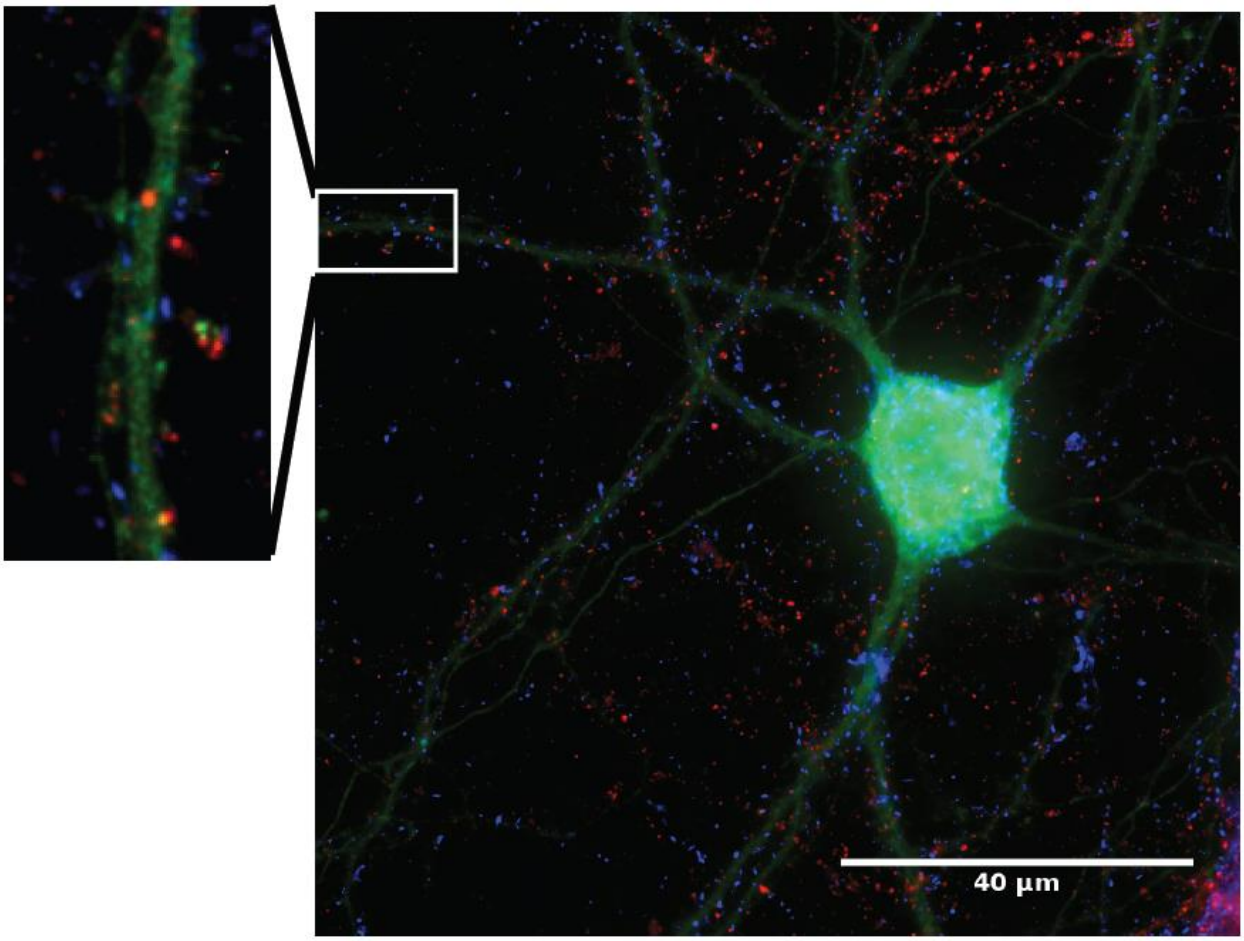
40 µm

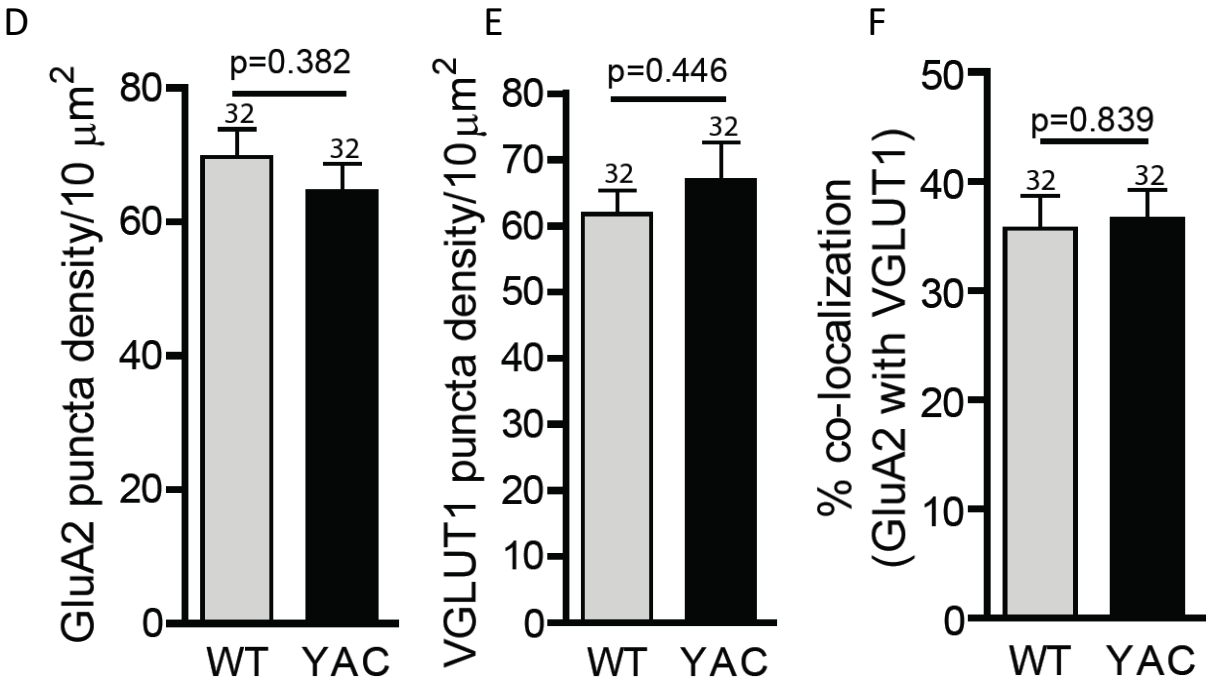
D
p=0.382
32
32
GluA2 puncta density/10 μm2
80
60
40
20
0
WT
YAC
E
p=0.446
32
32
VGLUT1 puncta density/10μm2
80
70
60
50
40
30
20
10
0
WT
YAC
F
p=0.839
32
32
% co-localization
(GluA2 with VGLUT1)
50
40
30
20
10
0
WT
YAC

Figure 4-7 Similar density of excitatory synapses on SPN dendrites at DIV21 in WT and YAC128 C-S cocultures.

A. Representative images of YFP-positive immunostaining (green) is shown on the left for both WT and YAC128 SPNs at DIV21, and the enlarged images to the right show immunostaining for PSD95 (red) and vGlut1 (blue) within the mask drawn around the YFP-stained dendritic segment bounded by the white rectangles. Yellow arrows point to the co-localized PSD95-vGlut1 puncta. The scale bar is 40 µm. ***B.*** The density of synapses defined by vGlut1 co-localized with PSD-95, as measured from SPN dendrites in coculture with cortical neurons (n=23-32 different cells for both genotypes and p-values were obtained by unpaired t-tests). ***C.*** Representative image of YAC128 SPN showing vGlut1 (blue), YFP (green) and GluA2 (red) immunostaining; scale bar is 40µm in the right image, and higher gain image is shown in left. Bar graphs show no difference between WT and YAC128 in terms of GluA2 (***D.***) and vGlut1 (***E.***) puncta densities, or the percent co-localization of GluA2 with vGlut1 (***F.***). There are 32 cells from 4 different culture batches for both WT and YAC128 analyzed for the bar graphs in ***D***-***F***.

4.3.4 Elevated Action Potential-independent, Impaired Action Potential-dependent Vesicle Release from Cortico-striatal Presynapses

To extend our observations of miniature excitatory synaptic activity, reflecting function of C-S connections, in recordings at the whole-cell level (Figure 4-3 A and B), we wanted to understand the function of individual C-S synapses in SPNs from HD mice under various conditions.

Firstly, we tested miniature release of presynaptic vesicles from C-S synapses at the single synaptic level by conducting a Synaptotagmin1 (Syt1) antibody uptake assay (referred as "Syt1 assay" in the following) in the presence of tetrodotoxin (TTX), an action potential blocker, in YAC128 vs. WT DIV21 C-S coculture. The Syt1 assay allows us to assess vesicular release at single synapses by incubating with an antibody against the luminal domain of Syt1, which is exposed to the extracellular bath solution as the vesicles undergo exocytosis (466). The cells were incubated at 37^{o}C in conditioned medium (containing TTX) with or without the Syt1 antibody for a range of time periods (Figure 4-8 A). The results showed that the average Syt1 intensity under a vGlut1 mask within PSD95-GFP-labeled SPN dendrites (C-S synapses) was significantly higher in YAC128 than in WT coculture under the same antibody exposure times (Figure 4-8 A and B), implying that the C-S synaptic vesicle release mechanism independent of action potentials is likely upregulated in our YAC128 coculture model. Moreover, the basal expression of Syt1 in presynapses (cortical terminals) was indistinguishable between the two genotypes as indicated by its puncta size in permeabilized immunostaining (Figure 4-8 C), further supporting our proposition that action potential-independent vesicle release is elevated at C-S synapses in the YAC128 coculture model. Therefore, we concluded that mHtt expression promotes quantal release at C-S synapses.

This outcome led us to question whether the elevated quantal release of presynaptic vesicles from C-S synapses is a consequence of an increased number of vesicles in the readily releasable pool (RRP) vs. enhanced release probability of individual vesicles. To answer this question, we conducted electrophysiological experiments to estimate the amount of glutamate vesicles in the C-S RRP by recording mEPSC events and the subsequent sucrose-evoked (500 mM, 4 second) EPSC amplitude with whole-cell patch clamp from striatal SPNs in WT and YAC128 DIV21 cocultures, in the presence of the $GABA_A$ receptor and voltage-gated sodium channel blockers (PTX and TTX; Figure 4-9 A).

The sucrose pulse depletes the RRP and boosts its replenishment up to the maximum rate (463,467). In the sucrose-evoked EPSC trace (Figure 4-9 A, trace on the right side), the steady-state charge [blank area under the curve (AUC); referred to as "new pool charge"] is largely induced by glutamate from newly replenished vesicles, whereas the rest (AUC with green stripes; referred to as "original pool charge") is mediated by that from the originally docked vesicles in the RRP (467). Therefore, the number of vesicles in the initial RRP was quantified by dividing the original pool charge by the average charge of mEPSC events recorded from the same cell; in contrast, the RRP maximum replenishment rate (by vesicle) was calculated by dividing the new pool charge by the product of the average mEPSC charge and sucrose-EPSC time duration (467) (Figure 4-9 A). Using this approach, we obtained a small trend toward a reduced number of vesicles in the original RRP in YAC128 compared with WT from DIV21 C-S coculture (Figure 4-9 B). Importantly, vesicle "density", calculated by normalizing vesicle number in the original RRP to cell membrane capacitance (Figure 4-9 C), was comparable between the two genotypes. Considering the similar density of C-S synapses on SPN dendrites between WT and YAC128 in our coculture (Figure 4-7 C), we concluded that the number of readily-releasable vesicles at

individual C-S synapses is not influenced by the presence of mHtt. Therefore, the enhanced live-staining of C-S synapses with Syt1 antibody (Figure 4-8) was most likely due to elevated release probability of individual vesicles. Together, we concluded that mHtt facilitates release of glutamate-containing vesicles at C-S synapses. Likewise, vesicle replenishment rate at C-S synapses, shown by the number of vesicles replenished per membrane capacitance per second, was similar between YAC128 and WT (Figure 4-9 D), suggesting that vesicle renewal at individual C-S synapses is not a subject of alteration by mHtt in this simple coculture system.

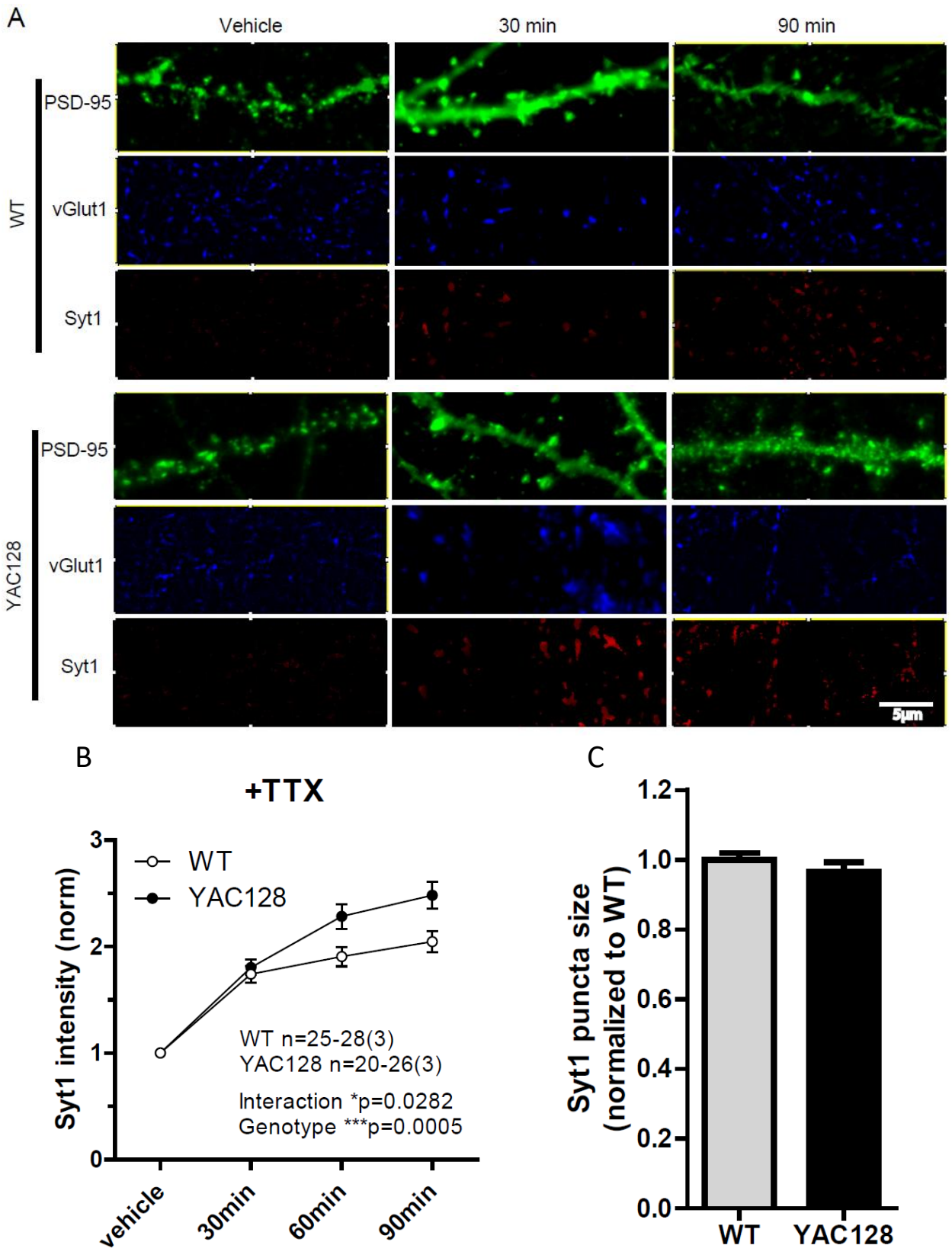
A
Vehicle
30 min
90 min
WT
PSD-95
vGlut1
Syt1
YAC128
PSD-95
vGlut1
Syt1
5μm
B
+TTX
WT
YAC128
Syt1 intensity (norm)
WT n=25-28(3)
YAC128 n=20-26(3)
Interaction *p=0.0282
Genotype ***p=0.0005
vehicle
30min
60min
90min
C
Syt1 puncta size (normalized to WT)
WT
YAC128

Figure 4-8 Action potential-independent vesicle release at C-S synapses is tuned up in YAC128 C-S coculture at DIV21

A. Representative pictures of live-immunostaining of Synaptotagmin1 (Syt1) with an anti-Syt1 luminal domain antibody (red) and cell membrane permeabilized immunostaining of vGlut1 (blue) in WT and YAC128 C-S coculture at DIV21. Striatal neurons were labeled with PSD95-GFP (green) construct when plated, and the fluorescent signal was later enhanced with anti-GFP antibody during immunostaining. ***B.*** With TTX present, YAC128 C-S synapses showed higher Syt1 live-staining intensity under the vGlut1 mask than WT [WT n=25-28(3) and YAC128 n=20-26(3); by 2-way ANOVA test, genotype ***p=0.0005, interaction *p=0.0282 and exposure time ***p<0.0001; by Bonferroni's post-test *p<0.05 at 60 min and **p<0.01 at 90 min]. ***C.*** When measured after cell membrane permeabilization followed by immunostaining, the average puncta size of Syt1 in C-S coculture at DIV21 is comparable between the two genotypes [WT n=48(4) and YAC128 n=51(4); by unpaired t-test p=0.302].

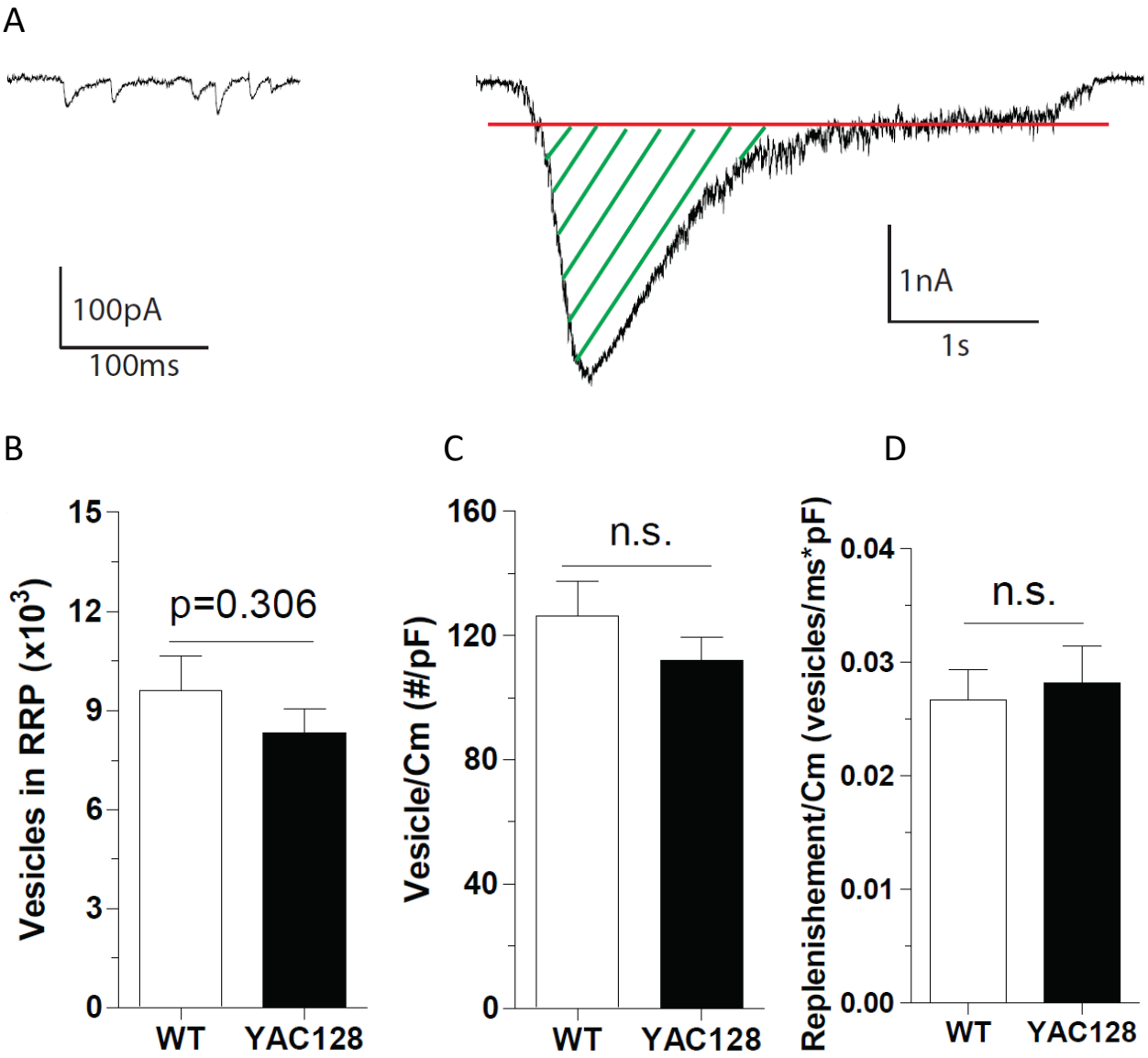
A
100pA
100ms
1nA
1s
B
Vesicles in RRP (x10^3)
p=0.306
WT
YAC128
C
Vesicle/Cm (#/pF)
n.s.
WT
YAC128
D
Replenishement/Cm (vesicles/ms*pF)
n.s.
WT
YAC128

Figure 4-9 The amount of readily releasable vesicles in individual C-S synapses is not affected in YAC128 compared with WT, nor vesicle replenishment.

A. An example of quantifying the number of vesicles in RRP and measuring vesicle replenishment speed. mEPSC events were recorded from striatal SPNs in WT and YAC128 C-S cocultures at DIV21 before sucrose (500 mM, 4 s)-evoked EPSC, which is composed of two components: a triangular region of peak current charge [area under the curve (AUC) with green stripes below red line; original pool charge] and a rectangular region of steady-state current charge (blank AUC above red line; new pool charge). Division of the original pool charge by the average charge of the preceding mEPSCs from the same cell estimates vesicle quantity in RRP, whereas that of new pool charge divided by the product of the average mEPSC charge and sucrose duration generates RRP vesicle replenishing speed. ***B.*** The estimated number of vesicles in original RRP is lower in YAC128 C-S connections, but not significant, compared with WT in DIV21 C-S cocultures [WT n=21(5) and YAC128 n=27(6); p=0.306 by unpaired t-test]. ***C.*** The number of RRP vesicles per membrane capacitance is comparable between the two genotypes [WT n=21(5) and YAC128 n=27(6); p=0.2816 by unpaired t-test], and so is the average number of replenished vesicles per membrane capacitance per second [***D.***: WT n=21(5) and YAC128 n=27(6); p=0.7352 by unpaired t-test].

Secondly, we were interested in learning about action potential-dependent vesicle release at C-S synapses in HD that determines synaptic efficacy, as this contributes to learning efficiency and capacity *in vivo*. To answer this question, we performed the Syt1 assay on WT and YAC128 C-S coculture at DIV21 in the absence of TTX for a range of exposure times. Our results demonstrated that the average Syt1 intensity under the vGlut1 mask [within striatal dendrites (C-S synapses) identified with PSD95-GFP transfection or DARPP32 immunostained dendritic processes] was significantly lower in YAC128 than in WT cocultures with the same exposure times (Figure 4-10 Ai and Aii), suggestive of reduced cortical neuronal activity or impaired action potential-dependent vesicle release at YAC128 C-S synapses. Interestingly, cortical neuronal firing rate was similar between the two genotypes, as indicated in whole-cell current clamp recording of cortical neuronal (YFP-transfected) membrane potential in response to various current injections (Figure 4-10 Bi and Bii), confirming impairment in action potential-dependent vesicle release in YAC128 C-S synapses. Notably, using immunocytochemistry we found a significant reduction in puncta size of cysteine string protein (CSP) in YAC128 DIV21 coculture compared with WT (Figure 4-10 C). CSP is a presynaptic machinery protein whose function is to facilitate action potential-dependent exocytosis of presynaptic vesicles via interaction with SNAP-25 (468). Intriguingly, CSP has stronger association with mHtt over wild-type Htt (202), and mHtt sequesters CSP from presynaptic terminals by suppressing its palmitoylation by HIP14 (202,469). Therefore, we concluded that neuronal activity-dependent vesicle release at C-S synapses is impaired with mHtt expression, which likely interferes with synaptic machinery by disrupting localization of synaptic proteins such as CSP.

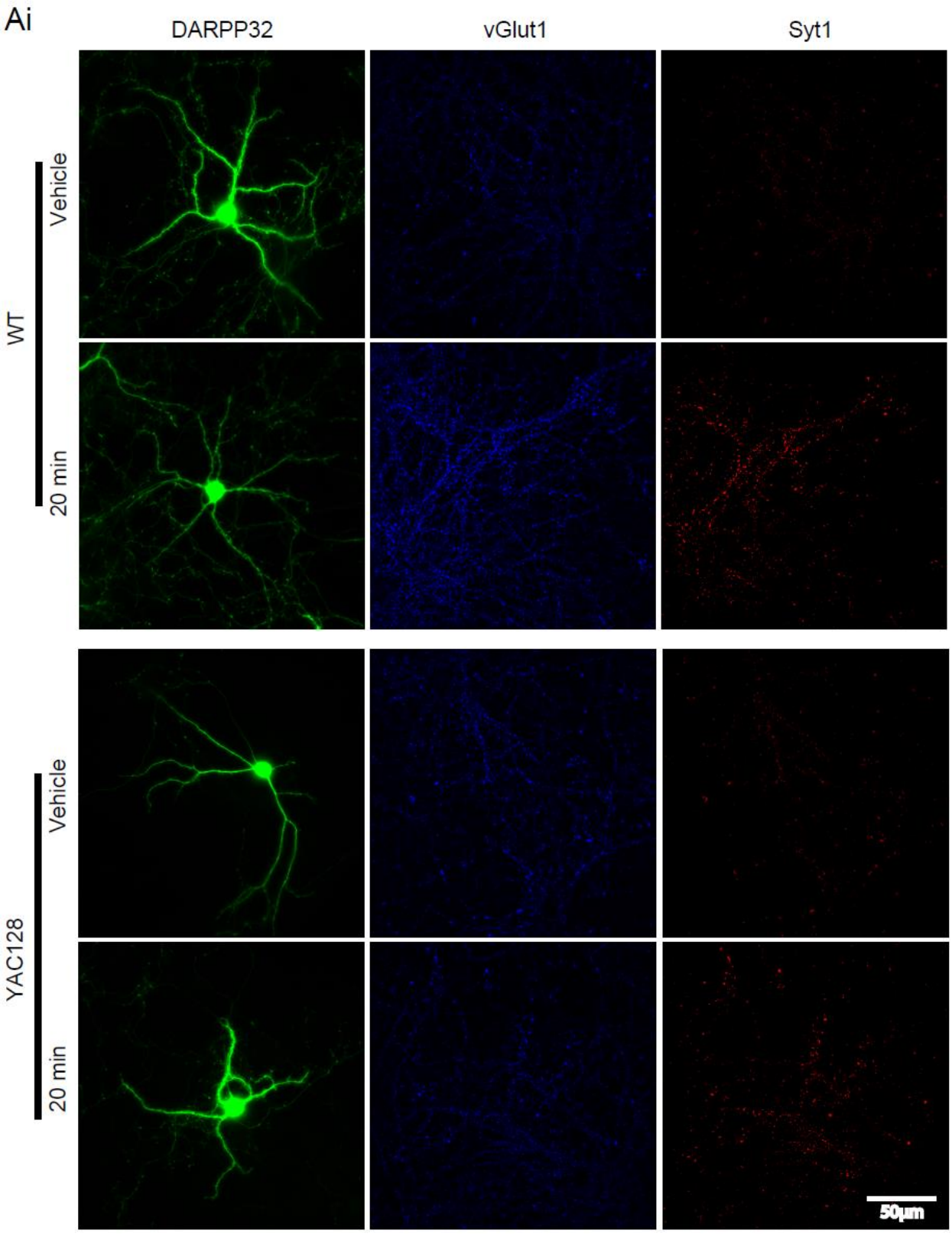
Ai
DARPP32
vGlut1
Syt1
WT
Vehicle
20 min
YAC128
Vehicle
20 min
50µm

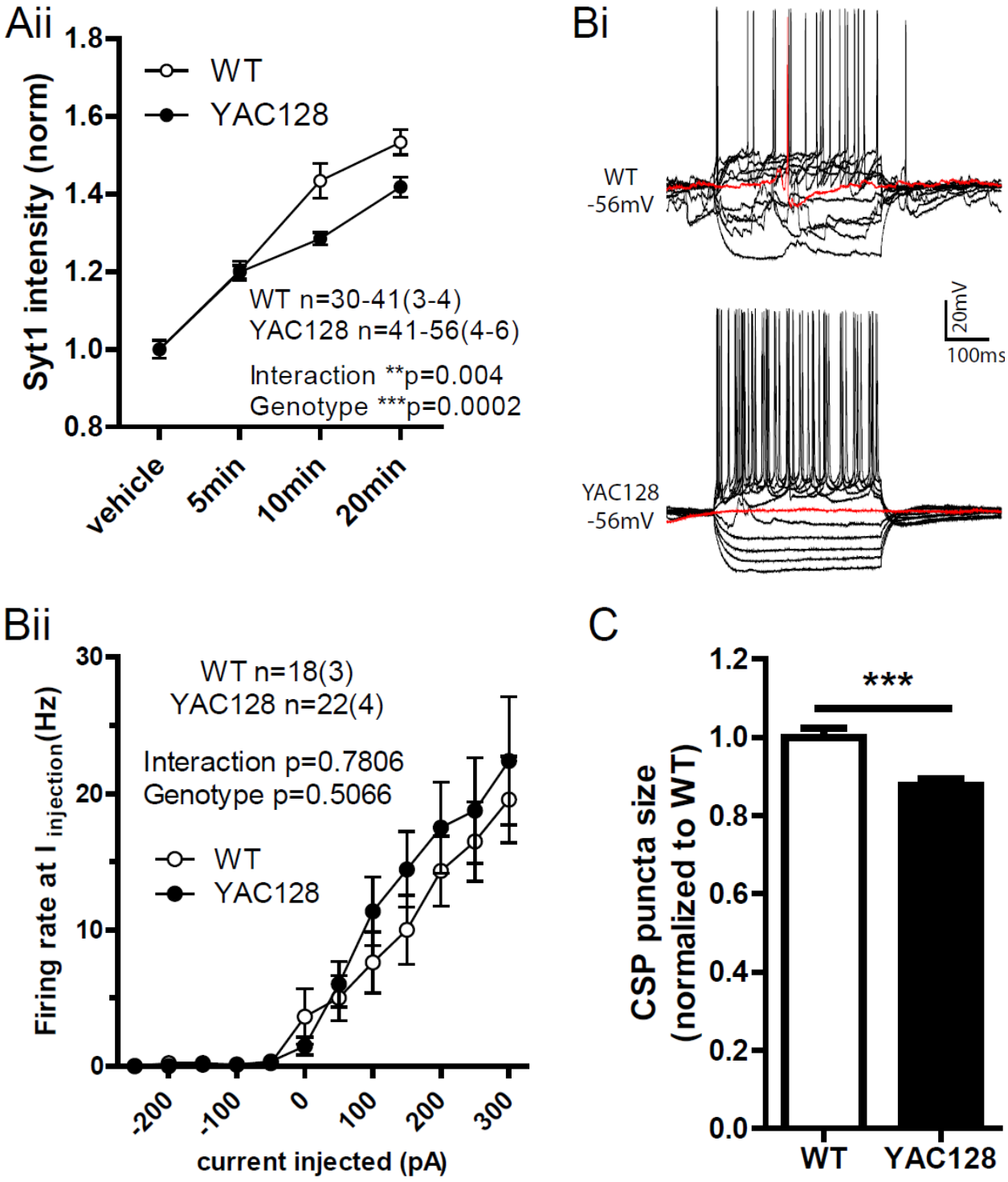
Aii
Syt1 intensity (norm)
1.8
1.6
1.4
1.2
1.0
0.8
WT
YAC128
WT n=30-41(3-4)
YAC128 n=41-56(4-6)
Interaction **p=0.004
Genotype ***p=0.0002
vehicle
5min
10min
20min
Bi
WT
-56mV
YAC128
-56mV
20mV
100ms
Bii
Firing rate at I injection (Hz)
30
20
10
0
WT n=18(3)
YAC128 n=22(4)
Interaction p=0.7806
Genotype p=0.5066
WT
YAC128
-200
-100
0
100
200
300
current injected (pA)
C
CSP puncta size
(normalized to WT)
1.2
1.0
0.8
0.6
0.4
0.2
0.0
***
WT
YAC128

Figure 4-10 Neuronal activity-dependent vesicle release at C-S synapses, but not cortical neuronal activity, is dysregulated by mHtt in YAC128 DIV21 C-S coculture

Ai. Representative photomicrographs of live-stained Syt1 (red; Syt1 assay without TTX) and permeabilized immunostaining of vGlut1 (blue) and DARPP32 (green) in WT and YAC128 C-S cocultures at DIV21 (controls were incubated in conditioned medium containing only glycerol). ***Aii*** The basal background intensity of Syt1 channel at C-S synapses is similar between WT and YAC128, but with same time exposure to Syt1 antibody YAC128 revealed lower Syt1 intensity under vGlut1 mask within DARPP32-positive dendrites compared with WT [normalized to control conditions; WT n=30-41(3-4) and YAC128 n=41-56(4-6); by 2-way ANOVA test genotype ***p=0.0002, interaction **p=0.004 and exposure time ***p<0.0001; ***p<0.001 at 10 min and **p<0.01 at 20 min exposure time by Bonferroni's post-test]. ***Bi.*** Representative traces of membrane potential (Vm) responses recorded from WT and YAC128 cortical neurons with whole-cell patch clamp in response to current injections from -250 to 300 pA with increments of 50 pA in C-S coculture at DIV21. Red trace indicates Vm response at 0 current injection. ***Bii.*** Firing frequency of YAC128 cortical neurons is not significantly different from that of WT at a given current injection [WT n=18(3) and YAC128 n=22(4); by 2-way ANOVA test genotype p=0.5066, interaction p=0.7806 and current ***p<0.0001]. ***C.*** Immunostained puncta size of CSP protein in YAC128 C-S coculture is significantly smaller than in WT at DIV21 [WT n=35(3) and YAC128 n=30(3); by unpaired t-test ***p<0.0001].

4.3.4.1 From Cortico-striatal Coculture to Acute Brain Slice

Results shown above, comparing C-S synapses in YAC128 vs. WT coculture, indicated that: *i)* the presynaptic vesicle RRP and replenishment rate is similar; *ii)* AP-independent presynaptic vesicle release is elevated whereas AP-dependent (calcium-induced, synchronous) vesicle release is impaired; and *iii)* glutamate content of individual vesicles is reduced. To investigate these processes in a more intact system, I used direct measurement of cortical glutamate release in acute cortical-striatal slices from 6-month old YAC128 and WT mice. This age was chosen because 6-month YAC128 mice show motor deficits but no significant reduction in striatal volume (90,93) and are considered to be at an early symptomatic stage.

To directly measure synaptically-released glutamate I used the intensity-based glutamate-sensing fluorescent reporter (iGluSnFr), a sensor protein that is capable of indicating the glutamate level in the extracellular space in a concentration-dependent manner when expressed on neuronal or astrocyte cell membranes (327,470). Due to the limited sensitivity of iGluSnFr to quantal release of glutamate, and difficulty in isolating quantal vesicle release of cortical glutamatergic terminals from that of thalamic, we were able to determine only action potential-dependent glutamate release from C-S synapses by electrically stimulating in corpus callosum.

Adeno-associated virus (AAV) carrying the iGluSnFr construct was injected into the dorsal striatum of 4 to 6-week old anaesthetized mice. By 6 months of age when the sensor was abundantly expressed, the imaging experiment was conducted on sagittal acute brain slices (thickness: 300µm) containing striatum prepared from WT and YAC128 mice. A series of electrical stimuli (300µA) were generated within corpus callosum adjacent to the dorsal striatum where iGluSnFr was highly abundant (Figure 4-11 A and B). The iGluSnFR fluorescence was excited with a blue LED for the duration of video acquisition (150Hz, 6.67ms frame-rate). A

stimulation paradigm shown in Figure 4-11 C was applied: paired stimuli (10 ms apart), applied six times at 30s intervals, were followed by a train stimulation (100 Hz for 500 ms). The average intensity of a 6x6-pixel region of interest (in 128x128 pixel image) within the striatum was acquired from each frame after background subtraction, and was plotted as an intensity response curve against time (Figure 4-11 D). The peak intensity average of all paired stimuli was normalized to that of the following train stimuli within each slice, and it is regarded as a C-S presynaptic glutamate vesicle release indicator in response to action potentials, triggered here with electrical stimulation of axon fibers projecting from cortex through corpus callosum to striatum. We found that the proportion of maximal action potential-dependent release of the presynaptic glutamate pool trended to be reduced in YAC128 compared to WT striatum ($p = 0.0968$), although this was not significant (Figure 4-11 D and E). This suggests that the disruptive effect of mHtt on AP-dependent vesicle release is still minimal at this age *in vivo*.

A

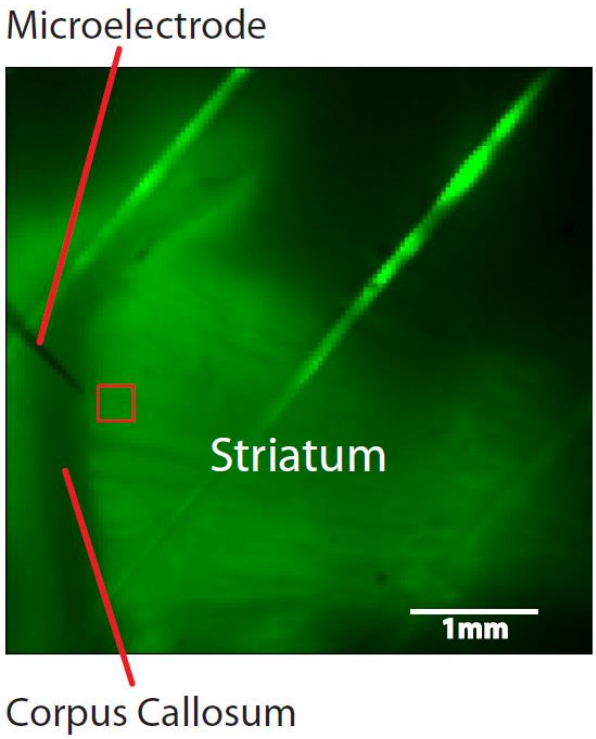
Microelectrode
Striatum
1mm
Corpus Callosum

B

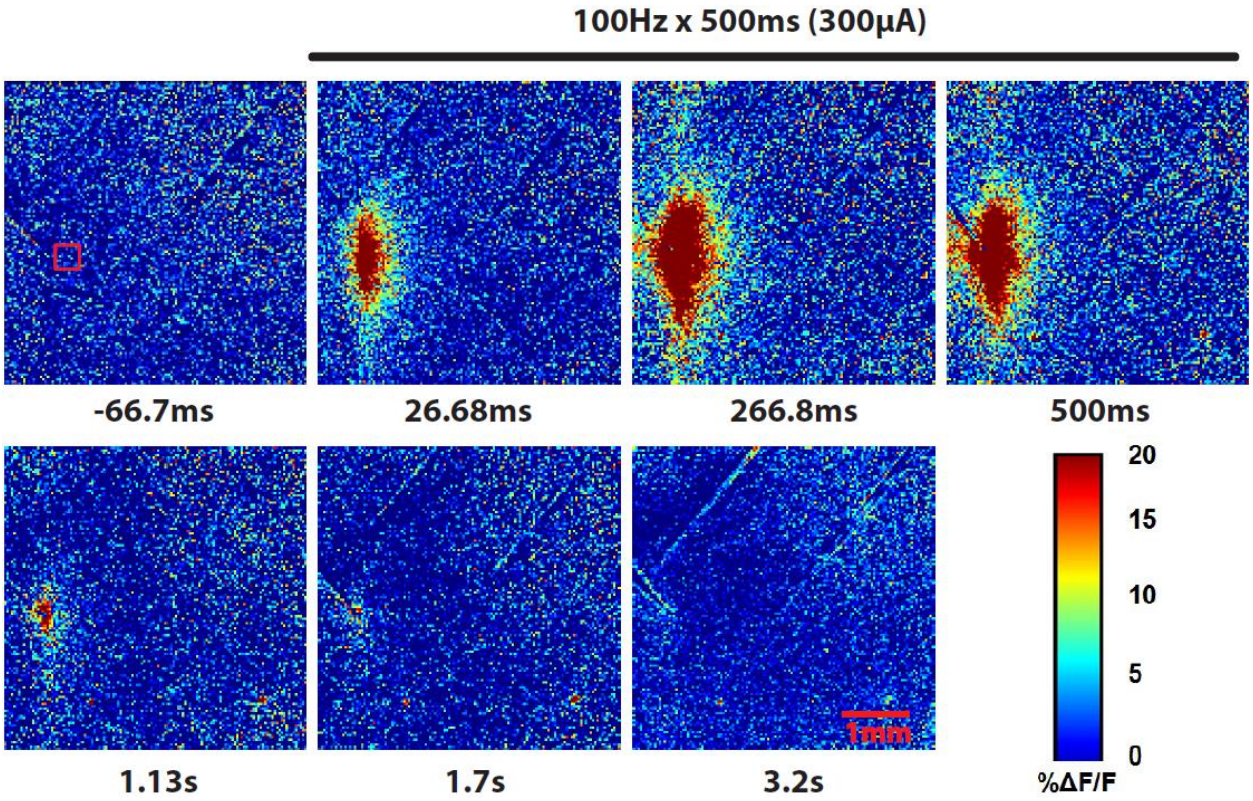
100Hz x 500ms (300µA)
-66.7ms
26.68ms
266.8ms
500ms
1.13s
1.7s
3.2s
1mm
20
15
10
5
0
%ΔF/F

C

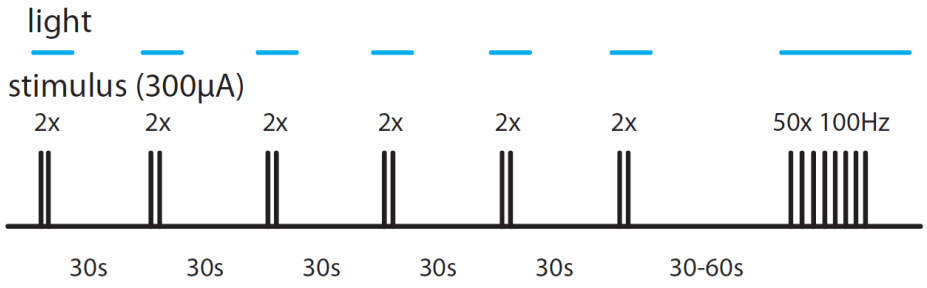
light
stimulus (300µA)
2x
2x
2x
2x
2x
2x
50x 100Hz
30s
30s
30s
30s
30s
30-60s

D

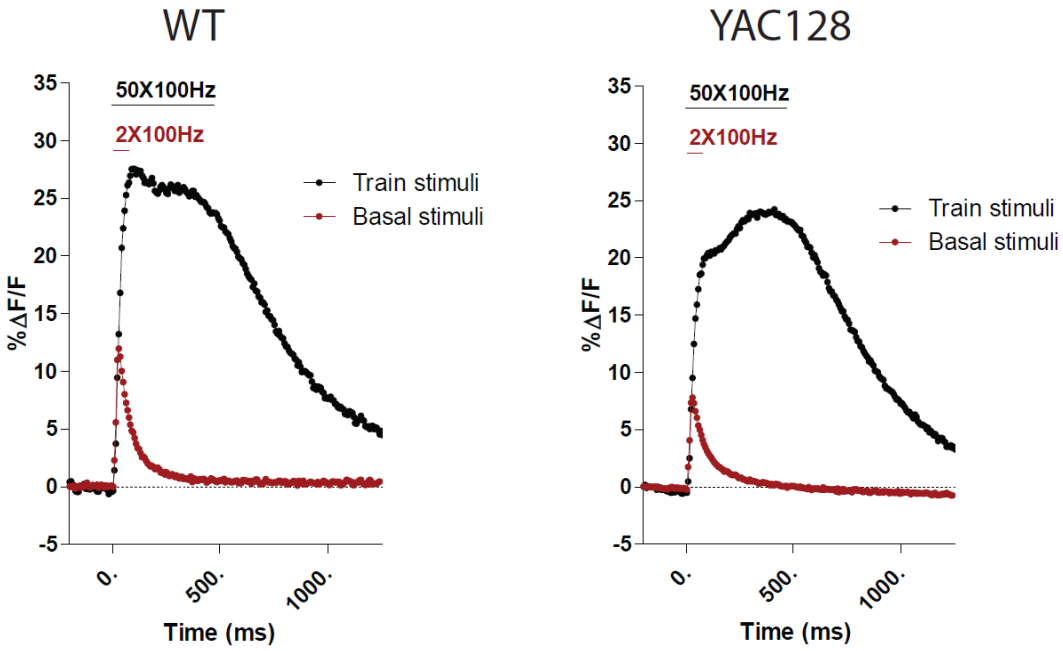
WT
YAC128
50X100Hz
2X100Hz
Train stimuli
Basal stimuli
%ΔF/F
Time (ms)
0.
500.
1000.

E

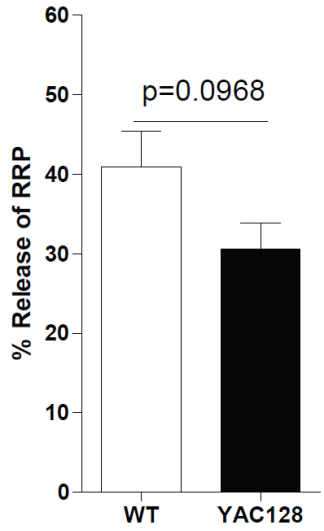
p=0.0968
% Release of RRP
WT
YAC128

Figure 4-11 Direct measurement of action potential-dependent glutamate release from C-S connections in acute brain slices prepared from 6-month old YAC128

A. An example picture showing expression of intensity-based glutamate sensor fluorescent reporter (iGluSnFr) in dorsal striatum in acute brain slice from 6-month old mouse with stimulating micro-electrode in corpus callosum. Red box indicates the region of interest (ROI) for analysis within striatum. ***B.*** Heat-map graph of fluorescence in the example slice under 100-Hz, 500-ms train electrical stimulation (300 μA) showed a corresponding, long-lasting response in ROI (red box) next to the stimulation site after subtraction of fluorescence depletion. In iGluSnFr graphs, %ΔF/F indicates percent change of fluorescence in contrast to basal intensity. ***C.*** Schematic diagram of electrical stimulation paradigm adopted to assess action potential-dependent vesicle release from C-S synapses: 6 pairs of basal stimuli (10 ms apart; 300 μA) were succeeded by a train stimulation (100 Hz; 500 ms; 300 μA), all accompanied with light (blue LED). ***D.*** Representative traces of iGluSnFr fluorescence changes in striatal ROIs imaged from acute brain slices from 6-month old WT and YAC128 mice under electrical stimulation with paradigm shown in ***C***, with background subtracted. Red (responses to basal stimuli) and black traces (to train stimulation) are overlapped to compare. ***E.*** Average peak intensity of iGluSnFr response to basal stimuli (example %ΔF/F in red in ***C***) was normalized to peak intensity of train stimulation (black %ΔF/F in ***C***) within slices. This measurement strongly trended to be reduced in YAC128 compared with WT, yet insignificant [WT n=12(4) and YAC128 n=9(4); by unpaired t-test p=0.0968; the n's indicate the numbers of slices analyzed whereas the animal numbers are shown in parentheses].

4.3.5 Suppressed Glutamate Pool Recovery at Cortico-striatal Connections in both YAC128 Three-week Cortico-striatal Cocultures and Acute Brain Slices from 6-month Old YAC128 Mice

Previously, we demonstrated that vesicle replenishment at C-S synapses is unaffected in YAC128 (Figure 4-9 D), but glutamate content in vesicles is reduced (Figure 4-3 D). Here, we asked whether recovery of the readily-releasable glutamate pool (referred as "glutamate recovery" hereafter) is slowed by the presence of mHtt, by measuring at various recovery times after a hypertonic sucrose and a high frequency train challenge *in vitro* and *in vivo*, respectively.

At first, we wanted to assess glutamate recovery at C-S synapses at more than a single recovery time (Figure 4-4 F and G) in our C-S coculture by implementing whole-cell patch clamp recording from striatal SPNs in response to paired-sucrose pulses (PSP) at a depleting concentration (500 mM; 3 s) with various inter-pulse intervals. The peak current of the second sucrose-EPSC was normalized to that of the first within the pair (Figure 4-12 Ai). Our results showed a significant genotype effect (*p=0.0415) by repeated measure 2-way ANOVA comparing percent recovery of sucrose-EPSC between WT and YAC128 cocultures at DIV21 (Figure 4-12 Aii), but there was no significant difference at any measured time point by Bonferroni's post-test. Given that the mEPSC amplitude was not differentially affected between the two genotypes after a sucrose pulse (4.3.2, Results, Chapter 4), we concluded that mHtt impedes glutamate recovery at C-S excitatory synapses, but does not promote AMPA receptor desensitization/inactivation/internalization. In contrast, the percent recovery of the sucrose-evoked IPSC, which is predominantly from inhibitory connections established between SPNs, was not significantly different between YAC128 and WT (Figure 4-12 B) under the same coculture

conditions and experimental protocol. This suggests selective suppression of glutamate recovery by mHtt at C-S synapses.

Ai

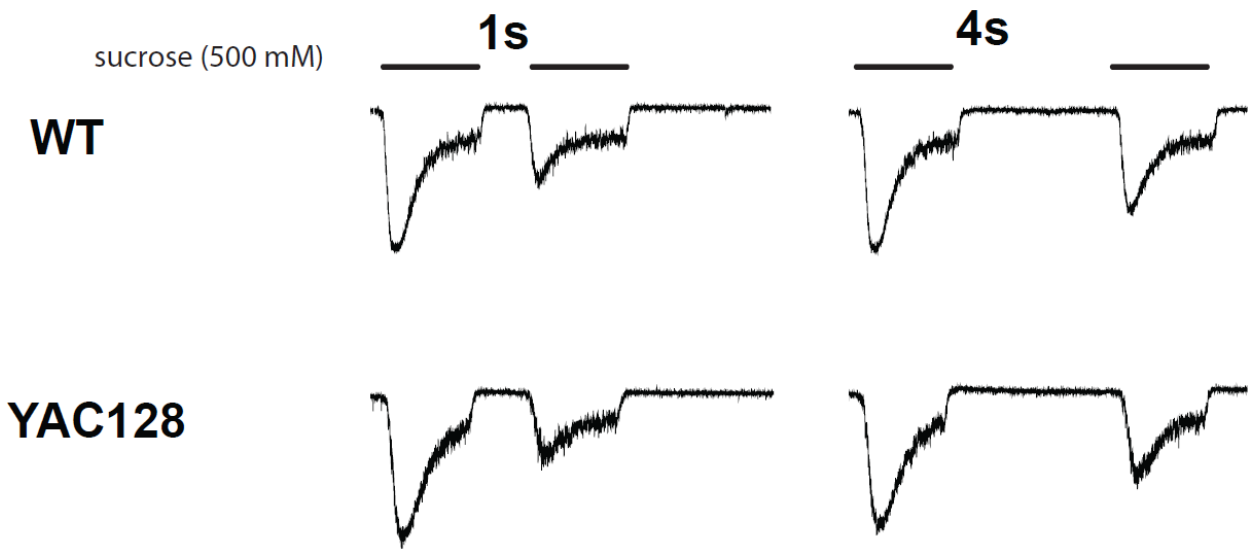
sucrose (500 mM)
1s
4s
WT
YAC128

Aii

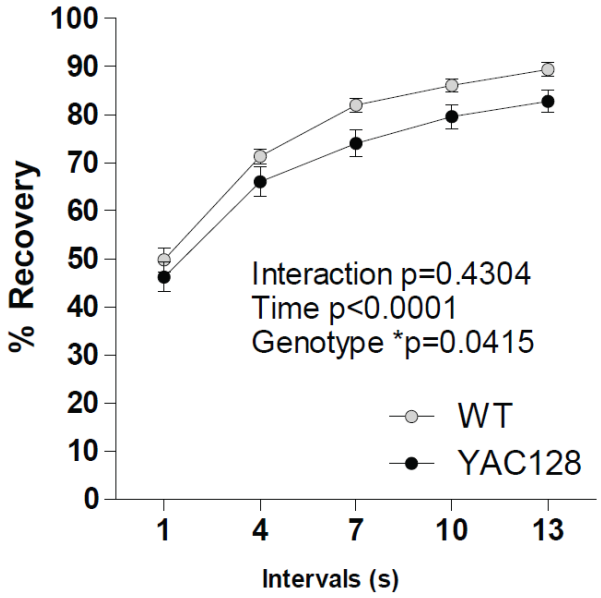
% Recovery
Intervals (s)
Interaction p=0.4304
Time p<0.0001
Genotype *p=0.0415
WT
YAC128

B

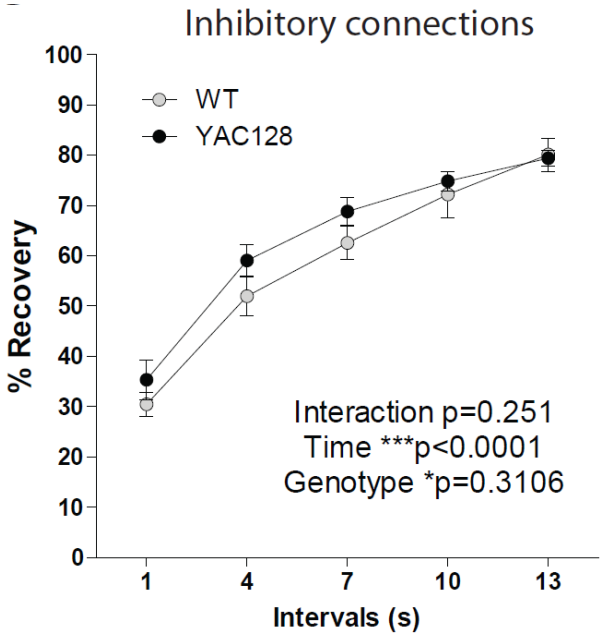
Inhibitory connections
% Recovery
Intervals (s)
WT
YAC128
Interaction p=0.251
Time ***p<0.0001
Genotype *p=0.3106

Figure 4-12 After sucrose challenge, percent recovery of EPSC recorded from striatal SPNs is significantly lower, but not that of IPSC, in YAC128 than in WT at DIV21 in C-S coculture.

Ai. Illustrative EPSC traces recorded from striatal SPNs in response to paired-sucrose pulses (PSP; 500 mM; 3 s) with different inter-pulse intervals but fixed inter-pair time (1 min for full recovery) in WT and YAC128 C-S cocultures at DIV21. PSP EPSC traces with 1 s and 4 s intervals are shown here. Peak current of later sucrose-EPSC normalized to that of former in pair was regarded as an indicator of presynaptic neurotransmitter (excitatory) pool recovery. ***Aii.*** The percent recovery of sucrose-EPSC recorded from striatal SPNs is lower in YAC128 than in WT [WT n=20(3) and YAC128 n=19(3); by repeated measure 2-way ANOVA interaction $p=0.4304$, intervals ***$p<0.0001$, and genotype *$p=0.0415$; with Bonferroni's post-test $p>0.05$ at all intervals]; in comparison, the percent recovery of sucrose-IPSC is similar in YAC128 compared with WT at DIV21 in C-S coculture [***B.***: WT n=10(3) and YAC128 n=10(4); by repeated measure 2-way ANOVA interaction $p=0.251$, intervals ***$p<0.0001$, and genotype **$p=0.3106$; with Bonferroni's post-test $p>0.05$ at all intervals].

Next, we asked whether the impaired glutamate recovery that we observed *in vitro* is also present *in vivo*. To answer this question, we recorded EPSCs from striatal SPNs in acute brain slices prepared from 6-month old WT and YAC128 mice that are regarded as at an early phenotypic stage, under paired electrical train stimuli (300-500 μA; 20Hz for 4s per train; Figure 4-13 A) in corpus callosum (stimulating electrode was 150-450 μm distant from the recorded striatal SPN) with a variety of inter-train intervals (with 1 min full-recovery time between pairs). Like the PSP in coculture (Figure 4-12 Ai and Aii), the total charge of first 1 second response of the second train response in each pair was divided by that of the first (because the majority of RRP is released in response to the first 1 second stimuli in each train stimulation), and was considered as an index of glutamate recovery. We found a reduced proportion of second SPN EPSC charge relative to that of the first in YAC128 compared with WT (Figure 4-13 Bi, Bii and C) as revealed by a significant genotype effect by repeated measure 2-way ANOVA (genotype *p=0.018; by Bonferroni's post-test p>0.05 at all intervals), similar to our observation in C-S coculture (Figure 4-12 Aii). This is suggestive of impaired glutamate recovery at C-S synapses in the HD condition. Enhanced AMPA receptor desensitization/internalization in YAC128 SPNs is a less likely explanation, since AMPA receptor desensitization is actually reduced in YAC128 SPNs compared to WT (in acutely dissociated neurons at 7 months) (312). Therefore, we concluded that mHtt inhibits recovery of the readily-releasable glutamate pool at C-S synapses both *in vitro* and in acute brain slices. Furthermore, a significantly faster decay of EPSC amplitude in the first train responses was recorded in YAC128 compared with WT (Figure 4-13 D), also similar to our finding in C-S coculture (Figure 4-4 E). These data provide further evidence supporting our conclusion that mHtt suppresses glutamate recovery at C-S connections.

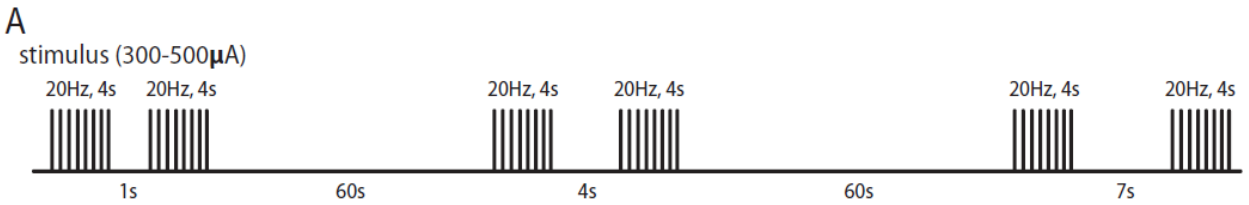
A
stimulus (300-500µA)
20Hz, 4s
20Hz, 4s
20Hz, 4s
20Hz, 4s
20Hz, 4s
20Hz, 4s
1s
60s
4s
60s
7s

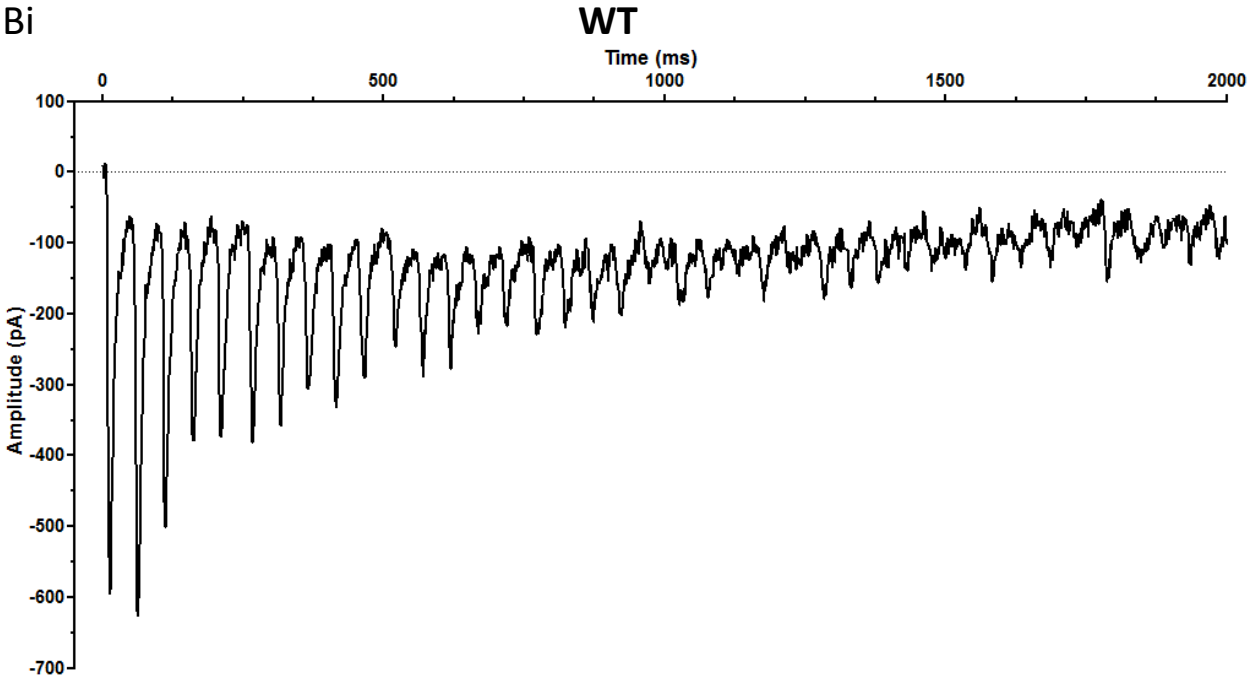
Bi
WT
Time (ms)
0
500
1000
1500
2000
100
0
-100
-200
-300
-400
-500
-600
-700
Amplitude (pA)

Bii

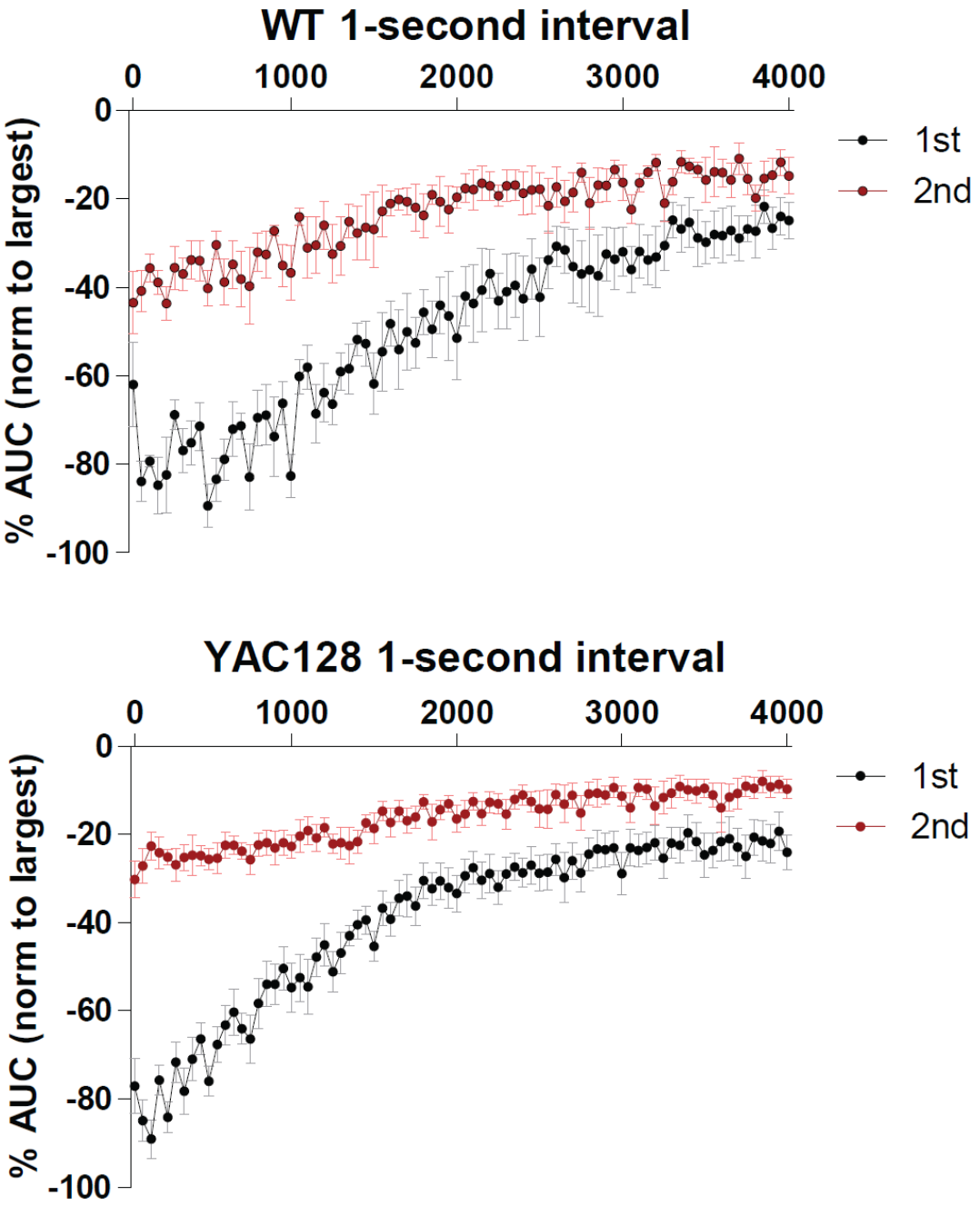
WT 1-second interval
0
1000
2000
3000
4000
0
-20
-40
-60
-80
-100
% AUC (norm to largest)
1st
2nd
YAC128 1-second interval
0
1000
2000
3000
4000
0
-20
-40
-60
-80
-100
% AUC (norm to largest)
1st
2nd

C

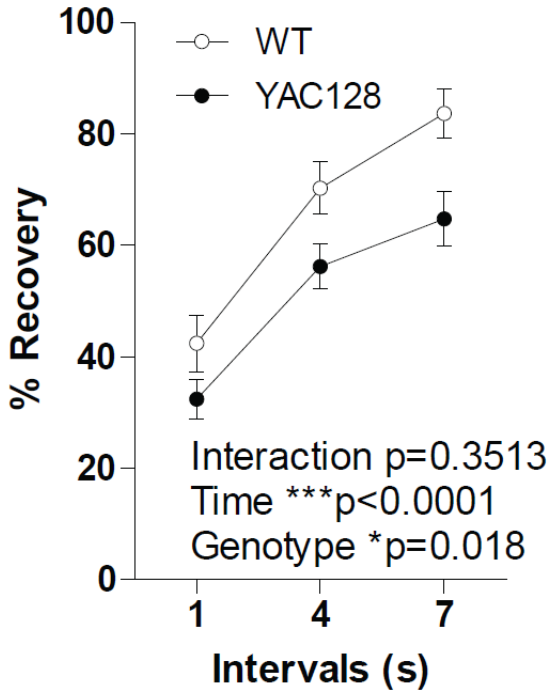
100
80
60
40
20
0
% Recovery
WT
YAC128
Interaction p=0.3513
Time ***p<0.0001
Genotype *p=0.018
1
4
7
Intervals (s)

D

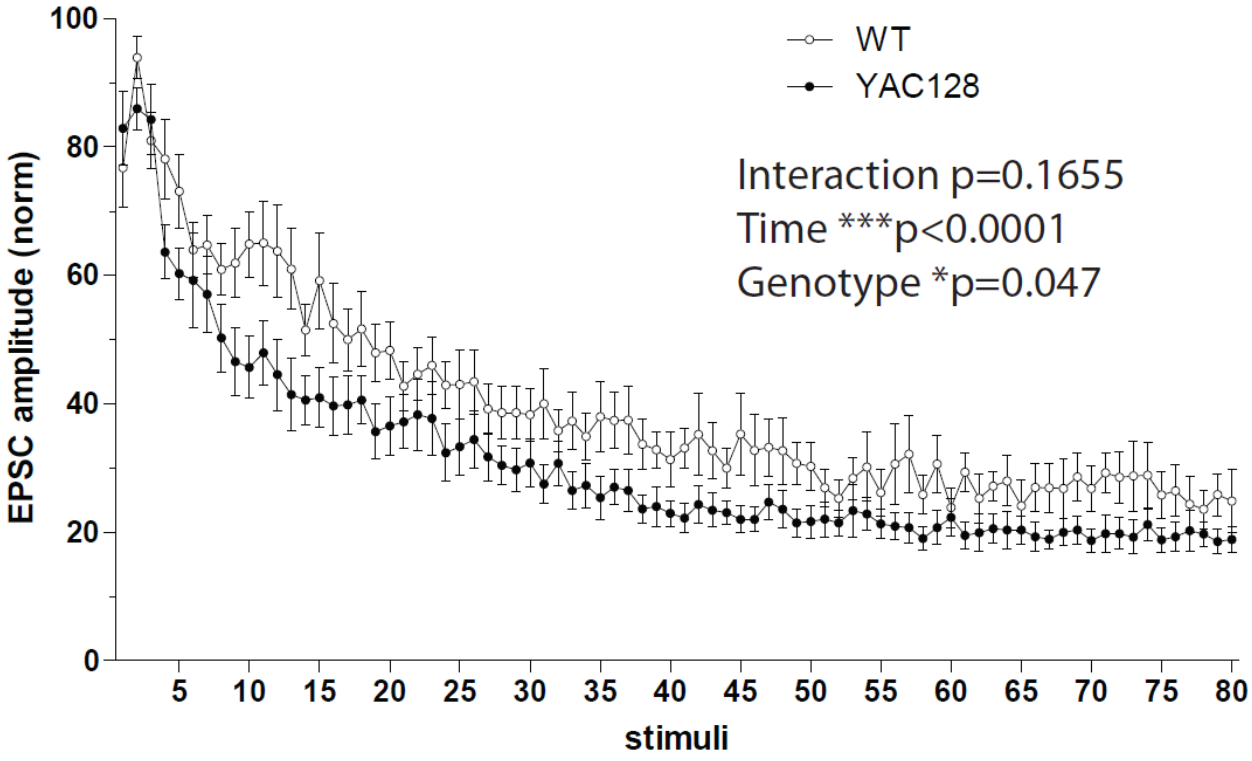
100
80
60
40
20
0
EPSC amplitude (norm)
WT
YAC128
Interaction p=0.1655
Time ***p<0.0001
Genotype *p=0.047
5
10
15
20
25
30
35
40
45
50
55
60
65
70
75
80
stimuli

Figure 4-13 Whole-cell patch-clamp electrophysiological study of striatal SPNs revealed reduced percent recovery EPSC under paired electrical train stimulation of corpus callosum at C-S synapses in acute brain slices from 6-month old YAC128.

A. Schematic diagram showing electrical stimulation paradigm of corpus callosum in sagittal slices of striatum. ***Bi.*** A representative trace recorded from WT striatal SPNs under electrical train stimulation (300-500 μA; 20 Hz for 4 s; only first 2 s response was shown here) in corpus callosum in acute brain slice prepared from a 6-month old mouse. ***Bii.*** Averaged responses of the first pairs (1-second interval) recorded from striatal SPNs under the repeated stimuli in acute brain slices from 6-month old WT and YAC128. Black traces indicate EPSC charge response to 1st train stimulation, while red shows that to 2nd. Event charge of each response was normalized to largest one in 1st train stimulation from same cells, which often appears within initial ten responses. ***C.*** The percent recovery of striatal EPSC charge of electrical train stimuli (Only the responses to the first 1-second stimuli in each train stimulation was considered) is lower in YAC128 compared to that in WT at 6 months [WT n=7(5) and YAC128 n=11(7); by repeated measure 2-way ANOVA interaction p=0.3513, interval ***p<0.001 and genotype *p=0.018; by Bonferroni's post-test p>0.05 at all intervals]. ***D.*** Amplitude of EPSC in train stimulation decays faster in YAC128 than in WT [normalized to largest amplitude peak within each cell; WT n=9(6) and YAC128 n=12(6); by repeated 2-way ANOVA interaction p=0.1655, ***time p<0.0001 and genotype *p=0.047; by Bonferroni's post-test p>0.05 at all stimuli]. In this figure, the n's indicate the numbers of slices used whereas the animal numbers are shown in parentheses.

To further confirm our result -- disrupted recovery of the glutamate pool at C-S synapses in an HD model *ex vivo*, using a more direct assessment with less involvement of postsynaptic striatal SPNs, I adopted iGluSnFr as beforehand described (Figure 4-11) and measured glutamate content released from cortical terminals into the striatum under train electrical stimulation in corpus callosum. In this experiment, as applied above in slice electrophysiology, pairs of train stimuli (300 μA; 100 Hz; 500 ms) with various inter-train intervals (4, 7 and 10 s) were generated with 60 seconds between pairs (full-recovery time; Figure 4-14 A). The peak amplitude of the second train response was normalized to that of the first in each pair, and this value indicates glutamate pool recovery within a given inter-train interval.

Our results showed that the percent recovery of iGluSnFr fluorescence under train stimulation was lower in YAC128, at least at 4-second inter-train intervals, as suggested by repeated measure 2-way ANOVA (interaction **$p=0.0046$) and Bonferroni's post-test (*$p<0.05$ at 4 s), compared to that in WT at 6 months (Figure 4-14 B and C). These results are consistent with our electrophysiological experiment results (Figure 4-13 C) and suggestive of reduced glutamate recovery at C-S synapses in YAC128, at least at the early recovery time. Together, this result further supports our conclusion that recovery of the glutamate pool at C-S synapses is impeded in HD at an early symptomatic stage.

A

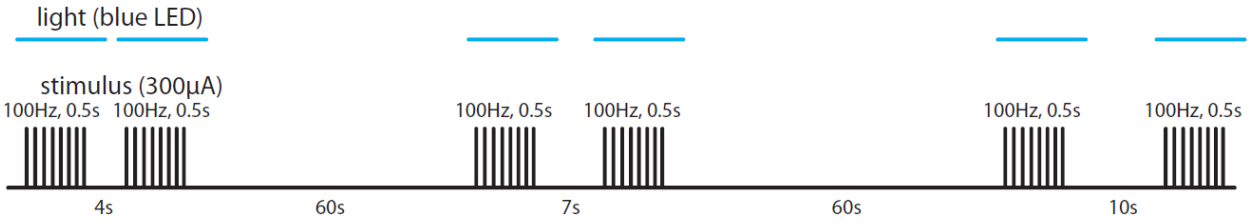
light (blue LED)
stimulus (300µA)
100Hz, 0.5s
100Hz, 0.5s
100Hz, 0.5s
100Hz, 0.5s
100Hz, 0.5s
100Hz, 0.5s
4s
60s
7s
60s
10s

B

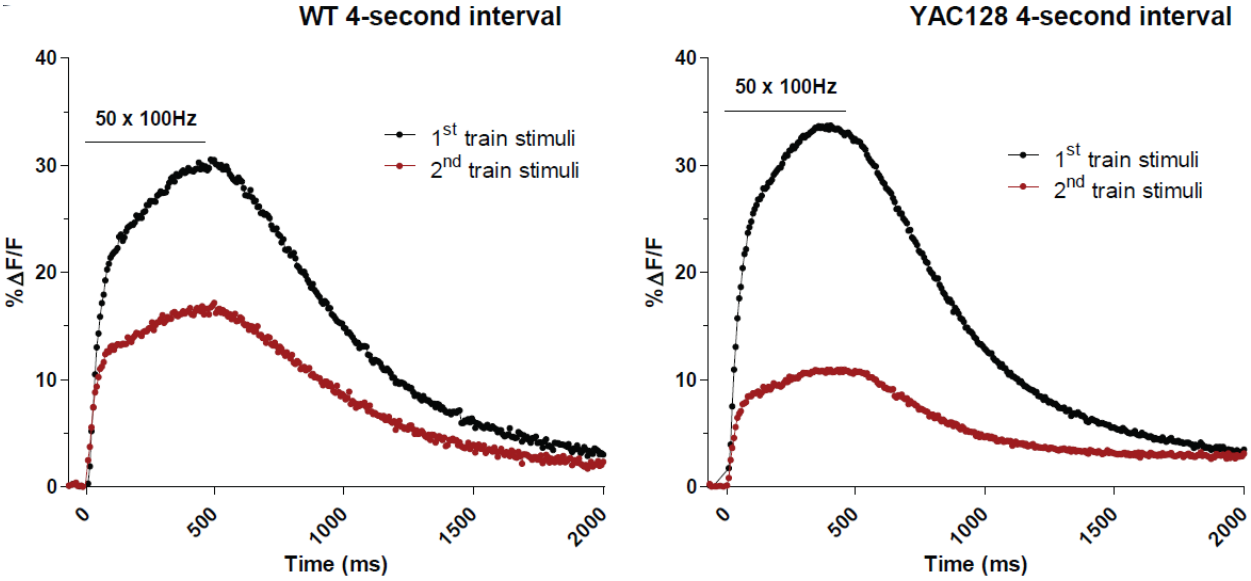
WT 4-second interval
YAC128 4-second interval
50 x 100Hz
1st train stimuli
2nd train stimuli
%ΔF/F
Time (ms)
0
500
1000
1500
2000
10
20
30
40

C

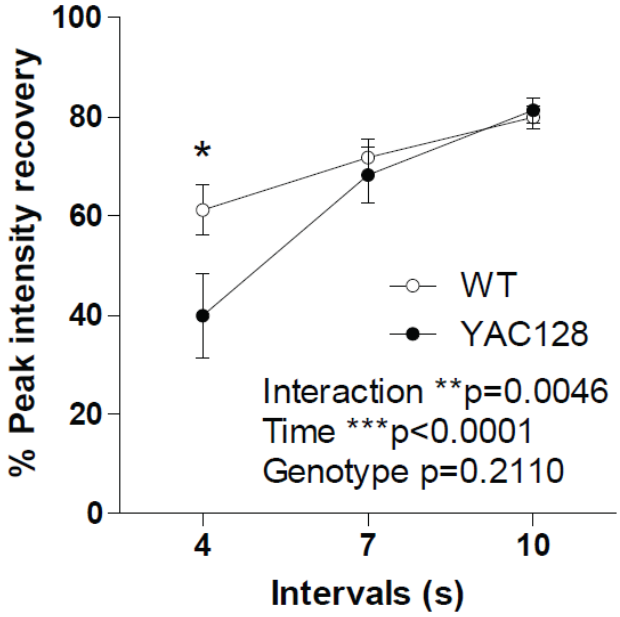
% Peak intensity recovery
Intervals (s)
WT
YAC128
*
Interaction **p=0.0046
Time ***p<0.0001
Genotype p=0.2110
0
20
40
60
80
100
4
7
10

Figure 4-14 Assessment of recovery of readily-releasable glutamate pool at C-S synapses under electrical stimulation in corpus callosum in acute brain slices obtained from 6-month old WT and YAC128 with iGluSnFr

A. Schematic diagram shows train stimulation (electrical) paradigm and iGluSnFr fluorescence excitation with blue LED. ***B.*** Representative responses of iGluSnFr fluorescent signal recorded from 6-month old WT and YAC128 striatal slices under paired-train stimulation with 4-second interval. First train stimulation responses are shown in black and seconds are in red. Normalized peak response of second train stimulation to that of first is an indicator of recovery of readily-releasable glutamate pool at C-S connections. ***C.*** Under paired-train stimulation with various inter-train intervals, YAC128 shows reduced percent recovery of fluorescent peak intensity at 4-second inter-train interval compared with WT at 6 months [WT n=10(5) and YAC128 n=10(3); by repeated measure 2-way ANOVA interaction **p=0.0046, interval ***p<0.0001 and genotype p=0.211; by Bonferroni's post-test *p<0.05 at 4 s; the n's indicate the numbers of slices analyzed whereas the animal numbers are shown in parentheses].

4.4 Discussion

HD is viewed as a synaptopathy, in which measurable early synaptic changes precede later neurodegeneration and may be a prerequisite for neuronal death. Using a coculture system to study the C-S synapse in relative isolation provides us with an accessible means to investigate the mechanisms underlying HD-associated synaptic dysfunction and to assess the potential value of various therapeutic avenues to restore normal synaptic neurotransmission. Here, we demonstrate that many of the synaptic changes previously reported to occur in the striatum at mid-to-late stages of HD in animal models (28) can be detected as early as three weeks *in vitro* where striatal SPNs are cocultured with cortical neurons. Detectable differences were observed in striatal SPN dendritic complexity, frequency of excitatory events, presynaptic vesicle release under different conditions and recovery of the presynaptic glutamate pool following sustained stimulation at C-S synapses. Thus, C-S cocultures can be a useful platform for understanding the mechanisms underlying synaptic dysfunction in HD and for investigating therapeutics for preventing/restoring synaptic changes in HD.

4.4.1 mHtt Does Not Impact Basal Neuronal Survival in Cortico-striatal Coculture by Three Weeks *In Vitro*

When mHtt is expressed, striatal neurons become more vulnerable to harmful stimuli (300). However, in this chapter, we found that the basal cell survival of DARPP-32-expressing SPNs is very similar between WT and YAC128 three weeks after plating with cortical neurons (Figure 4-1); as well, DARPP32-negative neurons (MAP2-positive), which represent a combination of striatal interneurons and cortical neurons [but may also include some striatal SPNs that do not express DARPP32 (471)], are preserved equally in the two genotypes. Surprisingly, the percentage

of MAP2-positive cells that are also DARPP32-positive (~8% for WT and ~8.5% for YAC128) is far less than the expected 50%. Either insufficient expression of DARPP32 in SPNs by three weeks *in vitro* or death of striatal SPNs could explain this result. In either case, the basal level of SPNs expressing DARPP32 is not affected by mHtt by DIV21 when we investigated C-S synaptopathy. Likewise, DARPP32-negative neurons that constitute a similar proportion of all MAP2-positive cells in the two genotypes could consist of similar or different ratios of cortical neurons to striatal interneurons, or possibly even DARPP32-negative striatal SPNs. Nonetheless, the density of vGlut1-positive terminals onto the DARPP32-expressing SPN dendritic tree is similar between WT and YAC128 (Figure 4-7 E), supporting the view that cortical neurons and their connections exist at a similar level.

Synaptic activity can promote downstream cell survival signaling, including phosphorylation of the transcription factor CREB (293,297). CREB activity is reduced in HD, an effect that has been attributed largely to repressed CREB transcription due to a mHtt-induced sequestration of the CREB binding protein (197). Notably, reduced basal levels of pCREB are found in nuclear fractions from striatal tissue of YAC128 mice at a stage when they exhibit an overt motor phenotype (472). However, in the present study, despite reduced synaptic activity and the presence of mHtt both pre- and postsynaptically, YAC128 C-S cocultures did not differ from WT in terms of basal nuclear-to-cytosolic expression of pCREB in SPNs. It is possible that differences in basal pCREB would be detected in cocultures at a later stage, although concerns of general culture health prevented any quantification outside of the employed three-week period. Alternatively, experimental manipulations of glutamate receptor activity may be prerequisite to observe genotype differences in pCREB expression. Indeed, we have shown previously that

extrasynaptic NMDA receptor activation induces a greater reduction of nuclear pCREB in DIV 14 YAC128 than WT cocultured SPNs (299).

Taken together, there is no genotype difference in terms of basal neuronal survival and pro-survival signaling by three weeks *in vitro* in C-S coculture between WT and YAC128. Therefore, day *in vitro* (DIV) 21 is an ideal time to investigate synaptopathy, free from differential cell-death.

4.4.2 mHtt Perturbs Miniature Excitatory Postsynaptic Currents and Dendritic Tree Development, but Not Cortico-striatal Synapse Density, in Striatal SPNs

In situ data from mouse models have provided ample evidence in support of altered dendritic morphology in HD. For example, reductions in spine density, somatic area and diameter of the dendritic field have been reported for SPNs in R6/2 mice only after development of an HD-like phenotype (398). This reduced neuronal size is consistent with the lower membrane capacitance that is typically recorded from R6/2 SPNs in whole-cell electrophysiological experiments (398,473). Similar reductions in dendritic complexity and spine density have been observed in knock-in HD mice (462). In the present study SPN dendritic complexity, as measured by Sholl analysis, was reduced in DIV21 but not DIV14 YAC128 cocultures. In agreement with the morphological findings, there was a significant interaction effect of DIV and genotype on membrane capacitance, reflected by an increase and decrease in the mean capacitance in WT and YAC128 SPN, respectively, from DIV 14 to 21. On the other hand, we did not observe a significant decrease in density of spine-like dendritic protrusions in YAC128 SPN as other researchers observed (415). It is most likely because our cocultures were prepared from embryonic neurons (day 17/18) from a mild form of HD model (YAC128 line 55) with abundant cortical neurons (1:1 cortical-to-striatal plating ratio) whereas Wu et al. (415) plated C-S coculture using postnatal day

1 neurons from YAC128 line 53, which is more aggressive compared with line 55, at a 1:3 ratio (cortical: striatal). Therefore, these data demonstrate that some, but not all of the HD-associated dendritic morphology impairments can also be recapitulated as early as three weeks in C-S cocultures.

A progressive loss in EPSC frequency has been widely reported in acute striatal brain slices from HD mice. This phenotype of reduced excitatory transmission shows remarkable consistency among the various HD models (474), including N-terminal fragment models (322), full-length transgenic models (419,474) and knock-in models of HD (102,400,474). These changes are not evident at birth; rather, HD mice typically age up to a number of months before quantifiable differences occur, with the exception of the rapidly-progressing R6/2 mice in which spontaneous EPSCs are reduced at 5 weeks of age (322). In the present study, mEPSCs measured from YAC128 striatal SPNs cocultured with cortical neurons are altered by as early as three weeks *in vitro*, whereas in acute slices, a deficit in spontaneous EPSCs was observed at 6 months of age or later in this model (474). Thus, when grown in isolation under the currently employed culture conditions, we observed accelerated synaptic impairment, which mirrors the synaptic dysfunction at relatively late stages *in situ*. This suggests that C-S cocultures may be useful for future work for investigating the precise mechanisms underlying the reduction of excitatory transmission that occurs with progression of the HD phenotype. Indeed, using a chimeric culture strategy, we were able to demonstrate a mechanistic requirement for both pre- and postsynaptic mHtt expression to observe this pathogenic effect (475) (not shown in the Result section). This result is in line with the finding that selective expression of mHtt in either striatal or cortical neurons is insufficient to recapitulate the full behavioral and neuropathological phenotypes of HD (476,477).

Differences in sucrose-induced EPSCs were also observed between WT and YAC128 C-S cocultures at DIV21. The reduced area under the curve (normalized to membrane capacitance) of sucrose-EPSC responses in YAC128 cocultured SPNs (Figure 4-4 C) suggests that there is a smaller amount of glutamate in the C-S synaptic readily releasable pool per SPN membrane capacitance. In acute brain slices, a reduction in the size of EPSCs evoked by electrical stimulation is evident in mid- to late-stage HD mouse models (28,312). The amplitude of evoked EPSCs is determined by a number of factors, including the total size of the readily releasable pool (RRP). It is thought that both electrically-evoked and sucrose-evoked EPSCs act on the same vesicle population (465). Thus, it is likely that the C-S EPSC glutamate pool itself is reduced in the HD model, since our immunocytochemical results show that the major AMPA receptor subunit (GluA2) is expressed at similar levels in WT and YAC128 C-S synapses (section 4.3.3) and our data indicate no difference in vesicle numbers in the RRP between genotypes. Indeed, reduction of the mEPSC amplitude in our YAC128 coculture at the same DIV (section 4.3.2) further supports our conclusion, and implies that glutamate content in presynaptic vesicles at C-S synapses is decreased by mHtt. This is in line with our finding that vGlut1 puncta size is reduced at C-S synapses in our system (section 4.3.3). However, functional study is necessary to prove effects of reduction of synaptic vGlut1 in HD. An additional direct and precise method to measure quantal release of glutamate would be helpful here, but a previous study has already provided evidence of this relationship to a certain degree (478) and measurement of glutamate released from individual vesicles is difficult. Consistent with our results, vGlut1 expression was reported to be reduced in the CAG140 HD model prior to striatal cell-death (119,192). Undoubtedly, we cannot exclude other factors that could also contribute to glutamate reduction in vesicles, such as impaired energy supply caused by mitochondria impairment in HD (479,480) or impaired function of vGlut1, or

reduced size of vesicles. Future experiments to increase synaptic vGlut1 expression in YAC128 cortical terminals back to WT levels could help determine whether vGlut1 reduction is causative.

A possible explanation for why excitatory connections are greatly affected by mHtt, whereas inhibitory connections are relatively preserved, in terms of miniature event frequency could be, in part, a result of formation of excitatory synapses largely onto distal dendrites and distribution of inhibitory synapses closer to the soma; therefore, dendritic tree attenuation in YAC128 SPNs may have impacted excitatory synapses more than inhibitory ones.

4.4.3 Presynaptic Vesicle Release at Cortico-striatal Synapses in Huntington's Disease Culture and Slice Models

While a number of investigations were conducted to determine the presynaptic release probability at various synapses with artificial stimuli in HD models (91,312,419), few have studied the spontaneous release of presynaptic vesicles at C-S synapses. However, the synaptotagmin 1 (Syt1) antibody uptake assay allows us to compare vesicle release at individual synapses in various conditions unlike mEPSC event recording at the whole-cell level, which involves both pre- and post-synaptic factors, such as dendritic tree arborization and postsynaptic receptor expression. Results of the Syt1 assay experiments demonstrate synaptic vesicle release in our C-S coculture as the basal expression of Syt1 at synapses is unaffected by the presence of mHtt (Figure 4-8 C). With action potentials blocked, vesicle release at C-S synapses was elevated with mHtt expressed. Although vesicle release measured as spontaneous or miniature EPSC events recorded from SPNs at the cellular level were reported to be reduced in frequency in various HD models (102,311,322), little was known about quantal release at individual synapses; to our knowledge, our data is the first evidence suggesting action potential-independent vesicle release is enhanced at C-S synapses

in the HD condition. More investigation is needed to uncover the underlying mechanism of elevated quantal release at C-S synapses in our HD condition and to test whether similar enhancement is present in HD animal models. In contrast, with action potentials naturally occurring in C-S coculture, we found that C-S synaptic vesicle release was suppressed by the presence of mHtt (Figure 4-10 Ai-Bii). On the other hand, in iGluSnFr experiments in acute brain slice we observed no difference in glutamate release in striatum during electrical stimulation in corpus callosum in 6-month old YAC128 compared with WT (Figure 4-11). Similarly, Joshi et al. also found no change in vesicle release at C-S synapses using the FM dye FM1-43 in acute brain slices prepared from YAC128 at 7 months, with 10Hz train electrical stimulation in cortical layer V-VI (312). However, the vesicle release is impaired at 12 months when striatal neuronal loss becomes evident (312). Thus, our 3-week old C-S coculture system is able to recapitulate the mid-to-late stage HD C-S synaptopathy without evident neuronal loss.

When it comes to cortical neuronal activity, we found it unaffected by mHtt in the DIV21 C-S cocultures (Figure 4-10). In comparison, cortical neuronal firing rate *in* vivo was found elevated in the R/2 model and not changed in the knock-in model in prefrontal cortex by recording extracellular spike activity in freely moving mice, even at the symptomatic stage (481); whereas in YAC128, cortex exhibited hyperexcitability at early ages (251).

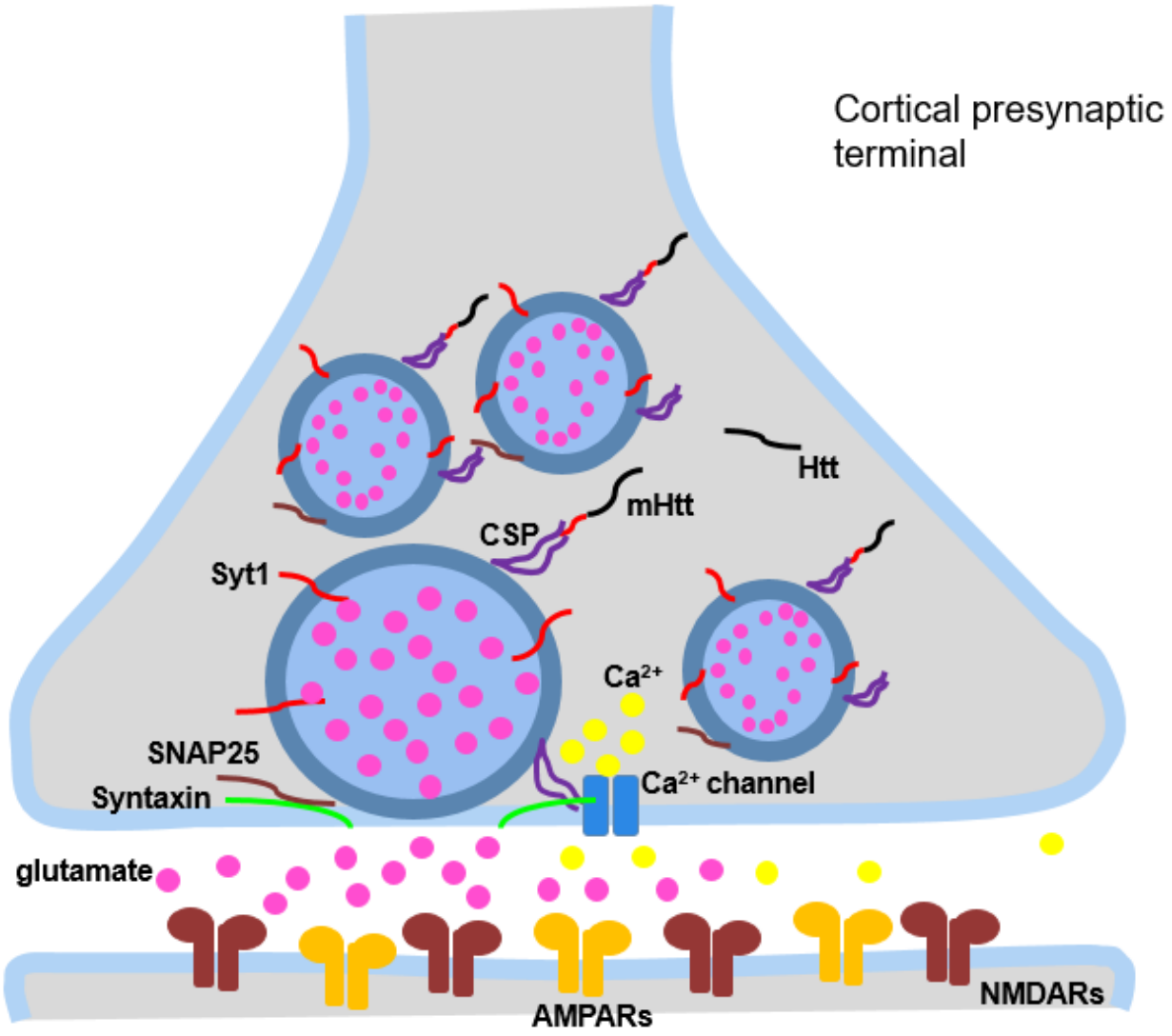

Figure 4-15 Schematic diagram of presynaptic terminal of cortico-striatal connections and mHtt interactions with presynaptic proteins.

In the presynaptic side, mHtt interferes functions of vesicular proteins. For instance, its interaction with Cysteine String Protein (CSP) removes CSP blockade of Ca^{2+} channels, thereafter alters presynaptic vesicle release.

Interestingly, we found that cysteine string protein (CSP) expression level at synapses was significantly reduced in YAC128 C-S coculture. CSP functions as a facilitator for calcium-dependent presynaptic vesicle secretion via interaction with SNAP-25 (468); in HD, CSP interacts with mHtt but not wild-type Htt (wtHtt) (202). Moreover, a Drosophila study found that when CSP is knocked out, stimulus-release coupling is impaired but not vesicle recycling (482–484). On the other hand, it has been demonstrated that CSP together with a G-protein forms a complex with N-type calcium channels and regulates vesicle secretion (484,485). Furthermore, CSP can be displaced from N-type calcium channels by the fragment encoded by *HTT* exon 1 (485) which contains the CAG expansion in the case of HD (202), thereby removing CSP inhibition of N-type Ca^{2+} channels, while wtHtt does not (202). Therefore, further experiments are necessary to examine how vesicle release at C-S synapses is affected when expression of CSP is reduced at the synapse.

Aside from CSP, expression of other synaptic proteins is likely disturbed by the poly-glutamine expansion, such as SNAP-25, PSD-95, complexin II, syntaxin 1A, synapsin 1, and GAD65 (141), in part by mHtt's failure to modulate HIP14 enzymatic activity properly (193). For example: Morton et al. found that expression of complexin II, which facilitates synchronous release but acts as a brake on spontaneous vesicle fusion (486,487) (i.e. miniature release), is progressively reduced in the R6/2 mouse model but not complexin I (184). Interestingly, the expression of mHtt suppresses neurotransmitter release as well as complexin II expression in non-neuronal cells (488); syntaxin 1A, whose inhibition on the N-type calcium channel is removed by wtHtt (489), is redistributed in the presence of mHtt in HEK cells (490) and was found decreased in striatal synaptosomes from 6-month old homozygous CAG140 knock-in HD mice (192) but not changed in whole-brain synaptosomes from phenotypic 13-week old R6/2 (184) or in

sensory/motor cortex of grade I-IV HD patients (188). In contrast, SNAP-25, a t-SNARE protein that directly executes vesicle fusion with cell membranes, was found reduced in grade I-IV HD patients cortex (188) and in striatal synaptosomes from 12-month old homozygous CAG140 knock-in mice (192) and in striatum and hippocampus of the Q175 knock-in model at 12 months (103), but both SNAP-25 and CSP were reported increased in the neuromuscular junction, that typically does not degenerate in HD, in 5 to 6-month old R6/1 (58). mHtt also binds to synapsin 1 (171), whose action potential/Ca^{2+}-based phosphorylation is critical for neurotransmitter release (491,492), and suppresses its phosphorylation (493). Therefore, a combination of multiple changes may contribute to the altered vesicle release at C-S synapses depending on the model and age. Interestingly, synaptotagmin 1 (Syt1), the major calcium sensor protein in presynapses, which was reported to be reduced in the late-stage homozygous CAG140 knock-in model (192) though not in transgenic R6/2 (184), is also a substrate of HIP14 (141) but its expression level is unaffected in our YAC128 C-S coculture.

4.4.4 Reduced Glutamate Content per Vesicle in YAC128 Cortico-striatal Synapses

In coculture and acute brain slice experiments we concluded that glutamate content in individual vesicles at C-S synapses is likely reduced in YAC128, mainly based on the following observations:

1. YAC128 mEPSC amplitude is reduced significantly (Figure 4-3 D) at DIV21 compared with WT, but GluA2 puncta size is unchanged (section 4.3.3).

2. RRP vesicle number is similar (Figure 4-9 C), yet sucrose-evoked EPSC charge is reduced (Figure 4-4 C).

3. in slices from 6-month YAC128 mice, glutamate recovery is impaired (Figure 4-13 and Figure 4-14), despite the fact that vesicular release is equal in WT and YAC128 C-S synapses at 7 months (312).

4. the recovery rate of the neurotransmitter pool at inhibitory synapses is not reduced in C-S coculture (Figure 4-12 B). This also argues for a specific reduction in vesicle filling with glutamate at excitatory synapses rather than a general problem with the vesicle release machinery.

4.4.5 Expression of mHtt Influences Recovery of Glutamate Pool but Not Vesicle Replenishment in RRP

In the present chapter, we estimated the vesicle quantity in the RRP (Figure 4-9) as previously described (467) and found a trend toward reduced number of vesicles in the RRP (~14%) at C-S synapses in YAC128, along with the decreased total dendritic length (~25%; Figure 4-6 E) observed on the same DIV. Interestingly, the density of C-S synapses along dendrites (Figure 4-7) was not significantly affected by mHtt, nor was the density of presynaptic vesicles (Figure 4-9 C), together suggesting that the number of presynaptic vesicles in the RRP at individual C-S synapses was not significantly influenced by mHtt. Moreover, mHtt expression did not change the RRP vesicle replenishment rate at C-S synapses (Figure 4-9 D), which is distinct from recovery of the glutamate pool in the RRP (glutamate recovery). One neuronal protein that is worth paying attention to is HAP1, which regulates vesicular transport, exocytosis and RRP size (494,495). Nevertheless, neither vesicle replenishment in the RRP nor RRP size at C-S synapses was impacted in our present study or reported in previous research even though HAP1's interaction strength with mHtt is proportionally correlated with CAG repeat length (496). This seems consistent with a

previous molecular interaction study, which came to the conclusion that HAP1-Htt interactions do not contribute to the molecular pathology in HD transgenic mice (497).

To our knowledge, our results are the first to demonstrate that glutamate recovery is impaired at C-S synapses in both HD C-S coculture (Figure 4-12) and acute brain slice (Figure 4-13 and Figure 4-14). The reason why glutamate recovery, but not the RRP vesicle replenishment rate, is impeded by mHtt at C-S synapses is likely because of the moderate reduction of vGlut1 expression at C-S synapses (section 4.3.3), which could result in decreased glutamate content in vesicles and mEPSC events with smaller amplitude (Figure 4-3 D). As to the question of why vGlut1 reduction could also contribute to impaired glutamate recovery, we propose that hypertonic sucrose solution/electrical train stimulation challenges the RRP, boosting vesicle mobilization and docking, and shortening the retention time of primed vesicles in the presynaptic active zone; we postulate that these challenging conditions unmask a difference in the amount of glutamate pumped into the vesicles. Certainly, this is an assumption that needs to be tested and we cannot exclude other possibilities, such as altered expression of other synaptic proteins or suppressed function of vGlut1.

4.4.6 In Summary

We demonstrated that C-S connections are affected by mHtt after three weeks *in vitro*, a time when survival of both cortical and striatal neurons is unaffected: mHtt causes dendritic tree degeneration but not synapse loss, thereby reducing the total number of C-S synapses formed onto SPNs, but not altering inhibitory connections. Attenuated frequency of excitatory events recorded at the soma is compensated to some degree by increased miniature release of presynaptic vesicles, although mHtt-expressing C-S synapses still show reduced vesicle exocytosis to action potential

invasion into cortical presynaptic terminals. Cortical neurons fire normally, but decreased vGlut1 in the presynaptic terminals results in less glutamate in vesicles and slower recovery of the glutamate pool. However, the readily releasable pool size and replenishment is not impacted by HD pathology in our C-S coculture system by three weeks. Together, these findings lay a foundation for potential treatments targeting HD synaptopathy in the future.

Chapter 5: Concluding Chapter

In Chapter 2, we studied striatal neuronal properties in various cortico-striatal (C-S) cocultures which were later adopted to investigate neuroprotective function of wild-type huntingtin (wtHtt) in more neuronal types in Chapter 3 as well as to examine synaptopathy caused by mutant huntingtin (mHtt) together with tests in acute brain slices in Chapter 4.

5.1 Summary of the Findings

The creation of C-S coculture allowed researchers to investigate neurons and synapses of interest in a relatively isolated condition, which is highly accessible to genetic and pharmacological manipulations. I used this platform to investigate how synaptic formation and function are affected by the expanded poly-glutamine in huntingtin (Htt) prior to striatal neuronal loss, as well as whether the neuroprotective function of wtHtt is universal. The main goal of this thesis was to further uncover function of wtHtt as neuroprotective in a broader view, and to investigate pathophysiology of mHtt in synaptic dysfunction both *in vitro* and *ex vivo*. The experiments conducted in this thesis examined cellular and subcellular structure and function of striatal and cortical neurons, as well as C-S and striatal-striatal synapses, when Htt is expressed with normal vs. mutant poly-glutamine repeat lengths.

The objectives of the present work were to:

Aim 1. Uncover an optimal plating ratio of cortical and striatal neurons in C-S coculture to more closely reproduce C-S connections *in vivo*.

In order to investigate wtHtt function and C-S synaptic dysfunctions caused by *HTT* mutation in C-S cocultures, we first studied the coculture system. We found that the plating ratio

of cortical and striatal neurons does impact striatal neuronal properties as well as the C-S synapses. However, due to its mild effects on C-S connections and pro-survival signaling of striatal spiny projection neurons (SPNs) and because of the wide application of C-S coculture plated at 1:1 cortical-to-striatal ratio we decided to adopt the 1:1 plating ratio in later studies.

Aim 2. Examine how wtHtt protects striatal neurons in C-S coculture and whether it is also neuroprotective for neurons originating from cortex and hippocampus by enhancing pro-survival signaling through nuclear pCREB.

By over-expressing wtHtt in cortical, striatal and hippocampal neurons, we determined that wtHtt provides global neuroprotection for neurons originating from these three brain regions; however, only striatal neurons are protected via the nuclear pCREB-dependent pro-survival signaling pathway.

Aim 3. How mHtt impacts C-S connections in C-S coculture and in Huntington's disease mouse model at the early symptomatic stage.

Using immunostaining and electrophysiological methodologies, we demonstrated that mHtt impacts C-S over striatal-striatal synapses, largely by suppressing SPN dendritic tree growth, altering synaptic protein expressions, shifting vesicle exocytosis and reducing neurotransmitter content in the vesicles.

5.2 Overall Significance and Limitations of the Present Study

5.2.1 Cortico-striatal Coculture and How Cortical Neuronal Abundance Modulates Striatal SPN Properties and Cortico-striatal Communications

The C-S coculture system is superior to investigate C-S synapses and both cortical and striatal neurons *in vitro*, especially when techniques that are only available to cultured neurons are applied: Firstly, the coculture system allows us to manipulate pharmacological components in the extracellular environment at a precise concentration with high temporal resolution. Drug treatment can be achieved with 10-millisecond precision and at a defined concentration to a target cell, whereas such precision is almost impossible *in vivo* or in acute brain slices. For example, application of hypertonic sucrose solution with 10-millisecod precision can be made only for a mono-layer of cells plated on coverslips, and not in brain slices. Secondly, numerous genetic tools are suitable for the C-S coculture system. For instance, knocking down a specific gene globally with siRNA or expressing a protein of interest in a target population of neurons (striatal SPNs vs. cortical neurons) via nucleofection on the plating day can be implemented easily in C-S coculture, free from time-consuming breeding or surgery in animals. Another application is that a disease-causing gene or a factor of interest can be expressed on either side the synapse to study pre- vs. post-synaptic and cell-autonomous vs. non-autonomous effects. Thirdly, as we have shown in Chapter 4, a number of synaptic and morphological changes, which are not evident *in vivo* until at least the early stage of HD (6 to 9 months in YAC128), were successfully reproduced in our three-week old C-S coculture, including altered mEPSC events and dendritic tree morphology. Lastly, the isolated environment of the coculture is rather clean to study cortical and striatal neuronal interactions and their connections, free from thalamo-striatal glutamatergic synapses and modulatory dopaminergic synapses from SNc. Together, C-S coculture is a powerful platform to

investigate synaptic dysfunctions and their underlying mechanisms, and to search for therapeutics to the malfunctions as a start *in vitro*.

When it comes to optimizing the C-S coculture system, varying the plating ratio of the two types of neurons is one of the influential changes that can be made easily. However, consequently it decreases the comparability of experimental results across studies (the most common plating ratios of cortical-to-striatal are 1:1 and 1:3). Thus, a study that examines how striatal neuronal properties and C-S connections differ between the two plating ratios was needed. Our study of C-S neuronal plating ratio fulfills the necessity by showing that the relative abundance of cortical neurons impacts several features of striatal neurons over others. For instance, membrane distribution of NMDA receptor and dendritic tree morphology are influenced more strongly than mEPSC frequency and amplitude. Therefore, our results provide a reference to compare experimental outcomes from C-S cocultures plated at different cortical-to-striatal ratios.

5.2.2 Insight on Neuroprotective Role of wtHtt and Its Mechanism

The neuroprotective effect of wtHtt is well known in the striatum and striatal SPNs, but not in other brain regions. In this thesis, we demonstrated that wtHtt is globally neuroprotective, at least for cortical and hippocampal neurons via nuclear pCREB-independent signaling and for striatal neurons through a pCREB-dependent pathway. It may hint why neurodegeneration spreads throughout cortex and hippocampus but with less severity compared to striatum in HD. Moreover, we showed that increased neuronal survival in response to an excitotoxic challenge does not always correlate with elevated basal nuclear pCREB, as has been well accepted in striatal neurons. Instead, there may be other neuroprotective mechanisms that do not engage gene transcription through nuclear pCREB in cortical and hippocampal neurons. These results suggest there may be

treatments that protect neurons from the *HTT* mutation in a gene transcription-independent manner.

5.2.3 Significance of Understanding Disrupted Cortico-striatal Connections

Despite the fact that the striatal SPN dendritic tree is known to be degenerated in numerous HD culture and animal models (398,462,498), and we observed a similar change in our C-S coculture model, much less is understood about how the glutamate pool in the C-S coculture is affected by the *HTT* mutation. In this thesis, my findings that glutamate content in the vesicles is reduced, and that the recovery of the glutamate pool is disrupted, in the HD condition at C-S synapses in the coculture system are new in this field, to our knowledge. Although we previously reported reduced mEPSC amplitude in YAC128 thalamo-striatal coculture (413), we did not determine whether this was a result of decreased glutamate content or reduced expression of AMPA receptors in thalamo-striatal synapses.

There are several limitations to our study. For example, the conclusion of reduced glutamate content was drawn from multiple indirect measures, including mEPSC amplitude and GluA2 AMPA receptor puncta size at C-S synapses, and we did not directly measure the vesicle size with electron microscopy or glutamate content with a sensor, or AMPA receptor-mediated current using cyclothiazide that removes receptor desensitization. After all, in the present work we focused more on the presynaptic side of C-S connections in this pre-neurodegenerative HD model, and our results suggested a number of pathogenic changes in presynaptic function that potentially impact motor learning efficiency and capacity, which rely on C-S communications. Apart from that, our choice of working in HD models free from enhanced SPN cell-death emphasizes HD as a synaptopathy and pushes the research frontiers of synaptic dysfunction forward.

5.2.4 Importance of Uncovering Functional Impairments of Presynaptic Vesicle Release at Cortico-striatal Synapses

Like HD, many other neurodegenerative diseases, including Parkinson's disease and Alzheimer's disease, have been suggested to be synaptopathies. Therefore, understanding how synaptic functions are altered before severe neurodegeneration occurs is key to uncover the disease mechanisms and to develop treatments; our finding of altered action potential-independent presynaptic vesicle release at C-S synapses as the first evidence, to our knowledge, is valuable for future research.

The limitations in our study of neurotransmitter release at C-S synapses are: it is better to conduct the iGluSnFr-based measurement of action potential-dependent glutamate release in acute striatal slices at multiple time-points prior to neurodegeneration, such as at 4, 8 and 10 months besides at 6 months; additionally, an alternative method of testing activity-dependent and -independent vesicle release would be valuable, such as optogenetic manipulation of cortical neuronal activity together with an ultra-sensitive measurement for glutamate released into the extracellular medium. Nonetheless, the advantage of our study is that we conducted electrophysiological experiments that are not suitable to acute brain slices in C-S coculture, which is superior to mono-striatal culture lacking abundant C-S excitatory connection, at an *in vitro* age when SPN cell-death is not evident. Our findings on altered release of presynaptic vesicles at C-S synapses were not reported with such details in previous research in HD and it opens up a new research direction in synaptopathy of neurodegenerative diseases beyond HD.

5.3 Future Directions

5.3.1 The Underlying Molecular Mechanism of Disrupted Presynaptic Vesicle Release, Reduced Glutamate Content in Presynaptic Vesicle and Impaired Recovery of Glutamate Pool at Cortico-striatal Synapses

Functional changes are often mediated by structural alterations in biology. Changes in vesicle release at C-S synapses in the present study, both action potential-dependent and -independent ways, may be not an exception. We proposed that CSP (cysteine string protein) is one of the candidates, as its expression has been shown to be reduced in our C-S coculture. Hence, further effort can be made in knocking down CSP in WT C-S coculture and examining action potential-dependent and -independent vesicle release at C-S synapses with the Syt1 assay with or without TTX at the same DIV.

Even if the results from the experiment above are positive, researchers should search further for other possibilities. For instance, immunostaining for other presynaptic proteins that play key roles in vesicle exocytosis, such as SNAP-25 and complexin II, would be important. In this regard, several synaptic proteins directly interact with wtHtt/mHtt (171), while others are indirectly regulated by post-translational modification enzymes, such as HIP14 (141), which is in turn modulated by Htt.

For the reduced glutamate in presynaptic vesicles at C-S synapses, we postulated that the moderate decrease of vGlut1 at C-S synapses is causative. However, further examination in striatal tissue and slice are necessary, such as western blotting for vGlut1 in homogenized striatal tissue and immunostaining for vGlut1 in striatal tissue slices from 6 to 9-month old WT and YAC128 mice.

We proposed that vGlut1 reduction at C-S synapses is the major cause for impaired glutamate recovery. But a knocking-down experiment of vGlut1 in WT C-S coculture with siRNA followed by paired-sucrose pulse whole-cell electrophysiology for striatal SPNs would be more decisive. Certainly, attempt to test the glutamate recovery after vGlut1 knockdown *in vivo* or *ex vivo* would be invaluable.

5.3.2 Uncovering Behavioral Outcomes of the Altered Functions of Cortico-striatal Synapses

In the present study, we uncovered the impaired recovery of the glutamate pool in both 3-week old YAC128 C-S coculture and acute brain slices from 6-month old YAC128 mice, likely by suppressed vGlut1 expression at C-S synapses caused by *HTT* mutation. On the other hand, it was found previously that motor learning that highly relies on C-S connections (499,500), such as in the rotarod task, is impaired in YAC128 mice as early as 2 months of age and worsens over time (93); by 8 months of age, YAC128 mice show deficits also in various cognitive tests, including a simple swimming test, open-field habituation and T-maze swimming test, suggesting significant cognitive dysfunction at this stage, such as changing strategy (93). Therefore, we propose that pursuing the question of how C-S synaptic changes that are evident prior to cell-death in the striatum in HD contributes to the behavior outcomes would be very meaningful. For example, if vGlut1 expression at C-S synapses is also decreased in 6 to 9-month old YAC128, then a genetic rescue experiment could be conducted to answer whether the vGlut1 reduction causes reduced glutamate content in C-S synaptic vesicles, as well as the impaired glutamate recovery, and to address whether the deficits contribute to any impairment in motor learning or cognitive ability.

Whether vesicle release impairment from C-S synapses or other synapses at various conditions exists in pre-SPN death and how it influences behavioral performances that involve learning and cognition are another avenue to pursue in the future.

5.3.3 Therapeutic Search for Preventing/Restoring Cortico-striatal Synaptic Malfunctions in Cortico-striatal Coculture System

The C-S coculture is a convenient tool to uncover pathological changes, study disease mechanisms and to develop therapeutics, especially for C-S synapses. Using the C-S cocultures, we were able to find numerous SPN and C-S connection-specific alterations and partially uncovered the underlying mechanisms in the YAC128 HD model. As mentioned previously this C-S coculture platform is accessible to pharmacological and genetic manipulations, and it can be further applied with medium-to-high throughput automated examination of numerous parameters to discover drugs, such as using fluorescent glutamate sensors or voltage/Ca^{2+} sensitive dyes.

References

1. de la Monte SM, Vonsattel JP, Richardson EPJ. Morphometric demonstration of atrophic changes in the cerebral cortex, white matter, and neostriatum in Huntington's disease. J Neuropathol Exp Neurol. 1988 Sep;47(5):516–25.

2. Soutar CA. Tetrabenazine for Huntington's chorea. Br Med J. 1970 Oct 3;4(5726):55.

3. Walker F. Huntington's disease. Lancet. 2007 Jan 20;369(9557):218–28.

4. A novel gene containing a trinucleotide repeat that is expanded and unstable on Huntington's disease chromosomes. The Huntington's Disease Collaborative Research Group. Cell. 1993 Mar 26;72(6):971–83.

5. Fisher ER, Hayden MR. Multisource ascertainment of Huntington disease in Canada: prevalence and population at risk. Mov Disord Off J Mov Disord Soc. 2014 Jan;29(1):105–14.

6. Kremer B, Weber B, Hayden MR. New insights into the clinical features, pathogenesis and molecular genetics of Huntington disease. Brain Pathol Zurich Switz. 1992 Oct;2(4):321–35.

7. Evans SJW, Douglas I, Rawlins MD, Wexler NS, Tabrizi SJ, Smeeth L. Prevalence of adult Huntington's disease in the UK based on diagnoses recorded in general practice records. J Neurol Neurosurg Psychiatry. 2013 Oct;84(10):1156–60.

8. Bates G, Dorsey R, Gusella J, Hayden M, Kay C, Leavitt B, et al. Huntington disease. Nat Rev Dis Primers. 2015 Apr 23;1:15005.

9. Dayalu P, Albin R. Huntington disease: pathogenesis and treatment. Neurol Clin. 2015 Feb;33(1):101–14.

10. McLellan DL. The suppression of involuntary movements with tetrabenazine. Scott Med J. 1972 Nov;17(11):367–70.

11. Pakkenberg H. The effect of tetrabenazine in some hyperkinetic syndromes. Acta Neurol Scand. 1968;44(3):391–3.

12. Swash M, Roberts AH, Zakko H, Heathfield KW. Treatment of involuntary movement disorders with tetrabenazine. J Neurol Neurosurg Psychiatry. 1972 Apr;35(2):186–91.

13. Erickson JD, Eiden LE, Hoffman BJ. Expression cloning of a reserpine-sensitive vesicular monoamine transporter. Proc Natl Acad Sci U S A. 1992 Nov 15;89(22):10993–7.

14. Frank S. Treatment of Huntington's disease. Neurotherapeutics. 2014 Jan;11(1):153–60.

15. Unti E, Mazzucchi S, Palermo G, Bonuccelli U, Ceravolo R. Antipsychotic drugs in Huntington's disease. Expert Rev Neurother. 2016 Aug 23;1–11.

16. Jones C, Busse M, Quinn L, Dawes H, Drew C, Kelson M, et al. The societal cost of Huntington's disease: are we underestimating the burden? Eur J Neurol. 2016 Oct;23(10):1588–90.

17. Kirkwood SC, Siemers E, Viken R, Hodes ME, Conneally PM, Christian JC, et al. Longitudinal personality changes among presymptomatic Huntington disease gene carriers. Neuropsychiatry Neuropsychol Behav Neurol. 2002 Sep;15(3):192–7.

18. Fritz NE, Hamana K, Kelson M, Rosser A, Busse M, Quinn L. Motor-cognitive dual-task deficits in individuals with early-mid stage Huntington disease. Gait Posture. 2016 Sep;49:283–9.

19. Paulsen JS, Langbehn DR, Stout JC, Aylward E, Ross CA, Nance M, et al. Detection of Huntington's disease decades before diagnosis: the Predict-HD study. J Neurol Neurosurg Psychiatry. 2008 Aug;79(8):874–80.

20. Pirogovsky E, Nicoll DR, Challener DM, Breen E, Gluhm S, Corey-Bloom J, et al. The Visual Spatial Learning Test: differential impairment during the premanifest and manifest stages of Huntington's disease. J Neuropsychol. 2015 Mar;9(1):77–86.

21. Siemers E, Foroud T, Bill DJ, Sorbel J, Norton JAJ, Hodes ME, et al. Motor changes in presymptomatic Huntington disease gene carriers. Arch Neurol. 1996 Jun;53(6):487–92.

22. Aylward EH, Nopoulos PC, Ross CA, Langbehn DR, Pierson RK, Mills JA, et al. Longitudinal change in regional brain volumes in prodromal Huntington disease. J Neurol Neurosurg Psychiatry. 2011 Apr;82(4):405–10.

23. Crawford HE, Hobbs NZ, Keogh R, Langbehn DR, Frost C, Johnson H, et al. Corpus callosal atrophy in premanifest and early Huntington's disease. J Huntingt Dis. 2013;2(4):517–26.

24. Schippling S, Schneider SA, Bhatia KP, Munchau A, Rothwell JC, Tabrizi SJ, et al. Abnormal motor cortex excitability in preclinical and very early Huntington's disease. Biol Psychiatry. 2009 Jun 1;65(11):959–65.

25. Orth M, Schippling S, Schneider SA, Bhatia KP, Talelli P, Tabrizi SJ, et al. Abnormal motor cortex plasticity in premanifest and very early manifest Huntington disease. J Neurol Neurosurg Psychiatry. 2010 Mar;81(3):267–70.

26. Li J-Y, Plomann M, Brundin P. Huntington's disease: a synaptopathy? Trends Mol Med. 2003 Oct;9(10):414–20.

27. Plotkin JL, Surmeier DJ. Corticostriatal synaptic adaptations in Huntington's disease. Curr Opin Neurobiol. 2015 Aug;33:53–62.

28. Raymond LA, Andre VM, Cepeda C, Gladding CM, Milnerwood AJ, Levine MS. Pathophysiology of Huntington's disease: time-dependent alterations in synaptic and receptor function. Neuroscience. 2011 Dec 15;198:252–73.

29. Warner JH, Sampaio C. Modeling Variability in the Progression of Huntington's Disease A Novel Modeling Approach Applied to Structural Imaging Markers from TRACK-HD. CPT Pharmacomet Syst Pharmacol. 2016 Aug;5(8):437–45.

30. Cubo E, Ramos-Arroyo MA, Martinez-Horta S, Martinez-Descalls A, Calvo S, Gil-Polo C. Clinical manifestations of intermediate allele carriers in Huntington disease. Neurology. 2016 Aug 9;87(6):571–8.

31. Alexandrov V, Brunner D, Menalled LB, Kudwa A, Watson-Johnson J, Mazzella M, et al. Large-scale phenome analysis defines a behavioral signature for Huntington's disease genotype in mice. Nat Biotechnol. 2016 Aug;34(8):838–44.

32. Langbehn DR, Hayden MR, Paulsen JS. CAG-repeat length and the age of onset in Huntington disease (HD): a review and validation study of statistical approaches. Am J Med Genet Part B Neuropsychiatr Genet Off Publ Int Soc Psychiatr Genet. 2010 Mar 5;153B(2):397–408.

33. Gatto EM, Parisi V, Etcheverry JL, Sanguinetti A, Cordi L, Binelli A, et al. Juvenile Huntington disease in Argentina. Arq Neuropsiquiatr. 2016 Jan;74(1):50–4.

34. Patra KC, Shirolkar MS. Childhood-onset (Juvenile) Huntington's disease: A rare case report. J Pediatr Neurosci. 2015 Sep;10(3):276–9.

35. Arning L. The search for modifier genes in Huntington disease - Multifactorial aspects of a monogenic disorder. Mol Cell Probes. 2016 Jul 12;

36. Identification of Genetic Factors that Modify Clinical Onset of Huntington's Disease. Cell. 2015 Jul 30;162(3):516–26.

37. Gusella JF, MacDonald ME, Lee J-M. Genetic modifiers of Huntington's disease. Mov Disord Off J Mov Disord Soc. 2014 Sep 15;29(11):1359–65.

38. Li X-J, Friedman M, Li S. Interacting proteins as genetic modifiers of Huntington disease. Trends Genet TIG. 2007 Nov;23(11):531–3.

39. Kaltenbach L, Romero E, Becklin R, Chettier R, Bell R, Phansalkar A, et al. Huntingtin interacting proteins are genetic modifiers of neurodegeneration. PLoS Genet. 2007 May 11;3(5):e82.

40. de Diego-Balaguer R, Schramm C, Rebeix I, Dupoux E, Durr A, Brice A, et al. COMT Val158Met Polymorphism Modulates Huntington's Disease Progression. PloS One. 2016;11(9):e0161106.

41. Rubinsztein DC, Leggo J, Chiano M, Dodge A, Norbury G, Rosser E, et al. Genotypes at the GluR6 kainate receptor locus are associated with variation in the age of onset of Huntington disease. Proc Natl Acad Sci U S A. 1997 Apr 15;94(8):3872–6.

42. Tartaglione AM, Armida M, Potenza RL, Pezzola A, Popoli P, Calamandrei G. Aberrant self-grooming as early marker of motor dysfunction in a rat model of Huntington's disease. Behav Brain Res. 2016 Oct 15;313:53–7.

43. Brandt J, Folstein SE, Folstein MF. Differential cognitive impairment in Alzheimer's disease and Huntington's disease. Ann Neurol. 1988 Jun;23(6):555–61.

44. Ouk K, Aungier J, Morton AJ. Progressive gene dose-dependent disruption of the methamphetamine-sensitive circadian oscillator-driven rhythms in a knock-in mouse model of Huntington's disease. Exp Neurol. 2016 Sep 16;

45. Rodrigues FB, Wild EJ. Psychogenic non-epileptic seizures in early Huntington's disease. Pract Neurol. 2016 Jun 21;

46. Morkl S, Muller NJ, Blesl C, Wilkinson L, Tmava A, Wurm W, et al. Problem solving, impulse control and planning in patients with early- and late-stage Huntington's disease. Eur Arch Psychiatry Clin Neurosci. 2016 Jul 2;

47. Montoya A, Price B, Menear M, Lepage M. Brain imaging and cognitive dysfunctions in Huntington's disease. J Psychiatry Neurosci. 2006 Jan;31(1):21–9.

48. Stout JC, Glikmann-Johnston Y, Andrews SC. Cognitive assessment strategies in Huntington's disease research. J Neurosci Methods. 2016 May 30;265:19–24.

49. Diamond A. Executive functions. Annu Rev Psychol. 2013;64:135–68.

50. Wright DJ, Gray LJ, Finkelstein DI, Crouch PJ, Pow D, Pang TY, et al. N-acetylcysteine modulates glutamatergic dysfunction and depressive behavior in Huntington's disease. Hum Mol Genet. 2016 May 14;

51. Dale M, van Duijn E. Anxiety in Huntington's Disease. J Neuropsychiatry Clin Neurosci. 2015 Fall;27(4):262–71.

52. Philpott AL, Andrews SC, Staios M, Churchyard A, Fisher F. Emotion Evaluation and Social Inference Impairments in Huntington's Disease. J Huntingt Dis. 2016 May 3;5(2):175–83.

53. Hubers AAM, Hamming A, Giltay EJ, von Faber M, Roos RAC, van der Mast RC, et al. Suicidality in Huntington's Disease: A Qualitative Study on Coping Styles and Support Strategies. J Huntingt Dis. 2016 May 31;5(2):185–98.

54. Martinez-Horta S, Perez-Perez J, van Duijn E, Fernandez-Bobadilla R, Carceller M, Pagonabarraga J, et al. Neuropsychiatric symptoms are very common in premanifest and early stage Huntington's Disease. Parkinsonism Relat Disord. 2016 Apr;25:58–64.

55. Sanberg PR, Fibiger HC, Mark RF. Body weight and dietary factors in Huntington's disease patients compared with matched controls. Med J Aust. 1981 Apr 18;1(8):407–9.

56. Zielonka D, Piotrowska I, Marcinkowski JT, Mielcarek M. Skeletal muscle pathology in Huntington's disease. Front Physiol. 2014;5:380.

57. Carroll JB, Bates GP, Steffan J, Saft C, Tabrizi SJ. Treating the whole body in Huntington's disease. Lancet Neurol. 2015 Nov;14(11):1135–42.

58. Rozas JL, Gomez-Sanchez L, Tomas-Zapico C, Lucas JJ, Fernandez-Chacon R. Increased neurotransmitter release at the neuromuscular junction in a mouse model of polyglutamine disease. J Neurosci Off J Soc Neurosci. 2011 Jan 19;31(3):1106–13.

59. Rocha NP, Ribeiro FM, Furr-Stimming E, Teixeira AL. Neuroimmunology of Huntington's Disease: Revisiting Evidence from Human Studies. Mediators Inflamm. 2016;2016:8653132.

60. Myers RH, Vonsattel JP, Paskevich PA, Kiely DK, Stevens TJ, Cupples LA, et al. Decreased neuronal and increased oligodendroglial densities in Huntington's disease caudate nucleus. J Neuropathol Exp Neurol. 1991 Nov;50(6):729–42.

61. Sapp E, Kegel KB, Aronin N, Hashikawa T, Uchiyama Y, Tohyama K, et al. Early and progressive accumulation of reactive microglia in the Huntington disease brain. J Neuropathol Exp Neurol. 2001 Feb;60(2):161–72.

62. van der Burg J, Bjorkgvist M, Brundin P. Beyond the brain: widespread pathology in Huntington's disease. Lancet Neurol. 2009 Aug;8(8):765–74.

63. Dufour BD, McBride JL. Corticosterone dysregulation exacerbates disease progression in the R6/2 transgenic mouse model of Huntington's disease. Exp Neurol. 2016 Sep;283(Pt A):308–17.

64. Mina E, van Roon-Mom W, Hettne K, van Zwet E, Goeman J, Neri C, et al. Common disease signatures from gene expression analysis in Huntington's disease human blood and brain. Orphanet J Rare Dis. 2016;11(1):97.

65. McCourt AC, Jakobsson L, Larsson S, Holm C, Piel S, Elmer E, et al. White Adipose Tissue Browning in the R6/2 Mouse Model of Huntington's Disease. PloS One. 2016;11(8):e0159870.

66. Garrett MC, Soares-da-Silva P. Increased cerebrospinal fluid dopamine and 3,4-dihydroxyphenylacetic acid levels in Huntington's disease: evidence for an overactive dopaminergic brain transmission. J Neurochem. 1992 Jan;58(1):101–6.

67. Quinn L, Hamana K, Kelson M, Dawes H, Collett J, Townson J, et al. A randomized, controlled trial of a multi-modal exercise intervention in Huntington's disease. Parkinsonism Relat Disord. 2016 Jul 1;

68. Kreilaus F, Spiro AS, Hannan AJ, Garner B, Jenner AM. Therapeutic Effects of Anthocyanins and Environmental Enrichment in R6/1 Huntington's Disease Mice. J Huntingt Dis. 2016 Aug 12;

69. Kreilaus F, Spiro AS, McLean CA, Garner B, Jenner AM. Evidence for altered cholesterol metabolism in Huntington's disease post mortem brain tissue. Neuropathol Appl Neurobiol. 2015 Sep 16;

70. Kreilaus F, Spiro AS, Hannan AJ, Garner B, Jenner AM. Brain Cholesterol Synthesis and Metabolism is Progressively Disturbed in the R6/1 Mouse Model of Huntington's Disease: A Targeted GC-MS/MS Sterol Analysis. J Huntingt Dis. 2015;4(4):305–18.

71. Peng C, Wang X, Chen J, Jiao R, Wang L, Li YM, et al. Biology of ageing and role of dietary antioxidants. BioMed Res Int. 2014;2014:831841.

72. Mollersen L, Moldestad O, Rowe AD, Bjolgerud A, Holm I, Tveteras L, et al. Effects of Anthocyanins on CAG Repeat Instability and Behaviour in Huntington's Disease R6/1 Mice. PLoS Curr. 2016;8.

73. Jodeiri Farshbaf M, Ghaedi K, Megraw TL, Curtiss J, Shirani Faradonbeh M, Vaziri P, et al. Does PGC1alpha/FNDC5/BDNF Elicit the Beneficial Effects of Exercise on Neurodegenerative Disorders? Neuromolecular Med. 2016 Mar;18(1):1–15.

74. Hartmann CJ, Groiss SJ, Vesper J, Schnitzler A, Wojtecki L. Brain stimulation in Huntington's disease. Neurodegener Dis Manag. 2016 Jun;6(3):223–36.

75. Spiegel EA, Wycis HT, Marks M, Lee AJ. Stereotaxic Apparatus for Operations on the Human Brain. Science. 1947 Oct 10;106(2754):349–50.

76. Wojtecki L, Groiss SJ, Ferrea S, Elben S, Hartmann CJ, Dunnett SB, et al. A Prospective Pilot Trial for Pallidal Deep Brain Stimulation in Huntington's Disease. Front Neurol. 2015;6:177.

77. McGregor AL, Dysart J, Tingle MD, Russell BR, Kydd RR, Finucane G. Varenicline improves motor and cognitive symptoms in early Huntington's disease. Neuropsychiatr Dis Treat. 2016;12:2381–6.

78. Deng P, Torrest A, Pollock K, Dahlenburg H, Annett G, Nolta JA, et al. Clinical trial perspective for adult and juvenile Huntington's disease using genetically-engineered mesenchymal stem cells. Neural Regen Res. 2016 May;11(5):702–5.

79. Luca G, Bellezza I, Arato I, Di Pardo A, Mancuso F, Calvitti M, et al. Terapeutic Potential of Microencapsulated Sertoli Cells in Huntington Disease. CNS Neurosci Ther. 2016 Aug;22(8):686–90.

80. Vadori M, Denaro L, D'Avella D, Cozzi E. Indications and prospects of neural transplantation for chronic neurological diseases. Curr Opin Organ Transplant. 2016 Oct;21(5):490–6.

81. Shin JW, Kim K-H, Chao MJ, Atwal RS, Gillis T, MacDonald ME, et al. Permanent inactivation of Huntington's disease mutation by personalized allele-specific CRISPR/Cas9. Hum Mol Genet. 2016 Sep 15;

82. Malkki H. Huntington disease: Selective deactivation of Huntington disease mutant allele by. Nat Rev Neurol. 2016 Sep 30;

83. Kay C, Collins JA, Skotte NH, Southwell AL, Warby SC, Caron NS, et al. Huntingtin Haplotypes Provide Prioritized Target Panels for Allele-specific Silencing in Huntington Disease Patients of European Ancestry. Mol Ther J Am Soc Gene Ther. 2015 Nov;23(11):1759–71.

84. Keeler AM, Sapp E, Chase K, Sottosanti E, Danielson E, Pfister E, et al. Cellular Analysis of Silencing the Huntington's Disease Gene Using AAV9 Mediated Delivery of Artificial Micro RNA into the Striatum of Q140/Q140 Mice. J Huntingt Dis. 2016 Sep 24;

85. Sanberg PR, Calderon SF, Giordano M, Tew JM, Norman AB. The quinolinic acid model of Huntington's disease: locomotor abnormalities. Exp Neurol. 1989 Jul;105(1):45–53.

86. Chang R, Liu X, Li S, Li X-J. Transgenic animal models for study of the pathogenesis of Huntington's disease and therapy. Drug Des Devel Ther. 2015;9:2179–88.

87. Raper J, Bosinger S, Johnson Z, Tharp G, Moran SP, Chan AWS. Increased irritability, anxiety, and immune reactivity in transgenic Huntington's disease monkeys. Brain Behav Immun. 2016 Jul 7;

88. Abada Y-SK, Ellenbroek BA. Of rodents and men: understanding the emergence of motor and cognitive symptoms in Huntington disease. Behav Pharmacol. 2016 Aug;27(5):403–14.

89. Pouladi MA, Morton AJ, Hayden MR. Choosing an animal model for the study of Huntington's disease. Nat Rev Neurosci. 2013 Oct;14(10):708–21.

90. Slow EJ, van Raamsdonk J, Rogers D, Coleman SH, Graham RK, Deng Y, et al. Selective striatal neuronal loss in a YAC128 mouse model of Huntington disease. Hum Mol Genet. 2003 Jul 1;12(13):1555–67.

91. Milnerwood AJ, Raymond LA. Corticostriatal synaptic function in mouse models of Huntington's disease: early effects of huntingtin repeat length and protein load. J Physiol. 2007 Dec 15;585(Pt 3):817–31.

92. Carroll JB, Lerch JP, Franciosi S, Spreeuw A, Bissada N, Henkelman RM, et al. Natural history of disease in the YAC128 mouse reveals a discrete signature of pathology in Huntington disease. Neurobiol Dis. 2011 Jul;43(1):257–65.

93. Van Raamsdonk JM, Pearson J, Slow EJ, Hossain SM, Leavitt BR, Hayden MR. Cognitive dysfunction precedes neuropathology and motor abnormalities in the YAC128 mouse model of Huntington's disease. J Neurosci Off J Soc Neurosci. 2005 Apr 20;25(16):4169–80.

94. Hodgson JG, Agopyan N, Gutekunst CA, Leavitt BR, LePiane F, Singaraja R, et al. A YAC mouse model for Huntington's disease with full-length mutant huntingtin, cytoplasmic toxicity, and selective striatal neurodegeneration. Neuron. 1999 May;23(1):181–92.

95. Cha JH, Kosinski CM, Kerner JA, Alsdorf SA, Mangiarini L, Davies SW, et al. Altered brain neurotransmitter receptors in transgenic mice expressing a portion of an abnormal human huntington disease gene. Proc Natl Acad Sci U S A. 1998 May 26;95(11):6480–5.

96. Mangiarini L, Sathasivam K, Seller M, Cozens B, Harper A, Hetherington C, et al. Exon 1 of the HD gene with an expanded CAG repeat is sufficient to cause a progressive neurological phenotype in transgenic mice. Cell. 1996 Nov 1;87(3):493–506.

97. Hansson O, Petersen A, Leist M, Nicotera P, Castilho RF, Brundin P. Transgenic mice expressing a Huntington's disease mutation are resistant to quinolinic acid-induced striatal excitotoxicity. Proc Natl Acad Sci U S A. 1999 Jul 20;96(15):8727–32.

98. Hickey MA, Kosmalska A, Enayati J, Cohen R, Zeitlin S, Levine MS, et al. Extensive early motor and non-motor behavioral deficits are followed by striatal neuronal loss in knock-in Huntington's disease mice. Neuroscience. 2008 Nov 11;157(1):280–95.

99. Strong MK, Southwell AL, Yonan JM, Hayden MR, Macgregor GR, Thompson LM, et al. Age-Dependent Resistance to Excitotoxicity in Htt CAG140 Mice and the Effect of Strain Background. J Huntingt Dis. 2012;1(2):221–41.

100. Menalled L, Brunner D. Animal models of Huntington's disease for translation to the clinic: best practices. Mov Disord Off J Mov Disord Soc. 2014 Sep 15;29(11):1375–90.

101. Loh DH, Kudo T, Truong D, Wu Y, Colwell CS. The Q175 mouse model of Huntington's disease shows gene dosage- and age-related decline in circadian rhythms of activity and sleep. PloS One. 2013;8(7):e69993.

102. Indersmitten T, Tran CH, Cepeda C, Levine MS. Altered excitatory and inhibitory inputs to striatal medium-sized spiny neurons and cortical pyramidal neurons in the Q175 mouse model of Huntington's disease. J Neurophysiol. 2015 Apr 1;113(7):2953–66.

103. Smith GA, Rocha EM, McLean JR, Hayes MA, Izen SC, Isacson O, et al. Progressive axonal transport and synaptic protein changes correlate with behavioral and neuropathological abnormalities in the heterozygous Q175 KI mouse model of Huntington's disease. Hum Mol Genet. 2014 Sep 1;23(17):4510–27.

104. Menalled LB, Kudwa AE, Miller S, Fitzpatrick J, Watson-Johnson J, Keating N, et al. Comprehensive behavioral and molecular characterization of a new knock-in mouse model of Huntington's disease: zQ175. PloS One. 2012;7(12):e49838.

105. El Massioui N, Ouary S, Cheruel F, Hantraye P, Brouillet E. Perseverative behavior underlying attentional set-shifting deficits in rats chronically treated with the neurotoxin 3-nitropropionic acid. Exp Neurol. 2001 Nov;172(1):172–81.

106. Yang S-H, Cheng P-H, Banta H, Piotrowska-Nitsche K, Yang J-J, Cheng ECH, et al. Towards a transgenic model of Huntington's disease in a non-human primate. Nature. 2008 Jun 12;453(7197):921–4.

107. Chan HY, Bonini NM. Drosophila models of human neurodegenerative disease. Cell Death Differ. 2000 Nov;7(11):1075–80.

108. Steinert JR, Campesan S, Richards P, Kyriacou CP, Forsythe ID, Giorgini F. Rab11 rescues synaptic dysfunction and behavioural deficits in a Drosophila model of Huntington's disease. Hum Mol Genet. 2012 Jul 1;21(13):2912–22.

109. Carter RJ, Lione LA, Humby T, Mangiarini L, Mahal A, Bates GP, et al. Characterization of progressive motor deficits in mice transgenic for the human Huntington's disease mutation. J Neurosci Off J Soc Neurosci. 1999 Apr 15;19(8):3248–57.

110. Cao Y, Bartolome-Martin D, Rotem N, Rozas C, Dellal SS, Chacon MA, et al. Rescue of homeostatic regulation of striatal excitability and locomotor activity in a mouse model of Huntington's disease. Proc Natl Acad Sci U S A. 2015 Feb 17;112(7):2239–44.

111. Spires TL, Grote HE, Varshney NK, Cordery PM, van Dellen A, Blakemore C, et al. Environmental enrichment rescues protein deficits in a mouse model of Huntington's disease,

indicating a possible disease mechanism. J Neurosci Off J Soc Neurosci. 2004 Mar 3;24(9):2270–6.

112. Bolivar VJ, Manley K, Messer A. Early exploratory behavior abnormalities in R6/1 Huntington's disease transgenic mice. Brain Res. 2004 Apr 16;1005(1–2):29–35.

113. Gray M, Shirasaki DI, Cepeda C, Andre VM, Wilburn B, Lu X-H, et al. Full-length human mutant huntingtin with a stable polyglutamine repeat can elicit progressive and selective neuropathogenesis in BACHD mice. J Neurosci Off J Soc Neurosci. 2008 Jun 11;28(24):6182–95.

114. Menalled LB. Knock-in mouse models of Huntington's disease. NeuroRx J Am Soc Exp Neurother. 2005 Jul;2(3):465–70.

115. Menalled LB, Sison JD, Dragatsis I, Zeitlin S, Chesselet M-F. Time course of early motor and neuropathological anomalies in a knock-in mouse model of Huntington's disease with 140 CAG repeats. J Comp Neurol. 2003 Oct 6;465(1):11–26.

116. Lione LA, Carter RJ, Hunt MJ, Bates GP, Morton AJ, Dunnett SB. Selective discrimination learning impairments in mice expressing the human Huntington's disease mutation. J Neurosci Off J Soc Neurosci. 1999 Dec 1;19(23):10428–37.

117. Meade CA, Deng Y-P, Fusco FR, Del Mar N, Hersch S, Goldowitz D, et al. Cellular localization and development of neuronal intranuclear inclusions in striatal and cortical neurons in R6/2 transgenic mice. J Comp Neurol. 2002 Jul 29;449(3):241–69.

118. Alves A, Gritsch K, Villle V, Drevon-Gaillotl E, Bayon Y, Clermont G, et al. Abdominal Wall: Register & Miscellaneous. Hernia J Hernias Abdom Wall Surg. 2015 Apr;19 Suppl 1:S139-143.

119. Deng YP, Wong T, Bricker-Anthony C, Deng B, Reiner A. Loss of corticostriatal and thalamostriatal synaptic terminals precedes striatal projection neuron pathology in heterozygous Q140 Huntington's disease mice. Neurobiol Dis. 2013 Dec;60:89–107.

120. Freese A, DiFiglia M, Koroshetz WJ, Beal MF, Martin JB. Characterization and mechanism of glutamate neurotoxicity in primary striatal cultures. Brain Res. 1990 Jun 25;521(1–2):254–64.

121. Zeron MM, Hansson O, Chen N, Wellington CL, Leavitt BR, Brundin P, et al. Increased sensitivity to N-methyl-D-aspartate receptor-mediated excitotoxicity in a mouse model of Huntington's disease. Neuron. 2002 Mar 14;33(6):849–60.

122. Zhang N, An MC, Montoro D, Ellerby LM. Characterization of Human Huntington's Disease Cell Model from Induced Pluripotent Stem Cells. PLoS Curr. 2010 Oct 28;2:RRN1193.

123. Eva C, Bovolin P, Balzac F, Botta C, Gamalero S, Vaccarino F. Primary cultures of corticostriatal cells from newborn rats: a model to study muscarinic receptor subtypes regulation and function. J Mol Neurosci. 1990;2(3):143–53.

124. Kaufman A, Milnerwood A, Sepers M, Coquinco A, She K, Wang L, et al. Opposing roles of synaptic and extrasynaptic NMDA receptor signaling in cocultured striatal and cortical neurons. J Neurosci. 2012 Mar 21;32(12):3992–4003.

125. Parsons MP, Kang R, Buren C, Dau A, Southwell AL, Doty CN, et al. Bidirectional control of postsynaptic density-95 (PSD-95) clustering by Huntingtin. J Biol Chem. 2014 Feb 7;289(6):3518–28.

126. Tartari M, Gissi C, Lo Sardo V, Zuccato C, Picardi E, Pesole G, et al. Phylogenetic comparison of huntingtin homologues reveals the appearance of a primitive polyQ in sea urchin. Mol Biol Evol. 2008 Feb;25(2):330–8.

127. White JK, Auerbach W, Duyao MP, Vonsattel JP, Gusella JF, Joyner AL, et al. Huntingtin is required for neurogenesis and is not impaired by the Huntington's disease CAG expansion. Nat Genet. 1997 Dec;17(4):404–10.

128. Duyao MP, Auerbach AB, Ryan A, Persichetti F, Barnes GT, McNeil SM, et al. Inactivation of the mouse Huntington's disease gene homolog Hdh. Science. 1995 Jul 21;269(5222):407–10.

129. Nasir J, Floresco S, O'Kusky J, Diewert V, Richman J, Zeisler J, et al. Targeted disruption of the Huntington's disease gene results in embryonic lethality and behavioral and morphological changes in heterozygotes. Cell. 1995 Jun 2;81(5):811–23.

130. Zeitlin S, Liu JP, Chapman DL, Papaioannou VE, Efstratiadis A. Increased apoptosis and early embryonic lethality in mice nullizygous for the Huntington's disease gene homologue. Nat Genet. 1995 Oct;11(2):155–63.

131. Leavitt BR, Guttman JA, Hodgson JG, Kimel GH, Singaraja R, Vogl AW, et al. Wild-type huntingtin reduces the cellular toxicity of mutant huntingtin in vivo. Am J Hum Genet. 2001 Feb;68(2):313–24.

132. Van Raamsdonk JM, Pearson J, Rogers DA, Bissada N, Vogl AW, Hayden MR, et al. Loss of wild-type huntingtin influences motor dysfunction and survival in the YAC128 mouse model of Huntington disease. Hum Mol Genet. 2005 May 15;14(10):1379–92.

133. Kaltenbach LS, Romero E, Becklin RR, Chettier R, Bell R, Phansalkar A, et al. Huntingtin interacting proteins are genetic modifiers of neurodegeneration. PLoS Genet. 2007 May 11;3(5):e82.

134. Shirasaki D, Greiner E, Al-Ramahi I, Gray M, Boontheung P, Geschwind D, et al. Network organization of the huntingtin proteomic interactome in mammalian brain. Neuron. 2012 Jul 12;75(1):41–57.

135. Zuccato C, Ciammola A, Rigamonti D, Leavitt B, Goffredo D, Conti L, et al. Loss of huntingtin-mediated BDNF gene transcription in Huntington's disease. Science. 2001 Jul 20;293(5529):493–8.

136. Hoffner G, Djian P. Protein aggregation in Huntington's disease. Biochimie. 2002 Apr;84(4):273–8.

137. Humbert S, Bryson EA, Cordelieres FP, Connors NC, Datta SR, Finkbeiner S, et al. The IGF-1/Akt pathway is neuroprotective in Huntington's disease and involves Huntingtin phosphorylation by Akt. Dev Cell. 2002 Jun;2(6):831–7.

138. Jeong H, Then F, Melia TJJ, Mazzulli JR, Cui L, Savas JN, et al. Acetylation targets mutant huntingtin to autophagosomes for degradation. Cell. 2009 Apr 3;137(1):60–72.

139. Arnesen T, Starheim KK, Van Damme P, Evjenth R, Dinh H, Betts MJ, et al. The chaperone-like protein HYPK acts together with NatA in cotranslational. Mol Cell Biol. 2010 Apr;30(8):1898–909.

140. Cong X, Held JM, DeGiacomo F, Bonner A, Chen JM, Schilling B, et al. Mass spectrometric identification of novel lysine acetylation sites in huntingtin. Mol Cell Proteomics MCP. 2011 Oct;10(10):M111.009829.

141. Huang K, Yanai A, Kang R, Arstikaitis P, Singaraja RR, Metzler M, et al. Huntingtin-interacting protein HIP14 is a palmitoyl transferase involved in palmitoylation and trafficking of multiple neuronal proteins. Neuron. 2004 Dec 16;44(6):977–86.

142. Yanai A, Huang K, Kang R, Singaraja RR, Arstikaitis P, Gan L, et al. Palmitoylation of huntingtin by HIP14 is essential for its trafficking and function. Nat Neurosci. 2006 Jun;9(6):824–31.

143. Steffan JS, Agrawal N, Pallos J, Rockabrand E, Trotman LC, Slepko N, et al. SUMO modification of Huntingtin and Huntington's disease pathology. Science. 2004 Apr 2;304(5667):100–4.

144. Kratter IH, Zahed H, Lau A, Tsvetkov AS, Daub AC, Weiberth KF, et al. Serine 421 regulates mutant huntingtin toxicity and clearance in mice. J Clin Invest. 2016 Sep 1;126(9):3585–97.

145. Bhat KP, Yan S, Wang C-E, Li S, Li X-J. Differential ubiquitination and degradation of huntingtin fragments modulated by ubiquitin-protein ligase E3A. Proc Natl Acad Sci U S A. 2014 Apr 15;111(15):5706–11.

146. Zhao T, Hong Y, Li S, Li X-J. Compartment-Dependent Degradation of Mutant Huntingtin Accounts for Its Preferential Accumulation in Neuronal Processes. J Neurosci Off J Soc Neurosci. 2016 Aug 10;36(32):8317–28.

147. DiGiovanni LF, Mocle AJ, Xia J, Truant R. Huntingtin N17 domain is a reactive oxygen species sensor regulating huntingtin phosphorylation and localization. Hum Mol Genet. 2016 Jul 27;

148. Chaibva M, Jawahery S, Pilkington AW 4th, Arndt JR, Sarver O, Valentine S, et al. Acetylation within the First 17 Residues of Huntingtin Exon 1 Alters Aggregation and Lipid Binding. Biophys J. 2016 Jul 26;111(2):349–62.

149. Mende-Mueller LM, Toneff T, Hwang SR, Chesselet MF, Hook VY. Tissue-specific proteolysis of Huntingtin (htt) in human brain: evidence of enhanced levels of N- and C-terminal

htt fragments in Huntington's disease striatum. J Neurosci Off J Soc Neurosci. 2001 Mar 15;21(6):1830–7.

150. Sahoo B, Arduini I, Drombosky KW, Kodali R, Sanders LH, Greenamyre JT, et al. Folding Landscape of Mutant Huntingtin Exon1: Diffusible Multimers, Oligomers and Fibrils, and No Detectable Monomer. PloS One. 2016;11(6):e0155747.

151. Casaca-Carreira J, Toonen LJA, Evers MM, Jahanshahi A, van-Roon-Mom WMC, Temel Y. In vivo proof-of-concept of removal of the huntingtin caspase cleavage motif-encoding exon 12 approach in the YAC128 mouse model of Huntington's disease. Biomed Pharmacother Biomedecine Pharmacother. 2016 Sep 15;84:93–6.

152. Hermel E, Gafni J, Propp SS, Leavitt BR, Wellington CL, Young JE, et al. Specific caspase interactions and amplification are involved in selective neuronal vulnerability in Huntington's disease. Cell Death Differ. 2004 Apr;11(4):424–38.

153. Graham RK, Deng Y, Carroll J, Vaid K, Cowan C, Pouladi MA, et al. Cleavage at the 586 amino acid caspase-6 site in mutant huntingtin influences caspase-6 activation in vivo. J Neurosci Off J Soc Neurosci. 2010 Nov 10;30(45):15019–29.

154. Gafni J, Hermel E, Young JE, Wellington CL, Hayden MR, Ellerby LM. Inhibition of calpain cleavage of huntingtin reduces toxicity: accumulation of calpain/caspase fragments in the nucleus. J Biol Chem. 2004 May 7;279(19):20211–20.

155. Clemens LE, Weber JJ, Wlodkowski TT, Yu-Taeger L, Michaud M, Calaminus C, et al. Olesoxime suppresses calpain activation and mutant huntingtin fragmentation in the BACHD rat. Brain J Neurol. 2015 Dec;138(Pt 12):3632–53.

156. Nissley DA, O'Brien EP. Altered Co-Translational Processing Plays a Role in Huntington's Pathogenesis-A Hypothesis. Front Mol Neurosci. 2016;9:54.

157. Gipson TA, Neueder A, Wexler NS, Bates GP, Housman D. Aberrantly spliced HTT, a new player in Huntington's disease pathogenesis. RNA Biol. 2013 Nov;10(11):1647–52.

158. Gauthier LR, Charrin BC, Borrell-Pages M, Dompierre JP, Rangone H, Cordelieres FP, et al. Huntingtin controls neurotrophic support and survival of neurons by enhancing BDNF vesicular transport along microtubules. Cell. 2004 Jul 9;118(1):127–38.

159. Slow EJ, Graham RK, Osmand AP, Devon RS, Lu G, Deng Y, et al. Absence of behavioral abnormalities and neurodegeneration in vivo despite widespread neuronal huntingtin inclusions. Proc Natl Acad Sci U S A. 2005 Aug 9;102(32):11402–7.

160. Reiner A, Dragatsis I, Zeitlin S, Goldowitz D. Wild-type huntingtin plays a role in brain development and neuronal survival. Mol Neurobiol. 2003 Dec;28(3):259–76.

161. Schulte J, Littleton JT. The biological function of the Huntingtin protein and its relevance to Huntington's Disease pathology. Curr Trends Neurol. 2011 Jan 1;5:65–78.

162. Clabough EBD, Zeitlin SO. Deletion of the triplet repeat encoding polyglutamine within the mouse Huntington's disease gene results in subtle behavioral/motor phenotypes in vivo and elevated levels of ATP with cellular senescence in vitro. Hum Mol Genet. 2006 Feb 15;15(4):607–23.

163. Neveklovska M, Clabough EBD, Steffan JS, Zeitlin SO. Deletion of the huntingtin proline-rich region does not significantly affect normal huntingtin function in mice. J Huntingt Dis. 2012;1(1):71–87.

164. Rigamonti D, Sipione S, Goffredo D, Zuccato C, Fossale E, Cattaneo E. Huntingtin's neuroprotective activity occurs via inhibition of procaspase-9 processing. J Biol Chem. 2001 May 4;276(18):14545–8.

165. Chen N, Luo T, Wellington C, Metzler M, McCutcheon K, Hayden MR, et al. Subtype-specific enhancement of NMDA receptor currents by mutant huntingtin. J Neurochem. 1999 May;72(5):1890–8.

166. Li L, Murphy TH, Hayden MR, Raymond LA. Enhanced striatal NR2B-containing N-methyl-D-aspartate receptor-mediated synaptic currents in a mouse model of Huntington disease. J Neurophysiol. 2004 Nov;92(5):2738–46.

167. Fan MMY, Fernandes HB, Zhang LYJ, Hayden MR, Raymond LA. Altered NMDA receptor trafficking in a yeast artificial chromosome transgenic mouse model of Huntington's disease. J Neurosci Off J Soc Neurosci. 2007 Apr 4;27(14):3768–79.

168. Hardingham GE, Fukunaga Y, Bading H. Extrasynaptic NMDARs oppose synaptic NMDARs by triggering CREB shut-off and cell death pathways. Nat Neurosci. 2002 May;5(5):405–14.

169. Hardingham GE, Bading H. Synaptic versus extrasynaptic NMDA receptor signalling: implications for neurodegenerative disorders. Nat Rev Neurosci. 2010 Oct;11(10):682–96.

170. Langfelder P, Cantle J, Chatzopoulou D, Wang N, Gao F, Al-Ramahi I, et al. Integrated genomics and proteomics define huntingtin CAG length-dependent networks in mice. Nat Neurosci. 2016 Apr;19(4):623–33.

171. Shirasaki DI, Greiner ER, Al-Ramahi I, Gray M, Boontheung P, Geschwind DH, et al. Network organization of the huntingtin proteomic interactome in mammalian brain. Neuron. 2012 Jul 12;75(1):41–57.

172. Rozas JL, Gomez-Sanchez L, Tomas-Zapico C, Lucas JJ, Fernandez-Chacon R. Presynaptic dysfunction in Huntington's disease. Biochem Soc Trans. 2010 Apr;38(2):488–92.

173. Sanders SS, Hayden MR. Aberrant palmitoylation in Huntington disease. Biochem Soc Trans. 2015 Apr;43(2):205–10.

174. DiFiglia M, Sapp E, Chase K, Schwarz C, Meloni A, Young C, et al. Huntingtin is a cytoplasmic protein associated with vesicles in human and rat brain neurons. Neuron. 1995 May;14(5):1075–81.

175. Velier J, Kim M, Schwarz C, Kim TW, Sapp E, Chase K, et al. Wild-type and mutant huntingtins function in vesicle trafficking in the secretory and endocytic pathways. Exp Neurol. 1998 Jul;152(1):34–40.

176. Hoffner G, Kahlem P, Djian P. Perinuclear localization of huntingtin as a consequence of its binding to microtubules through an interaction with beta-tubulin: relevance to Huntington's disease. J Cell Sci. 2002 Mar 1;115(Pt 5):941–8.

177. Li H, Wyman T, Yu Z-X, Li S-H, Li X-J. Abnormal association of mutant huntingtin with synaptic vesicles inhibits glutamate release. Hum Mol Genet. 2003 Aug 15;12(16):2021–30.

178. Harjes P, Wanker EE. The hunt for huntingtin function: interaction partners tell many different stories. Trends Biochem Sci. 2003 Aug;28(8):425–33.

179. Giralt A, Carreton O, Lao-Peregrin C, Martin ED, Alberch J. Conditional BDNF release under pathological conditions improves Huntington's disease pathology by delaying neuronal dysfunction. Mol Neurodegener. 2011 Oct 10;6(1):71.

180. Nithianantharajah J, Barkus C, Murphy M, Hannan AJ. Gene-environment interactions modulating cognitive function and molecular correlates of synaptic plasticity in Huntington's disease transgenic mice. Neurobiol Dis. 2008 Mar;29(3):490–504.

181. Anglada-Huguet M, Vidal-Sancho L, Giralt A, Garcia-Diaz Barriga G, Xifro X, Alberch J. Prostaglandin E2 EP2 activation reduces memory decline in R6/1 mouse model of Huntington's

disease by the induction of BDNF-dependent synaptic plasticity. Neurobiol Dis. 2016 Nov;95:22–34.

182. Puigdellivol M, Cherubini M, Brito V, Giralt A, Suelves N, Ballesteros J, et al. A role for Kalirin-7 in corticostriatal synaptic dysfunction in Huntington's disease. Hum Mol Genet. 2015 Dec 20;24(25):7265–85.

183. Cai H, Reim K, Varoqueaux F, Tapechum S, Hill K, Sorensen JB, et al. Complexin II plays a positive role in Ca2+-triggered exocytosis by facilitating vesicle priming. Proc Natl Acad Sci U S A. 2008 Dec 9;105(49):19538–43.

184. Morton AJ, Edwardson JM. Progressive depletion of complexin II in a transgenic mouse model of Huntington's disease. J Neurochem. 2001 Jan;76(1):166–72.

185. Morton AJ, Faull RL, Edwardson JM. Abnormalities in the synaptic vesicle fusion machinery in Huntington's disease. Brain Res Bull. 2001 Sep 15;56(2):111–7.

186. Glynn D, Bortnick RA, Morton AJ. Complexin II is essential for normal neurological function in mice. Hum Mol Genet. 2003 Oct 1;12(19):2431–48.

187. Glynn D, Reim K, Brose N, Morton AJ. Depletion of Complexin II does not affect disease progression in a mouse model of Huntington's disease (HD); support for role for complexin II in behavioural pathology in a mouse model of HD. Brain Res Bull. 2007 Apr 30;72(2–3):108–20.

188. Smith R, Klein P, Koc-Schmitz Y, Waldvogel HJ, Faull RLM, Brundin P, et al. Loss of SNAP-25 and rabphilin 3a in sensory-motor cortex in Huntington's disease. J Neurochem. 2007 Oct;103(1):115–23.

189. Singaraja RR, Huang K, Sanders SS, Milnerwood AJ, Hines R, Lerch JP, et al. Altered palmitoylation and neuropathological deficits in mice lacking HIP14. Hum Mol Genet. 2011 Oct 15;20(20):3899–909.

190. Smith R, Petersen A, Bates GP, Brundin P, Li J-Y. Depletion of rabphilin 3A in a transgenic mouse model (R6/1) of Huntington's disease, a possible culprit in synaptic dysfunction. Neurobiol Dis. 2005 Dec;20(3):673–84.

191. Lynch G, Kramar EA, Rex CS, Jia Y, Chappas D, Gall CM, et al. Brain-derived neurotrophic factor restores synaptic plasticity in a knock-in mouse model of Huntington's disease. J Neurosci Off J Soc Neurosci. 2007 Apr 18;27(16):4424–34.

192. Valencia A, Sapp E, Kimm JS, McClory H, Ansong KA, Yohrling G, et al. Striatal synaptosomes from Hdh140Q/140Q knock-in mice have altered protein levels, novel sites of methionine oxidation, and excess glutamate release after stimulation. J Huntingt Dis. 2013;2(4):459–75.

193. Huang K, Sanders SS, Kang R, Carroll JB, Sutton L, Wan J, et al. Wild-type HTT modulates the enzymatic activity of the neuronal palmitoyl transferase HIP14. Hum Mol Genet. 2011 Sep 1;20(17):3356–65.

194. Rush DB, Leon RT, McCollum MH, Treu RW, Wei J. Palmitoylation and trafficking of GAD65 are impaired in a cellular model of Huntington's disease. Biochem J. 2012 Feb 15;442(1):39–48.

195. Young FB, Butland SL, Sanders SS, Sutton LM, Hayden MR. Putting proteins in their place: palmitoylation in Huntington disease and other neuropsychiatric diseases. Prog Neurobiol. 2012 May;97(2):220–38.

196. Valor LM. Transcription, epigenetics and ameliorative strategies in Huntington's Disease: a genome-wide perspective. Mol Neurobiol. 2015 Feb;51(1):406–23.

197. Steffan JS, Kazantsev A, Spasic-Boskovic O, Greenwald M, Zhu YZ, Gohler H, et al. The Huntington's disease protein interacts with p53 and CREB-binding protein and represses transcription. Proc Natl Acad Sci U S A. 2000 Jun 6;97(12):6763–8.

198. Sugars KL, Brown R, Cook LJ, Swartz J, Rubinsztein DC. Decreased cAMP response element-mediated transcription: an early event in exon 1 and full-length cell models of Huntington's disease that contributes to polyglutamine pathogenesis. J Biol Chem. 2004 Feb 6;279(6):4988–99.

199. Labadorf A, Hoss AG, Lagomarsino V, Latourelle JC, Hadzi TC, Bregu J, et al. RNA Sequence Analysis of Human Huntington Disease Brain Reveals an Extensive Increase in Inflammatory and Developmental Gene Expression. PloS One. 2015;10(12):e0143563.

200. Lin L, Park JW, Ramachandran S, Zhang Y, Tseng Y-T, Shen S, et al. Transcriptome sequencing reveals aberrant alternative splicing in Huntington's disease. Hum Mol Genet. 2016 Jul 4;

201. Kim S-H, Shahani N, Bae B-I, Sbodio JI, Chung Y, Nakaso K, et al. Allele-specific regulation of mutant Huntingtin by Wig1, a downstream target of p53. Hum Mol Genet. 2016 May 19;

202. Miller LC, Swayne LA, Chen L, Feng Z-P, Wacker JL, Muchowski PJ, et al. Cysteine string protein (CSP) inhibition of N-type calcium channels is blocked by mutant huntingtin. J Biol Chem. 2003 Dec 26;278(52):53072–81.

203. Graybiel AM, Aosaki T, Flaherty AW, Kimura M. The basal ganglia and adaptive motor control. Science. 1994 Sep 23;265(5180):1826–31.

204. Carpenter MB. Anatomical organization of the corpus striatum and related nuclei. Res Publ - Assoc Res Nerv Ment Dis. 1976;55:1–36.

205. Smith Y, Shink E, Sidibe M. Neuronal circuitry and synaptic connectivity of the basal ganglia. Neurosurg Clin N Am. 1998 Apr;9(2):203–22.

206. Groenewegen HJ, Berendse HW, Wolters JG, Lohman AH. The anatomical relationship of the prefrontal cortex with the striatopallidal system, the thalamus and the amygdala: evidence for a parallel organization. Prog Brain Res. 1990;85:95-116-118.

207. Finch DM. Neurophysiology of converging synaptic inputs from the rat prefrontal cortex, amygdala, midline thalamus, and hippocampal formation onto single neurons of the caudate/putamen and nucleus accumbens. Hippocampus. 1996;6(5):495–512.

208. Swanson LW. The projections of the ventral tegmental area and adjacent regions: a combined fluorescent retrograde tracer and immunofluorescence study in the rat. Brain Res Bull. 1982 Dec;9(1–6):321–53.

209. Phillipson OT, Griffiths AC. The topographic order of inputs to nucleus accumbens in the rat. Neuroscience. 1985 Oct;16(2):275–96.

210. Ena S, de Kerchove d'Exaerde A, Schiffmann SN. Unraveling the differential functions and regulation of striatal neuron sub-populations in motor control, reward, and motivational processes. Front Behav Neurosci. 2011;5:47.

211. Yin HH. The Basal Ganglia in Action. Neurosci Rev J Bringing Neurobiol Neurol Psychiatry. 2016 Jun 15;

212. Delgado MR. Reward-related responses in the human striatum. Ann N Y Acad Sci. 2007 May;1104:70–88.

213. Balleine BW, Delgado MR, Hikosaka O. The role of the dorsal striatum in reward and decision-making. J Neurosci Off J Soc Neurosci. 2007 Aug 1;27(31):8161–5.

214. Baez-Mendoza R, Schultz W. The role of the striatum in social behavior. Front Neurosci. 2013 Dec 10;7:233.

215. Bhanji JP, Delgado MR. The Social Brain and Reward: Social Information Processing in the Human Striatum. Wiley Interdiscip Rev Cogn Sci. 2014 Jan;5(1):61–73.

216. van den Bos R. The dorsal striatum and ventral striatum play different roles in the programming of social behaviour: a tribute to Lex Cools. Behav Pharmacol. 2015 Feb;26(1–2):6–17.

217. Zeighami Y, Moustafa AA. Differential functions of ventral and dorsal striatum. Brain J Neurol. 2015 Oct;138(Pt 10):e381.

218. O'Doherty J, Dayan P, Schultz J, Deichmann R, Friston K, Dolan RJ. Dissociable roles of ventral and dorsal striatum in instrumental conditioning. Science. 2004 Apr 16;304(5669):452–4.

219. Everitt BJ, Robbins TW. From the ventral to the dorsal striatum: devolving views of their roles in drug addiction. Neurosci Biobehav Rev. 2013 Nov;37(9 Pt A):1946–54.

220. Sleezer BJ, Hayden BY. Differential Contributions of Ventral and Dorsal Striatum to Early and Late Phases of Cognitive Set Reconfiguration. J Cogn Neurosci. 2016 Dec;28(12):1849–64.

221. Ferre S, Lluis C, Justinova Z, Quiroz C, Orru M, Navarro G, et al. Adenosine-cannabinoid receptor interactions. Implications for striatal function. Br J Pharmacol. 2010 Jun;160(3):443–53.

222. Vonsattel JP, Myers RH, Stevens TJ, Ferrante RJ, Bird ED, Richardson EPJ. Neuropathological classification of Huntington's disease. J Neuropathol Exp Neurol. 1985 Nov;44(6):559–77.

223. Ferrante RJ, Kowall NW, Beal MF, Martin JB, Bird ED, Richardson EPJ. Morphologic and histochemical characteristics of a spared subset of striatal neurons in Huntington's disease. J Neuropathol Exp Neurol. 1987 Jan;46(1):12–27.

224. Kemp JM, Powell TP. The structure of the caudate nucleus of the cat: light and electron microscopy. Philos Trans R Soc Lond B Biol Sci. 1971 Sep 30;262(845):383–401.

225. Freund TF, Powell JF, Smith AD. Tyrosine hydroxylase-immunoreactive boutons in synaptic contact with identified striatonigral neurons, with particular reference to dendritic spines. Neuroscience. 1984 Dec;13(4):1189–215.

226. Xu ZC, Wilson CJ, Emson PC. Restoration of the corticostriatal projection in rat neostriatal grafts: electron microscopic analysis. Neuroscience. 1989;29(3):539–50.

227. Maeno H. Dopamine receptors in canine caudate nucleus. Mol Cell Biochem. 1982 Mar 19;43(2):65–80.

228. Richfield EK, Penney JB, Young AB. Anatomical and affinity state comparisons between dopamine D1 and D2 receptors in the rat central nervous system. Neuroscience. 1989;30(3):767–77.

229. Gerfen CR, Surmeier DJ. Modulation of striatal projection systems by dopamine. Annu Rev Neurosci. 2011;34:441–66.

230. Albin RL, Young AB, Penney JB. The functional anatomy of basal ganglia disorders. Trends Neurosci. 1989 Oct;12(10):366–75.

231. DeLong MR. Primate models of movement disorders of basal ganglia origin. Trends Neurosci. 1990 Jul;13(7):281–5.

232. Rosell A, Gimenez-Amaya JM. Anatomical re-evaluation of the corticostriatal projections to the caudate nucleus: a retrograde labeling study in the cat. Neurosci Res. 1999 Sep;34(4):257–69.

233. Lei W, Jiao Y, Del Mar N, Reiner A. Evidence for differential cortical input to direct pathway versus indirect pathway striatal projection neurons in rats. J Neurosci Off J Soc Neurosci. 2004 Sep 22;24(38):8289–99.

234. Reiner A, Jiao Y, Del Mar N, Laverghetta AV, Lei WL. Differential morphology of pyramidal tract-type and intratelencephalically projecting-type corticostriatal neurons and their intrastriatal terminals in rats. J Comp Neurol. 2003 Mar 17;457(4):420–40.

235. Ballion B, Mallet N, Bezard E, Lanciego JL, Gonon F. Intratelencephalic corticostriatal neurons equally excite striatonigral and striatopallidal neurons and their discharge activity is selectively reduced in experimental parkinsonism. Eur J Neurosci. 2008 May;27(9):2313–21.

236. Glass M, Dragunow M, Faull RL. The pattern of neurodegeneration in Huntington's disease: a comparative study of cannabinoid, dopamine, adenosine and GABA(A) receptor alterations in the human basal ganglia in Huntington's disease. Neuroscience. 2000;97(3):505–19.

237. Reiner A, Albin RL, Anderson KD, D'Amato CJ, Penney JB, Young AB. Differential loss of striatal projection neurons in Huntington disease. Proc Natl Acad Sci U S A. 1988 Aug;85(15):5733–7.

238. Augood SJ, Faull RL, Love DR, Emson PC. Reduction in enkephalin and substance P messenger RNA in the striatum of early grade Huntington's disease: a detailed cellular in situ hybridization study. Neuroscience. 1996 Jun;72(4):1023–36.

239. Deng YP, Albin RL, Penney JB, Young AB, Anderson KD, Reiner A. Differential loss of striatal projection systems in Huntington's disease: a quantitative immunohistochemical study. J Chem Neuroanat. 2004 Jun;27(3):143–64.

240. Albin RL, Reiner A, Anderson KD, Penney JB, Young AB. Striatal and nigral neuron subpopulations in rigid Huntington's disease: implications for the functional anatomy of chorea and rigidity-akinesia. Ann Neurol. 1990 Apr;27(4):357–65.

241. Deng Y-P, Reiner A. Cholinergic interneurons in the Q140 knock-in mouse model of Huntington's disease: Reductions in dendritic branching and thalamostriatal input. J Comp Neurol. 2016 May 24;

242. Rub U, Hentschel M, Stratmann K, Brunt E, Heinsen H, Seidel K, et al. Huntington's disease (HD): degeneration of select nuclei, widespread occurrence of neuronal nuclear and axonal inclusions in the brainstem. Brain Pathol Zurich Switz. 2014 Apr;24(3):247–60.

243. Lambeck J, Niesen W-D, Reinhard M, Weiller C, Dose M, Zucker B. Substantia nigra hyperechogenicity in hypokinetic Huntington's disease patients. J Neurol. 2015 Mar;262(3):711–7.

244. Bamford NS, Robinson S, Palmiter RD, Joyce JA, Moore C, Meshul CK. Dopamine modulates release from corticostriatal terminals. J Neurosci Off J Soc Neurosci. 2004 Oct 27;24(43):9541–52.

245. Bamford NS, Zhang H, Schmitz Y, Wu N-P, Cepeda C, Levine MS, et al. Heterosynaptic dopamine neurotransmission selects sets of corticostriatal terminals. Neuron. 2004 May 27;42(4):653–63.

246. Bamford NS, Zhang H, Joyce JA, Scarlis CA, Hanan W, Wu N-P, et al. Repeated exposure to methamphetamine causes long-lasting presynaptic corticostriatal depression that is renormalized with drug readministration. Neuron. 2008 Apr 10;58(1):89–103.

247. Cepeda C, Murphy KPS, Parent M, Levine MS. The role of dopamine in Huntington's disease. Prog Brain Res. 2014;211:235–54.

248. Singh-Bains MK, Tippett LJ, Hogg VM, Synek BJ, Roxburgh RH, Waldvogel HJ, et al. Globus pallidus degeneration and clinicopathological features of Huntington disease. Ann Neurol. 2016 Aug;80(2):185–201.

249. Du Z, Chazalon M, Bestaven E, Leste-Lasserre T, Baufreton J, Cazalets J-R, et al. Early GABAergic transmission defects in the external globus pallidus and rest/activity rhythm alteration in a mouse model of Huntington's disease. Neuroscience. 2016 Aug 4;329:363–79.

250. Callahan JW, Abercrombie ED. Age-dependent alterations in the cortical entrainment of subthalamic nucleus neurons in the YAC128 mouse model of Huntington's disease. Neurobiol Dis. 2015 Jun;78:88–99.

251. Callahan JW, Abercrombie ED. Relationship between subthalamic nucleus neuronal activity and electrocorticogram is altered in the R6/2 mouse model of Huntington's disease. J Physiol. 2015 Aug 15;593(16):3727–38.

252. Hedreen JC, Peyser CE, Folstein SE, Ross CA. Neuronal loss in layers V and VI of cerebral cortex in Huntington's disease. Neurosci Lett. 1991 Dec 9;133(2):257–61.

253. Cudkowicz M, Kowall NW. Degeneration of pyramidal projection neurons in Huntington's disease cortex. Ann Neurol. 1990 Feb;27(2):200–4.

254. Rosas HD, Koroshetz WJ, Chen YI, Skeuse C, Vangel M, Cudkowicz ME, et al. Evidence for more widespread cerebral pathology in early HD: an MRI-based morphometric analysis. Neurology. 2003 May 27;60(10):1615–20.

255. Waldvogel HJ, Thu D, Hogg V, Tippett L, Faull RLM. Selective neurodegeneration, neuropathology and symptom profiles in Huntington's disease. Adv Exp Med Biol. 2012;769:141–52.

256. Spargo E, Everall IP, Lantos PL. Neuronal loss in the hippocampus in Huntington's disease: a comparison with HIV infection. J Neurol Neurosurg Psychiatry. 1993 May;56(5):487–91.

257. Ransome MI, Renoir T, Hannan AJ. Hippocampal neurogenesis, cognitive deficits and affective disorder in Huntington's disease. Neural Plast. 2012;2012:874387.

258. Begeti F, Schwab LC, Mason SL, Barker RA. Hippocampal dysfunction defines disease onset in Huntington's disease. J Neurol Neurosurg Psychiatry. 2016 Sep;87(9):975–81.

259. Rub U, Hoche F, Brunt ER, Heinsen H, Seidel K, Del Turco D, et al. Degeneration of the cerebellum in Huntington's disease (HD): possible relevance for the clinical picture and potential gateway to pathological mechanisms of the disease process. Brain Pathol Zurich Switz. 2013 Mar;23(2):165–77.

260. Wolf RC, Thomann PA, Sambataro F, Wolf ND, Vasic N, Landwehrmeyer GB, et al. Abnormal cerebellar volume and corticocerebellar dysfunction in early manifest Huntington's disease. J Neurol. 2015;262(4):859–69.

261. Hansotia P, Wall R, Berendes J. Sleep disturbances and severity of Huntington's disease. Neurology. 1985 Nov;35(11):1672–4.

262. Morton AJ, Wood NI, Hastings MH, Hurelbrink C, Barker RA, Maywood ES. Disintegration of the sleep-wake cycle and circadian timing in Huntington's disease. J Neurosci Off J Soc Neurosci. 2005 Jan 5;25(1):157–63.

263. Heuser IJ, Chase TN, Mouradian MM. The limbic-hypothalamic-pituitary-adrenal axis in Huntington's disease. Biol Psychiatry. 1991 Nov 1;30(9):943–52.

264. Bartlett DM, Cruickshank TM, Hannan AJ, Eastwood PR, Lazar AS, Ziman MR. Neuroendocrine and Neurotrophic Signaling in Huntington's Disease: Implications for Pathogenic Mechanisms and Treatment Strategies. Neurosci Biobehav Rev. 2016 Sep 13;

265. Rona-Voros K, Weydt P. The role of PGC-1alpha in the pathogenesis of neurodegenerative disorders. Curr Drug Targets. 2010 Oct;11(10):1262–9.

266. Cui L, Jeong H, Borovecki F, Parkhurst CN, Tanese N, Krainc D. Transcriptional repression of PGC-1alpha by mutant huntingtin leads to mitochondrial dysfunction and neurodegeneration. Cell. 2006 Oct 6;127(1):59–69.

267. Cong S-Y, Pepers BA, Evert BO, Rubinsztein DC, Roos RAC, van Ommen G-JB, et al. Mutant huntingtin represses CBP, but not p300, by binding and protein degradation. Mol Cell Neurosci. 2005 Dec;30(4):560–71.

268. Jiang H, Nucifora FCJ, Ross CA, DeFranco DB. Cell death triggered by polyglutamine-expanded huntingtin in a neuronal cell line is associated with degradation of CREB-binding protein. Hum Mol Genet. 2003 Jan 1;12(1):1–12.

269. Lin J, Wu P-H, Tarr PT, Lindenberg KS, St-Pierre J, Zhang C-Y, et al. Defects in adaptive energy metabolism with CNS-linked hyperactivity in PGC-1alpha null mice. Cell. 2004 Oct 1;119(1):121–35.

270. Zuccato C, Tartari M, Crotti A, Goffredo D, Valenza M, Conti L, et al. Huntingtin interacts with REST/NRSF to modulate the transcription of. Nat Genet. 2003 Sep;35(1):76–83.

271. Goodman LJ, Valverde J, Lim F, Geschwind MD, Federoff HJ, Geller AI, et al. Regulated release and polarized localization of brain-derived neurotrophic factor in hippocampal neurons. Mol Cell Neurosci. 1996 Mar;7(3):222–38.

272. Altar CA, Cai N, Bliven T, Juhasz M, Conner JM, Acheson AL, et al. Anterograde transport of brain-derived neurotrophic factor and its role in the brain. Nature. 1997 Oct 23;389(6653):856–60.

273. Engelender S, Sharp AH, Colomer V, Tokito MK, Lanahan A, Worley P, et al. Huntingtin-associated protein 1 (HAP1) interacts with the p150Glued subunit of dynactin. Hum Mol Genet. 1997 Dec;6(13):2205–12.

274. Li SH, Gutekunst CA, Hersch SM, Li XJ. Interaction of huntingtin-associated protein with dynactin P150Glued. J Neurosci Off J Soc Neurosci. 1998 Feb 15;18(4):1261–9.

275. Baquet ZC, Gorski JA, Jones KR. Early striatal dendrite deficits followed by neuron loss with advanced age in the absence of anterograde cortical brain-derived neurotrophic factor. J Neurosci Off J Soc Neurosci. 2004 Apr 28;24(17):4250–8.

276. Canals JM, Pineda JR, Torres-Peraza JF, Bosch M, Martin-Ibanez R, Munoz MT, et al. Brain-derived neurotrophic factor regulates the onset and severity of motor dysfunction associated with enkephalinergic neuronal degeneration in Huntington's disease. J Neurosci Off J Soc Neurosci. 2004 Sep 1;24(35):7727–39.

277. Pineda JR, Canals JM, Bosch M, Adell A, Mengod G, Artigas F, et al. Brain-derived neurotrophic factor modulates dopaminergic deficits in a transgenic mouse model of Huntington's disease. J Neurochem. 2005 Jun;93(5):1057–68.

278. Gines S, Bosch M, Marco S, Gavalda N, Diaz-Hernandez M, Lucas JJ, et al. Reduced expression of the TrkB receptor in Huntington's disease mouse models and in human brain. Eur J Neurosci. 2006 Feb;23(3):649–58.

279. Gines S, Paoletti P, Alberch J. Impaired TrkB-mediated ERK1/2 activation in huntington disease knock-in striatal cells involves reduced p52/p46 Shc expression. J Biol Chem. 2010 Jul 9;285(28):21537–48.

280. Brito V, Puigdellivol M, Giralt A, del Toro D, Alberch J, Gines S. Imbalance of p75(NTR)/TrkB protein expression in Huntington's disease: implication for neuroprotective therapies. Cell Death Dis. 2013 Apr 18;4:e595.

281. Plotkin JL, Day M, Peterson JD, Xie Z, Kress GJ, Rafalovich I, et al. Impaired TrkB receptor signaling underlies corticostriatal dysfunction in Huntington's disease. Neuron. 2014 Jul 2;83(1):178–88.

282. Plotkin JL, Surmeier DJ. Impaired striatal function in Huntington's disease is due to aberrant p75NTR signaling. Rare Dis Austin Tex. 2014;2(1):e968482.

283. Reick C, Ellrichmann G, Tsai T, Lee D-H, Wiese S, Gold R, et al. Expression of brain-derived neurotrophic factor in astrocytes - Beneficial effects of glatiramer acetate in the R6/2 and YAC128 mouse models of Huntington's disease. Exp Neurol. 2016 Aug 29;285(Pt A):12–23.

284. Pan Y, Daito T, Sasaki Y, Chung YH, Xing X, Pondugula S, et al. Inhibition of DNA Methyltransferases Blocks Mutant Huntingtin-Induced Neurotoxicity. Sci Rep. 2016;6:31022.

285. Geva M, Kusko R, Soares H, Fowler KD, Birnberg T, Barash S, et al. Pridopidine activates neuroprotective pathways impaired in Huntington Disease. Hum Mol Genet. 2016 Jul 27;

286. Zimmermann T, Remmers F, Lutz B, Leschik J. ESC-Derived BDNF-Overexpressing Neural Progenitors Differentially Promote Recovery in Huntington's Disease Models by Enhanced Striatal Differentiation. Stem Cell Rep. 2016 Sep 21;

287. Simmons DA, Belichenko NP, Ford EC, Semaan S, Monbureau M, Aiyaswamy S, et al. A small molecule p75NTR ligand normalizes signaling and reduces Huntington's Disease phenotypes in R6/2 and BACHD mice. Hum Mol Genet. 2016 Sep 16;

288. Paoletti P, Bellone C, Zhou Q. NMDA receptor subunit diversity: impact on receptor properties, synaptic plasticity and disease. Nat Rev Neurosci. 2013 Jun;14(6):383–400.

289. Sattler R, Xiong Z, Lu WY, MacDonald JF, Tymianski M. Distinct roles of synaptic and extrasynaptic NMDA receptors in excitotoxicity. J Neurosci Off J Soc Neurosci. 2000 Jan 1;20(1):22–33.

290. Steigerwald F, Schulz TW, Schenker LT, Kennedy MB, Seeburg PH, Kohr G. C-Terminal truncation of NR2A subunits impairs synaptic but not extrasynaptic localization of NMDA receptors. J Neurosci Off J Soc Neurosci. 2000 Jun 15;20(12):4573–81.

291. Groc L, Heine M, Cousins SL, Stephenson FA, Lounis B, Cognet L, et al. NMDA receptor surface mobility depends on NR2A-2B subunits. Proc Natl Acad Sci U S A. 2006 Dec 5;103(49):18769–74.

292. Martel M-A, Wyllie DJA, Hardingham GE. In developing hippocampal neurons, NR2B-containing N-methyl-D-aspartate receptors (NMDARs) can mediate signaling to neuronal survival and synaptic potentiation, as well as neuronal death. Neuroscience. 2009 Jan 12;158(1):334–43.

293. Hardingham GE, Arnold FJ, Bading H. Nuclear calcium signaling controls CREB-mediated gene expression triggered by synaptic activity. Nat Neurosci. 2001 Mar;4(3):261–7.

294. Hardingham GE, Bading H. Coupling of extrasynaptic NMDA receptors to a CREB shut-off pathway is developmentally regulated. Biochim Biophys Acta. 2002 Nov 4;1600(1–2):148–53.

295. Papadia S, Soriano FX, Leveille F, Martel M-A, Dakin KA, Hansen HH, et al. Synaptic NMDA receptor activity boosts intrinsic antioxidant defenses. Nat Neurosci. 2008 Apr;11(4):476–87.

296. Xu J, Kurup P, Zhang Y, Goebel-Goody SM, Wu PH, Hawasli AH, et al. Extrasynaptic NMDA receptors couple preferentially to excitotoxicity via calpain-mediated cleavage of STEP. J Neurosci Off J Soc Neurosci. 2009 Jul 22;29(29):9330–43.

297. Parsons MP, Raymond LA. Extrasynaptic NMDA receptor involvement in central nervous system disorders. Neuron. 2014 Apr 16;82(2):279–93.

298. Milnerwood A, Gladding C, Pouladi M, Kaufman A, Hines R, Boyd J, et al. Early increase in extrasynaptic NMDA receptor signaling and expression contributes to phenotype onset in Huntington's disease mice. Neuron. 2010 Jan 28;65(2):178–90.

299. Milnerwood AJ, Kaufman AM, Sepers MD, Gladding CM, Zhang L, Wang L, et al. Mitigation of augmented extrasynaptic NMDAR signaling and apoptosis in cortico-striatal co-cultures from Huntington's disease mice. Neurobiol Dis. 2012 Oct;48(1):40–51.

300. Fan J, Gladding CM, Wang L, Zhang LYJ, Kaufman AM, Milnerwood AJ, et al. P38 MAPK is involved in enhanced NMDA receptor-dependent excitotoxicity in YAC transgenic mouse model of Huntington disease. Neurobiol Dis. 2012 Mar;45(3):999–1009.

301. Gladding CM, Sepers MD, Xu J, Zhang LYJ, Milnerwood AJ, Lombroso PJ, et al. Calpain and STriatal-Enriched protein tyrosine phosphatase (STEP) activation contribute to extrasynaptic NMDA receptor localization in a Huntington's disease mouse model. Hum Mol Genet. 2012 Sep 1;21(17):3739–52.

302. Gladding CM, Fan J, Zhang LYJ, Wang L, Xu J, Li EHY, et al. Alterations in STriatal-Enriched protein tyrosine Phosphatase expression, activation, and downstream signaling in early

and late stages of the YAC128 Huntington's disease mouse model. J Neurochem. 2014 Jul;130(1):145–59.

303. Fan J, Cowan CM, Zhang LYJ, Hayden MR, Raymond LA. Interaction of postsynaptic density protein-95 with NMDA receptors influences excitotoxicity in the yeast artificial chromosome mouse model of Huntington's disease. J Neurosci Off J Soc Neurosci. 2009 Sep 2;29(35):10928–38.

304. Dau A, Gladding CM, Sepers MD, Raymond LA. Chronic blockade of extrasynaptic NMDA receptors ameliorates synaptic dysfunction and pro-death signaling in Huntington disease transgenic mice. Neurobiol Dis. 2014 Feb;62:533–42.

305. Saavedra A, Puigdellivol M, Tyebji S, Kurup P, Xu J, Gines S, et al. BDNF Induces Striatal-Enriched Protein Tyrosine Phosphatase 61 Degradation Through the Proteasome. Mol Neurobiol. 2016 Aug;53(6):4261–73.

306. Xu J, Kurup P, Azkona G, Baguley TD, Saavedra A, Nairn AC, et al. Down-regulation of BDNF in cell and animal models increases striatal-enriched protein tyrosine phosphatase 61 (STEP61) levels. J Neurochem. 2016 Jan;136(2):285–94.

307. Marco S, Giralt A, Petrovic MM, Pouladi MA, Martinez-Turrillas R, Martinez-Hernandez J, et al. Suppressing aberrant GluN3A expression rescues synaptic and behavioral impairments in Huntington's disease models. Nat Med. 2013 Aug;19(8):1030–8.

308. Modregger J, DiProspero NA, Charles V, Tagle DA, Plomann M. PACSIN 1 interacts with huntingtin and is absent from synaptic varicosities in presymptomatic Huntington's disease brains. Hum Mol Genet. 2002 Oct 1;11(21):2547–58.

309. Sun Y, Savanenin A, Reddy PH, Liu YF. Polyglutamine-expanded huntingtin promotes sensitization of N-methyl-D-aspartate receptors via post-synaptic density 95. J Biol Chem. 2001 Jul 6;276(27):24713–8.

310. Ho GPH, Selvakumar B, Mukai J, Hester LD, Wang Y, Gogos JA, et al. S-nitrosylation and S-palmitoylation reciprocally regulate synaptic targeting of. Neuron. 2011 Jul 14;71(1):131–41.

311. Mandal M, Wei J, Zhong P, Cheng J, Duffney LJ, Liu W, et al. Impaired alpha-amino-3-hydroxy-5-methyl-4-isoxazolepropionic acid (AMPA) receptor trafficking and function by mutant huntingtin. J Biol Chem. 2011 Sep 30;286(39):33719–28.

312. Joshi P, Wu N, Andre V, Cummings D, Cepeda C, Joyce J, et al. Age-dependent alterations of corticostriatal activity in the YAC128 mouse model of Huntington disease. J Neurosci. 2009 Feb 25;29(8):2414–27.

313. Arzberger T, Krampfl K, Leimgruber S, Weindl A. Changes of NMDA receptor subunit (NR1, NR2B) and glutamate transporter (GLT1) mRNA expression in Huntington's disease--an in situ hybridization study. J Neuropathol Exp Neurol. 1997 Apr;56(4):440–54.

314. Lievens JC, Woodman B, Mahal A, Spasic-Boscovic O, Samuel D, Kerkerian-Le Goff L, et al. Impaired glutamate uptake in the R6 Huntington's disease transgenic mice. Neurobiol Dis. 2001 Oct;8(5):807–21.

315. Behrens PF, Franz P, Woodman B, Lindenberg KS, Landwehrmeyer GB. Impaired glutamate transport and glutamate-glutamine cycling: downstream effects of the Huntington mutation. Brain J Neurol. 2002 Aug;125(Pt 8):1908–22.

316. Shin J-Y, Fang Z-H, Yu Z-X, Wang C-E, Li S-H, Li X-J. Expression of mutant huntingtin in glial cells contributes to neuronal excitotoxicity. J Cell Biol. 2005 Dec 19;171(6):1001–12.

317. Rebec GV. Dysregulation of corticostriatal ascorbate release and glutamate uptake in transgenic models of Huntington's disease. Antioxid Redox Signal. 2013 Dec 10;19(17):2115–28.

318. Hassel B, Tessler S, Faull RLM, Emson PC. Glutamate uptake is reduced in prefrontal cortex in Huntington's disease. Neurochem Res. 2008 Feb;33(2):232–7.

319. Faideau M, Kim J, Cormier K, Gilmore R, Welch M, Auregan G, et al. In vivo expression of polyglutamine-expanded huntingtin by mouse striatal astrocytes impairs glutamate transport: a correlation with Huntington's disease subjects. Hum Mol Genet. 2010 Aug 1;19(15):3053–67.

320. Li X, Valencia A, Sapp E, Masso N, Alexander J, Reeves P, et al. Aberrant Rab11-dependent trafficking of the neuronal glutamate transporter EAAC1 causes oxidative stress and cell death in Huntington's disease. J Neurosci Off J Soc Neurosci. 2010 Mar 31;30(13):4552–61.

321. Petr GT, Bakradze E, Frederick NM, Wang J, Armsen W, Aizenman E, et al. Glutamate transporter expression and function in a striatal neuronal model of Huntington's disease. Neurochem Int. 2013 Jun;62(7):973–81.

322. Cepeda C, Hurst RS, Calvert CR, Hernandez-Echeagaray E, Nguyen OK, Jocoy E, et al. Transient and progressive electrophysiological alterations in the corticostriatal pathway in a mouse model of Huntington's disease. J Neurosci Off J Soc Neurosci. 2003 Feb 1;23(3):961–9.

323. Estrada-Sanchez AM, Rebec GV. Corticostriatal dysfunction and glutamate transporter 1 (GLT1) in Huntington's disease: interactions between neurons and astrocytes. Basal Ganglia. 2012 Jul 1;2(2):57–66.

324. Rothstein JD, Patel S, Regan MR, Haenggeli C, Huang YH, Bergles DE, et al. Beta-lactam antibiotics offer neuroprotection by increasing glutamate transporter expression. Nature. 2005 Jan 6;433(7021):73–7.

325. Miller BR, Dorner JL, Shou M, Sari Y, Barton SJ, Sengelaub DR, et al. Up-regulation of GLT1 expression increases glutamate uptake and attenuates the Huntington's disease phenotype in the R6/2 mouse. Neuroscience. 2008 Apr 22;153(1):329–37.

326. Petr GT, Schultheis LA, Hussey KC, Sun Y, Dubinsky JM, Aoki C, et al. Decreased expression of GLT-1 in the R6/2 model of Huntington's disease does not worsen disease progression. Eur J Neurosci. 2013 Aug;38(3):2477–90.

327. Parsons MP, Vanni MP, Woodard CL, Kang R, Murphy TH, Raymond LA. Real-time imaging of glutamate clearance reveals normal striatal uptake in Huntington disease mouse models. Nat Commun. 2016;7:11251.

328. Kiechle T, Dedeoglu A, Kubilus J, Kowall NW, Beal MF, Friedlander RM, et al. Cytochrome C and caspase-9 expression in Huntington's disease. Neuromolecular Med. 2002;1(3):183–95.

329. Rigamonti D, Bauer JH, De-Fraja C, Conti L, Sipione S, Sciorati C, et al. Wild-type huntingtin protects from apoptosis upstream of caspase-3. J Neurosci Off J Soc Neurosci. 2000 May 15;20(10):3705–13.

330. Zhang Y, Leavitt BR, van Raamsdonk JM, Dragatsis I, Goldowitz D, MacDonald ME, et al. Huntingtin inhibits caspase-3 activation. EMBO J. 2006 Dec 13;25(24):5896–906.

331. Zhang Y, Ona VO, Li M, Drozda M, Dubois-Dauphin M, Przedborski S, et al. Sequential activation of individual caspases, and of alterations in Bcl-2 proapoptotic signals in a mouse model of Huntington's disease. J Neurochem. 2003 Dec;87(5):1184–92.

332. Wang X, Wang H, Figueroa BE, Zhang W-H, Huo C, Guan Y, et al. Dysregulation of receptor interacting protein-2 and caspase recruitment domain only protein mediates aberrant

caspase-1 activation in Huntington's disease. J Neurosci Off J Soc Neurosci. 2005 Dec 14;25(50):11645–54.

333. Skotte NH, Sanders SS, Singaraja RR, Ehrnhoefer DE, Vaid K, Qiu X, et al. Palmitoylation of caspase-6 by HIP14 regulates its activation. Cell Death Differ. 2017 Mar;24(3):433–44.

334. Warby SC, Doty CN, Graham RK, Carroll JB, Yang Y-Z, Singaraja RR, et al. Activated caspase-6 and caspase-6-cleaved fragments of huntingtin specifically colocalize in the nucleus. Hum Mol Genet. 2008 Aug 1;17(15):2390–404.

335. Wellington CL, Ellerby LM, Gutekunst C-A, Rogers D, Warby S, Graham RK, et al. Caspase cleavage of mutant huntingtin precedes neurodegeneration in Huntington's disease. J Neurosci Off J Soc Neurosci. 2002 Sep 15;22(18):7862–72.

336. Tebbenkamp ATN, Green C, Xu G, Denovan-Wright EM, Rising AC, Fromholt SE, et al. Transgenic mice expressing caspase-6-derived N-terminal fragments of mutant huntingtin develop neurologic abnormalities with predominant cytoplasmic inclusion pathology composed largely of a smaller proteolytic derivative. Hum Mol Genet. 2011 Jul 15;20(14):2770–82.

337. Wellington CL, Singaraja R, Ellerby L, Savill J, Roy S, Leavitt B, et al. Inhibiting caspase cleavage of huntingtin reduces toxicity and aggregate formation in neuronal and nonneuronal cells. J Biol Chem. 2000 Jun 30;275(26):19831–8.

338. Graham RK, Deng Y, Slow EJ, Haigh B, Bissada N, Lu G, et al. Cleavage at the caspase-6 site is required for neuronal dysfunction and degeneration due to mutant huntingtin. Cell. 2006 Jun 16;125(6):1179–91.

339. Pouladi MA, Graham RK, Karasinska JM, Xie Y, Santos RD, Petersen A, et al. Prevention of depressive behaviour in the YAC128 mouse model of Huntington disease by mutation at residue 586 of huntingtin. Brain J Neurol. 2009 Apr;132(Pt 4):919–32.

340. Wong BKY, Ehrnhoefer DE, Graham RK, Martin DDO, Ladha S, Uribe V, et al. Partial rescue of some features of Huntington Disease in the genetic absence of caspase-6 in YAC128 mice. Neurobiol Dis. 2015 Apr;76:24–36.

341. Uribe V, Wong BKY, Graham RK, Cusack CL, Skotte NH, Pouladi MA, et al. Rescue from excitotoxicity and axonal degeneration accompanied by age-dependent behavioral and neuroanatomical alterations in caspase-6-deficient mice. Hum Mol Genet. 2012 May 1;21(9):1954–67.

342. Panov AV, Gutekunst C-A, Leavitt BR, Hayden MR, Burke JR, Strittmatter WJ, et al. Early mitochondrial calcium defects in Huntington's disease are a direct effect of polyglutamines. Nat Neurosci. 2002 Aug;5(8):731–6.

343. Panov AV, Burke JR, Strittmatter WJ, Greenamyre JT. In vitro effects of polyglutamine tracts on Ca2+-dependent depolarization of rat and human mitochondria: relevance to Huntington's disease. Arch Biochem Biophys. 2003 Feb 1;410(1):1–6.

344. Milakovic T, Quintanilla RA, Johnson GVW. Mutant huntingtin expression induces mitochondrial calcium handling defects in clonal striatal cells: functional consequences. J Biol Chem. 2006 Nov 17;281(46):34785–95.

345. Chang DTW, Rintoul GL, Pandipati S, Reynolds IJ. Mutant huntingtin aggregates impair mitochondrial movement and trafficking in cortical neurons. Neurobiol Dis. 2006 May;22(2):388–400.

346. Gu M, Gash MT, Mann VM, Javoy-Agid F, Cooper JM, Schapira AH. Mitochondrial defect in Huntington's disease caudate nucleus. Ann Neurol. 1996 Mar;39(3):385–9.

347. Benchoua A, Trioulier Y, Zala D, Gaillard M-C, Lefort N, Dufour N, et al. Involvement of mitochondrial complex II defects in neuronal death produced by. Mol Biol Cell. 2006 Apr;17(4):1652–63.

348. Quintanilla RA, Tapia C, Perez MJ. Possible role of mitochondrial permeability transition pore in the pathogenesis of Huntington disease. Biochem Biophys Res Commun. 2016 Sep 13;

349. Naia L, Rosenstock TR, Oliveira AM, Oliveira-Sousa SI, Caldeira GL, Carmo C, et al. Comparative Mitochondrial-Based Protective Effects of Resveratrol and Nicotinamide in Huntington's Disease Models. Mol Neurobiol. 2016 Sep 2;

350. Guo X, Sun X, Hu D, Wang Y-J, Fujioka H, Vyas R, et al. VCP recruitment to mitochondria causes mitophagy impairment and neurodegeneration in models of Huntington's disease. Nat Commun. 2016;7:12646.

351. Lastres-Becker I, Fezza F, Cebeira M, Bisogno T, Ramos JA, Milone A, et al. Changes in endocannabinoid transmission in the basal ganglia in a rat model of Huntington's disease. Neuroreport. 2001 Jul 20;12(10):2125–9.

352. Lastres-Becker I, Berrendero F, Lucas JJ, Martin-Aparicio E, Yamamoto A, Ramos JA, et al. Loss of mRNA levels, binding and activation of GTP-binding proteins for cannabinoid CB1 receptors in the basal ganglia of a transgenic model of Huntington's disease. Brain Res. 2002 Mar 8;929(2):236–42.

353. McCaw EA, Hu H, Gomez GT, Hebb ALO, Kelly MEM, Denovan-Wright EM. Structure, expression and regulation of the cannabinoid receptor gene (CB1) in Huntington's disease transgenic mice. Eur J Biochem. 2004 Dec;271(23–24):4909–20.

354. Dowie MJ, Bradshaw HB, Howard ML, Nicholson LFB, Faull RLM, Hannan AJ, et al. Altered CB1 receptor and endocannabinoid levels precede motor symptom onset in a transgenic mouse model of Huntington's disease. Neuroscience. 2009 Sep 29;163(1):456–65.

355. Van Laere K, Casteels C, Dhollander I, Goffin K, Grachev I, Bormans G, et al. Widespread decrease of type 1 cannabinoid receptor availability in Huntington disease in vivo. J Nucl Med Off Publ Soc Nucl Med. 2010 Sep;51(9):1413–7.

356. Pazos MR, Sagredo O, Fernandez-Ruiz J. The endocannabinoid system in Huntington's disease. Curr Pharm Des. 2008;14(23):2317–25.

357. Blazquez C, Chiarlone A, Bellocchio L, Resel E, Pruunsild P, Garcia-Rincon D, et al. The CB(1) cannabinoid receptor signals striatal neuroprotection via a PI3K/Akt/mTORC1/BDNF pathway. Cell Death Differ. 2015 Oct;22(10):1618–29.

358. Scotter EL, Goodfellow CE, Graham ES, Dragunow M, Glass M. Neuroprotective potential of CB1 receptor agonists in an in vitro model of Huntington's disease. Br J Pharmacol. 2010 Jun;160(3):747–61.

359. Lastres-Becker I, Hansen HH, Berrendero F, De Miguel R, Perez-Rosado A, Manzanares J, et al. Alleviation of motor hyperactivity and neurochemical deficits by endocannabinoid uptake inhibition in a rat model of Huntington's disease. Synap N Y N. 2002 Apr;44(1):23–35.

360. Dowie MJ, Howard ML, Nicholson LFB, Faull RLM, Hannan AJ, Glass M. Behavioural and molecular consequences of chronic cannabinoid treatment in Huntington's disease transgenic mice. Neuroscience. 2010 Sep 29;170(1):324–36.

361. Mievis S, Blum D, Ledent C. Worsening of Huntington disease phenotype in CB1 receptor knockout mice. Neurobiol Dis. 2011 Jun;42(3):524–9.

362. Meunier C, Merienne N, Jolle C, Deglon N, Pellerin L. Astrocytes are key but indirect contributors to the development of the symptomatology and pathophysiology of Huntington's disease. Glia. 2016 Nov;64(11):1841–56.

363. Benraiss A, Wang S, Herrlinger S, Li X, Chandler-Militello D, Mauceri J, et al. Human glia can both induce and rescue aspects of disease phenotype in Huntington disease. Nat Commun. 2016;7:11758.

364. Selkoe DJ, Salazar FJ, Abraham C, Kosik KS. Huntington's disease: changes in striatal proteins reflect astrocytic gliosis. Brain Res. 1982 Aug 5;245(1):117–25.

365. Stevens CD, Altshuler LL, Bogerts B, Falkai P. Quantitative study of gliosis in schizophrenia and Huntington's chorea. Biol Psychiatry. 1988 Oct;24(6):697–700.

366. Takemoto T, Ishihara Y, Ishida A, Yamazaki T. Neuroprotection elicited by nerve growth factor and brain-derived neurotrophic factor released from astrocytes in response to methylmercury. Environ Toxicol Pharmacol. 2015 Jul;40(1):199–205.

367. Degos V, Charpentier TL, Chhor V, Brissaud O, Lebon S, Schwendimann L, et al. Neuroprotective effects of dexmedetomidine against glutamate agonist-induced neuronal cell death are related to increased astrocyte brain-derived neurotrophic factor expression. Anesthesiology. 2013 May;118(5):1123–32.

368. Miyamoto N, Maki T, Shindo A, Liang AC, Maeda M, Egawa N, et al. Astrocytes Promote Oligodendrogenesis after White Matter Damage via Brain-Derived Neurotrophic Factor. J Neurosci Off J Soc Neurosci. 2015 Oct 14;35(41):14002–8.

369. Wang L, Lin F, Wang J, Wu J, Han R, Zhu L, et al. Truncated N-terminal huntingtin fragment with expanded-polyglutamine (htt552-100Q) suppresses brain-derived neurotrophic factor transcription in astrocytes. Acta Biochim Biophys Sin. 2012 Mar;44(3):249–58.

370. Wang L, Lin F, Wang J, Wu J, Han R, Zhu L, et al. Expression of mutant N-terminal huntingtin fragment (htt552-100Q) in astrocytes suppresses the secretion of BDNF. Brain Res. 2012 Apr 17;1449:69–82.

371. Hong Y, Zhao T, Li X-J, Li S. Mutant Huntingtin Impairs BDNF Release from Astrocytes by Disrupting Conversion of Rab3a-GTP into Rab3a-GDP. J Neurosci Off J Soc Neurosci. 2016 Aug 24;36(34):8790–801.

372. Simmons DA, Casale M, Alcon B, Pham N, Narayan N, Lynch G. Ferritin accumulation in dystrophic microglia is an early event in the development of Huntington's disease. Glia. 2007 Aug 1;55(10):1074–84.

373. Ma L, Morton AJ, Nicholson LFB. Microglia density decreases with age in a mouse model of Huntington's disease. Glia. 2003 Sep;43(3):274–80.

374. Politis M, Su P, Piccini P. Imaging of microglia in patients with neurodegenerative disorders. Front Pharmacol. 2012;3:96.

375. Politis M, Lahiri N, Niccolini F, Su P, Wu K, Giannetti P, et al. Increased central microglial activation associated with peripheral cytokine levels in premanifest Huntington's disease gene carriers. Neurobiol Dis. 2015 Nov;83:115–21.

376. Kaushik DK, Basu A. A friend in need may not be a friend indeed: role of microglia in neurodegenerative diseases. CNS Neurol Disord Drug Targets. 2013 Sep;12(6):726–40.

377. Moresco RM, Lavazza T, Belloli S, Lecchi M, Pezzola A, Todde S, et al. Quinolinic acid induced neurodegeneration in the striatum: a combined in vivo and in vitro analysis of receptor changes and microglia activation. Eur J Nucl Med Mol Imaging. 2008 Apr;35(4):704–15.

378. Chakraborty J, Rajamma U, Jana N, Mohanakumar KP. Quercetin improves the activity of the ubiquitin-proteasomal system in 150Q mutated huntingtin-expressing cells but exerts detrimental effects on neuronal survivability. J Neurosci Res. 2015 Oct;93(10):1581–91.

379. Yamada T, Akiyama H, McGeer PL. Complement-activated oligodendroglia: a new pathogenic entity identified by immunostaining with antibodies to human complement proteins C3d and C4d. Neurosci Lett. 1990 May 4;112(2–3):161–6.

380. Teo RTY, Hong X, Yu-Taeger L, Huang Y, Tan LJ, Xie Y, et al. Structural and molecular myelination deficits occur prior to neuronal loss in the YAC128 and BACHD models of Huntington disease. Hum Mol Genet. 2016 Apr 28;

381. Lawrence AD, Hodges JR, Rosser AE, Kershaw A, ffrench-Constant C, Rubinsztein DC, et al. Evidence for specific cognitive deficits in preclinical Huntington's disease. Brain J Neurol. 1998 Jul;121 (Pt 7):1329–41.

382. Watkins LH, Rogers RD, Lawrence AD, Sahakian BJ, Rosser AE, Robbins TW. Impaired planning but intact decision making in early Huntington's disease: implications for specific fronto-striatal pathology. Neuropsychologia. 2000;38(8):1112–25.

383. Julien CL, Thompson JC, Wild S, Yardumian P, Snowden JS, Turner G, et al. Psychiatric disorders in preclinical Huntington's disease. J Neurol Neurosurg Psychiatry. 2007 Sep;78(9):939–43.

384. Birrell JM, Brown VJ. Medial frontal cortex mediates perceptual attentional set shifting in the rat. J Neurosci Off J Soc Neurosci. 2000 Jun 1;20(11):4320–4.

385. Bissonette GB, Martins GJ, Franz TM, Harper ES, Schoenbaum G, Powell EM. Double dissociation of the effects of medial and orbital prefrontal cortical lesions on attentional and affective shifts in mice. J Neurosci Off J Soc Neurosci. 2008 Oct 29;28(44):11124–30.

386. Thompson-Schill SL, Swick D, Farah MJ, D'Esposito M, Kan IP, Knight RT. Verb generation in patients with focal frontal lesions: a neuropsychological test of neuroimaging findings. Proc Natl Acad Sci U S A. 1998 Dec 22;95(26):15855–60.

387. Jurado MA, Mataro M, Verger K, Bartumeus F, Junque C. Phonemic and semantic fluencies in traumatic brain injury patients with focal frontal lesions. Brain Inj. 2000 Sep;14(9):789–95.

388. Lawrence AD, Sahakian BJ, Hodges JR, Rosser AE, Lange KW, Robbins TW. Executive and mnemonic functions in early Huntington's disease. Brain J Neurol. 1996 Oct;119 (Pt 5):1633–45.

389. Lawrence AD, Weeks RA, Brooks DJ, Andrews TC, Watkins LH, Harding AE, et al. The relationship between striatal dopamine receptor binding and cognitive performance in Huntington's disease. Brain J Neurol. 1998 Jul;121 (Pt 7):1343–55.

390. Lawrence AD, Sahakian BJ, Robbins TW. Cognitive functions and corticostriatal circuits: insights from Huntington's disease. Trends Cogn Sci. 1998 Oct 1;2(10):379–88.

391. Stout JC, Paulsen JS, Queller S, Solomon AC, Whitlock KB, Campbell JC, et al. Neurocognitive signs in prodromal Huntington disease. Neuropsychology. 2011 Jan;25(1):1–14.

392. Duff K, Paulsen J, Mills J, Beglinger LJ, Moser DJ, Smith MM, et al. Mild cognitive impairment in prediagnosed Huntington disease. Neurology. 2010 Aug 10;75(6):500–7.

393. Smith MM, Mills JA, Epping EA, Westervelt HJ, Paulsen JS. Depressive symptom severity is related to poorer cognitive performance in prodromal Huntington disease. Neuropsychology. 2012 Sep;26(5):664–9.

394. Kirkwood SC, Siemers E, Stout JC, Hodes ME, Conneally PM, Christian JC, et al. Longitudinal cognitive and motor changes among presymptomatic Huntington disease gene carriers. Arch Neurol. 1999 May;56(5):563–8.

395. Kirkwood SC, Siemers E, Bond C, Conneally PM, Christian JC, Foroud T. Confirmation of subtle motor changes among presymptomatic carriers of the Huntington disease gene. Arch Neurol. 2000 Jul;57(7):1040–4.

396. Zhang J, Peng Q, Li Q, Jahanshad N, Hou Z, Jiang M, et al. Longitudinal characterization of brain atrophy of a Huntington's disease mouse model by automated morphological analyses of magnetic resonance images. NeuroImage. 2010 Feb 1;49(3):2340–51.

397. Cheng Y, Peng Q, Hou Z, Aggarwal M, Zhang J, Mori S, et al. Structural MRI detects progressive regional brain atrophy and neuroprotective effects in N171-82Q Huntington's disease mouse model. NeuroImage. 2011 Jun 1;56(3):1027–34.

398. Klapstein GJ, Fisher RS, Zanjani H, Cepeda C, Jokel ES, Chesselet MF, et al. Electrophysiological and morphological changes in striatal spiny neurons in R6/2 Huntington's disease transgenic mice. J Neurophysiol. 2001 Dec;86(6):2667–77.

399. Cummings DM, Cepeda C, Levine MS. Alterations in striatal synaptic transmission are consistent across genetic mouse models of Huntington's disease. ASN Neuro. 2010;2(3):e00036.

400. Heikkinen T, Lehtimaki K, Vartiainen N, Puolivali J, Hendricks SJ, Glaser JR, et al. Characterization of neurophysiological and behavioral changes, MRI brain volumetry and 1H MRS in zQ175 knock-in mouse model of Huntington's disease. PloS One. 2012;7(12):e50717.

401. Grant SGN, Bagni C, O'Dell TJ. Synaptopathy--From Biology to Therapy. Neuropharmacology. 2016 Jan;100:1.

402. Leavitt BR, van Raamsdonk JM, Shehadeh J, Fernandes H, Murphy Z, Graham RK, et al. Wild-type huntingtin protects neurons from excitotoxicity. J Neurochem. 2006 Feb;96(4):1121–9.

403. Harrison R. The outgrowth of the nerve fiber as a mode of protoplasmic movement. J Exp Zool. 1959 Dec;142:5–73.

404. Fischbach G. Synaptic potentials recorded in cell cultures of nerve and muscle. Science. 1970 Sep 25;169(3952):1331–3.

405. Millet L, Gillette M. Over a century of neuron culture: from the hanging drop to microfluidic devices. Yale J Biol Med. 2012 Dec;85(4):501–21.

406. Segal M, Greenberger V, Korkotian E. Formation of dendritic spines in cultured striatal neurons depends on excitatory afferent activity. Eur J Neurosci. 2003 Jun;17(12):2573–85.

407. Snyder-Keller A. Pattern of corticostriatal innervation in organotypic cocultures is dependent on the age of the cortical tissue.

408. Melcangi RC, Magnaghi V, Cavarretta I, Riva MA, Martini L. Corticosteroid effects on gene expression of myelin basic protein in oligodendrocytes and of glial fibrillary acidic protein in type 1 astrocytes. J Neuroendocrinol. 1997 Oct;9(10):729–33.

409. Li Y-N, Pan R, Qin X-J, Yang W-L, Qi Z, Liu W, et al. Ischemic neurons activate astrocytes to disrupt endothelial barrier via increasing VEGF expression. J Neurochem. 2014 Apr;129(1):120–9.

410. Marchetti C, Marie H. Hippocampal synaptic plasticity in Alzheimer's disease: what have we learned so far from transgenic models? Rev Neurosci. 2011;22(4):373–402.

411. Tian X, Kai L, Hockberger PE, Wokosin DL, Surmeier DJ. MEF-2 regulates activity-dependent spine loss in striatopallidal medium spiny neurons. Mol Cell Neurosci. 2010 May;44(1):94–108.

412. Lalchandani RR, Vicini S. Inhibitory collaterals in genetically identified medium spiny neurons in mouse primary corticostriatal cultures. Physiol Rep. 2013 Nov;1(6):e00164.

413. Kolodziejczyk K, Raymond LA. Differential changes in thalamic and cortical excitatory synapses onto striatal spiny projection neurons in a Huntington disease mouse model. Neurobiol Dis. 2016 Feb;86:62–74.

414. Buren C, Wang L, Smith-Dijak A, Raymond LA. Region-specific pro-survival signaling and global neuronal protection by wild-type Huntingtin. J Huntingt Dis. 2014;3(4):365–76.

415. Wu J, Ryskamp DA, Liang X, Egorova P, Zakharova O, Hung G, et al. Enhanced Store-Operated Calcium Entry Leads to Striatal Synaptic Loss in a Huntington's Disease Mouse Model. J Neurosci Off J Soc Neurosci. 2016 Jan 6;36(1):125–41.

416. Mahon S, Vautrelle N, Pezard L, Slaght SJ, Deniau J-M, Chouvet G, et al. Distinct patterns of striatal medium spiny neuron activity during the natural sleep-wake cycle. J Neurosci Off J Soc Neurosci. 2006 Nov 29;26(48):12587–95.

417. Cazorla M, Shegda M, Ramesh B, Harrison NL, Kellendonk C. Striatal D2 receptors regulate dendritic morphology of medium spiny neurons via Kir2 channels. J Neurosci Off J Soc Neurosci. 2012 Feb 15;32(7):2398–409.

418. Lalchandani R, van der Goes M, Partridge J, Vicini S. Dopamine D2 receptors regulate collateral inhibition between striatal medium spiny neurons. J Neurosci. 2013 Aug 28;33(35):14075–86.

419. Kolodziejczyk K, Parsons MP, Southwell AL, Hayden MR, Raymond LA. Striatal synaptic dysfunction and hippocampal plasticity deficits in the Hu97/18 mouse model of Huntington disease. PloS One. 2014;9(4):e94562.

420. Halliday GM, McRitchie DA, Macdonald V, Double KL, Trent RJ, McCusker E. Regional specificity of brain atrophy in Huntington's disease. Exp Neurol. 1998 Dec;154(2):663–72.

421. Vonsattel JP, DiFiglia M. Huntington disease. J Neuropathol Exp Neurol. 1998 May;57(5):369–84.

422. Thu DCV, Oorschot DE, Tippett LJ, Nana AL, Hogg VM, Synek BJ, et al. Cell loss in the motor and cingulate cortex correlates with symptomatology in Huntington's disease. Brain J Neurol. 2010 Apr;133(Pt 4):1094–110.

423. Zuccato C, Valenza M, Cattaneo E. Molecular mechanisms and potential therapeutical targets in Huntington's disease. Physiol Rev. 2010 Jul;90(3):905–81.

424. Okamoto S, Pouladi MA, Talantova M, Yao D, Xia P, Ehrnhoefer DE, et al. Balance between synaptic versus extrasynaptic NMDA receptor activity influences inclusions and neurotoxicity of mutant huntingtin. Nat Med. 2009 Dec;15(12):1407–13.

425. Sepers MD, Raymond LA. Mechanisms of synaptic dysfunction and excitotoxicity in Huntington's disease. Drug Discov Today. 2014 Jul;19(7):990–6.

426. Silva AJ, Kogan JH, Frankland PW, Kida S. CREB and memory. Annu Rev Neurosci. 1998;21:127–48.

427. Lonze BE, Ginty DD. Function and regulation of CREB family transcription factors in the nervous system. Neuron. 2002 Aug 15;35(4):605–23.

428. Walton M, Woodgate AM, Muravlev A, Xu R, During MJ, Dragunow M. CREB phosphorylation promotes nerve cell survival. J Neurochem. 1999 Nov;73(5):1836–42.

429. Walton MR, Dragunow I. Is CREB a key to neuronal survival? Trends Neurosci. 2000 Feb;23(2):48–53.

430. Tao X, Finkbeiner S, Arnold DB, Shaywitz AJ, Greenberg ME. Ca2+ influx regulates BDNF transcription by a CREB family transcription factor-dependent mechanism. Neuron. 1998 Apr;20(4):709–26.

431. Zheng C-Y, Seabold GK, Horak M, Petralia RS. MAGUKs, synaptic development, and synaptic plasticity. Neurosci Rev J Bringing Neurobiol Neurol Psychiatry. 2011 Oct;17(5):493–512.

432. El-Husseini AE, Schnell E, Chetkovich DM, Nicoll RA, Bredt DS. PSD-95 involvement in maturation of excitatory synapses. Science. 2000 Nov 17;290(5495):1364–8.

433. Schnell E, Sizemore M, Karimzadegan S, Chen L, Bredt DS, Nicoll RA. Direct interactions between PSD-95 and stargazin control synaptic AMPA receptor number. Proc Natl Acad Sci U S A. 2002 Oct 15;99(21):13902–7.

434. Ehrlich I, Malinow R. Postsynaptic density 95 controls AMPA receptor incorporation during long-term potentiation and experience-driven synaptic plasticity. J Neurosci Off J Soc Neurosci. 2004 Jan 28;24(4):916–27.

435. Murer MG, Yan Q, Raisman-Vozari R. Brain-derived neurotrophic factor in the control human brain, and in Alzheimer's disease and Parkinson's disease. Prog Neurobiol. 2001 Jan;63(1):71–124.

436. Bruyn RP, Stoof JC. The quinolinic acid hypothesis in Huntington's chorea. J Neurol Sci. 1990 Jan;95(1):29–38.

437. Li L, Fan M, Icton CD, Chen N, Leavitt BR, Hayden MR, et al. Role of NR2B-type NMDA receptors in selective neurodegeneration in Huntington disease. Neurobiol Aging. 2003 Dec;24(8):1113–21.

438. Fan MMY, Raymond LA. N-methyl-D-aspartate (NMDA) receptor function and excitotoxicity in Huntington's disease. Prog Neurobiol. 2007 Apr;81(5–6):272–93.

439. Graham RK, Pouladi MA, Joshi P, Lu G, Deng Y, Wu N-P, et al. Differential susceptibility to excitotoxic stress in YAC128 mouse models of Huntington disease between initiation and progression of disease. J Neurosci Off J Soc Neurosci. 2009 Feb 18;29(7):2193–204.

440. Reddy PH, Shirendeb UP. Mutant huntingtin, abnormal mitochondrial dynamics, defective axonal transport of mitochondria, and selective synaptic degeneration in Huntington's disease. Biochim Biophys Acta. 2012 Feb;1822(2):101–10.

441. Tourette C, Li B, Bell R, O'Hare S, Kaltenbach LS, Mooney SD, et al. A large scale Huntingtin protein interaction network implicates Rho GTPase signaling pathways in Huntington disease. J Biol Chem. 2014 Mar 7;289(10):6709–26.

442. Hackam AS, Singaraja R, Wellington CL, Metzler M, McCutcheon K, Zhang T, et al. The influence of huntingtin protein size on nuclear localization and cellular toxicity. J Cell Biol. 1998 Jun 1;141(5):1097–105.

443. Ho LW, Brown R, Maxwell M, Wyttenbach A, Rubinsztein DC. Wild type Huntingtin reduces the cellular toxicity of mutant Huntingtin in mammalian cell models of Huntington's disease. J Med Genet. 2001 Jul;38(7):450–2.

444. Gervais FG, Singaraja R, Xanthoudakis S, Gutekunst C-A, Leavitt BR, Metzler M, et al. Recruitment and activation of caspase-8 by the Huntingtin-interacting protein Hip-1 and a novel partner Hippi. Nat Cell Biol. 2002 Feb;4(2):95–105.

445. Lau D, Bengtson CP, Buchthal B, Bading H. BDNF Reduces Toxic Extrasynaptic NMDA Receptor Signaling via Synaptic NMDA Receptors and Nuclear-Calcium-Induced Transcription of inhba/Activin A. Cell Rep. 2015 Aug 25;12(8):1353–66.

446. Liot G, Zala D, Pla P, Mottet G, Piel M, Saudou F. Mutant Huntingtin alters retrograde transport of TrkB receptors in striatal dendrites. J Neurosci Off J Soc Neurosci. 2013 Apr 10;33(15):6298–309.

447. Jiang M, Peng Q, Liu X, Jin J, Hou Z, Zhang J, et al. Small-molecule TrkB receptor agonists improve motor function and extend survival in a mouse model of Huntington's disease. Hum Mol Genet. 2013 Jun 15;22(12):2462–70.

448. Simmons DA, Belichenko NP, Yang T, Condon C, Monbureau M, Shamloo M, et al. A small molecule TrkB ligand reduces motor impairment and neuropathology in R6/2 and BACHD mouse models of Huntington's disease. J Neurosci Off J Soc Neurosci. 2013 Nov 27;33(48):18712–27.

449. Todd D, Gowers I, Dowler SJ, Wall MD, McAllister G, Fischer DF, et al. A monoclonal antibody TrkB receptor agonist as a potential therapeutic for Huntington's disease. PloS One. 2014;9(2):e87923.

450. Lee B, Butcher GQ, Hoyt KR, Impey S, Obrietan K. Activity-dependent neuroprotection and cAMP response element-binding protein (CREB): kinase coupling, stimulus intensity, and temporal regulation of CREB phosphorylation at serine 133. J Neurosci Off J Soc Neurosci. 2005 Feb 2;25(5):1137–48.

451. Lin C-H, Chen C-C, Chou C-M, Wang C-Y, Hung C-C, Chen JY, et al. Knockdown of the aryl hydrocarbon receptor attenuates excitotoxicity and enhances. J Neurochem. 2009 Nov;111(3):777–89.

452. Lai TW, Zhang S, Wang YT. Excitotoxicity and stroke: identifying novel targets for neuroprotection. Prog Neurobiol. 2014 Apr;115:157–88.

453. Mehta SL, Mendelev N, Kumari S, Andy Li P. Overexpression of human selenoprotein H in neuronal cells enhances mitochondrial biogenesis and function through activation of protein kinase A, protein kinase B, and cyclic adenosine monophosphate response element-binding protein pathway. Int J Biochem Cell Biol. 2013 Mar;45(3):604–11.

454. Khodagholi F, Ashabi G. Dietary supplementation with Salvia sahendica attenuates memory deficits, modulates CREB and its down-stream molecules and decreases apoptosis in amyloid beta-injected rats. Behav Brain Res. 2013 Mar 15;241:62–9.

455. Puddifoot C, Martel M-A, Soriano FX, Camacho A, Vidal-Puig A, Wyllie DJA, et al. PGC-1alpha negatively regulates extrasynaptic NMDAR activity and excitotoxicity. J Neurosci Off J Soc Neurosci. 2012 May 16;32(20):6995–7000.

456. Luo Y, Zhu W, Jia J, Zhang C, Xu Y. NMDA receptor dependent PGC-1alpha up-regulation protects the cortical neuron against oxygen-glucose deprivation/reperfusion injury. J Mol Neurosci MN. 2009 Sep;39(1–2):262–8.

457. Brose N, O'Connor V, Skehel P. Synaptopathy: dysfunction of synaptic function? Biochem Soc Trans. 2010 Apr;38(2):443–4.

458. Selkoe DJ. Alzheimer's disease is a synaptic failure. Science. 2002 Oct 25;298(5594):789–91.

459. Marttinen M, Kurkinen KM, Soininen H, Haapasalo A, Hiltunen M. Synaptic dysfunction and septin protein family members in neurodegenerative diseases. Mol Neurodegener. 2015;10:16.

460. Cattaneo E, Zuccato C, Tartari M. Normal huntingtin function: an alternative approach to Huntington's disease. Nat Rev Neurosci. 2005 Dec;6(12):919–30.

461. Smith R, Brundin P, Li J-Y. Synaptic dysfunction in Huntington's disease: a new perspective. Cell Mol Life Sci CMLS. 2005 Sep;62(17):1901–12.

462. Lerner RP, Trejo Martinez LDCG, Zhu C, Chesselet M-F, Hickey MA. Striatal atrophy and dendritic alterations in a knock-in mouse model of Huntington's disease. Brain Res Bull. 2012 Apr 10;87(6):571–8.

463. Rosenmund C, Stevens CF. Definition of the readily releasable pool of vesicles at hippocampal synapses. Neuron. 1996 Jun;16(6):1197–207.

464. Wierenga CJ, Ibata K, Turrigiano GG. Postsynaptic expression of homeostatic plasticity at neocortical synapses. J Neurosci Off J Soc Neurosci. 2005 Mar 16;25(11):2895–905.

465. Moulder KL, Mennerick S. Reluctant vesicles contribute to the total readily releasable pool in glutamatergic hippocampal neurons. J Neurosci Off J Soc Neurosci. 2005 Apr 13;25(15):3842–50.

466. Xu W, Tse YC, Dobie FA, Baudry M, Craig AM, Wong TP, et al. Simultaneous monitoring of presynaptic transmitter release and postsynaptic receptor trafficking reveals an enhancement of presynaptic activity in metabotropic glutamate receptor-mediated long-term depression. J Neurosci Off J Soc Neurosci. 2013 Mar 27;33(13):5867–77.

467. Pyott SJ, Rosenmund C. The effects of temperature on vesicular supply and release in autaptic cultures of rat and mouse hippocampal neurons. J Physiol. 2002 Mar 1;539(Pt 2):523–35.

468. Sheng J, Wu L-G. Cysteine string protein alpha: a new role in vesicle recycling. Neuron. 2012 Apr 12;74(1):6–8.

469. Ohyama T, Verstreken P, Ly CV, Rosenmund T, Rajan A, Tien A-C, et al. Huntingtin-interacting protein 14, a palmitoyl transferase required for exocytosis and targeting of CSP to synaptic vesicles. J Cell Biol. 2007 Dec 31;179(7):1481–96.

470. Marvin JS, Borghuis BG, Tian L, Cichon J, Harnett MT, Akerboom J, et al. An optimized fluorescent probe for visualizing glutamate neurotransmission. Nat Methods. 2013 Feb;10(2):162–70.

471. Ivkovic S, Ehrlich ME. Expression of the striatal DARPP-32/ARPP-21 phenotype in GABAergic neurons requires neurotrophins in vivo and in vitro. J Neurosci Off J Soc Neurosci. 1999 Jul 1;19(13):5409–19.

472. Milnerwood AJ, Raymond LA. Early synaptic pathophysiology in neurodegeneration: insights from Huntington's disease. Trends Neurosci. 2010 Nov;33(11):513–23.

473. Cepeda C, Ariano MA, Calvert CR, Flores-Hernandez J, Chandler SH, Leavitt BR, et al. NMDA receptor function in mouse models of Huntington disease. J Neurosci Res. 2001 Nov 15;66(4):525–39.

474. Cummings DM, Cepeda C, Levine MS. Alterations in striatal synaptic transmission are consistent across genetic mouse models of Huntington's disease. ASN Neuro. 2010;2(3):e00036.

475. Buren C, Parsons MP, Smith-Dijak A, Raymond LA. Impaired development of cortico-striatal synaptic connectivity in a cell culture model of Huntington's disease. Neurobiol Dis. 2016 Mar;87:80–90.

476. Gu X, Andre VM, Cepeda C, Li S-H, Li X-J, Levine MS, et al. Pathological cell-cell interactions are necessary for striatal pathogenesis in a conditional mouse model of Huntington's disease. Mol Neurodegener. 2007;2:8.

477. Wang N, Gray M, Lu X-H, Cantle JP, Holley SM, Greiner E, et al. Neuronal targets for reducing mutant huntingtin expression to ameliorate disease in a mouse model of Huntington's disease. Nat Med. 2014 May;20(5):536–41.

478. Wojcik SM, Rhee JS, Herzog E, Sigler A, Jahn R, Takamori S, et al. An essential role for vesicular glutamate transporter 1 (VGLUT1) in postnatal development and control of quantal size. Proc Natl Acad Sci U S A. 2004 May 4;101(18):7158–63.

479. Brustovetsky N. Mutant Huntingtin and Elusive Defects in Oxidative Metabolism and Mitochondrial Calcium Handling. Mol Neurobiol. 2016 Jul;53(5):2944–53.

480. Mejia EM, Chau S, Sparagna GC, Sipione S, Hatch GM. Reduced Mitochondrial Function in Human Huntington Disease Lymphoblasts is Not Due to Alterations in Cardiolipin Metabolism or Mitochondrial Supercomplex Assembly. Lipids. 2016 May;51(5):561–9.

481. Walker AG, Miller BR, Fritsch JN, Barton SJ, Rebec GV. Altered information processing in the prefrontal cortex of Huntington's disease mouse models. J Neurosci Off J Soc Neurosci. 2008 Sep 3;28(36):8973–82.

482. Heckmann M, Adelsberger H, Dudel J. Evoked transmitter release at neuromuscular junctions in wild type and cysteine string protein null mutant larvae of Drosophila. Neurosci Lett. 1997 Jun 13;228(3):167–70.

483. Umbach JA, Gundersen CB. Evidence that cysteine string proteins regulate an early step in the Ca2+-dependent secretion of neurotransmitter at Drosophila neuromuscular junctions. J Neurosci Off J Soc Neurosci. 1997 Oct 1;17(19):7203–9.

484. Ranjan R, Bronk P, Zinsmaier KE. Cysteine string protein is required for calcium secretion coupling of evoked neurotransmission in drosophila but not for vesicle recycling. J Neurosci Off J Soc Neurosci. 1998 Feb 1;18(3):956–64.

485. Swayne LA, Beck KE, Braun JEA. The cysteine string protein multimeric complex. Biochem Biophys Res Commun. 2006 Sep 15;348(1):83–91.

486. Chang S, Reim K, Pedersen M, Neher E, Brose N, Taschenberger H. Complexin stabilizes newly primed synaptic vesicles and prevents their premature fusion at the mouse calyx of held synapse. J Neurosci Off J Soc Neurosci. 2015 May 27;35(21):8272–90.

487. Trimbuch T, Rosenmund C. Should I stop or should I go? The role of complexin in neurotransmitter release. Nat Rev Neurosci. 2016 Feb;17(2):118–25.

488. Edwardson JM, Wang C-T, Gong B, Wyttenbach A, Bai J, Jackson MB, et al. Expression of mutant huntingtin blocks exocytosis in PC12 cells by depletion of complexin II. J Biol Chem. 2003 Aug 15;278(33):30849–53.

489. Swayne LA, Chen L, Hameed S, Barr W, Charlesworth E, Colicos MA, et al. Crosstalk between huntingtin and syntaxin 1A regulates N-type calcium channels. Mol Cell Neurosci. 2005 Nov;30(3):339–51.

490. Swayne LA, Braun JEA. Aggregate-centered redistribution of proteins by mutant huntingtin. Biochem Biophys Res Commun. 2007 Mar 2;354(1):39–44.

491. Fornasiero EF, Bonanomi D, Benfenati F, Valtorta F. The role of synapsins in neuronal development. Cell Mol Life Sci CMLS. 2010 May;67(9):1383–96.

492. Shupliakov O, Haucke V, Pechstein A. How synapsin I may cluster synaptic vesicles. Semin Cell Dev Biol. 2011 Jun;22(4):393–9.

493. Xu Q, Huang S, Song M, Wang C-E, Yan S, Liu X, et al. Synaptic mutant huntingtin inhibits synapsin-1 phosphorylation and causes neurological symptoms. J Cell Biol. 2013 Sep 30;202(7):1123–38.

494. Wu LL, Zhou X-F. Huntingtin associated protein 1 and its functions. Cell Adhes Migr. 2009 Mar;3(1):71–6.

495. Mackenzie KD, Duffield MD, Peiris H, Phillips L, Zanin MP, Teo EH, et al. Huntingtin-associated protein 1 regulates exocytosis, vesicle docking, readily releasable pool size and fusion pore stability in mouse chromaffin cells. J Physiol. 2014 Apr 1;592(7):1505–18.

496. Li SH, Hosseini SH, Gutekunst CA, Hersch SM, Ferrante RJ, Li XJ. A human HAP1 homologue. Cloning, expression, and interaction with huntingtin. J Biol Chem. 1998 Jul 24;273(30):19220–7.

497. Bertaux F, Sharp AH, Ross CA, Lehrach H, Bates GP, Wanker E. HAP1-huntingtin interactions do not contribute to the molecular pathology in Huntington's disease transgenic mice. FEBS Lett. 1998 Apr 17;426(2):229–32.

498. Guo X, Disatnik M-H, Monbureau M, Shamloo M, Mochly-Rosen D, Qi X. Inhibition of mitochondrial fragmentation diminishes Huntington's disease-associated neurodegeneration. J Clin Invest. 2013 Dec;123(12):5371–88.

499. Costa RM, Cohen D, Nicolelis MAL. Differential corticostriatal plasticity during fast and slow motor skill learning in mice. Curr Biol CB. 2004 Jul 13;14(13):1124–34.

500. Rothwell JC. The motor functions of the basal ganglia. J Integr Neurosci. 2011 Sep;10(3):303–15.